Dynamical behaviour of semiconductor lasers for analogue applications

Wong, Allen Y. C.

Award date:
1993

Awarding institution:
University of Bath

DYNAMICAL BEHAVIOUR OF SEMICONDUCTOR LASERS FOR ANALOGUE APPLICATIONS

Submitted by Allen Y. C. Wong, BSc.(Hons)
for the degree of
Doctor of Philosophy
of the University of Bath
1993

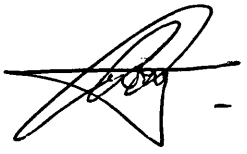

ProQuest LLC
789 East Eisenhower Parkway
P.O. Box 1346
Ann Arbor, MI 48106-1346

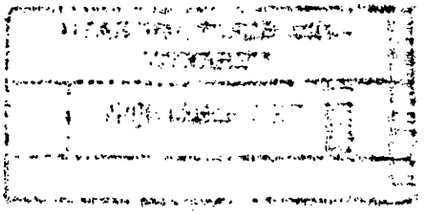

To my mother

Summary

This thesis is an investigation of the dynamical behaviour of semiconductor lasers for analogue lightwave systems, such as broadband subcarrier multiplexed systems. In particular, the following areas have been studied :

- relationship between the damping and bandwidth (both intrinsic and extrinsic bandwidth) of laser diodes;
- effects of gain non-linearities on the bandwidth;
- carrier transport effects on the dynamic response of quantum well laser devices;
- relaxation oscillation induced non-linear distortions; and
- non-linear distortions induced by longitudinal spatial hole burning and leakage current.

Acknowledgements

I would like to express my sincere thanks to Dr. K. Alan Shore for his superb guidance and supervision throughout the work of this course. I am also grateful to Dr. Adrian Jannsen of Northern Telecom for his participating interest in my research.

Thanks also to Drs. J. Sarma and Ian Middlemast with their useful discussions. I also want to thank Drs. C.S. Chang, Kevin Chan and Mr. C.H. Chong for their 24 hours computing service support; and Mr. Eric Cheung for his supply of video entertainment. Without these supports, the writing-up of this thesis would not have finished in such an efficient and enjoyable way. Particular thanks to Chong who has covered for me so many times in my absence while I was working so hard at my residence 15 miles away from the University. I will certainly be returning the favour now that he is frequently commuting to the North 100 miles from Bath !!!

I am greatly indebted to my better half, Priscilla, for her sensitivity, forbearance and loving support in the past few years. I would like to take this opportunity to wish her every success in the final Chartered Accountant Examinations. Last but not least, the names of the financial supporters, the University of Bath, the CVCP and Northern Telecom (Paignton) should also deserve acknowledgements.

Lists of Symbols

q	Electron charge ($1.602 \times 10^{-19} col$)
ϵ_o	Free space permittivity ($8.849 \times 10^{-12} Fm^{-1}$)
N	Carrier density (cm^{-3})
N_w	Carrier density bounded in the quantum well (cm^{-3})
N_b	Carrier density in the barrier (unbounded) (cm^{-3})
N_{tr}	Transparency carrier density (cm^{-3})
N_{th}	Threshold carrier density (cm^{-3})
I	Injection current (A)
I_l	Leakage current (A)
I_T	Total current (A)
I_{so}	Effective saturation current of leakage diode (A)
P	Photon density (cm^{-3})
$\tilde{(\cdot)}$	Denotes instantaneous values
$\delta(\cdot)$	Denotes small perturbations
L	Cavity length (μm)
d	Active region thickness (μm)
d_p	Thickness of ridge (μm)
d_s	Thickness of silicon nitride layer (mum)
w_{chip}	Entire width of the laser chip (mum)
w	Active region (or stripe) width (μm)

V	Volume of active region (m^3)
V_{qw}	Volume of quantum well active region (m^3)
V_{sch}	Volume of one-sided SCH region (m^3)
A_{nr}	Non-radiative carrier recombination rate (s^{-1})
B_r	Radiative bimolecular recombination rate ($cm^3 s^{-1}$)
C_{Auger}	Auger recombination rate ($cm^6 s^{-1}$)
R_{sp}	Spontaneous emission rate ($cm^{-3} s^{-1}$)
β	Spontaneous emission factor
γ_p	Optical loss (s^{-1})
γ_e	Electron recombination rate (s^{-1})
τ_p	Photon lifetime (s)
τ_e	Electron lifetime (s)
$\bar{\tau}_e$	Effective electron lifetime (s)
τ_{cap}	Quantum capture time (s)
τ_{esc}	Quantum escape time (s)
τ_{thm}	Thermionic emission time (s)
τ_{tp}	Carrier diffusion time across the SCH region (s)
τ_{eff}	Effective carrier transport time (s)
η_r	Quantum escape/capture rate ratio
Γ	Optical confinement factor
G	Optical gain
G_l	Linear optical gain
g_o	Gain coefficient ($cm^3 s^{-1}$)
A_o	Linear differential gain (cm^2)
ϵ	Gain suppression coefficient (cm^3)
v_g	Group velocity of optical wave (ms^{-1})
f	Frequency (Hz)
$\omega = 2\pi f$	Angular frequency (rad/s)

f_c	Carrier frequency spacing (Hz)
$f_{1,2,3}$	Arbitrary carrier frequency (Hz)
BW	Intrinsic -3 dB bandwidth (rad/s unless otherwise specified)
BW_{max}	Intrinsic maximum -3 dB bandwidth (rad/s)
BW_T	Extrinsic -3 dB bandwidth (rad/s)
BW_{Tmax}	Extrinsic maximum -3 dB bandwidth (rad/s)
BW_{QW}	Intrinsic -3 dB bandwidth for QW lasers (rad/s)
BW_{QWmax}	Intrinsic maximum -3 dB bandwidth for QW lasers
f_o	Undamped (Natural) frequency (Hz)
ω_o	Angular undamped frequency (rad/s)
α_r	Damping rate (s^{-1})
$\zeta = \alpha_r/\omega_o$	Damping factor
K	Olshansky's K factor
R_s	Series resistance (Ω)
R_l	Leakage diode resistance (Ω)
R_a	Active region resistance (Ω)
C_s	Shunt capacitance ($/pF$)
V_a	Voltage across active region (V)
η	Ideality factor of leakage diode
z	Longitudinal direction
$R(z)$, $S(z)$	Amplitude of forward and backward travelling waves
$\mathcal{F}$	Flatness parameter
r_o, r_L	Facets (power) reflectivities
$\mathcal{R}_o$, $\mathcal{R}_L$	Facets (amplitude) reflectivities
κ	Coupling coefficient of DFB lasers (cm^{-1})
α	Mode gain (cm^{-1})
σ	Detuning from Bragg frequency (cm^{-1})
φ	Propagation constant of optical wave

a_{th}	Threshold material gain (cm^{-1})
α_{int}	Internal cavity loss (cm^{-1})
Λ	Bragg wavelength (μm)
λ	Lasing wavelength (μm)
n	Refractive index
n_o	Refractive index at threshold
D	Diffusion coefficient (cm^2s^{-1})
μ_p	P-type semiconductor hole mobility ($cm^2V^{-1}s^{-1}$)
n_p	P-type semiconductor doping density (cm^{-3})

List of Figures

List of Tables

Contents

Chapter 1

Overview

1.1 Fiber optic systems for analogue applications

A great interest in communication at optical frequencies was created in the early 1960s after the invention of semiconductor laser which made available a compact coherent light source. Since the optical frequencies are of the order of 10^{14} Hz, the theoretical information capacity of an optical communication system exceeds that of microwave communication systems by a factor of 10^5. During the 1970s, the development of semiconductor lasers emitting in the near infrared red wavelength 0.8-0.9μm, resulted in their first usage as the light source of optical fibre communication systems designed for increased information throughput compared to that of the traditional telecommunication systems. The technology was then evolved towards a longer wavelength 1.3 and 1.55μm in order to take advantage of the very low losses occurring in silica fibre at these wavelengths and also the zero chromatic dispersion transmission at 1.3μm wavelength. In the early 1980s, intensive research efforts led to technological maturity of the semiconductor lasers to be used as a practical and economical light source for fibre point-to-point

links between cities (eg. long-haul telephony system). At that time, the digital revolution was at full swing in the telecommunication industry, almost all of the laser diodes used in the fibre links were subjected to direct digital intensity modulation (eg. simple on-off intensity signalling).

A simple schematic illustrating a digital fibre optic links is given in Figure 1.1. Analogue signals are first converted to digital data via an Analogue-to-Digital (A/D) converter and this digital data stream is used to modulate an electro-optical device, such as a laser diode, which produces the optical signal to transmit over the optical fibre. At the receiving end, digital optical data is converted back to an electrical digital signal through a photo-sensing device, such as a photodetector, and the digital signal is brought back to the analogue form by a Digital-to-Analogue (D/A) converter. An analogue fibre optic link, on the other hand, has a much simpler approach. It is obtained by removing the A/D and D/A converters at either end of the digital system as shown in the figure.

Due to the growth of information technology in the mid-1980s, there has been a strong demand from the subscriber loop for an interactive bi-directional communication system capable of handling multi-services. This gave birth to the concept of fibre-based Broadband Integrated Services Digital Network (BISDN) as a way to provide integrated voice, data and video services (eg. telephone, information retrieval and pay TV) reaching the subscriber loop. The original concept in the mid-1980s was later on improved to include new Synchronous Optical Network (SONET) standards and to incorporate new ideas like Asynchronous Transfer Mode (ATM) switching and transmission. Nevertheless, the main architecture and the pure digital approach of BISDN has not changed significantly. Although the proposal of BISDN is technically feasible at present, there has been a growing recognition that it is not a cost effective way of meeting such a broadband multi-

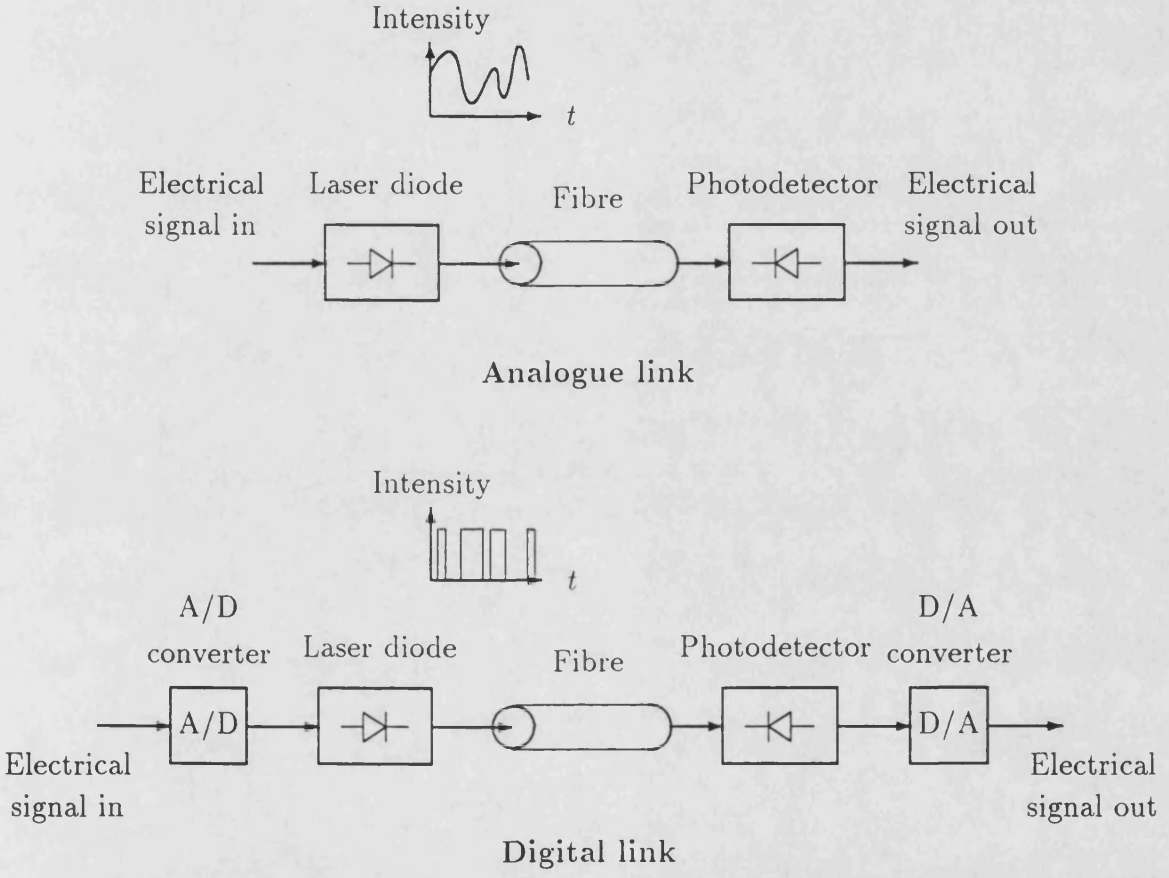

Figure 1.1: *The basic difference between analogue and digital fibre optic links.*

services demand, particularly, in the delivery of video signals to the residential subscribers. Several less expensive alternative approaches providing broadband multi-services were then developed in the late 1980s [1, 2, 3].

1.1.1 Subcarrier multiplexed lightwave system

Stepping into 1990s, the Subcarrier Multiplexed Broadband Service Network (SCM-BSN) seems to be the most promising solution for the future high capacity lightwave system as advocated by several research groups including GTE Laboratories [3] AT&T Bell Laboratories [4] and Bellcore [5]. The major revolution of the SCM-BSN approach is its capability of accommodating both multichannel analogue and digital signals. As the key element of the Subcarrier multiplexed (SCM) lightwave system, the laser diode is in continuous-wave operation and is directly intensity modulated by the upconverted microwave signals. This is then in fact an analogue optical communication system.

A basic SCM system configuration is shown in Figure 1.2. A number of baseband services (including voice, video and data channels) in analogue or digital format are first frequency division multiplexed (FDM) by using local oscillators (LO) of different radio frequencies (RF) or even microwave frequencies. The upconverted signals then combine to modulate a high speed laser diode. The local oscillator frequencies are the so-called *subcarrier* in contrast to the *optical carrier* frequencies. At the receiver end, a subscriber or end user can receive any one of the FDM channels by tuning a local oscillator and down-converting the microwave signals to baseband or intermediate frequencies (IF). The frequency spectrum of the SCM-BSN is therefore within the microwave frequency range, for instance a 2-6 GHz SCM with 60 FM (Frequency Modulation) video channels and data

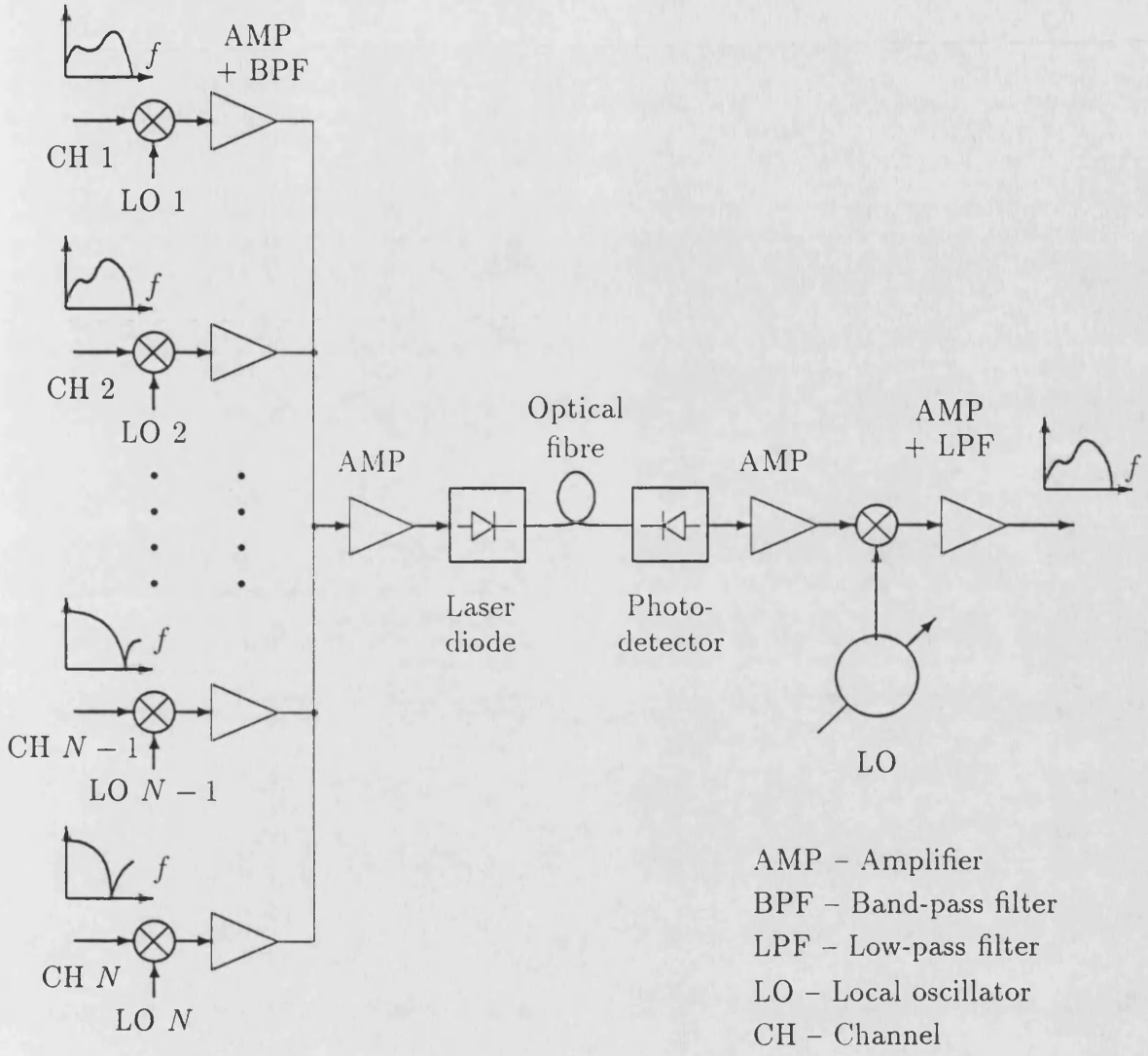

Figure 1.2: *Basic SCM system configuration*

channel of 100-Mbit/s as demonstrated by R. Olshansky [6].

1.1.2 Cable television systems

Another more obvious application of analogue lightwave system is the evolutionary upgrading of the existing cable television network, for example the Community Antenna Television (CATV) system in the United States. The CATV system is presently running on the coaxial (coax) cable network based on the technology in the 1970s. The performance of this coax technology has continuously improved throughout the years to meet growing requirements. But in order to meet the future high-quality broadband needs, fibre optics is an attractive option.

At the head office (headend), various video signal are AM-VSB (Amplitude Modulation-Vestigial Sideband) modulated, combined using FDM techniques, and then transmitted over the primary coax network (trunks or feeders) to various distribution points as show in Figure 1.3. From the distribution system, flexible coaxial cable is used to bring signals to the terminal equipment – TV set or video cassette recorder (VCR). Usually, a frequency span from 50 to 500 MHz is required to accommodate 40-50 channels.

In the late 1980s, a number of point-to-point links between headends (supertrunks) in the CATV network have been built using analogue lightwave systems [7]. These supertrunks generally use FM/FDM to directly modulate a laser diode feeding an optical fibre and have proven cost effective compared with other techniques. Later on T.E. Darcie [4] proposed the replacement of most of the headend trunks in the CATV network by fibre optics in order to improve the service quality and to prepare for the anticipated broadband multi-service system. In fact, by introducing the fibre trunk, the CATV system is equivalent to a SCM with AM-VSB format operating from 50 to 500 MHz.

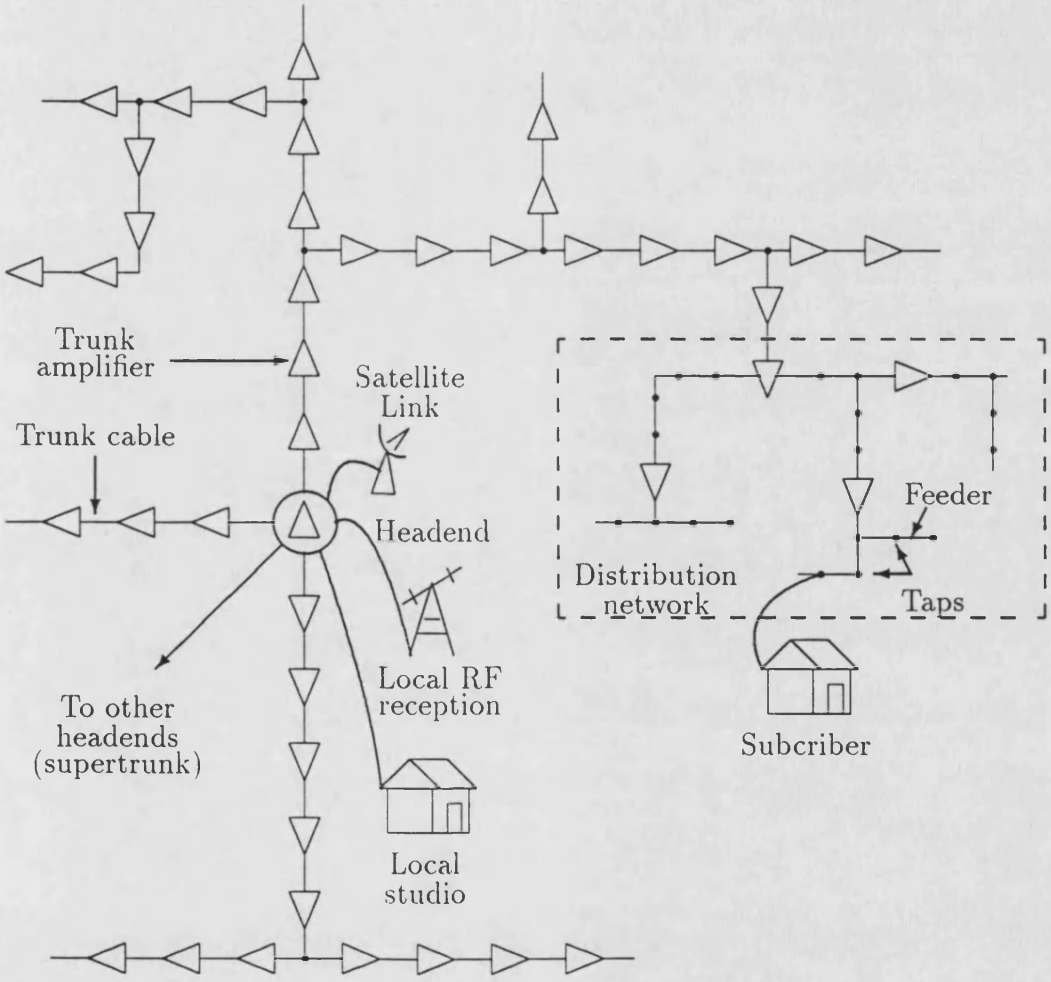

Figure 1.3: *Simplified schematic of a CATV system*

Although other modulation formats such as FM, FSK (Frequency Shift Keying) and even digital schemes were suggested to replaced the AM-VSB to improve the picture and sound qualities, AM-VSB is still the most cost effective choice to directly match with final interface – the consumer's TV receiver which has been based on AM-VSB technology for nearly three decades. Fortunately, fibre optic trunks with directly modulated distributed feedback (DFB) laser diode as the light source can compensate for the fragility of the signal with respect to the noise and non-linear distortions of the AM-VSB format. This is due to the high linearity and low noise characteristics of the carefully designed DFB laser diode. In early 1990, CATV operators began to install fibre trunk, usually in application where there was a requirement to make a substantial increase in channel capacity.

1.2 External modulators versus direct modulation

In the direct modulation scheme of a lightwave system, the laser diode is in fact performing two major functions :

(i) as an electro-optical converter; and

(ii) as a modulator whose optical output intensity varies in accordance with the modulating electrical signal.

With the laser operated in this way, the interaction between photons and electrons inside the laser diode can give rise to unwanted non-linear distortions. The two primary functions may be separated by the use of, external modulation illustrated by Figure 1.4. A diode-pumped $1.3\mu m$ Yttrium Aluminum Garnet (YAG) laser

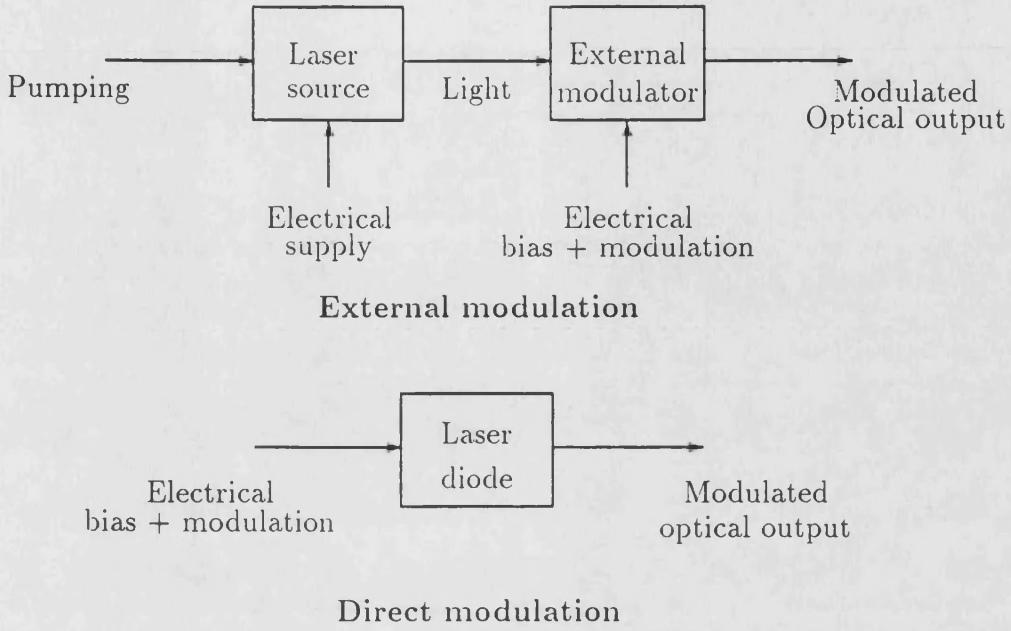

Figure 1.4: *The difference between direct modulation and external modulation scheme*

is generally used as the optical source to meet the optical power budget and the external modulator is usually formed by an optical waveguide interferometer using lithium niobate material.

Recently, there is a growing interest in the search of an external modulator to compete with the direct modulated laser diode in analogue applications. Experimental results by G.E. Bodeep [9] show that at some bias voltage the second-order non-linear distortion of an ordinary $LiNbO_3$ modulator can be eliminated, but the third-order distortion is much more serious than that with direct modulation ($\approx$ 25 dB worse) as seen in Figures 1.5 and 1.6. This result suggests either the modification of the structure or the addition of electronic [10] or optical [11] compensation is required to linearise the external modulator if it is to be used for an analogue optic link. Even if the results can match exactly those of direct modulation, the external modulation scheme must still pay the penalty of the cost for extra electronic or optical components for the linearisation and the external

modulator itself. However, the external modulation scheme has the advantage of providing a high optical power with narrow linewidth and low RIN if a YAG laser is used.

In the past five years, a lot of research activities have been undertaken to improve the linearity of laser diodes and a number of highly linear laser devices suitable for direct modulation in CATV AM-VSB system (which has the most stringent linearity requirement) have been made. It is the small size, low manufacturing cost, flexibility and simplicity that make the semiconductor laser an attractive candidate for direct modulation schemes.

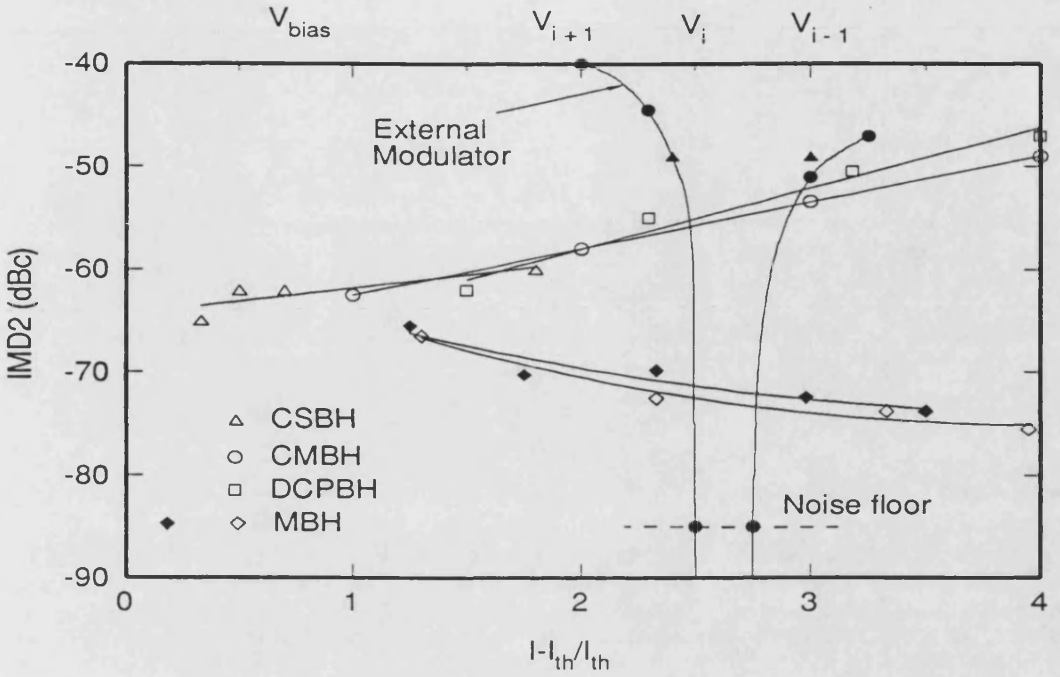

Figure 1.5: *Second-order non-linear distortions at optical modulation depth (OMD) of 4% versus normalised bias current (bottom axis) and bias voltage (top axis) for channel substrate buried heterostructure (CSBH) laser, covered mesa heterostructure (CMBH), double channel planner buried heterostructure (DCPBH) laser, and modified buried heterostructure (MBH) laser. Extracted from [9].*

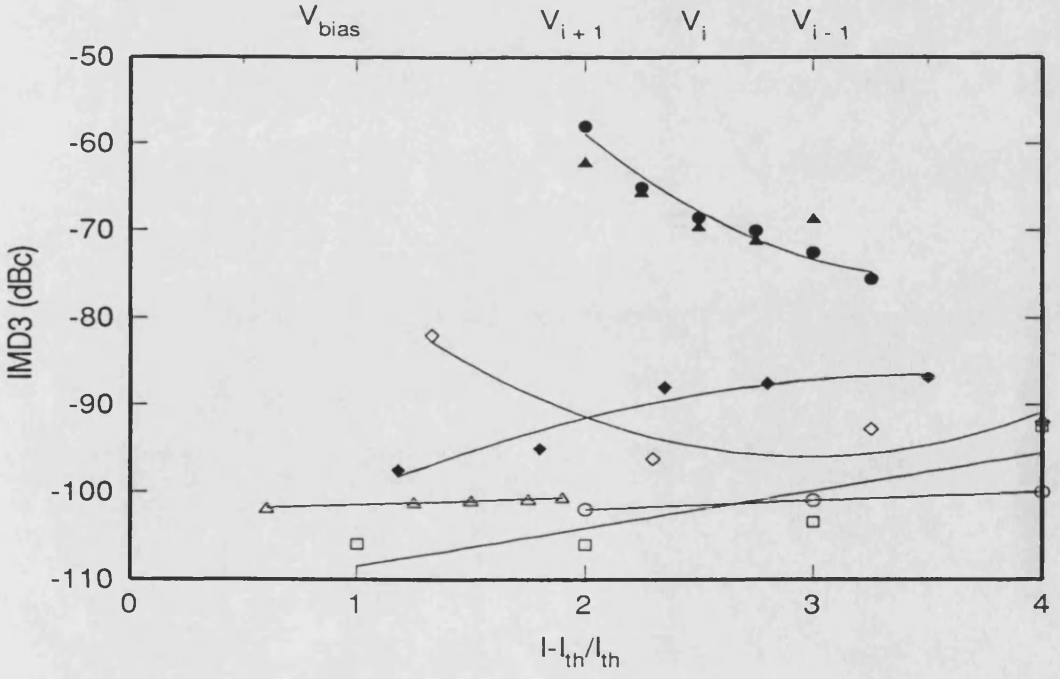

Figure 1.6: *Third-order non-linear distortion at OMD = 4% versus normalised bias current (bottom axis) and bias voltage (top axis). Same labels as above.*

1.3 Structure of the thesis

It appears that in the world of fibre optics communication, analogue application will become increasingly common. Different system applications will set different requirements on the laser diode dynamics, but there exist some common criteria for a laser diode used in an analogue system :

- large bandwidth and flat frequency response;
- low non-linear distortions;
- low Relative Intensity Noise (RIN).

The objective of this thesis is therefore to study these various dynamic properties of a laser diode when it is subject to direct analogue modulation. It is hoped that the results can be used as a guideline for designing laser diode for analogue lightwave system.

Chapters 2-5 are mainly concerned with the bandwidth of semiconductor lasers due to both intrinsic and extrinsic effects, such as gain non-linearities, chip parasitics and also carrier transport phenomena in quantum well (QW) devices. The word *intrinsic* here should be understood as referring to phenomena occurring in the active region of laser diode (and which can be described by the laser rate equations). Moreover, Chapters 6 and 7, concentrate on the non-linear distortion analysis of laser diodes.

The RIN for a solitary laser diode is known to be very small [5, 12, 13, 14] and it actually decreases as optical output power increases. In a practical lightwave

system, the situation is aggravated due to external feedback, for example, reflections from fibre discontinuities back into the laser cavity. However, the analysis of such a degradation factor due to the external environment is beyond the scope of this thesis and will not be discussed here.

In Chapter 2, the relationship of the damping effects and the intrinsic bandwidth for a laser diode is derived. From this relationship, bandwidth optimisation for analogue application purposes is performed. The implications of the intrinsic material properties, for instance, differential gain and gain suppression on the optimised bandwidth is also discussed. A comparison of the possible implications on the intrinsic bandwidth using two different non-linear gain models is discussed in Chapter 3.

Chip parasitics are a major extrinsic effect that imposes an early roll-off in the laser diode frequency response and thus results in the reduction of bandwidth. The relationship of the damping and the extrinsic (overall) bandwidth is given in Chapter 4. The results of a bandwidth measurement experiment, using the laser diodes provided by Northern Telecom, Paignton, UK, is also given in the same chapter. Recent progress on the rate-equation modelling of carrier transport effects in QW laser devices is summarised in Chapter 5. The analysis is extended to emphasis the influence of the carrier transport on the intrinsic bandwidth of a QW laser. Due to the similar frequency response roll-off effect of the carrier transport, the results in Chapter 4 are used for the prediction of the QW laser intrinsic bandwidth.

A perturbation method and Volterra series approach for analysing the non-linear distortion of a laser diode are introduced in Chapter 6. Particular attention is given to the high frequency relaxation oscillation (RO) induced non-linearity.

For the commonly used DFB laser diodes, two types of non-linearities : spatial hole burning and leakage current dominate at frequencies far below the RO frequency. The corresponding non-linear distortions are studied in Chapter 7. The Volterra series is then applied to study the effects of the low frequency non-linear distortions in order to identify the dominant mechanism. Finally, in Chapter 8 some conclusions are drawn based on the findings in the previous chapters for designing laser diodes used in an analogue optical communication system.

References

[1] J.R. Stern, "Passive optical local networks for telephony applications and beyond," *Electron. Letts., vol. 23, pp. 128-135, 1989.*

[2] D. Large, "A comparison of evolutionary paths : tapped fibre vs fibre-reinforced coaxial CATV systems", *IEEE LCS Mag., vol. 1, pp. 12-18, 1990.*

[3] R. Olshansky, "Subcarrier Multiplexed broadband service network : a migration path to BISDN", *IEEE LCS Mag., pp. 30-34, August 1990.*

[4] T. E. Darcie, "Subcarrier multiplexing for lightwave networks and video distribution systems", *IEEE J. Selected Areas in Commun., vol. 8, pp. 1240-1248, 1990.*

[5] W. I. Way,"Subcarrier multiplexed lightwave system design considerations for subscriber loop applications", *J. Lightwave Technol., vol. 7, pp. 1806-1818, 1989.*

[6] R. Olshansky and V. A. Lanzisera, "60-channel FM video subcarrier multiplexed optical communication system", *Electron lett., vol. 22, pp. 1119, 1987.*

[7] J.A. Chiddix, "Optical fibre supertrunking. The time has come : A performance report on a real-world system", *IEEE J. Selected Areas in Commun., vol. 4, no. 5, 1986.*

[8] P. Hill and R. Olshansky, " A 20-channel optical communication system using subcarrier multiplexing for the transmission of digital video signals", *J. Lightwave Technol., vol. 8, pp. 554-560, 1990.*

[9] G.E. Bodeep and T.E. Darcie, "Semiconductor lasers versus external modulators : A comparison of non-linear distortion for lightwave subcarrier CATV applications", *IEEE Photonics Technol. Lett., vol. 1, pp. 401-403, 1989.*

[10] A.H. Guanck, T.E. Darcie and G.E. Bodeep, "Comparison of direct and external modulation for CATV lightwave transmission at 1.5 μm wavelength", *Electron. Lett., vol. 28, pp. 1875-1876, 1992.*

[11] L.M. Johnson and H.V. Roussell, "Linearisation of interferometric modulator at microwave frequencies by polarisation mixing", *IEEE Photonics Technol. Lett., vol.2, pp. 810-811, 1990.*

[12] P. Hill, J. Schlafer and R. Olshansky, "Reduction of relative intensity noise in 1.3 μm InGaAsP semiconductor lasers", *Appl. Phys. Lett., vol. 50, pp. 1400-1402, 1987.*

[13] K. Sota," Intensity noise of semiconductor laser diodes in fibre-optic analog video transmission", *IEEE J. Quantum Electron., vol. QE-19, pp. 1380-1301, 1983.*

[14] K. Petermann, "Laser diode modulation and noise", *Kluwer Academic Publishers, Chap. 7, 1988.*

Chapter 2

Intrinsic Bandwidth and Damping

2.1 Introduction

In the design of a high performance broadband optical system, eg. broadband distribution SCM which operates at microwave frequencies, the following two basic criteria would be applied to the intrinsic properties of a directly modulated laser diode :

(i) the intrinsic -3 dB bandwidth of laser diode should be as high as possible in order to accommodate more channels and operate at high speed.

(ii) a flat and smooth frequency response should also be obtained to reduce the non-linear distortions and provide a near ideal communication channel.

In the absence of all extrinsic limitations, for example, package and chip parasitics, device over-heating and damage at high power, the intrinsic bandwidth of the semiconductor laser is greatly influenced by the damping of relaxation oscillations

(RO) arising due to gain suppression [1, 2, 3, 4]. It is also noted that the exact origin of this gain suppression is still a matter of debate; spectral hole burning and carrier heating effects are widely believed to be primary sources [5, 6, 7, 8]; whilst spatial carrier diffusion [9] may be considered as secondary mechanisms for this gain suppression. The main conclusions to be drawn in respect of the effect of relaxation oscillation damping are that if :

- the damping is too small, a high resonance peak is obtained in the frequency response – in contradiction with criterion (ii);
- the damping is too large a reduction in the intrinsic bandwidth occurs – violating criterion (i).

It is clear therefore that optimisation of both the bandwidth and the damping are required in order to satisfy the design criteria.

In this chapter, the relationship between the intrinsic bandwidth and damping is established by applying small signal analysis to the standard rate equations. Optimisation of the intrinsic bandwidth is then undertaken with the use of a damping factor ζ (defined in the following Section 3). A brief explanation of Olshansky's K factor [1] is also given. Finally, a consideration of the maximum bandwidth is given for different device materials, such as bulk, multi-quantum well (MQW) and strained-layer quantum well (SLQW).

2.2 Laser diode rate equations

One of the important properties of semiconductor lasers is that they can be directly modulated. The corresponding modulation dynamics of a laser diode active region can be studied by the following pair of single-mode rate equations which are derived base on the concept of energy conservation inside the lasing cavity :

$$\begin{aligned} \frac{d\tilde{N}}{dt} &= \frac{\tilde{I}}{qV} - G(\tilde{N},\tilde{P})\tilde{P} - \gamma_e(\tilde{N})\tilde{N} \\ \frac{d\tilde{P}}{dt} &= \Gamma G(\tilde{N},\tilde{P})\tilde{P} - \gamma_p\tilde{P} + R_{sp} \end{aligned} \tag{2.1}$$

with

$$\begin{aligned} \gamma_e(\tilde{N}) &= \frac{1}{\tau_e} = A_{nr} + B_r\tilde{N} + C_{Auger}\tilde{N}^2 \\ \gamma_p &= \frac{1}{\tau_p} \\ R_{sp} &= \beta(B_r\tilde{N})\tilde{N} \end{aligned}$$

where $\tilde{N}$ and $\tilde{P}$ are the (instantaneous) carrier and photon densities (cm^{-3}) respectively; $\tilde{I}$ is the (instantaneous) injection current (A), q and V are the electron charge (col) and active region volume (cm^3); G and γ_p are the optical gain and losses respectively; τ_e and τ_p are the carrier lifetime and the photon lifetime (s); γ_e is the electron recombination rate which includes : A_{nr} the non-radiative rate (s^{-1}), B_r the radiative rate (cm^3s^{-1}) and C_{Auger} the Auger (cm^6s^{-1}) recombination rate; Γ and β are the optical confinement and the spontaneous emission factors.

2.3 Intrinsic bandwidth and damping

By applying standard small signal analysis (see Appendix A) to the pair of rate equations in Chapter 1, one can obtain the intrinsic frequency response (transfer function) $F_{int}(\omega)$ of a laser diode, which is given by,

$$\begin{aligned} F_{int}(\omega) &= \frac{1}{eV}\frac{\Gamma\frac{\partial G}{\partial N}P}{\omega_o^2}H_{int}(\omega) \\ H_{int}(\omega) &= \frac{1}{\left(\frac{j\omega}{\omega_o}\right)^2 + 2\frac{\alpha_r}{\omega_o}\left(\frac{j\omega}{\omega_o}\right) + 1} \end{aligned} \tag{2.2}$$

where P is the steady state photon density; ω_o is the undamped angular frequency; α_r is the damping rate of the relaxation oscillation; $\frac{\partial G}{\partial N}$ is the gain derivative w.r.t. to the carrier density; $H_{int}(\omega) = F_{int}(\omega)/F_{int}(0)$ is the normalised response function. The damping factor ζ is therefore defined as

$$\zeta \equiv \frac{\alpha_r}{\omega_o} \tag{2.3}$$

By equating the magnitude of Eqn (2.2) to $1/\sqrt{2} = -3$ dB, a quadratic equation in $\left(\frac{BW}{\omega_o}\right)^2$ is obtained as shown below,

$$\left(\frac{BW}{\omega_o}\right)^4 - 2(1-2\zeta^2)\left(\frac{BW}{\omega_o}\right)^2 - 1 = 0 \tag{2.4}$$

here BW denotes the -3 dB intrinsic bandwidth (rad/s). In other words, the definition of intrinsic bandwidth BW is the bandwidth achieved by the active region of a laser diode. As extrinsic effects, for example parasitics and carrier transport effects are brought in, the resultant (extrinsic) bandwidth may be reduced.

The formula relating the intrinsic bandwidth BW and the damping factor ζ is therefore given by

$$BW = Y(\zeta)\,\omega_o \tag{2.5}$$

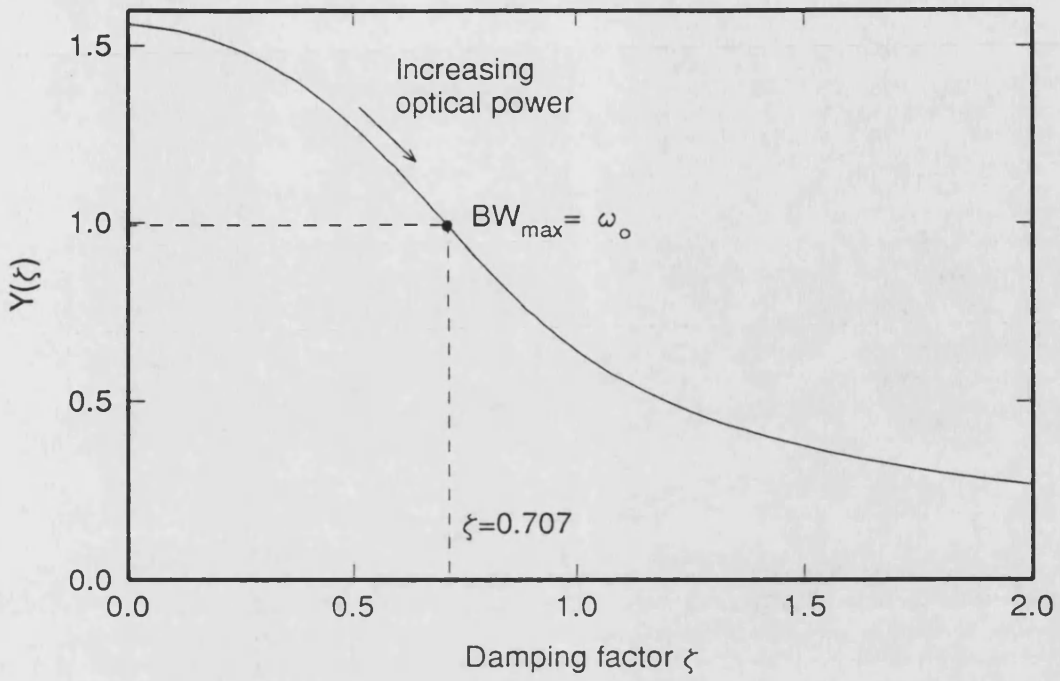

Figure 2.1: *The function $Y(\zeta)$ versus ζ*

where

$$Y(\zeta) = \sqrt{(1-2\zeta^2) + \sqrt{(1-2\zeta^2)^2 + 1}}$$

The function $Y(\zeta)$ is shown in Figure 2.1 from which it is seen that as ζ increases, the whole function $Y(\zeta)$ decreases. Typical range for damping factor ζ is $0 < \zeta < 1$.

Obviously, Eqn (2.5) shows that the damping and intrinsic bandwidth are closely related. As the damping factor ζ increases due to increase in optical output power, $Y(\zeta)$ begins to decrease while ω_o increases. Hence, a trade off between $Y(\zeta)$ and ω_o exists. Depending on the rate of change of these two terms with the increase in optical output power, the bandwidth BW will inevitably experience *suppression* or even undergo a maximum values, ie. *maximum bandwidth* BW_{max}, as the optical intensity increases.

Keeping the dominant terms, the above three parameters α_r, ω_o and ζ can be

approximately given by,

$$\begin{aligned}\alpha_r &= \frac{1}{2}\left(\frac{\partial G}{\partial N}P - \Gamma\frac{\partial G}{\partial P}P + \frac{d\gamma_e \cdot N}{dN}\right) \\ &\approx \frac{1}{2}\left(\frac{\partial G}{\partial N} - \Gamma\frac{\partial G}{\partial P}\right)P \qquad (2.6)\end{aligned}$$

$$\begin{aligned}{\omega_o}^2 &= \Gamma G\frac{\partial G}{\partial N}P - \frac{d\gamma_e \cdot N}{dN}\Gamma\frac{\partial G}{\partial P}P \\ &\approx \Gamma G\frac{\partial G}{\partial N}P \qquad (2.7)\end{aligned}$$

$$\zeta \approx \frac{1}{2}\sqrt{\frac{\partial G/\partial N}{\Gamma G}}\left(1 - \Gamma\frac{\partial G/\partial P}{\partial G/\partial N}\right)\sqrt{P} \qquad (2.8)$$

where the gain derivative w.r.t. photon density, $\partial G/\partial P$, is a gain non-linearity term; the term $d\gamma_e/dN$ is referred as the differential electron recombination rate.

As is apparent from the above equations these parameters are all functions of the steady state photon density P or functions of output optical power. Moreover, the material dependent parameters - optical gain $G(N,P)$ and its derivatives $\partial G/\partial N, \partial G/\partial P$ are therefore the key elements in determining the variational behaviour of α_r, ω_o and ζ against P.

2.4 The 'Two-level' non-linear gain model

A commonly used form of the optical gain is

$$\begin{aligned}G(N,P) &= \frac{G_l(N)}{1+\epsilon P} \\ &= \frac{g_o(N-N_{tr})}{1+\epsilon P} \qquad (2.9)\end{aligned}$$

where $G_l(N)$ is the linear gain and g_o is the gain coefficient (cm^3s^{-1}) and $A_o = \frac{dG_l}{dN}/v_g = g_o/v_g$ is often regarded as the linear differential gain (cm^2) with v_g as the group velocity of the optical wave. N_{tr} is the transparency carrier density;

and ϵ is the gain suppression coefficient. This non-linear gain model is obtained by considering a homogeneously broadened two-level system [6]. A more detailed discussion of other models of optical gain is given in next chapter. Typical device parameter values are given in Table 2.1.

A_{nr}	$1 \times 10^{8} s^{-1}$	Γ	0.3
B_r	$1 \times 10^{-10} cm^3 s^{-1}$	τ_p	$1.44 \times 10^{-12} s$
C_{Auger}	$3 \times 10^{-29} cm^6 s^{-1}$	τ_e	$2.11 \times 10^{-9} s$
β	1.7×10^{-4}	N_{th}	$2.22 \times 10^{18} cm^3$
$V = L \times w \times d$	$275 \times 2.5 \times 0.2 \mu m^3$	I_{th}	23.2 mA
N_{tr}	$1 \times 10^{18} cm^{-3}$	g_o	$1.875 \times 10^{-6} cm^{-3} s^{-1}$

Table 2.1: *Typical parameter values for a laser diode operating at a wavelength* $\lambda = 1.3 \mu m$. I_{th} *and* N_{th} *are the threshold current and threshold carrier density respectively. For the analysis of QW devices, the active region volume* V *and the optical confinement factor* Γ *is scaled up to that of the bulk for comparison.*

The relationship between the damping and the non-linear gain effect can be seen from Eqn (2.8). For example, a laser diode with high gain suppression coefficient ϵ and low differential gain A_o will therefore exhibits a high damping effect as indicated by the significant term $\frac{\partial G/\partial P}{\partial G/\partial N}$ of Eqn (2.8).

Substituting the expression of the non-linear optical gain G into the previous expressions, α_r, ω_o and ζ can then be rewritten as,

$$\alpha_r \approx \frac{1}{2}\left(1 + \frac{\epsilon}{g_o \tau_p}\right) \frac{g_o}{\epsilon} \frac{\epsilon P}{(1 + \epsilon P)} \tag{2.10}$$

$$\omega_o^2 \approx \frac{g_o}{\tau_p \epsilon} \frac{\epsilon P}{(1+\epsilon P)} \tag{2.11}$$

$$\zeta \approx \frac{1}{2} \frac{1}{\sqrt{\frac{\epsilon}{g_o \tau_p}}} \left(1 + \frac{\epsilon}{g_o \tau_p}\right) \sqrt{\frac{\epsilon P}{(1+\epsilon P)}} \tag{2.12}$$

The above analytic results have been justified by solving the pair of rate equations numerically in a static fashion (eg. Newton method), that is, setting $dN/dt, dP/dt = 0$. Some numerically examples are given in Figures 2.2 to 2.4, for various values of gain suppression coefficient ϵ.

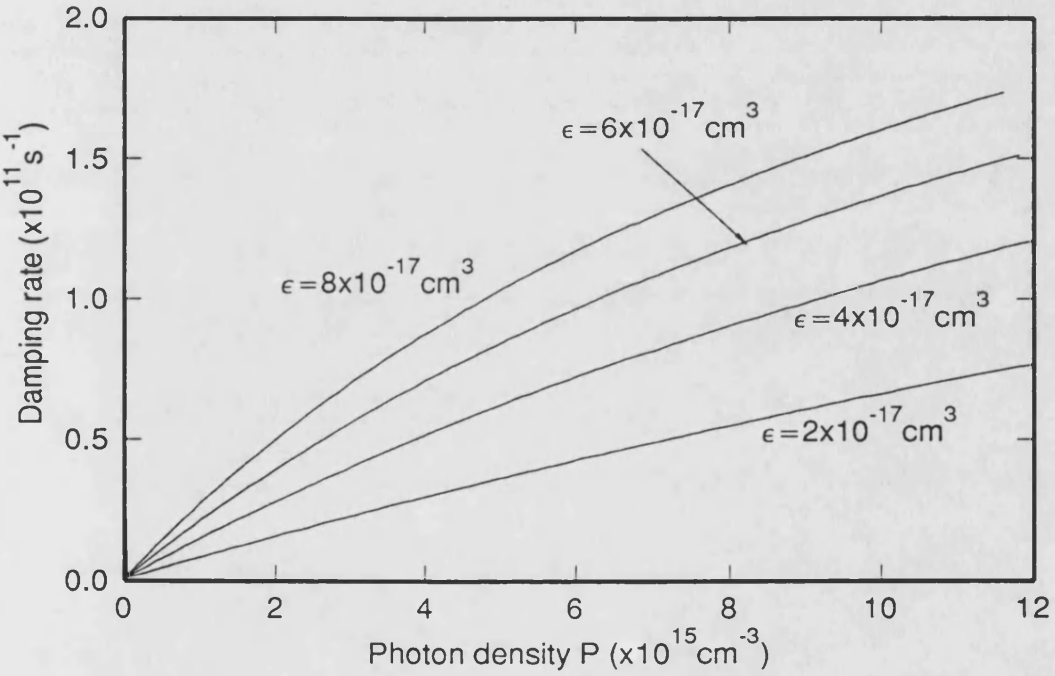

Figure 2.2: *Plot of damping rate α_r versus photon density P.*

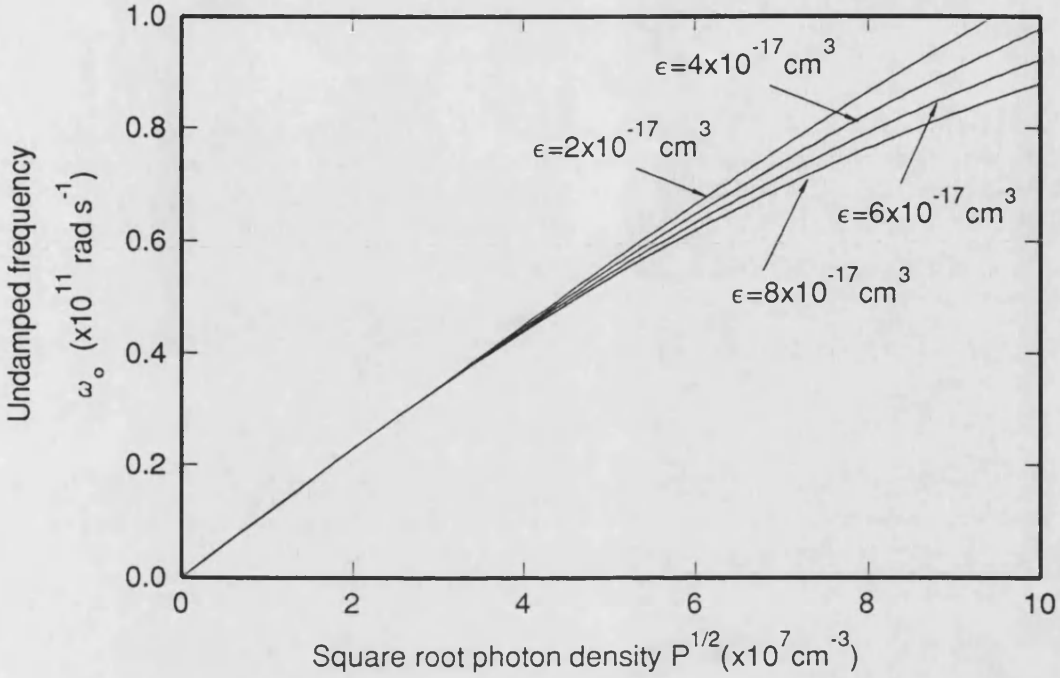

Figure 2.3: *Plot of squared undamped frequency f_o^2 versus square root photon density $P^{1/2}$.*

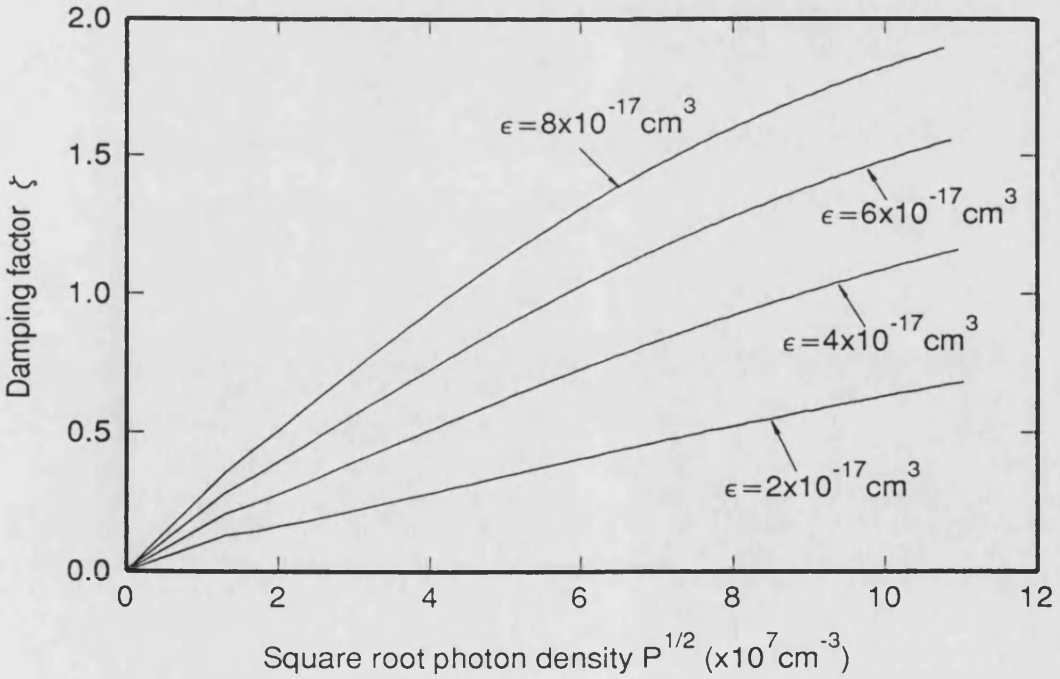

Figure 2.4: *Plot of damping factor ζ versus square root photon density $P^{1/2}$.*

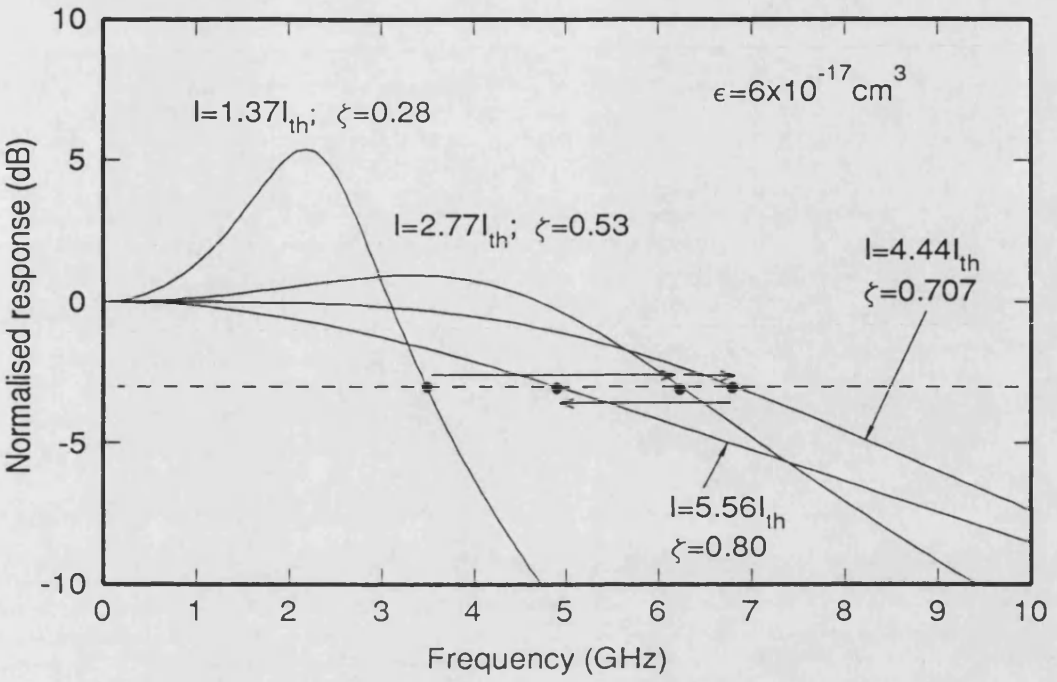

Figure 2.5: *Typical frequency response of a laser diode.*

Figure 2.5 shows a graph of the frequency response at various levels photon density and which corresponds to different level of damping factor ζ. As can be seen the higher the ζ, the flatter is the frequency response. In other words, the resonance peak shown in the frequency response is being suppressed as the damping factor ζ increases. In the graph, a -3 dB line was drawn to identify the bandwidth which varies non-linearly with the damping factor ζ. The BW starts to increase as the damping factor ζ increases, but then at a certain value of ζ heavy damping begins to cause reduction in the BW. This effect may be understood by computing the relationship between the BW and damping factor ζ as given in the previous section.

2.5 Bandwidth optimisation

The conditions for which the intrinsic maximum bandwidth BW_{max} exists can be found by setting $\frac{dBW}{dP} = 0$. This can be rewritten as

$$\frac{dBW}{dP} = \frac{dBW}{d\zeta}\frac{d\zeta}{dP} = 0$$

Since $\frac{d\zeta}{dP} \neq 0$, this forces $\frac{dBW}{d\zeta} = 0$ when maximum intrinsic bandwidth exists. This leads to the following relationship [11],

$$\frac{dBW}{d\zeta} = BW\left(\frac{-2\zeta}{\sqrt{(1-2\zeta^2)^2+1}} + \frac{1}{\frac{d\zeta}{d\omega_o}\omega_o}\right) = 0 \tag{2.13}$$

2.5.1 Criterion for the existence of maximum bandwidth

Assuming the term $\frac{d\zeta}{d\omega_o}\omega_o$ can be expressed as,

$$\frac{d\zeta}{d\omega_o}\omega_o = \phi(P)\zeta$$

where $\phi(P)$ is either a function of P or constant. Substituting this assumption back into Eqn (2.13), one can obtain

$$2(\phi^2-1)\zeta^4 + 2\zeta^2 - 1 = 0 \tag{2.14}$$

In order to ensure a root for the above equation, the discriminant has to be greater than or equal to zero. This implies the following criterion has to be satisfied, if an intrinsic maximum bandwidth BW_{max} does exist,

$$\frac{d\zeta}{d\omega_o}\omega_o \geq 0.707\zeta \tag{2.15}$$

This criterion is very important in determining whether or not an intrinsic maximum bandwidth BW_{max} would actually occur in a laser diode. The parameter

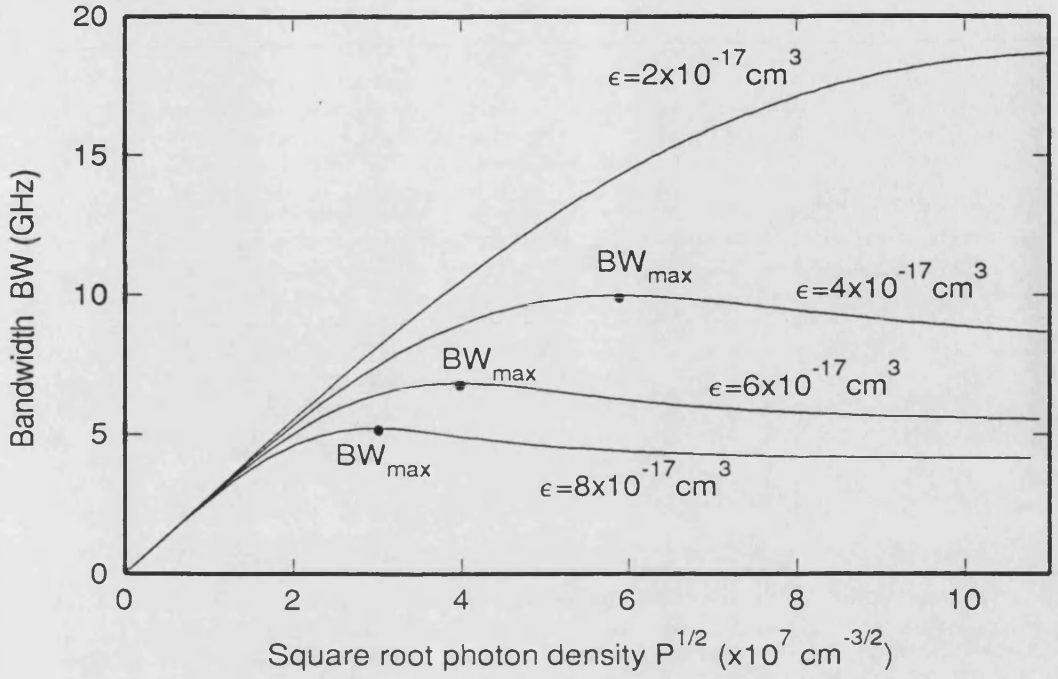

Figure 2.6: *Plot of intrinsic bandwidth BW versus square root photon density* $P^{1/2}$.

that affects both ζ and ω_o seriously is the non-linear gain G as evident in Eqns (2.7) and (2.8).

With the two-level non-linear gain model in Eqn (2.9) and the corresponding results in Eqns (2.11) and (2.12), it can be shown that

$$\begin{aligned} \frac{d\zeta}{d\omega_o}\omega_o &= \zeta \\ &> 0.707\zeta \end{aligned} \tag{2.16}$$

This proves that for this model of gain non-linearity Eqn (2.9), the intrinsic bandwidth of the laser diode always experiences a maximum value BW_{max}. The numerical results displayed in Figure 2.6 also confirms this conclusion. With a small gain suppression coefficient ϵ, a higher BW_{max} results.

2.5.2 Optimal damping factor and maximum bandwidth

The value of the damping factor ζ at which intrinsic maximum bandwidth occurred is found by substituting Eqn (2.15) back into Eqn (2.13). The following results are obtained :

(i) the intrinsic maximum bandwidth always equals the undamped frequency,

$$BW_{max} = \omega_o \tag{2.17}$$

(ii) the corresponding damping factor at this intrinsic maximum bandwidth is

$$\zeta = 0.707 \tag{2.18}$$

Clearly, at this particular value of $\zeta = 0.707$, the frequency response is just flat and shows no resonance peak, ie. critically damped system. This implies that the BW_{max} of a laser diode is actually the optimal bandwidth which satisfies the two basic criteria for a high performance analogue system stated in Section 1.

It is note worthy that the optimal value of ζ for a high performance digital system is usually bigger than 1 [12], that is corresponding to an overdamped system. This is because the optimisation for a high performance digital system requires a minimisation of the laser's ringing effect (relaxation oscillation). The present result indicates a difference in optimisation criteria which would seem to be of particular importance for the design of a high performance analogue system.

Substituting $\zeta = 0.707$ back into Eqn (2.8), and eliminating P using Eqn (2.17), the maximum bandwidth BW_{max} can be approximated in terms of device param-

eters as follows :

$$\begin{aligned} BW_{max}(\text{Hz}) &= \frac{\sqrt{2}}{2\pi}\frac{\Gamma G}{\left(1-\Gamma\frac{\partial G/\partial P}{\partial G/\partial N}\right)} \\ &= \frac{\sqrt{2}g_o}{2\pi(\epsilon+g_o\tau_p)} \\ &\approx \sqrt{2}(2\pi)\frac{1}{\frac{2\alpha_r}{f_o^2}} \end{aligned} \tag{2.19}$$

where $f_o = \omega_o/2\pi$. Note that the unit of bandwidth BW is often in rad/s unless specified. This equation stresses that the maximum bandwidth is power independent and further discussion of the effect of various device parameters on the BW_{max} will be given in Section 2.7.

By substituting the following static light-current (L-I) relationship (obtained by solving the rate equations Eqn (2.1) in a static manner),

$$P \approx \Gamma\frac{\tau_p}{qV}(I-I_{th}) \tag{2.20}$$

into Eqn (2.12) with $\zeta = 0.707$, the approximated bias current required to achieve the intrinsic maximum bandwidth BW_{max} is found to be,

$$I\,|_{BW=BW_{max}} \approx \frac{2qVg_o}{\Gamma(\epsilon+g_o\tau_p)^2} + I_{th} \tag{2.21}$$

where I_{th} is the threshold current.

2.6 The K factor

The term $2\alpha_r/f_o^2$ in Eqn (2.19) was originally defined by R. Olshansky as the K *damping* factor [1], that is

$$K = \frac{2\alpha_r}{f_o^2} = 2(2\pi)^2\frac{\zeta}{\omega_o}$$

$$= (2\pi)^2 \left(\frac{1 - \Gamma \frac{\partial G/\partial P}{\partial G/\partial N}}{\Gamma G} + \frac{\frac{d\gamma_e \cdot N}{dN}}{\Gamma G \frac{\partial G}{\partial N} P} \right)$$

$$\approx (2\pi)^2 \frac{(\epsilon + g_o \tau_p)}{g_o}$$

which is a power independent parameter. In the above derivation, the term containing $d(\gamma_e \cdot N)/dN$ has been neglected and therefore a better definition for the K factor would be given by :

$$K = \frac{2(\alpha_r - \frac{1}{2}\frac{d\gamma_e \cdot N}{dN})}{f_o^2}$$

$$= \frac{2\Delta\alpha_r}{\Delta f_o^2} \tag{2.22}$$

which represents a straight line relationship between the damping rate α_r and the squared undamped frequency f_o^2. Hence, by plotting a graph of α_r versus f_o^2, the slope of the graph is the K factor and the y-intercept or d.c. offset is the $d(\gamma_e \cdot N)/dN$ term. Is is clear therefore that the K factor contains no information in relation to the effects of damping which have been shown above to be of considerable relevance. However, the utility of the K factor may be appreciated by noting that it is actually directly proportional to the intrinsic maximum bandwidth given by Eqn (2.19), which implies

$$K = \frac{\sqrt{2}\ 2\pi}{BW_{max}(\text{Hz})} \tag{2.23}$$

Thus, the K factor is actually a fast and powerful method of evaluating the intrinsic maximum bandwidth BW_{max}. In contrast, the strength of the damping experienced by the laser diode and the flatness of the frequency response are manifested by the damping factor ζ defined in the last section.

In addition, as will be discussed in Chapter 3, there exists another functional form of non-linear gain which gives no maximum bandwidth at all and, in that case, the K factor loses its utility. In Chapters 4 and 5, a new relationship

between the K factor and the maximum bandwidth due to the parasitic and carrier transport effects will also be given. Therefore, the K factor will only be a useful parameter if the functional form of the laser diode gain is as given by Eqn (2.9). On the other hand, the damping factor ζ always shows the level of damping no matter what functional form of non-linear gain is used. In this way, the parameter ζ may always be used to identify the existence of the BW_{max} via the criterion given Eqn (2.15). It is these general applicabilities of the parameter ζ which justify its introduction as measure of the dynamical behaviour of the laser diode.

2.7 Device material considerations

The calculations of the previous sections emphasised the optical output power dependence of the maximum bandwidth BW_{max}. In this section, brief consideration is given to the dependence of the maximum bandwidth on a number of device material parameters and Eqn (2.19) highlights the available options. The maximum achievable bandwidth BW_{max} is now expressed as a function of the gain suppression coefficient ϵ, the photon lifetime τ_p, and the gain coefficient g_o (or linear differential gain A_o).

The photon lifetime τ_p can be changed by varying the cavity length, the facet reflectivities or even the grating of the device if it is of distributed feedback (DFB) type. Variation of the linear differential gain A_o can be achieved, for example, by varying the dopant concentrations in bulk semiconductor material or, more relevantly, by selecting a different device material. Of particular interest would be the use of advanced semiconductor materials such as quantum well (QW) [13, 18] or strained-layer quantum well (SLQW) materials [15, 16, 17, 23, 34]

for which higher differential gain than in bulk material are generally obtained due to their step-like band structure. In addition, by employing a number of quantum wells, ie. multi-quantum wells (MQW), grown on top of each other, the differential gain can increase even further compare to that of the single quantum well (SQW) material [13, 14].

However, theory reported in [30], for example, shows that QW devices also have a higher gain suppression ϵ than conventional bulk material whilst SLQW devices exhibit an even higher gain suppression compared with unstrained QWs [32, 36, 37]. The increases in gain suppression for such materials are largely attributable to the quantum confinement [30]. This relatively large material gain suppression in QW/SLQW devices will obviously increase the damping and thus reduces the bandwidth. From a different view point, results in [39] suggest that the carrier transport effects in the commonly used separate confined heterostructure (SCH) QW devices can also limit its maximum achievable bandwidth. A more detailed treatment of the SCH will be given in Chapter 5.

Published values of both the linear differential gain A_o and the gain suppression coefficient ϵ for several kind of devices are given in Tables 2.2 and 2.3. Apparently, the QW and SLQW devices are extremely structural dependent which results in a large deviation of differential gain and gain suppression values as evident in the table. Recent theoretical work [33] has also shown that in QW materials there is a dependence between the gain suppression and the material threshold gain (the gain require to sustain lasing condition) which governs the value of photon lifetime τ_p. However, in the present analysis the two parameters ϵ and τ_p are assumed to be independent of each other.

Material	Structure	A_o
Bulk	FP 1.3μm	$1.2 \sim 2.5 \times 10^{-16} cm^2$ [28]
	FP 1.5μm	$2.7 \times 10^{-16} cm^2$ [27]
	DFB 1.55μm	$2.5 \times 10^{-16} cm^2$ [26]
QW	10 wells DFB 1.55μm	$2.2 \times 10^{-16} cm^2$ [23]
	single well FP 1.0μm	$3 \times 10^{-16} cm^2$ [38]
	single well FP 1.0μm	$1.5 \sim 2 \times$ Bulk[18]
	6 wells DFB 1.55μm	$3.04 \times 10^{-16} cm^2$ [37]
	2 and 4 wells FP 1.5μm	$2.5 \times 10^{-16} cm^2$ [21]
	6 wells FP 1.0μm	$2.4 \times$ Bulk [20]
	5 wells FP 1.3μm	$2.5 \times$ Bulk [19]
	10 wells DFB 1.55μm	$1.4 \times$ Bulk [23]
SLQW	single well FP 1.0μm	$2.5 \sim 7.2 \times 10^{-16} cm^2$ for various carrier density [17]
	6 wells FP 1.0μm	$3.5 \sim 7.4 \times 10^{-16} cm^2$ for various AR coating [37]
	single well FP 1.55μm	$2.7 \sim 5.4 \times 10^{-16} cm^2$ for various cavity length L [35]
	2 and 4 wells FP 1.5μm	$2.5 \times 10^{16} cm^2$ [21]
	10 wells DFB 1.55μm	$3.0 \times$ Bulk[23]

Table 2.2: Typical linear differential gain A_o values for different material types. The values of gain coefficient g_o is obtained by $A_o \times v_g$.

Material	Structure	ϵ
Bulk	FP 1.3μm	$0.9 \times 10^{-17} cm^3$ [1]
	FP 1.3μm	$1.5 \sim 1.9 \times 10^{-17} cm^3$ [24]
	DFB 1.3μm	$2.7 \times 10^{-17} cm^3$ [25]
	DFB 1.55μm	$1.3 \times 10^{-17} cm^3$ [26]
	DFB & FP 1.55μm	$2.4 \times 10^{-17} cm^3$ [29]
QW	6 wells DFB 1.55μm	$2.45 \times 10^{-17} cm^3$ [37]
	4 wells DFB 1.55μm	$4.3 \times 10^{-17} cm^3$ [29]
	7 wells FP 1.3μm	$5.4 \times 10^{-17} cm^3$ [22]
SLQW	single well FP 1.55μm	$3.1 \sim 6.5 \times 10^{-17} cm^3$ for different cavity length L, measured by RIN method [35]
	single well FP 1.0μm	$7.4 \times 10^{-17} cm^3$ measured by RIN method [36]

Table 2.3: Typical gain suppression coefficient ϵ values for different material types.

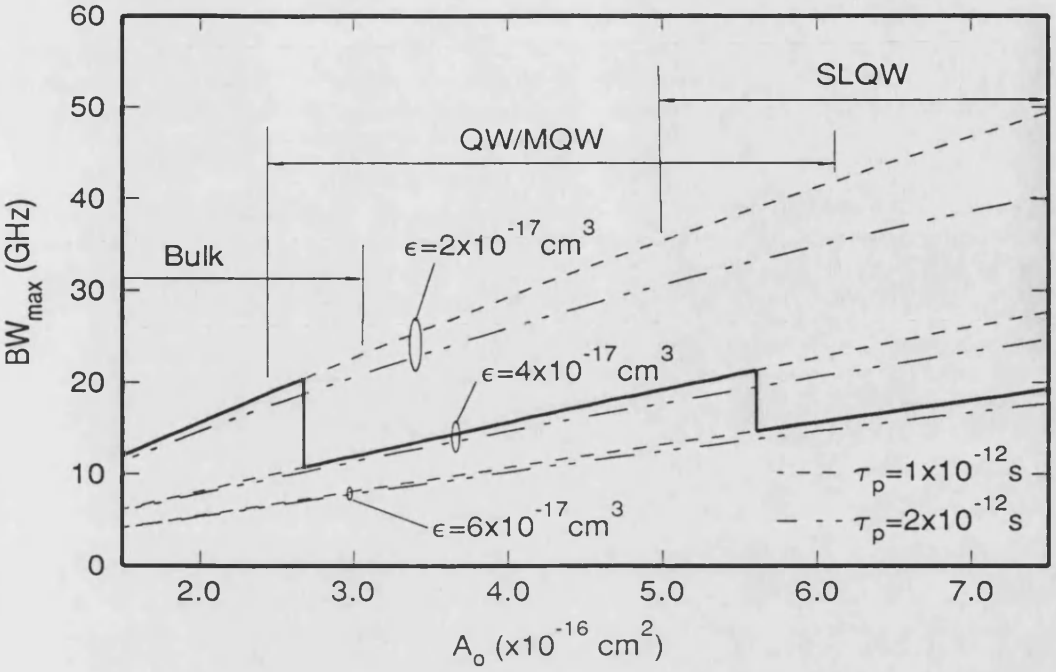

Figure 2.7: *Variation of intrinsic maximum bandwidth BW_{max} with increasing linear differential gain A_o.*

In order to perform a qualitative analysis on different materials, a plot of the maximum BW_{max} with the linear differential gain A_o at different gain suppression ϵ and photon lifetime τ_p is given in Figure 2.7. It is obvious that increase in differential gain A_o can increase the maximum bandwidth BW_{max}, however, the incremental change (slope of curve) is mainly limited by gain suppression and photon lifetime. In other words, high differential gain A_o devices do not always mean high maximum bandwidth BW_{max}, simply because they may have a high gain suppression ϵ.

Assuming the gain suppression rises accordingly with the benefit of increasing the differential gain by switching from bulk to QW/SLQW materials, a trace of the maximum achievable bandwidth BW_{max} is shown by the thick solid line in Figure 2.7. The trace shows that there is virtually no improvement on the maximum bandwidth BW_{max} if the gain suppression ϵ enhances with the high differential gain materials.

One recent example is the SLQW device in [36, 37]. Suppose a SLQW laser having an enhancement in the gain suppression of about three times that of a bulk laser for a given photon lifetime; then due to the linear relationship in Eqn (2.19), it would be required that the SLQW laser have a differential gain of also three times that of the bulk in order to maintain the same maximum achievable bandwidth. Real improvement in bandwidth can only be obtained if the differential gain of the SLQW laser is actually more than three times that of the bulk. This illustrates that both the differential gain and the gain suppression are of equal importance to the maximum bandwidth BW_{max} of a laser diode. Therefore, the effect of gain suppression on the bandwidth should not be overlooked.

A few years ago, the use of p-type doping to increase the differential gain of QW/SLQW material was proposed [40]. By controlling the quasi-Fermi level of the carriers in the QW active region via the use of doping, an enhancement in differential gain can be achieved *with no significant increase in gain suppression.* Theoretical predictions also pointed out that by selectively p-doped the barrier layers between the wells of a MQW device, ie. modulation doped (MD-MQW), the differential gain is expected to increase by 2-2.5 times that of ordinary MQW device and this was then confirmed by experiments [20, 41]. More recently, this implication of higher modulation bandwidth has been realised by experimental devices with p-doping on MQW [43] and strained layer MQW [42] respective-

ly, and a bandwidth of greater than 25 GHz is obtained for the first time in QW/SLQW materials. The MD-MQW device is clearly an example of achieving high modulation bandwidth using material with high differential gain and low gain suppression effect.

2.8 Conclusion

A damping factor ζ has been defined to take into account the effects of relaxation oscillation damping on the frequency response of a laser diode whose dynamics is described the pair of rate equations in Eqn (2.1). The relationship between this damping factor ζ and the intrinsic bandwidth is given in Eqn (2.4).

The criterion in determining the existence of a maximum achievable intrinsic bandwidth BW_{max} has been derived. Using the two-level nonlinear gain model, that is $g_o(N-Ntr)/(1+\epsilon P)$, it can be shown that there always exists a maximum achievable bandwidth BW_{max} due to the effect of damping.

In order to accomplish this maximum bandwidth BW_{max} together with a flat frequency response, ie. an optimal case for a high performance analogue system, the damping factor ζ should be equal to 0.707. It is also confirmed that the maximum bandwidth must equal the undamped frequency, ie. $BW_{max} = \omega_o$, at this optimal point.

Approximated expressions for the maximum intrinsic bandwidth have been found as given in Eqn (2.19). Both the differential gain A_o and the gain suppression ϵ should be carefully considered in order to achieve high bandwidth. It has been shown that high differential gain devices do not always have large bandwidths

due to the high gain suppression which may occur.

References

[1] R. Olshansky, P. Hill and W. Powazinik, "Frequency response of 1.3 μm InGaAsP high speed semiconductor lasers", *IEEE J. Quantum Electron., vol. QE-23, pp. 1410-1418, 1987.*

[2] R. S. Tucker, " High speed modulation of semiconductor lasers", *IEEE J. Lightwave Technol., vol. LT-3, pp. 1180-1192, 1985.*

[3] J. E. Bower, " High speed semiconductor laser design and performance", *Solid State Electron., vol. 30, pp. 1-11, 1987.*

[4] R. Olshansky, "Effect of non-linear gain on the bandwidth of semiconductor lasers", *Electron. Lett., vol. 21, pp. 721-722, 1985.*

[5] G. P. Agrawal,"Gain non-linearities in semiconductor lasers: theory and application to DFB lasers", *IEEE J. Quantum Electron., vol. QE-23, pp.860-868, 1987.*

[6] G. P. Agrawal," Modulation bandwidth of high-power single-mode semiconductor lasers : effects of intraband gain saturation", *Appl. Phys. Lett., vol. 57, pp. 1-3, 1990.*

[7] G. P. Agrawal,"Spectral hole-burning and gain saturation in semiconductor lasers : strong-signal theory", *J. Appl. Phys., vol. 63, pp. 1232-1235, 1988.*

[8] B. N. Gomatam and A. P. DeFonzo,"Theory of hot carrier effects on non-linear gain in GaAs-GaAlAs lasers and Amplifiers", *IEEE J. Quantum Electron., vol. QE-26, pp. 1689-1704, 1990.*

[9] R. S. Tucker and D. J. Pope,"Circuit modelling of effect of diffusion on damping in a narrow-stripe semiconductor laser", *IEEE J. Quantum Electron., vol. QE-19, pp. 1179-1183, 1983.*

[10] Y. C. A. Wong and K. A. Shore,"Diode laser bandwidth optimisation for analogue applications", *IEE Colloquium on Microwave Optoelectronics, London, Nov. 1990.*

[11] Y. C. A. Wong and K. A. Shore,"Influence of non-linear gain on the intrinsic bandwidth of quantum well and strained layer semiconductor lasers", *IEE Proc. J, vol.138, pp. 413-419, 1991*

[12] G. P. Agrawal and T. M. Shen, "Importance of rapid damping of relaxation oscillations for high-performance optical communication systems", *Electron. Lett., vol. 22, pp. 1087-1088, 1990.*

[13] Y. Arakawa and A. Yariv,"Quantum well lasers - Gain, spectra, dynamics", *IEEE Quantum Electron., vol. QE-22, pp. 1887-1899, 1986.*

[14] A. Yariv, "Quantum electronics", *John Wiley & Sons, 1989.*

[15] A. Ghiti, E. P. O'Reilly and A. R. Adams, "Improved dynamics and linewidth enhancement factor in strained-layer lasers", *Electron. Lett.,vol. 25, pp.821-823, 1989.*

[16] J. S. Osinski, P. Grodzinski, Y. Zou, P. D. Dapkus,"Evidence of gain enhancement in long wavelength strained quantum well laser diodes", *Electron. Lett., vol. 27, pp. 469-470, 1991.*

[17] W. Rideout, B. Yu, J. LaCourse, P. K. York, K. J. Beernink and J. J. Coleman,"Measurement of carrier dependence of differential gain, refractive index and linewidth enhancement factor in strained-layer quantum well lasers", *Appl. Phys. Lett., vol 56, pp. 706-708, 1990.*

[18] C. A. Zmudzinski, P. S. Zory, G. G. Lim, L. M. Miller, K. J. Beernink, T. L. Cockerill, J. J. Coleman, C. S. Hong and L. Figueroa,"Differential gain in bulk and quantum well diode lasers", *IEEE Photonics Tech. Lett., vol. 3, pp. 1057-1060, 1991.*

[19] Y. Sasai and M. Ogura, "Spectral linewidth and resonant frequency characteristics of InGaAsP/InP multiquantum well lasers", *J. Quantum Electron., vol. QE-25, pp. 662-667, 1989.*

[20] T. Takahashi, M. Nishioka and Y. Arakawa , " Differential gain of GaAs/AlGaAs quantum well and modulation-doped quantum well lasers ", *Appl. Phys. Lett., vol. 58, pp. 4-6, 1991.*

[21] Y. Zou, J. S. Osinski, P. Grodzinski, P. D. Dapkus, W. Rideout, W. F. Sharfin and F. D. Crawford, "Experimental certification of strain benefits in 1.5μm semiconductor lasers by carrier lifetime and gain measurement", *IEEE Photon. Technol. Lett., vol. 4, pp. 1315-1317, 1992.*

[22] M. Cavelier, J. M. Lourtioz, J. M. Xie, L. Chusseau, B. De Cremoux, M. Krawkowski and D. Rondi, "Gain compression and phase-amplitude coupling in InGaAs quantum well lasers with three, five and seven wells", *Electron. Lett., vol 27, pp. 513-514, 1991.*

[23] Y. Hirayama, M. Morinaga, N. suzuki and M. Nakamura,"Extremely reduced non-linear K-factor in high speed strained layer multiquantum well DFB lasers", *Electron. Lett., vol. 27, pp. 875-876, 1991.*

[24] E. Hemery, L. Chusseau and J. M. Lourtioz, "Dynamic behaviours of semiconductor lasers under strong sinusoidal current modulation : Modelling and experiments at 1.3 μm", *IEEE J. Quantum Electron., vol. QE-26, pp. 633-641, 1990.*

[25] R. J. Lang, H. P. Mayer, H. Schweizer, A. P. Mozer, P. Panknin and W. Elsasser, "Measurement of relaxation resonance, damping and nonlinear gain coefficient from the sidebands in the field spectrum of a 1.3μm InGaAsP distributed feedback laser", *Appl. Phys. Lett., vol. 54, pp. 1845-1847, 1989.*

[26] S. Tsuji, R. S. Vodhanel and M. M. Choy, "Measurements of nonlinear damping factor in 1.5μm distributed feedback lasers", *Appl. Phys. Lett., vol. 54, pp. 90-92, 1989.*

[27] L. D. Westbrook,"Measurements of dG/dN and dn/dN and their dependence on photon energy in $\lambda = 1.5\mu$m InGaAsP laser diodes," *IEE Proc. J, vol. 133, pp. 135-142, 1986.*

[28] G. P. Agrawal and N. K. Dutta, "Long wavelength semiconductor lasers",

[29] K. Uomi, T. Tsuchiya, M. Aoki and N. Chinone,"Oscillation wavelength and laser structure dependence of non-linear damping effect in semiconductor lasers", *Appl. Phys. Lett., vol. 58, pp. 675-677, 1991.*

[30] Y. Arakawa and T. Takahashi, "Effect of nonlinear gain on modulation dynamics in quantum well lasers", *Electron. Lett., vol. 25, pp. 169-170, 1989.*

[31] Y. Arakawa and T. Takahashi, "Nonlinear gain effects in quantum well, quantum well wire and quantum well box lasers", *IEEE J. Quantum Electron., vol QE-27, pp. 1824-1829, 1991.*

[32] A. Ghiti and E. P. O'Reilly, "Non-linear gain effects in strained-layer lasers", *Electron. Lett., vol. 26, pp. 1978-1980, 1990.*

[33] A. Tomita, "Dependence of nonlinear gain effect on threshold gain in semiconductor lasers - an optimization for high-speed modulation", *IEEE Photonics Tech. Lett., vol. 4, pp. 342-344, 1992.*

[34] S. D. Offsey, L. F. Lester, W. J. Schaff and L. F. Eastman,"High-speed modulation of strained-layer InGaAs-GaAs-AlGaAs ridge waveguide multiple quantum well lasers", *Appl. Phys. Lett., vol. 58, pp. 2336-2338, 1991.*

[35] T. C. Wu, S. C. Kan, D Vassilovski, K. Y. Lau, C. E. Zah, B. Pathak and T. P. Lee,"Gain compression in tensile-strained 1.55 μm quantum well lasers operating at first and second quantised states", *Appl. Phys. Lett., vol. 60, pp. 1794-1796, 1992.*

[36] W. F. Sharfin, J. Schlafer, W. Rideout, B. Elman, R. B. Lauer, J. LaCourse and F. D. Crawford,"Anomalously high damping in strained InGaAs/GaAs single quantum well lasers", *Photonics Tech. Lett., vol. 3, pp. 193-195, 1991.*

[37] H. Yasaka, K. Takahata and M. Naganuma,"Measurement of gain saturation coefficients in strained-layer multiple quantum-well distributed feedback lasers", *IEEE J. Quantum Eletron., vol. 28, pp. 1294-1304, 1992.*

[38] W. Rideout, W. F. Sharfin, E. S. Koteles, M. O. Vassell and B. Elman,"Well-barrier burning in quantum well lasers", *IEEE Photonics Tech. Lett., vol. 3, pp. 784-786, 1991.*

[39] R. Nagarajan, T. Fukushima, M. Ishikawa, J. E. Bowers, R. S. Geels and L. A Coldren,"Transport limits in high-speed quantum-well lasers : experiment and theory", *IEEE Photonics Tech. Lett., vol. 4, pp. 121-123, 1992.*

[40] K. Uomi, "Modulation-doped multi-quantum well (MD-MQW) lasers. I. Theory", *Japanese J. Appl. Phys., vol. 29, pp. 81-87, 1990.*

[41] K. Uomi, T. Mishima and N. Chinone, "Modulation-doped multi-quantum well (MD-MQW) lasers. II. Experiment", *Japanese J. Appl. Phys. vol. 29, pp. 88-94, 1990.*

[42] P.A. Morton, R.A. Logan, T. Tanbun-Ek, P.F.Sciortino Jr., A.M. Sergent, R.K. Montgomery and B.T. Lee, "25 GHz bandwidth 1.55 μm GaInAsP p-doped strained multiquantum-well lasers", *Electron Lett., vol. 28, pp. 2156-2157, 1992.*

[43] S. Weisser, J.D. Ralston, E.C. Larkins, I. Esquivias, P.J. Tasker, J. Fleissner and J. Rosenzweig, "Efficient high-speed direct modulation in p-doped $In_{0.35}Ga_{0.65}As/GaAs$ multiquantum well lasers", *Electron. Lett., vol. 28, pp. 2141-2143, 1992.*

Chapter 3

Non-linear Gain models

3.1 Introduction

As mentioned in Chapter 2, an important parameter, which can affect the damping rate α_r and indirectly controls the rate of change of $Y(\zeta)$ and ω_o as the optical output power increases, is the optical gain $G(N, P)$. Several forms of functional dependence of G on the photon density P and the carrier density N have been proposed in the literature in recent years. Two common functional forms for G which have been used are :

$$G(N,\ P) \ = \ g_o(N - N_{tr})(1 - \epsilon P) \tag{3.1}$$

$$G(N,\ P) \ = \ \frac{g_o(N - N_{tr})}{1 + \epsilon P} \tag{3.2}$$

where g_o is the gain coefficient or differential gain; N_{tr} is the transparency carrier density; and ϵ is the gain suppression coefficient. Eqn (3.1) is always used as a simple model related to small optical power, ie. $\epsilon P \ll 1$, since clearly the model actually breaks down when $\epsilon P \geq 1$. In dealing with the high-power regime of semiconductor laser operation, the two-level model [2] in Eqn (3.2) can be used. In fact, Eqn (3.1) is an approximation of Eqn (3.2) when ϵP is small.

More recently, G. P. Agrawal has derived another form of non-linear gain model [3, 4, 5],

$$G(N,\ P) = \frac{g_o(N - N_{tr})}{\sqrt{1 + \epsilon P}} \tag{3.3}$$

This 'non-perturbative' non-linear gain model is obtained by considering the intraband relaxation effects in high power lasers which have been neglected in the 'two-level' model. Both non-linear gain models (Eqns (3.2) and (3.3)), can be expected to have different effects on the damping rate α_r and undamped frequency ω_o of a laser diode and hence on the damping factor ζ and bandwidth BW as they are related by Eqn (2.5).

In this chapter, the implications on the dynamic response of a laser diode for the two different non-linear gain models (Eqn (3.2) and Eqn (3.3)) are compared theoretically. Based on small signal analysis of the single mode rate equations model, we obtain both numerical and analytical results for the α_r, ω_o and ζ of the two non-linear gain models. By utilising the maximum bandwidth criterion derived in Chapter 2, the effect of the two non-linear gain models on the bandwidth are compared. In addition, a comparison between the results of the present approach and those predicted by Agrawal for the 'non-perturbative' non-linear gain model is given. Finally, some consideration will be given to the possibilities of experimentally distinguishing the two non-linear gain models.

3.2 The non-perturbative model

Substituting the functional form of the non-perturbative model Eqn (3.3) into Eqns (2.6)-(2.8), it is found [1] that,

$$\alpha_r \approx \frac{1}{4}\left(2+\frac{\epsilon}{g_o\tau_p}\right)\frac{g_o}{\epsilon}\frac{\epsilon P}{(1+\epsilon P)} \tag{3.4}$$

$$\omega_o{}^2 \approx \frac{g_o}{\tau_p\epsilon}\frac{\epsilon P}{\sqrt{1+\epsilon P}} \tag{3.5}$$

$$\zeta \approx \frac{1}{4}\frac{1}{\sqrt{\frac{\epsilon}{g_o\tau_p}}}\left(2+\frac{\epsilon}{g_o\tau_p}\right)\sqrt{\frac{\epsilon P}{(1+\epsilon P)^{3/2}}} \tag{3.6}$$

Similarly, the results for the damping rate α_r, undamped frequency ω_o and damping factor ϵ of the two-level model have been given in Eqns (2.10)-(2.12).

Comparing Eqns (3.4) and (2.10), it can be observed that the growth rate of α_r versus ϵP (or optical output) produced by the two-level non-linear model is twice that obtained by the non-perturbative model as evident by numerical results shown in Figure 3.1. This shows that the two-level model implies a comparatively higher damping than that of the non-perturbative model. In Figure 3.2, numerical results also show that the two-level model is subject to a higher suppression in undamped frequency ω_o than of the non-perturbative model as $\sqrt{\epsilon P}$ (or square root intensity) increases which is obvious when viewing the denominators of the approximated expression in Eqns (3.5) and (2.11). All the parameter values used in the numerical calculations are based on Table 2.1.

Figure 3.3 displays the numerical calculations of the damping factor ζ against $\sqrt{\epsilon P}$ for the two different non-linear gain models. Within the practical regime of ζ (ie. $0 \leq \zeta \leq 1$), it is clear that the ζ of the non-perturbative model has a relatively smaller growth rate (approximately half that of the two-level model)

and tends to saturate at a certain optical output power.

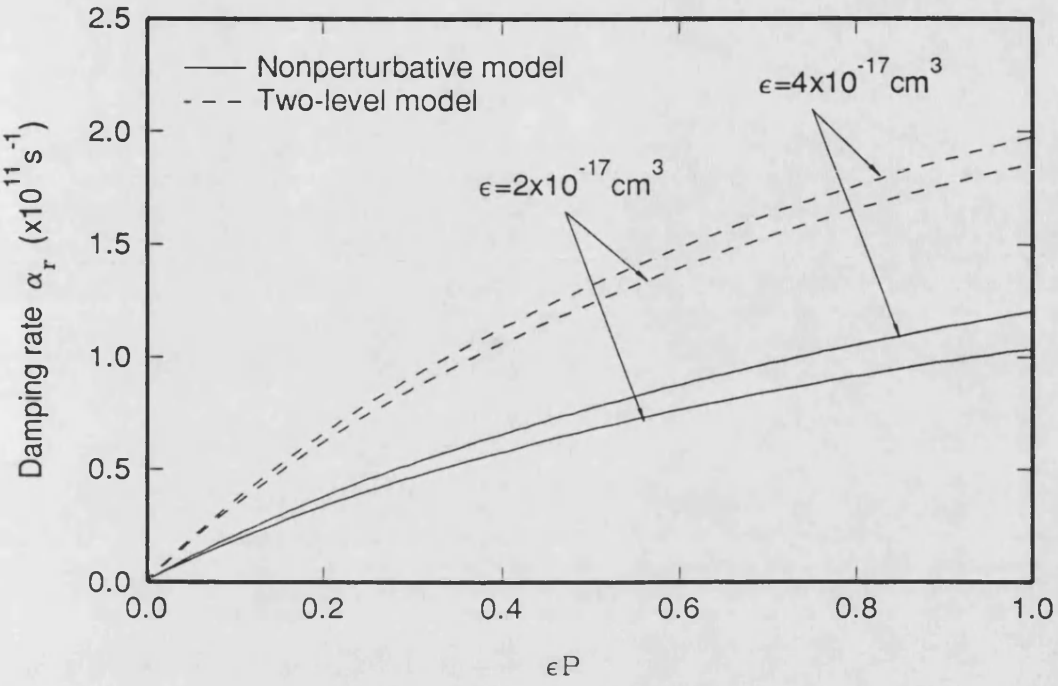

Figure 3.1: *Variation of the damping rate α_r against ϵP, for the two different forms of non-linear gain models.*

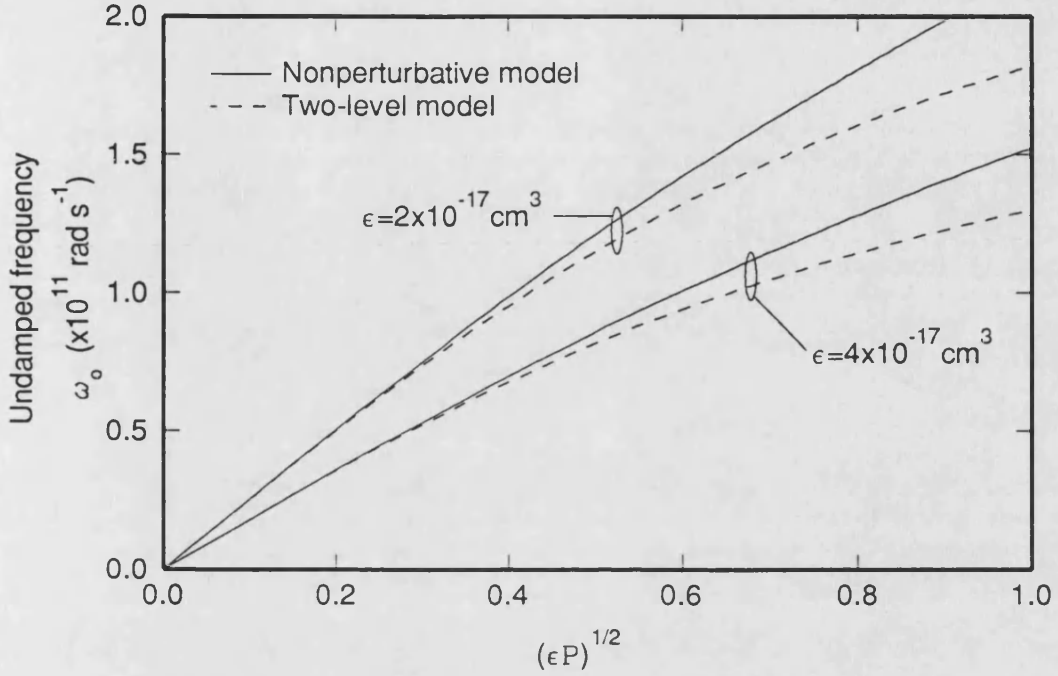

Figure 3.2: *Variation of the undamped frequency ω_o against $(\epsilon P)^{1/2}$, for the two different forms of non-linear gain models.*

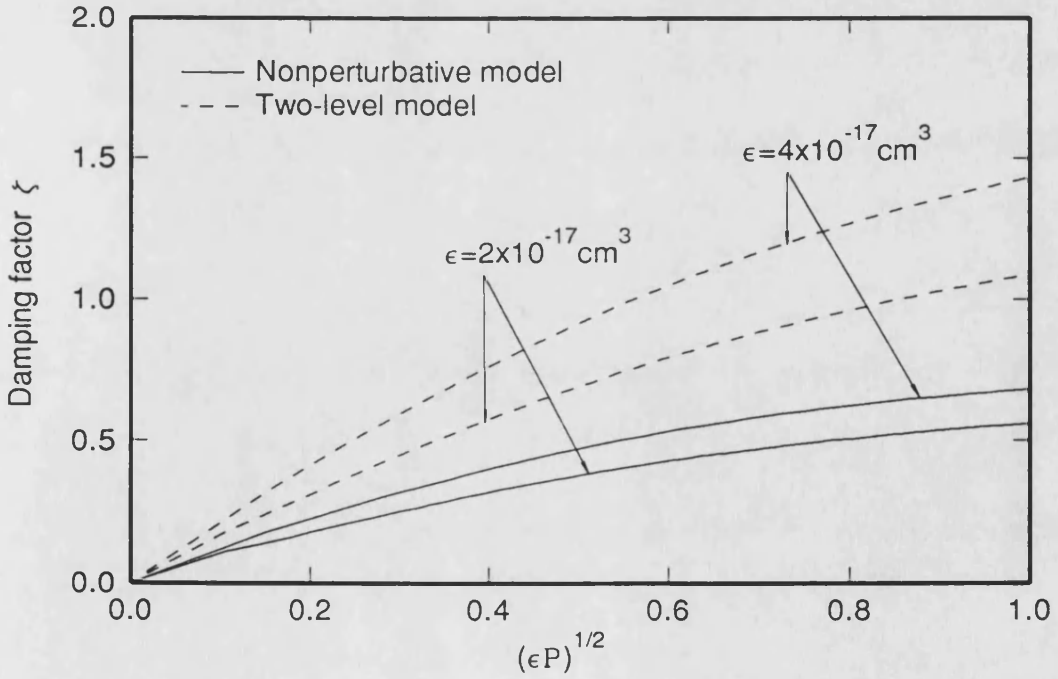

Figure 3.3: *Variation of the damping factor ζ against $(\epsilon P)^{1/2}$, for the two different forms of non-linear gain models.*

Notice that for low power operation, the prediction of the two models are roughly the same provided one takes a double ϵ value for the non-perturbative model. However, in the following discussions the emphasis is given on the maximum achievable bandwidth and hence implies high power operation.

By differentiating Eqn (3.6) w.r.t. ϵP, it is found that the ζ of the non-perturbative model always reaches its maximum at around $\epsilon P \approx 2$ region with a value of :

$$\zeta_{max} = 0.155 \frac{\left(2 + \frac{\epsilon}{g_o \tau_p}\right)}{\sqrt{\frac{\epsilon}{g_o \tau_p}}} \tag{3.7}$$

In fact, the damping factor ζ of the non-perturbative model begins to saturate fairly early at $\epsilon P \approx 0.5$ as illustrate in Figure 3.3. It is this saturation effect and the reduced growth rate of ζ of the non-perturbative model which causes a dramatic change in the intrinsic bandwidth BW when compared with that of the two-level model.

3.3 Bandwidth suppression and maximum bandwidth

The term *bandwidth suppression* means that at a certain optical output power, a *reduction* occurs in the rate of increase of bandwidth BW with increasing optical power. This happens due to the increase in damping effect which accompanies an increase of optical output power as explained in Section 2.3. If the damping effect in the system is strong enough, then the bandwidth versus intensity may reach a maximum – the *maximum achievable bandwidth* BW_{max}.

It has already been shown in Section 2.4 that the criterion for the maximum bandwidth BW_{max} to occur is:

$$\frac{d\zeta}{d\omega_o}\omega_o \geq 0.707\zeta \tag{3.8}$$

Checking this criterion for the two different non-linear gain models, the following results can be found :

3.3.1 Two-level model

$$\begin{aligned} \frac{d\zeta}{d\omega_o}\omega_o &= \zeta \\ &> 0.707\zeta \end{aligned} \tag{3.9}$$

This indicates that a maximum bandwidth BW_{max} always exists for this functional form of gain non-linearity. Further calculations in Section 2.5 shows that $\zeta = 0.707$ whenever the BW_{max} occurs while

$$BW_{max}\ (\text{Hz}) = \frac{\sqrt{2}g_o}{2\pi(\epsilon + g_o\tau_p)} \tag{3.10}$$

The implications of this equation has already been given in detail in Section 2.7. In brief, an increase in the gain coefficient g_o, say by using quantum well (QW) material, will usually achieve a higher maximum bandwidth BW_{max} provided the gain suppression coefficient ϵ remains unchanged or small [1].

Substituting $\zeta = 0.707$ back into Eqn (2.12), we find that at $BW = BW_{max}$

$$\epsilon P = \frac{2\left(\frac{\epsilon}{g_o\tau_p}\right)}{1 + \left(\frac{\epsilon}{g_o\tau_p}\right)^2} \tag{3.11}$$

which indicates that ϵP has a maximum value of unity at $\frac{\epsilon}{g_o \tau_p} = 1$. Therefore the maximum bandwidth BW_{max}, will always occur within the range of $0 < \epsilon P < 1$ and is purely depended on the value of $\frac{\epsilon}{g_o \tau_p}$. The typical value of $\frac{\epsilon}{g_o \tau_p}$ lies between 1 to 20 from bulk to SLQW materials as implied in Tables 2.2 and 2.3.

3.3.2 Non-perturbative model

$$\frac{d\zeta}{d\omega_o}\omega_o = \frac{2-\epsilon P}{2+\epsilon P}\zeta \tag{3.12}$$

which suggests that the BW_{max} may or may not exists, since $\frac{2-\epsilon P}{2+\epsilon P}\zeta$ can be bigger or smaller than 0.707 ζ.

However, it is certain that if there exists a local maximum or turning point in the bandwidth versus optical intensity then, (in order to meet the criterion in Eqn (2.15)) ϵP must fulfill the condition : $\frac{2-\epsilon P}{2+\epsilon P}\zeta \geq 0.707\zeta$, that is,

$$0 < \epsilon P \leq 0.34 \tag{3.13}$$

In fact, the existence of the local maximum for this non-perturbative non-linear gain model is also depend on the parameter $\frac{\epsilon}{g_o \tau_p}$. This can be visualised by manipulating Eqn (3.6) and expressing ϵP as a cubic equation of $\frac{\epsilon}{g_o \tau_p}$. For typical parameter values, such a local maximum point seldom exists (since the existence of the local maximum requires $\frac{\epsilon}{g_o \tau_p} > 60$). In addition, the K factor therefore, loses it utility as a measurement of maximum bandwidth and becomes a power dependent parameter.

Figure 3.4 shows the numerically calculated bandwidth BW versus $\sqrt{\epsilon P}$ using the two non-linear gain models. For the two-level model, the bandwidth always

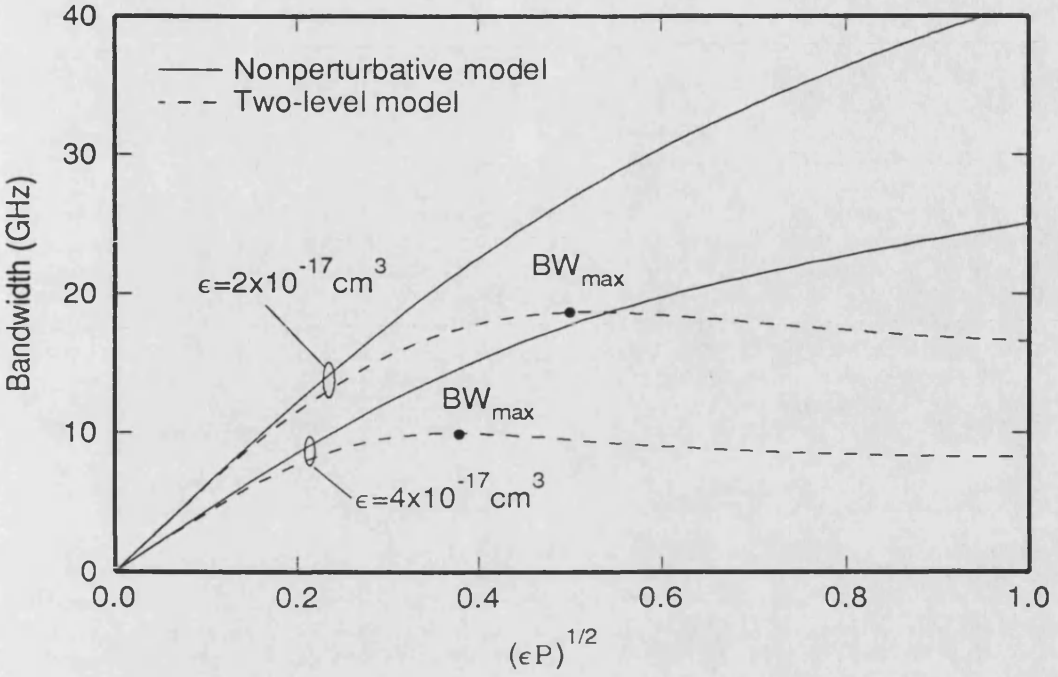

Figure 3.4: *Variation of the −3 dB intrinsic bandwidth BW against* $(\epsilon P)^{1/2}$*, for the two different non-linear gain models.*

experiences a *maximum bandwidth* at $\zeta = 0.707$ as that given in Section 2.5. In brief, when the intensity increases, ω_o begins to rise linearly while $Y(\zeta)$ decreases. As intensity increase further, the non-linear gain term $(1 + \epsilon P)$ in the denominator of Eqn (2.11) starts to cause ω_o to increase sub-linearly; and at the same time $Y(\zeta)$ decreases continuously. Hence a trade off between terms exists, and the damping effect is so strong that it actually causes a maximum point in the bandwidth versus intensity. Such a maximum bandwidth BW_{max} is also the optimal bandwidth of the laser diode for the use in an high performance analogue system.

On the other hand, for the non-perturbative model, *bandwidth suppression* exists which causes the bandwidth to increase sub-linearly at high intensity but no maximum point is observed. This is due to the fact that the growth rate of ζ is reduced when compared to the two-level model. Thus $Y(\zeta)$ decreases relatively

slowly and even become nearly constant as ζ starts to saturate at $\epsilon P \approx 0.5$ and reaches its maximum value at $\zeta = 2.0$. Furthermore, the sub-linear increase effect in ω_o is also comparatively weak (since the denominator is $\sqrt{1+\epsilon P}$ rather than $(1+\epsilon P)$ in the previous case, refer to Eqns (2.11) and (3.5) respectively). Consequently, the total bandwidth suppression effect is far less than that obtained from the two-level non-linear gain model and therefore a maximum point in the bandwidth versus ϵP is rarely seen for typical parameter values.

It is constructive to compare the results in this work to those obtained by Agrawal for the non-perturbative non-linear gain model. From references [4, 5], the analytical results obtained by Agrawal are (in the notation used in this work) :

$$\alpha_r = \frac{1}{4}\frac{1}{\tau_p}\frac{x}{(1+\epsilon P)^{3/2}} \tag{3.14}$$

$$\omega_o{}^2 = \frac{g_o}{\tau_p \epsilon}\left(1+\frac{x}{2}\right)\frac{x}{(1+\epsilon P)^2} \tag{3.15}$$

The comparison between these two sets of results are shown graphically in Figures 3.5-3.7 for α_r, ω_o and BW respectively. The reasons for the big discrepancy in the two sets of results can be explained as follows:

- In references [4, 5], Agrawal has implicitly assumed $\omega_o \approx \omega_r$ where ω_r is the relaxation frequency and is given by $\omega_r = \sqrt{\omega_o^2 - \alpha_r^2}$.
- A significant term, $(g_o \epsilon P)/(2\epsilon\sqrt{1+\epsilon P})$ in Eqn (3.5) has been omitted by Agrawal during the approximation procedure.
- An assumption that $\tau_p = 1/\Gamma g_o(N - N_{tr})$ has been made by Agrawal whereas $\tau_p = 1/\Gamma G = \sqrt{1+\epsilon P}/\Gamma g_o(N - N_{tr})$ should be utilised.

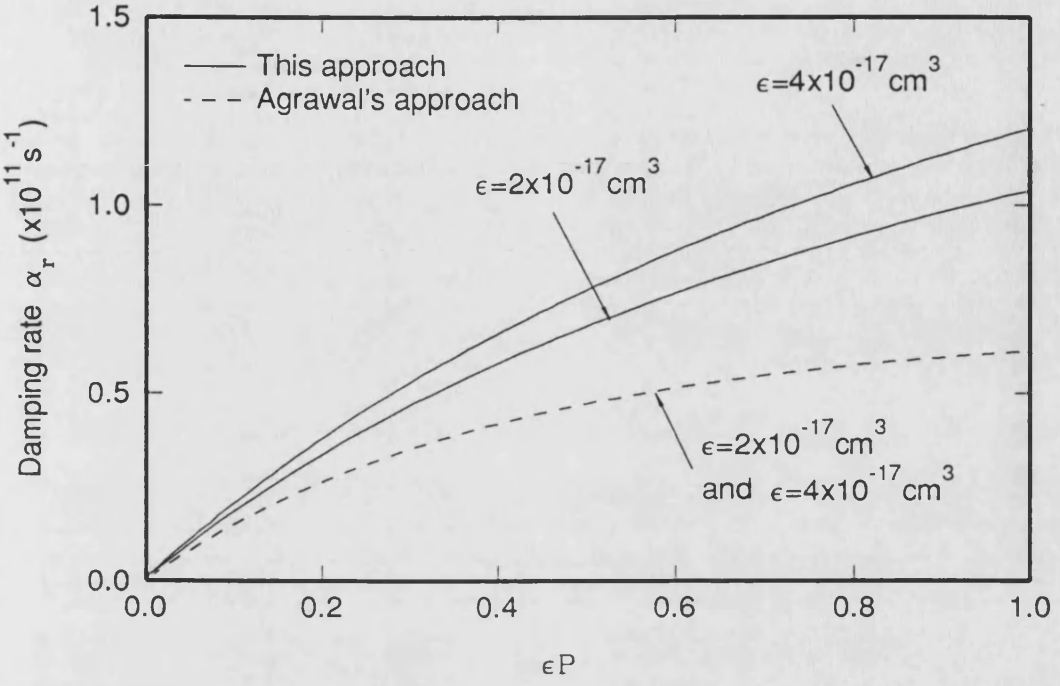

Figure 3.5: *Comparison of the results obtained by the two different approaches on the damping rate, α_r, for the 'non-perturbative' non-linear gain model.*

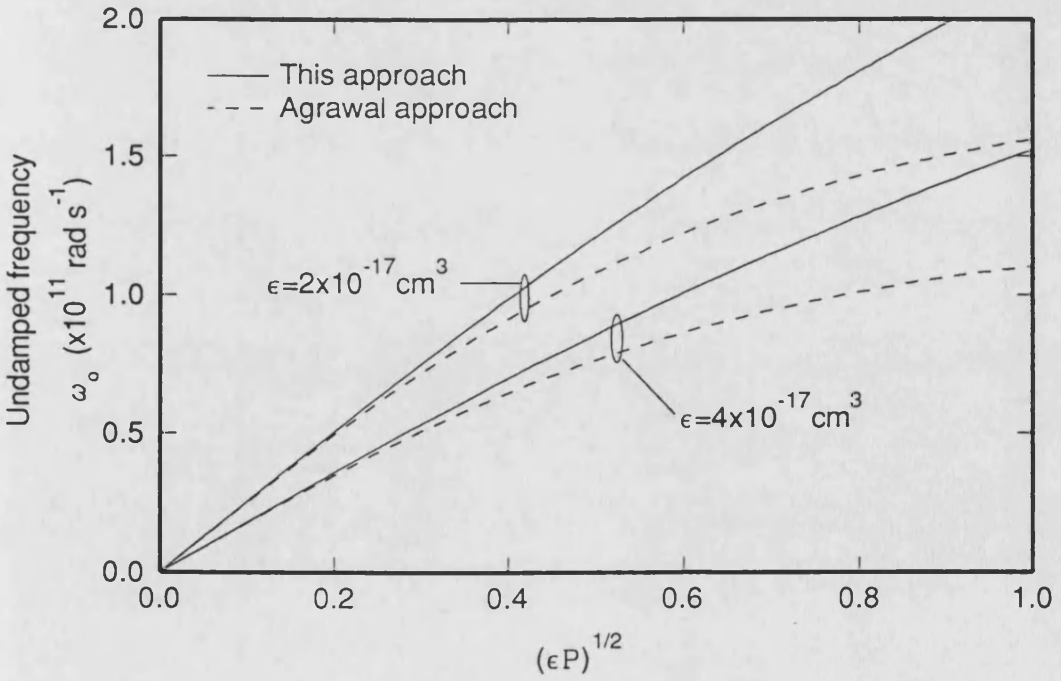

Figure 3.6: *Comparison of the results obtained by the two different approaches on the undamped frequency, ω_o, for the 'non-perturbative' non-linear gain model.*

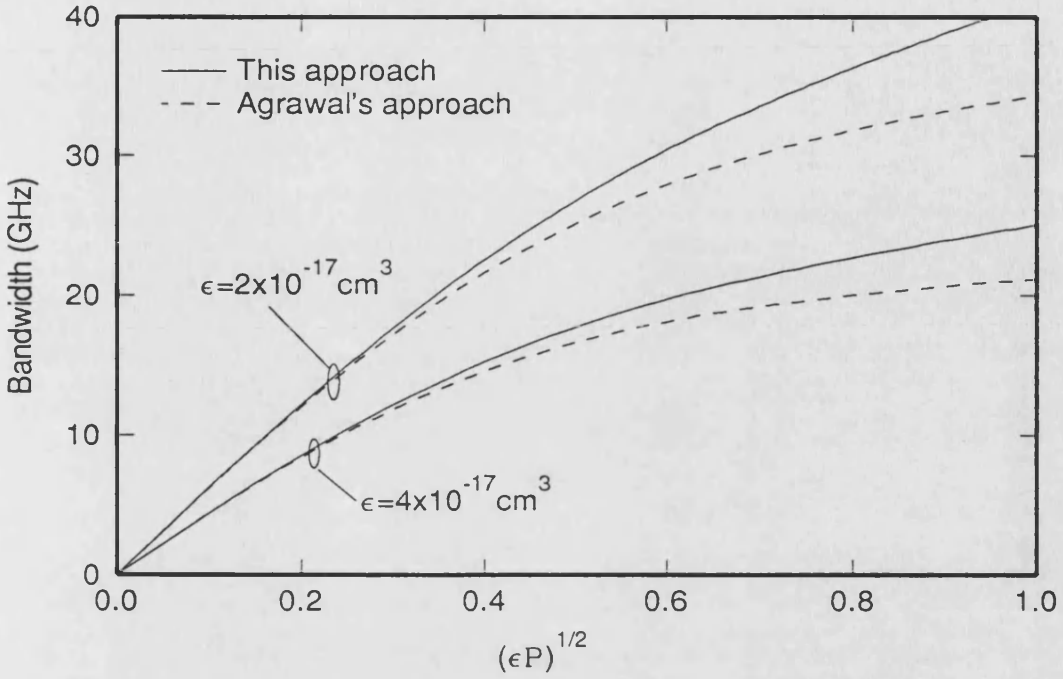

Figure 3.7: *Comparison of the results obtained by the two different approaches on the −3 dB intrinsic bandwidth, BW, for the 'non-perturbative' non-linear gain model.*

3.4 Practical considerations

As mentioned previously, a large intrinsic bandwidth BW is normally required for the laser diode deployed in a high performance analogue optical system. It has been shown that no matter which form of non-linear gain model is being used, bandwidth suppression always takes place. The most striking feature of the non-perturbative model is that there is virtually no limitation imposed on the intrinsic bandwidth as optical power increases; on the contrary, the bandwidth predicted by the two-level model always experiences a maximum point within $0 < \epsilon P < 1$.

Based on this difference in behaviour, one can determine the best described non-linear gain model of a particular laser diode by driving it up to high enough power, say $\epsilon P \approx 1$, to obtain a trace of the bandwidth BW versus square root

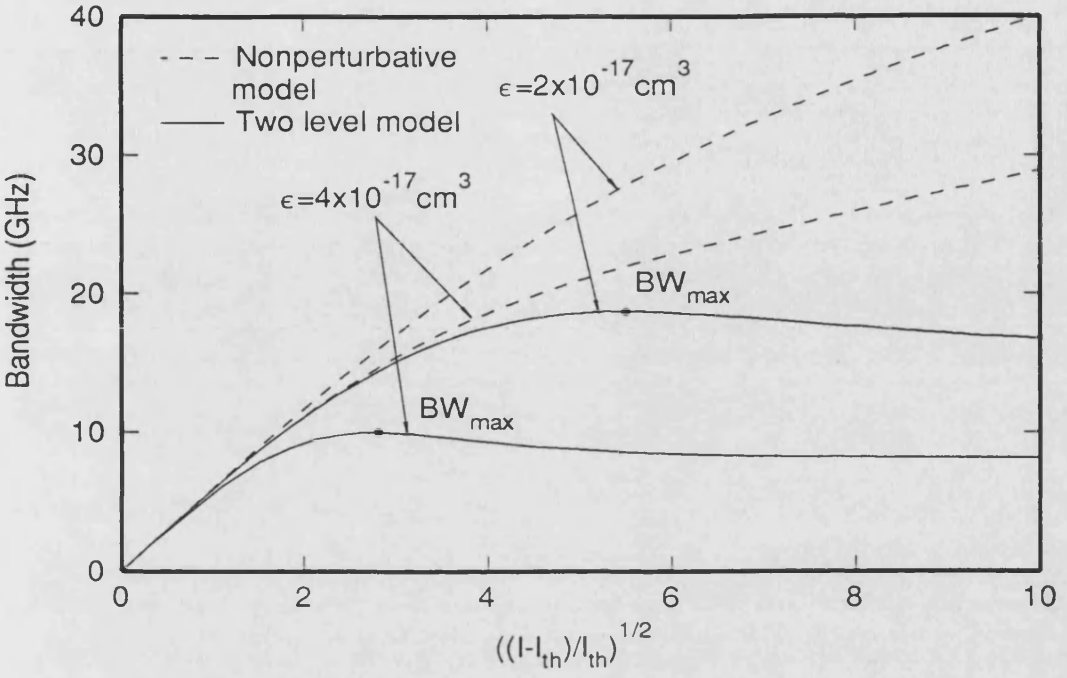

Figure 3.8: *Illustrate the differences in the intrinsic bandwidth causes by the two different forms of non-linear gain models at a practical range of intensity.*

output optical power or simply the normalised bias current $\sqrt{(I - I_{th})/I_{th}}$. If a maximum point exists then the two-level model would appear to be appropriate to describe the non-linear gain effect of the laser diode under test; otherwise, if a reasonably linear relationship persists between the bandwidth BW and the square root optical power, then the non-perturbative model could be a good alternative. This is demonstrated by the simulated results shown in Figure 3.8.

The K factor will be another parameter to observe in order to check whether the non-perturbative model should be used in place of the two-level model for an experiment. If the K factor measured is showing a moderate amount of or even strong power dependence, then it is suggested that one should switch from the two-level model to the non-perturbative model.

There is at present very little experimental work available which permits a test of

the model. Thermal effects restrict the nominal output power of a typical laser diode to $0 < \epsilon P < 0.3$, thus a specially designed high power laser diode would be required for the experimental observation. However, Agrawal [5] has suggested that the data obtained in an experiment described in [6] for high power DFB lasers actually support the use of non-perturbative non-linear gain model.

3.5 Conclusion

The effect of two different non-linear models on both the damping and bandwidth have been compared. The non-perturbative model does not cause any maximum bandwidth BW_{max} in the bandwidth versus intensity, in contrast the two-level model always induces a BW_{max} within $0 < \epsilon P < 1$. Such an unlimiting growth of bandwidth BW with increasing optical power in the non-perturbative model is due to the saturation effect of the damping factor ζ in this model. This could be an advantage to optical communication system like SCM which seek to exploit the multi-GHz bandwidth of a laser diode.

References

[1] Y.C.A. Wong and K.A. Shore, "Analysis of two forms of gain non-linearities on the dynamic response of a laser diode for high frequency applications", *IEE Proc. J, vol. 138, pp. 413-419, 1991.*

[2] J.E. Bowers, B.R. Hemenway, A.H. Gnauck and D.P. Wilt, "High-speed constricted-mesa lasers", *IEEE J. Quantum Electron., vol. QE-22, pp. 833-844, 1986.*

[3] G.P. Agrawal, "Effect of gain non-linearities on the dynamic response of single mode semiconductor laser", *IEEE Photonics Lett., vol. 1, pp. 419-421, 1989.*

[4] G.P. Agrawal, "Modulation bandwidth of high power single-mode semiconductor lasers: Effect of intraband gain saturation", *Appl. Phys. Lett., vol. 57, pp. 1-3, 1990.*

[5] G.P. Agrawal,"Effect of gain and index non-linearities on single-mode dynamics in semiconductor lasers", *IEEE J. Quantum Electron., vol. QE-26, pp. 1901-1909, 1990.*

[6] K. Kamite, H. Sudo, M. Yano, H. Ishikawa and H. Imai, "Ultra-high speed InGaAsP/InP DFB lasers emitting at 1.3 μm wavelength", *IEEE J. Quantum Electron., vol. QE-23, pp. 1054-1058, 1987.*

Chapter 4

Package and Chip Parasitics

4.1 Introduction

In the previous two chapters, theoretical presentation emphasis has been given to the intrinsic non-linear effects on the dynamics of laser diode. It has been shown that the intrinsic maximum bandwidth of a laser diode predicted by the rate equations is generally high, say 10-20 GHz, even under the influence of non-linear gain damping effect. In practice, diode lasers are limited to a relatively low bandwidth operation due to various extrinsic effects, most importantly,

(i) package/chip parasitics [1, 2, 3] and;

(ii) carrier transport effects in most quantum well (QW) devices [8].

The effects of the parasitics on the modulation response of a laser diode will be considered in this chapter, whilst the limitation on the bandwidth caused by the the carrier transport across a separated confinement heterostructure (SCH) of most QW lasers will be discussed in the next chapter.

In order to investigate the parasitics effects, a simple electrical equivalent circuit for the laser diode is established in Section 4.2 which basically consists of three cascaded stages with their own transfer function representation. They are :

- the package parasitics - generally include the mount capacitance and bond-wire inductance;
- the chip parasitics - normally the stray capacitance and resistance associated with the semiconductor material surrounding the active region; and
- the intrinsic laser with dynamics governed by the pair of rate equations.

Usually the package parasitics are of negligible effect on the modulation bandwidth of the laser diode when compared with the chip parasitics which consists of a simple RC stage.

By applying small signal analysis, the intrinsic diode can be represented by a second-order (low-pass filter) transfer function as given in Appendix A. Together with the chip parasitics RC stage, a practical laser diode can therefore be viewed as a third-order system and a general theoretical approach to such a system will be given in Section 4.3. Owing to the highly structural dependent nature of the parasitics, the discussion will be limited to ridge waveguide lasers which are supplied by Northern Telecom, Paignton. An experiment for measuring the chip parasitics and device parameters, for a group of $1.3\mu m$ ridge-waveguide lasers will be presented in Section 4.4.

4.2 Overall transfer function

A general small signal electrical equivalent circuit for a laser diode is given in Figure 4.1. This circuit has been proven to be reasonably adequate in describing most types of lasers [1, 4, 5], for example, ridge waveguide and buried heterostructure. This equivalent circuit is composed of three cascaded stages with the following transfer functions :

(i) the package parasitics, $F_{pack}(\omega) = \delta i_p/\delta i_{src}$ or $F_{pack+R_{src}}(\omega) = \delta i_p/\delta i_{src}$ for a non-ideal current drive with input impedance R_{src};

(ii) the chip parasitics, $F_{chip}(\omega) = \delta i/\delta i_p$; and

(iii) the intrinsic laser diode, $F_{int}(\omega) = \delta p/\delta i$.

where the corresponding small signal current components $\delta i_{src}, \delta i_p$ and δi are denoted in Figure 4.1. The overall laser diode frequency response (transfer function) defined as $F_T(\omega) = \delta p/\delta i_{src}$, can be given by,

$$\begin{aligned} F_T(\omega) &= \frac{\delta i_p}{\delta i_{src}} \times \frac{\delta i}{\delta i_p} \times \frac{\delta p}{\delta i} \\ &= F_{pack+R_{src}}(\omega) \times F_{chip}(\omega) \times F_{int}(\omega) \end{aligned} \tag{4.1}$$

The expressions for the transfer function of individual stage are given in the following subsections. These results are obtained based on the assumption that the input resistance of the intrinsic laser is very small and can therefore be viewed as *short circuit* with negligible error in calculating the overall bandwidth due to parasitic roll-off effect.

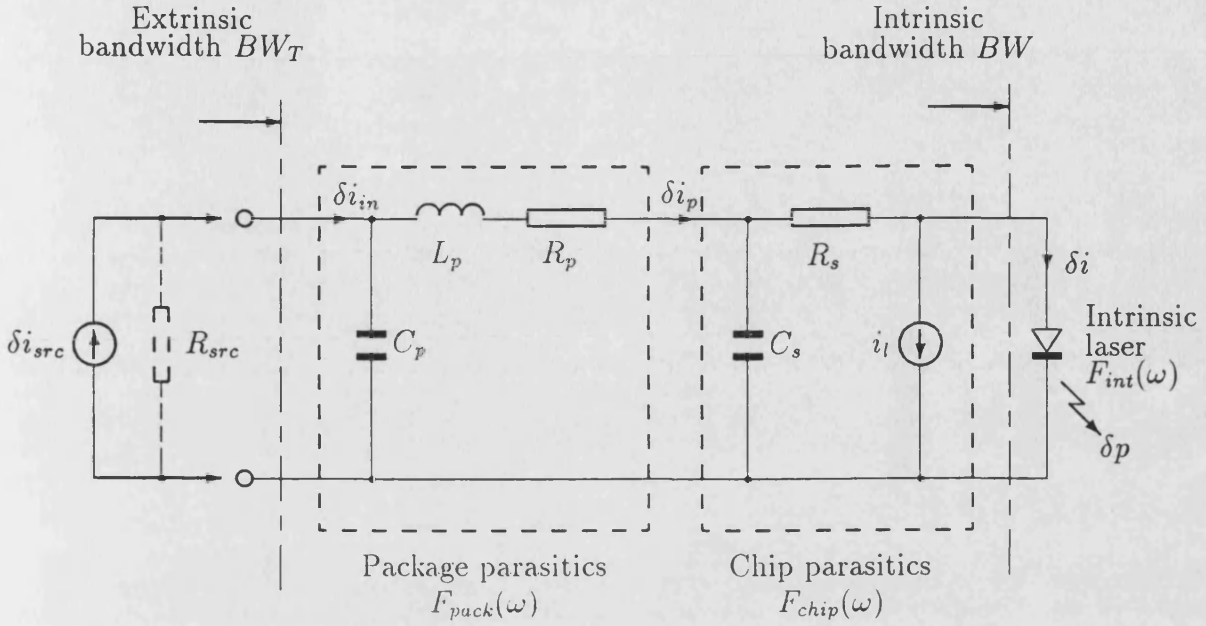

Figure 4.1: *Electrical equivalent circuit model of laser diode*

4.2.1 Package parasitics

The package parasitics are made up of the resistance R_p and inductance L_p of the bond-wire and the capacitance C_p of the metal stud on which the laser chip is mounted. For an ideal current source, ie. $\delta i_{src} = \delta i_{in}$, the transfer function may be expressed as

$$F_{pack}(\omega) = \frac{\delta i_p}{\delta i_{in}} = \frac{1}{1 + j\omega C_p(j\omega L_p + R_p + Z_s)}$$

where $Z_s = R_s/(1 + j\omega R_s C_s)$ is the loading from the chip parasitics stage. The typical values for the parameters are : $R_p \approx 1\Omega, L_p \approx$ 0.1-0.8nH, $C_p \approx$ 0.1-0.3pF, $R_s \approx$ 5-15Ω and $C_s \approx$ 5-20pF. Due to the relatively small values of $C_p < 0.2pF$ and $L_p < 0.2nH$, the frequency bandwidth of this $F_{pack}(\omega)$ stage is very high – about 35 GHz, for the ideal input current source. However, a sharp resonance appears at about 25 GHz because of C_p and L_p. In practice, when a non-ideal current source of input impedance 50 Ω is connected to the laser diode via a series matching resistor of 50 Ω giving a $R_{src} = 100\Omega$, the corresponding

package parasitics transfer function lumping R_{src} can be rewritten as,

$$F_{pack+R_{src}}(\omega) = \frac{\delta i_p}{\delta i_{src}} = \frac{1}{1+(j\omega C_p + \frac{1}{R_{src}})(j\omega L_p + R_p + Z_s)} \quad (4.2)$$

With $R_{src} = 100\Omega$, the resonance peak due to C_pL_p can be damped out substantially and this leaves a reasonably flat response upto a frequency of 20 GHz provided small L_p and C_p values are maintained [2]. On the other hand, if the bond wire inductance is large, say $L_p \geq 1nH$, then an early roll-off of about 6-7 GHz may be observed.

In other words, the frequency response of $F_{pack+R_{src}}(\omega)$ is dependent on the input impedance of the current source. For a conventional microwave instrumentation with equivalent $R_{src} = 100\Omega$ and small $L_p \approx 0.2nH$, the package parasitics stage lumped with R_{src} has virtually no effect on the overall bandwidth (ie. $F_{pack+R_{src}}(\omega) \approx 1$ for frequency upto 20 GHz) when compared to the dominant RC roll-off of chip parasitics [1, 5]. The experimental works and calculations related to the overall bandwidth of a laser diode in the following sections are therefore based on the above assumption since the measurements are for a frequency of about 7 GHz.

4.2.2 Chip parasitics

The chip parasitics which consist of the total resistance R_s and the shunt capacitance C_s of the semiconducting material surround the active region, can be described by a low-pass filter response, that is,

$$F_{chip}(\omega) = \frac{\delta i}{\delta i_p} = \frac{1}{1+j\omega R_s C_s} \quad (4.3)$$

For example, in a ridge waveguide laser diode, for which a typical structure is given in Figure 4.2, the resistance R_s is the total series resistance of the ridge

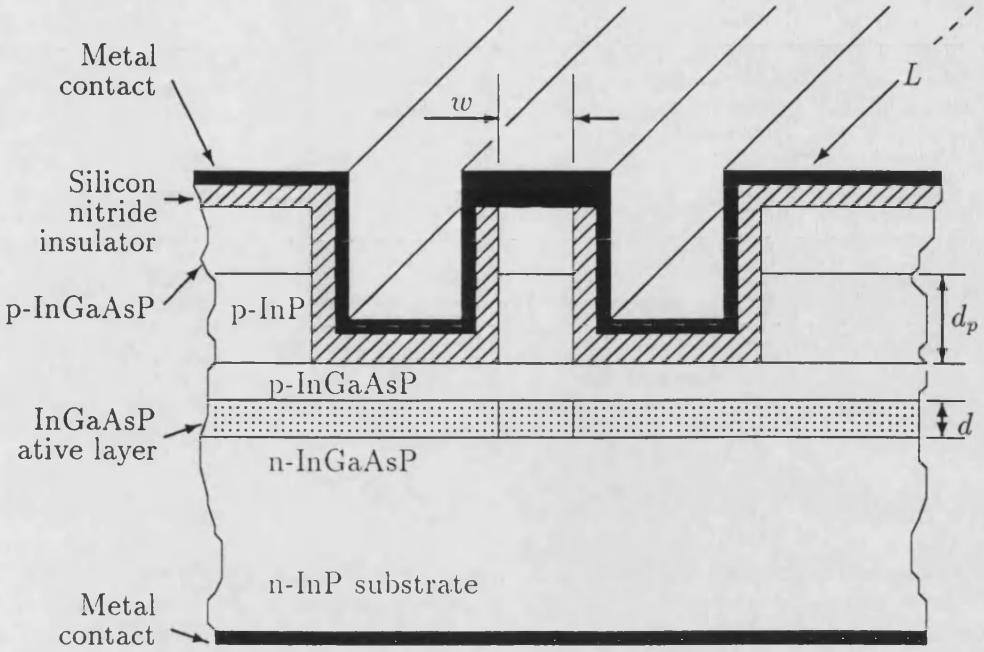

Figure 4.2: *Cross section a ridge waveguide laser*

and the substrate under the the active region; and the capacitance C_s is mainly associated with the silicon nitride insulator layer in the device. The typical R_sC_s product of, say a ridge waveguide laser, is 30-65 *ps* which corresponds to a roll-off frequency ($\frac{1}{2\pi R_sC_s}$) of 3-7 GHz for this stage. Consequently, the chip parasitics are usually the dominant effects on the overall laser diode bandwidth.

It is noteworthy that the current source i_l represents leakage current paths that bypass the active region. This leakage current is found to be very small for a ridge waveguide laser, but can be significant in some buried heterostructure devices [6].

4.2.3 Intrinsic laser diode

The active region which represents an intrinsic laser diode, can be specified by a second order transfer function obtained by applying small signal analysis to the pair of rate equations Eqn (2.1). The transfer function is given below (see

Appendix A)

$$\begin{aligned} F_{int}(\omega) &= \frac{1}{eV}\frac{\Gamma\frac{\partial G}{\partial N}P}{\omega_o^2}H(\omega) \\ H(\omega) &= \frac{1}{\left(\frac{j\omega}{\omega_o}\right)^2 + 2\left(\frac{\alpha_r}{\omega_o}\right)\left(\frac{j\omega}{\omega_o}\right) + 1} \end{aligned} \tag{4.4}$$

where α_r and ω_o are the damping rate and angular undamped frequency; $H(\omega)$ is the normalised transfer function, ie. $F_{int}(\omega)/F_{int}(0)$.

4.3 Bandwidth due to parasitic effects

Assuming the chip parasitics are causing the dominant frequency roll-off effect when compared to the package parasitics, therefore the overall laser response within the frequency range of interest, say 7 GHz, can be rewritten as ($F_{pack+R_{src}}(\omega) \approx 1$ for frequency upto 20 GHz with small C_p and L_p)

$$\begin{aligned} F_T(\omega) &= \frac{1}{eV}\frac{\Gamma\frac{\partial G}{\partial N}P}{\omega_o^2}H_T(\omega) \\ H_T(\omega) &\approx \frac{1}{(1+j\omega R_s C_s)}\,\frac{1}{\left(\frac{j\omega}{\omega_o}\right)^2 + 2\left(\frac{\alpha_r}{\omega_o}\right)\left(\frac{j\omega}{\omega_o}\right) + 1} \\ &\approx \frac{1}{(1+j\frac{\omega}{\omega_o}\chi)}\,\frac{1}{\left(\frac{j\omega}{\omega_o}\right)^2 + 2\zeta\left(\frac{j\omega}{\omega_o}\right) + 1} \end{aligned} \tag{4.5}$$

where

$$\begin{aligned} \zeta &= \frac{\alpha_r}{\omega_o} \\ \chi &= R_s C_s \omega_o \end{aligned} \tag{4.6}$$

which is the standard second order low-pass transfer function multiply by an extra pole $1/(1+j\omega R_s C_s)$ caused by the chip parasitics. The significant effects of this pole on the overall bandwidth is outlined by Figure 4.3 which shows that the -3 dB bandwidth reduces drastically as the $R_s C_s$ product (or χ) increases.

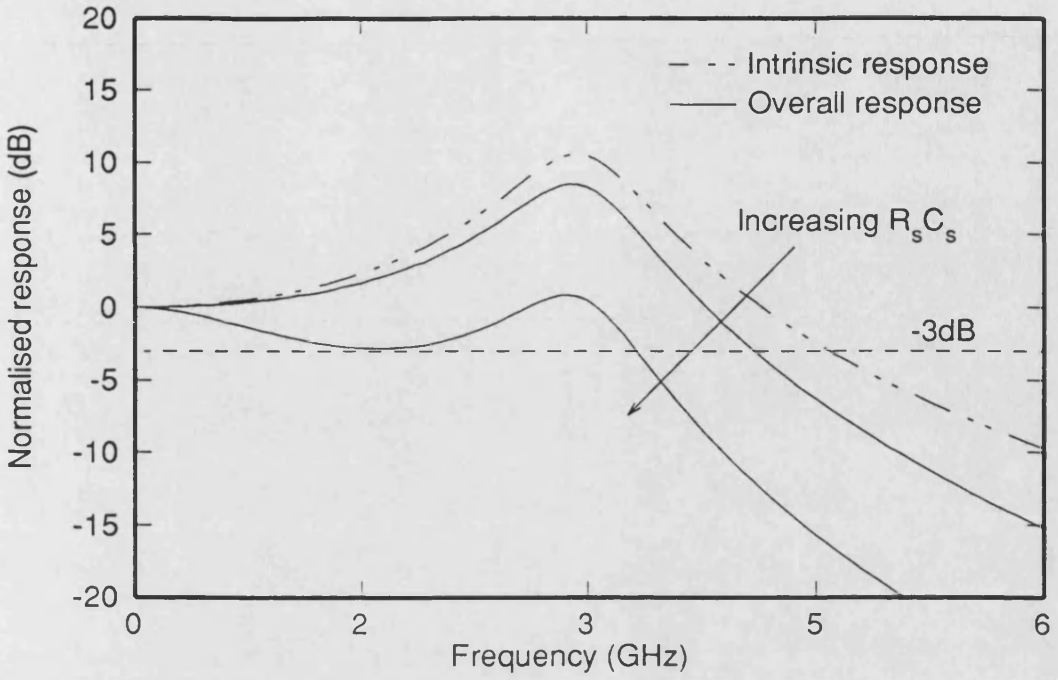

Figure 4.3: *Frequency response of laser diode including the parasitic effects*

Equating the magnitude of $H_T(\omega)$ to $1/\sqrt{2}$, the following third order equation in $\left(\frac{BW_T}{\omega_o}\right)^2$ can be obtained, where BW_T (in rad/s) denotes the -3 dB extrinsic bandwidth of the laser diode including the parasitic effects (see Figure 4.1),

$$\chi^2\left(\frac{BW_T}{\omega_o}\right)^6 + (1-2(1-2\zeta^2)\chi^2)\left(\frac{BW_T}{\omega_o}\right)^4 + (\chi^2 - 2(1-2\zeta^2))\left(\frac{BW_T}{\omega_o}\right)^2 - 1 = 0 \tag{4.7}$$

Clearly, excluding the effect of chip parasitics by setting $\chi = 0$, this equation reverts to the intrinsic bandwidth relationship Eqn (2.4). Eqn (4.7) can be solved either numerically or analytically, but an analytical result will not be significantly simpler than the original equation. Assume the solution of Eqn (4.7) is given by the function $Y(\zeta, \chi) = BW_T/\omega_o$ which is not only a function of ζ as in Section 2.3 but also a function of χ due to effect of chip RC roll-off. The numerical result of $Y(\zeta, \chi)$ is shown in Figure 4.4. Notice that the curve with $\chi = 0$, ie. without chip parasitics, is equivalent to that in Figure 2.1.

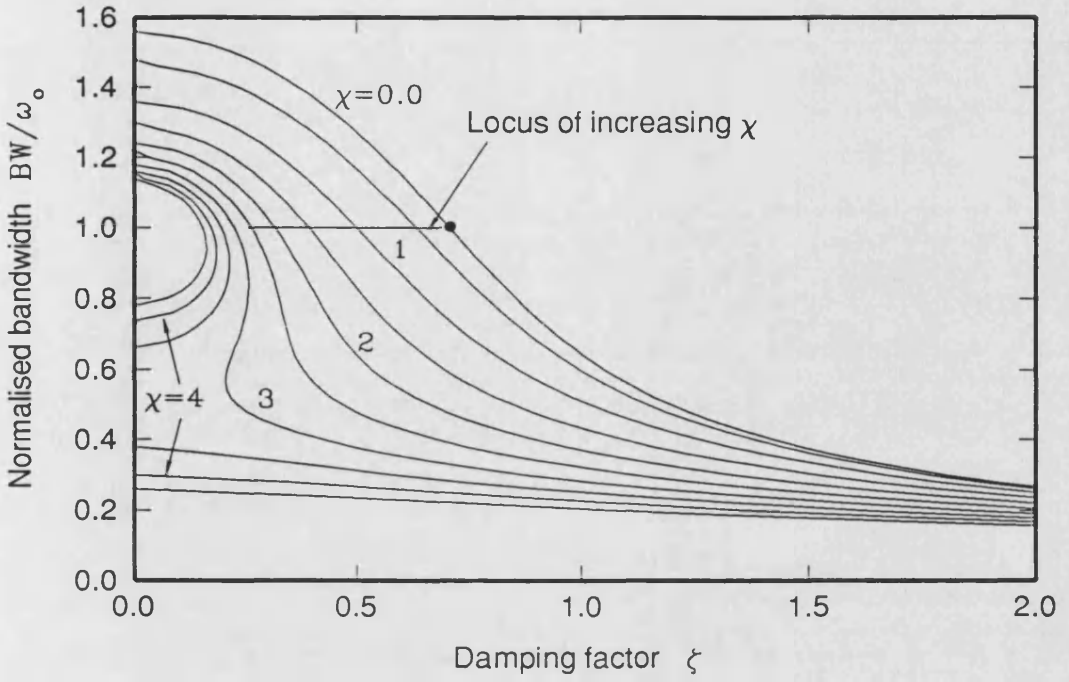

Figure 4.4: *The function $Y(\zeta, \chi)$ versus ζ for various level of χ governed by the parasitic effects*

The overall laser bandwidth BW_T is therefore becomes,

$$BW_T = Y(\zeta, \chi)\, \omega_o \tag{4.8}$$

The argument in Section 2.3 is still applicable to this case. When output optical power increases due to increased bias current, $Y(\zeta, \chi)$ will decrease whereas ω_o increases, therefore, a trade off between the $Y(\zeta, \chi)$ and ω_o exists as optical output escalates. This results in an extrinsic maximum achievable bandwidth BW_{Tmax}. The point where the maximum bandwidth takes place can be located by differentiating Eqn (4.7) w.r.t. ω_o^2, this gives the result $BW_{Tmax} = \omega_o$ which is similar to case of the intrinsic maximum achievable described in Section 2.5. However, the value of damping factor ζ for this BW_{Tmax} will no longer be fixed at $\zeta = 0.707$ as before because of the effect of χ, instead it is given by,

$$\zeta = \frac{1}{\sqrt{2(\chi^2 + 1)}} \tag{4.9}$$

As illustrated graphically in Figure 4.4, an increase in χ will reduce the function $Y(\zeta, \chi)$. Hence, the inclusion of χ enhances the reduction rate of $Y(\zeta, \chi)$ when photon density rises. As a result, the BW_{Tmax} must occur at $\zeta \leq 0.707$ but maintaining the relationship $BW_{Tmax} = \omega_o$ as depicted by the horizontal locus for BW_{Tmax} with varying χ in the figure.

When χ increases beyond a certain value, $\chi \approx 2.7$, one can observed that there exists more than one value of BW_T/ω_o for a single value of ζ. This is because the frequency dip on the laser diode response, due to the parasitic RC roll-off, has touched the -3 dB point and causes a sudden drop in the bandwidth as shown in Figure 4.3. That is also why the locus of the BW_{Tmax} ends around $\chi \approx 2.7$. Hence, in order to avoid that sudden drop in the bandwidth, one requires

$$2.7 \; > \; \omega_o R_s C_s \tag{4.10}$$

This imposes a certain maximum value of the R_sC_s product for a particular laser since ω_o, given by Eqn (2.11), contains device parameters such as gain coefficient g_o, photon lifetime, τ_p and gain suppression ϵ.

4.3.1 Modified K factor due to the effect of parasitics

It is possible to obtain an analytical result for the extrinsic maximum achievable bandwidth for $\chi < 2.7$, by using the relationship $BW_{Tmax} = \omega_o$ and Eqn (4.9),

$$BW_{max}^2 \; = \; BW_{Tmax}^2(1 + (R_sC_s)^2 BW_{Tmax}^2) \tag{4.11}$$

where BW_{max}(rad/s) denotes the intrinsic maximum bandwidth of the laser diode given in Chapter 2, and is given by

$$BW_{max} \; = \; \sqrt{2}\frac{\Gamma G}{1 - \Gamma\frac{\partial G/\partial P}{\partial G/\partial N}}$$

However, when $\chi > 2.7$, the parasitic effect is so strong that the bandwidth is severely limited to the RC roll-off frequency - $1/(2\pi R_s C_s)$, and the extrinsic maximum bandwidth is thus of no importance. It is noteworthy that Eqn (4.11) is only used for relating the intrinsic and extrinsic "maximum" bandwidths and not the bandwidth at any other values.

Consequently, in the presence of parasitic effects, the relationship between the K factor and the overall maximum bandwidth BW_{Tmax} is given by,

$$K = \frac{\sqrt{2}(2\pi)^2}{BW_{Tmax}} \left(\frac{1}{\sqrt{BW_{Tmax}^2 (R_s C_s)^2 + 1}} \right) \tag{4.12}$$

If the parasitic effects are neglected, ie. $R_s C_s = 0$, then Eqn (4.12) reverts back to the same form of Eqn (2.23) [7].

Solving Eqn (4.11), the overall laser bandwidth BW_{Tmax} can be obtained and is given by

$$BW_{Tmax} = \sqrt{\frac{-1 + \sqrt{1 + 4(R_s C_s)^2 BW_{max}^2}}{2(R_s C_s)^2}} \tag{4.13}$$

$$= \sqrt{\frac{-K + \sqrt{K^2 + 8(2\pi)^4 (R_s C_s)^2}}{2(R_s C_s)^2 K}} \tag{4.14}$$

Hence by extracting the K factor and the $R_s C_s$ product from the frequency response of a laser diode [7], the overall maximum modulation bandwidth due to the effect of the parasitics can be estimated via Eqn (4.14).

A simulated plot of the overall bandwidth BW_T versus the bias current I, based on the parameter values in Table 2.1, is given in Figure 4.5. It confirms that the parasitic RC roll-off causes a significant reduction on the laser diode bandwidth; furthermore, the overall maximum achievable bandwidth BW_{Tmax} always takes

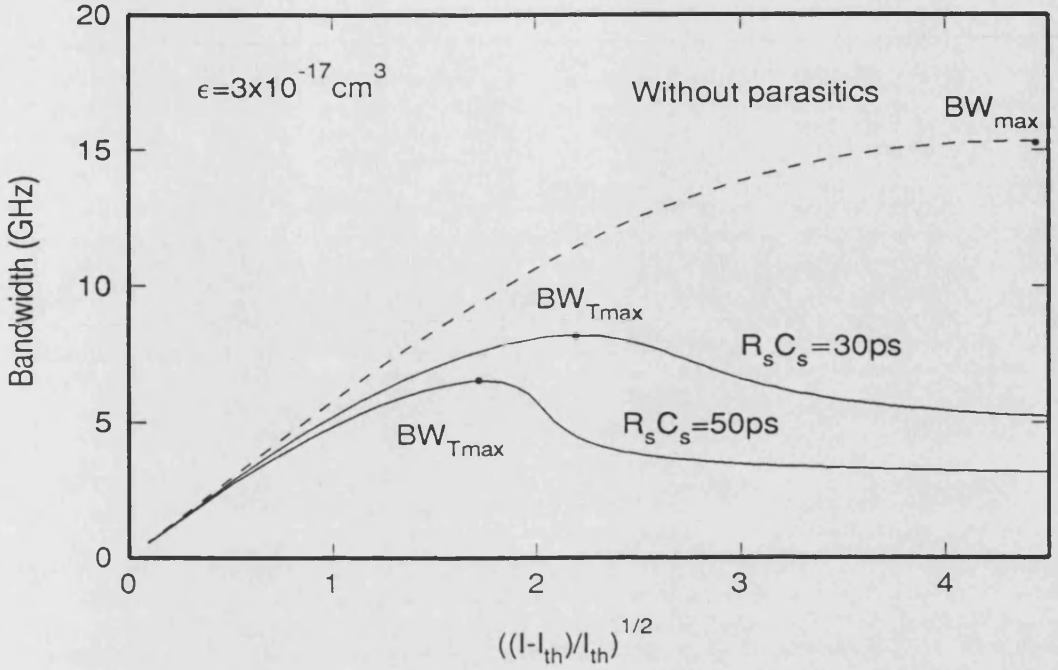

Figure 4.5: *Numerical results of the −3 dB bandwidth of laser diode with and without the effects of parasitic.*

place at $\zeta \leq 0.707$ under such an influence. The analytical values of the BW_{Tmax} predicted by Eqn (4.13) or (4.14) can also be identified by the numerical results.

4.4 Experimental results

The experimental setup for measuring the chip parasitics RC product of a diode laser under direct amplitude modulation is shown in Figure 4.6.

This experiment was performed at Northern Telecom's laboratory in Paignton with several DFB ridge waveguide laser diodes provided by the company. The setup is very standard, it consists of a sweep oscillator used in conjunction with a network analyser which incorporates a s-parameter test-set (All these are HP instruments and have internal impedance of 50 Ω). The photo-detector used is a

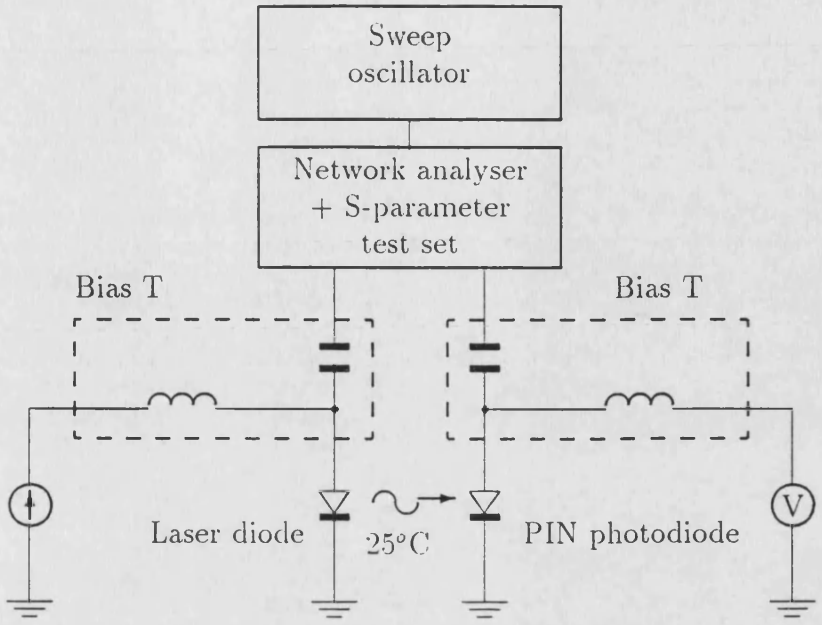

Figure 4.6: *The experimental setup for measuring the frequency response of laser diodes*

high speed InGaAs pin photodiode whose frequency response was calibrated up to 8.5 GHz. Each ridge waveguide laser is mounted n-side up on a gold-plated copper carrier. The copper carrier is attached to a high frequency mount which provides the necessary electrical connections for the T-bias and a.c. modulation (a 50 Ω matching resistor is used). An electronically controlled heat sink is placed underneath the mount to ensure a constant temperature environment of 25°C. The laser diodes are all lasing at $1.3\mu m$ with a ridge of dimension $2.5 \times 2 \times 380\mu m^3$ ($w \times d_p \times L$) and active layer thickness of $d = 0.2\mu m$. The inductances of the bond wires for these laser diodes are quite small, $L_p \approx 0.2nH$ because of their short lengths ($< 0.5mm$) and the shunt capacitance C_p is also small say $\approx 0.2pF$. As a result, package parasitics stage in Figure 4.1 can be neglected and this leaves the chip parasitics as a dominant effect limiting the laser diode bandwidth.

4.4.1 Measurement of chip parasitics

The measured normalised frequency response for one particular sample (LK-20) at different bias currents is given in Figure 4.7. One can easily observe the resonant peak and the dip caused by the chip parasitics. A group of five laser chips of the same structure from the same wafer has been measured (LK-20 to LK-24). Very little information can be obtained by simply looking at the frequency responses of these devices. Hence, the next step is to perform a least square fit to the measured frequency response to determine the three parameters ω_o, α_r and $R_s C_s$ of the overall normalised transfer given by Eqn (4.4). The fitted results are listed in Tables 4.1-4.3 for devices LK-20, LK-21 and LK-23. The results are also translated into several plots shown in Figures 4.8-4.10.

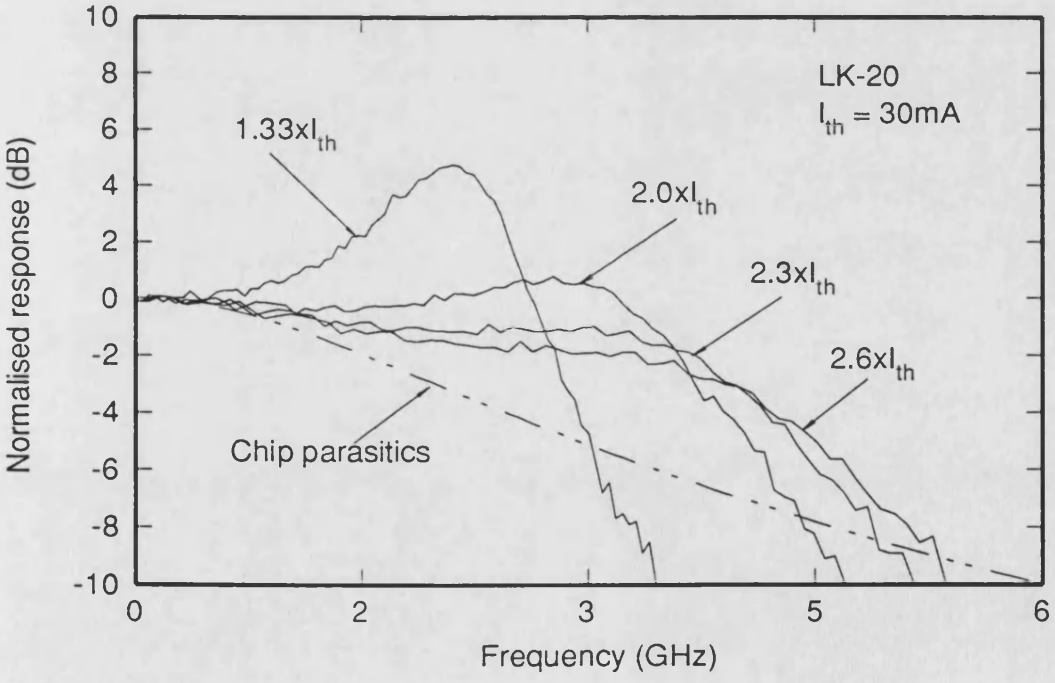

Figure 4.7: *Frequency response for ridge waveguide laser diode LK-20*

$I(mA)$	$\alpha_r(s^{-1})$	ω_o(rad/s)	ζ	R_sC_s (ps)
$1.2 \times I_{th}$	2.2×10^9	1.25×10^{10}	0.176	75.6
$1.33 \times I_{th}$	3.2×10^9	1.46×10^{10}	0.22	72.1
$1.6 \times I_{th}$	4.9×10^9	1.83×10^{10}	0.26	77.4
$2.0 \times I_{th}$	7.1×10^9	2.3×10^{10}	0.3	77.4
$2.3 \times I_{th}$	9.0×10^9	2.64×10^{10}	0.34	76.3

Table 4.1: *Fitted parameters for LK-20.* $I_{th} = 30mA$.

$I(mA)$	$\alpha_r(s^{-1})$	ω_o(rad/s)	ζ	R_sC_s (ps)
$1.28 \times I_{th}$	3.0×10^9	1.44×10^{10}	0.21	77.7
$1.4 \times I_{th}$	3.7×10^9	1.63×10^{10}	0.22	69.8
$1.57 \times I_{th}$	4.4×10^9	1.86×10^{10}	0.23	76.1
$1.85 \times I_{th}$	6.3×10^9	2.15×10^{10}	0.29	77.4
$2.14 \times I_{th}$	8.0×10^9	2.43×10^{10}	0.33	72.3

Table 4.2: *Fitted parameters for LK-21.* $I_{th} = 32mA$.

$I(mA)$	$\alpha_r(s^{-1})$	ω_o(rad/s)	ζ	R_sC_s (ps)
$1.2 \times I_{th}$	2.3×10^9	1.22×10^{10}	0.18	80.0
$1.36 \times I_{th}$	3.1×10^9	1.56×10^{10}	0.2	72.1
$1.6 \times I_{th}$	4.7×10^9	1.88×10^{10}	0.25	74.3
$1.9 \times I_{th}$	6.7×10^9	2.26×10^{10}	0.29	77.4
$2.2 \times I_{th}$	8.6×10^9	2.56×10^{10}	0.33	69.9

Table 4.3: *Fitted parameters for LK-23.* $I_{th} = 33mA$.

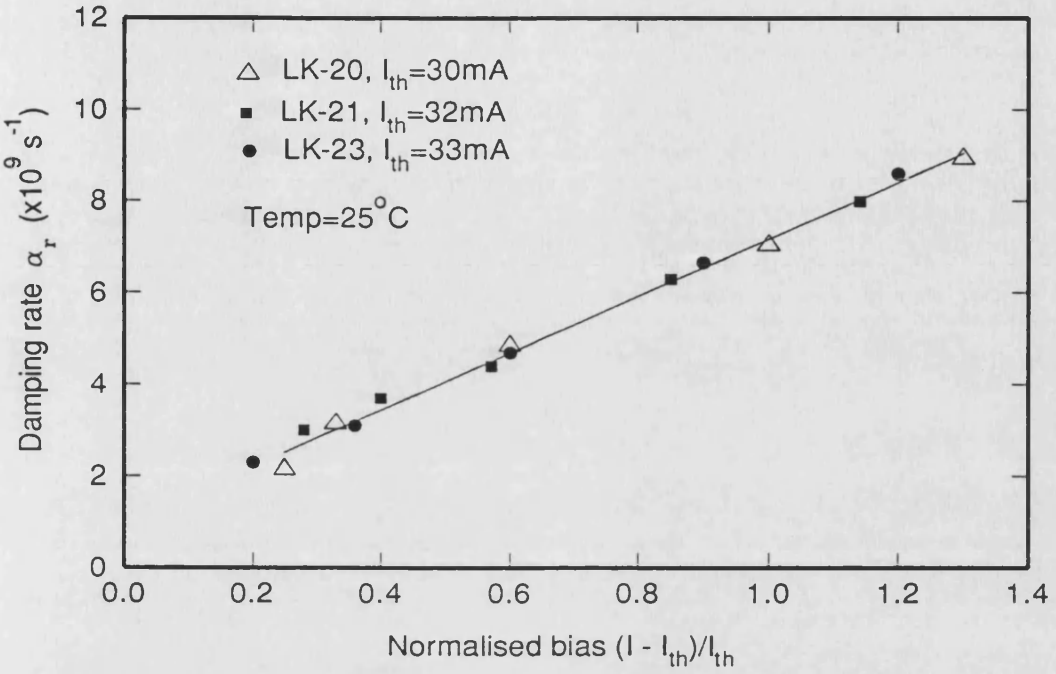

Figure 4.8: *Plot of (fitted) damping rate α_r versus bias current I for devices LK-20, 21 and 23*

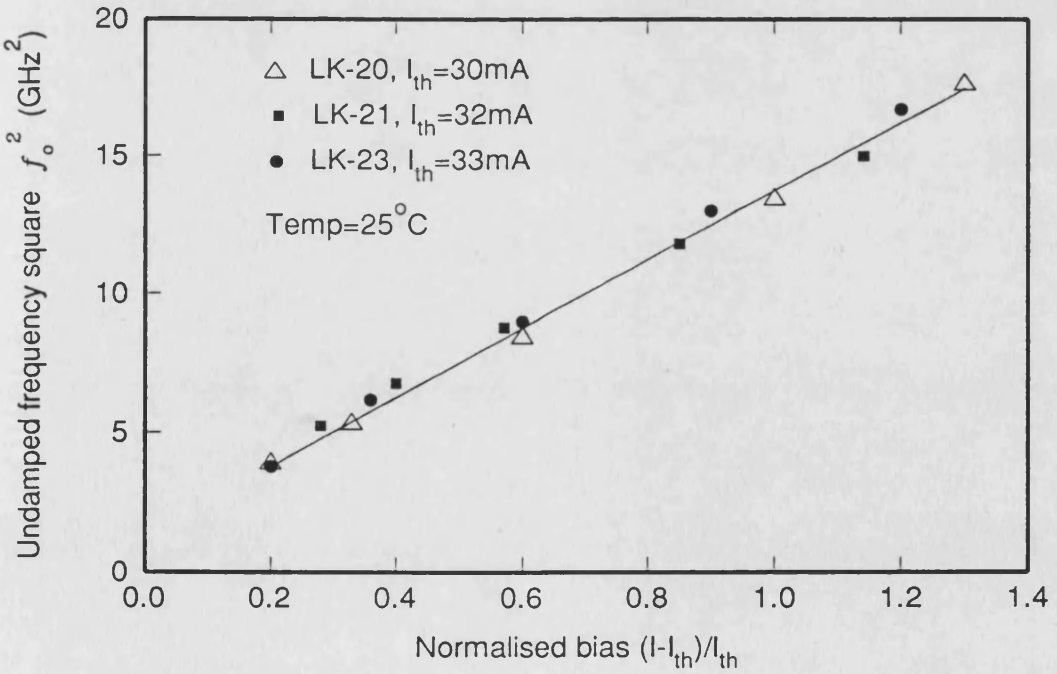

Figure 4.9: *Plot of (fitted) squared undamped frequency f_o^2 versus bias current I for devices LK-20, 21 and 23. From this diagram, the gain coefficient can be estimated using Eqn (4.17).*

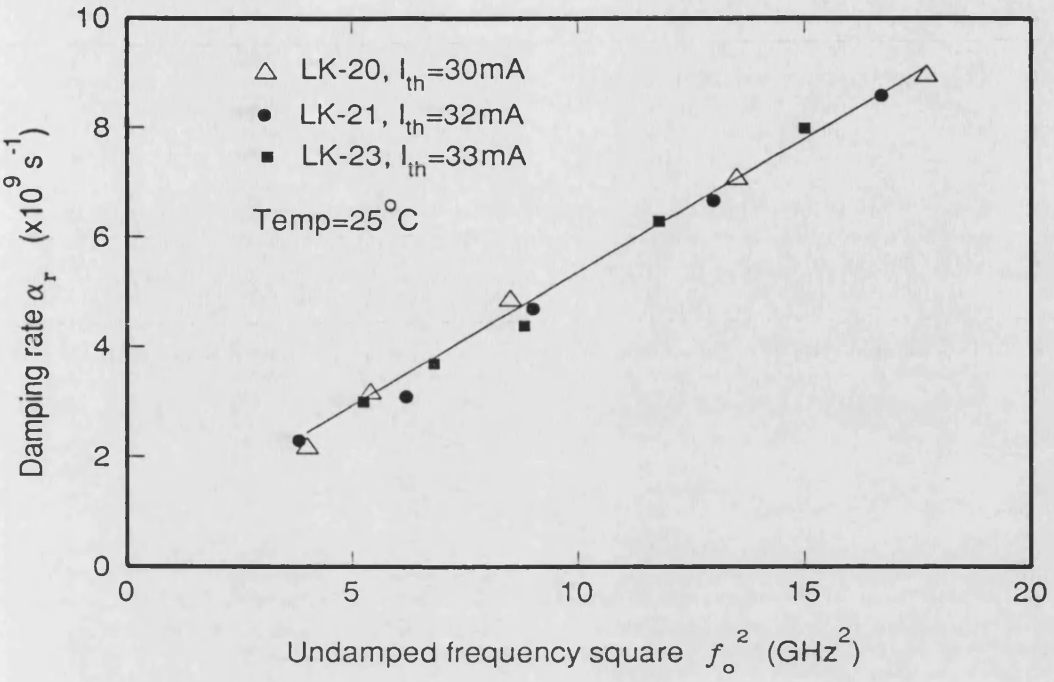

Figure 4.10: *Plot of damping rate α_r versus squared undamped frequency f_o^2 for devices LK-20, 21 and 23. The slope of this curve is directly proportional to the K factor which provides the information of the intrinsic maximum bandwidth of the device.*

It is found that the group of ridge waveguide laser diodes under test possess an average R_sC_s product of 75 ps. Utilising the given dimension of the ridge, a hole mobility μ_p of 70 $cm^2V^{-1}s^{-1}$ and a doping density n_p of $3.5 \times 10^{17}cm^{-3}$, the resistance R_s can be calculated by using

$$R_s = \frac{1}{n_p q \mu_p} \frac{d_p}{wL} \tag{4.15}$$

This gives a value of $R_s \approx 5\Omega$, hence the shunt capacitance $C_s \approx 15pF$. This result can be justified by using the equation for capacitance,

$$C_s = \epsilon_o \epsilon_r \frac{L w_{chip}}{d_s} \tag{4.16}$$

where ϵ_o is the permittivity of free space; ϵ_r is the relative permittivity of the silicon nitride layer; w_{chip} and d_s are the entire chip width and the thickness of the silicon nitride layer. Using $\epsilon_r \approx 2.9$, $w_{chip} = 320\mu m$ and $d_s = 0.25\mu m$, this gives a result of 12.5 pF which is close to the experimental result.

4.5 Estimation of device parameters

In this section, by using some of the equations derived in Chapter 2, estimations are made for several intrinsic device parameters, including gain coefficient g_o, gain suppression ϵ and maximum achievable bandwidth BW_{Tmax} are made.

Referring to Eqn (2.23), the intrinsic maximum bandwidth BW_{max} is inversely proportional to K factor which is defined as the slope of the α_r versus f_o^2 curve as given in Figure 4.10, that is,

$$\begin{aligned} BW_{max}(\text{Hz}) &= \frac{\sqrt{2}(2\pi)}{K} \\ &= \frac{\sqrt{2}\pi}{\frac{\alpha_r}{f_o^2}} \end{aligned}$$

Hence the estimated intrinsic BW_{max} for this group of ridge waveguide lasers is found to be 9.3 GHz with a K factor of $9.54 \times 10^{-10} s^{-1}$.

Substituting the L-I relationship in Eqn (2.20) into Eqn(2.10), the undamped frequency can be rewritten as

$$f_o^2 \approx \frac{1}{2\pi}\frac{\Gamma g_o}{qV}(I - I_{th}) \tag{4.17}$$

Therefore, it can be found from Figure 4.9 that the gain coefficient for these device is $g_o \approx 1.85 \times 10^{-6} cm^3 s^{-1}$ or the linear differential gain $A_o \approx 2.46 \times 10^{-16} cm^2$. Assuming $\tau_p = 1.6 \times 10^{-12}$, and fitting the values of BW_{max}, g_o and τ_p into Eqn (2.19), the estimated gain suppression value is $\epsilon \approx 4 \times 10^{-17} cm^3$.

Using the above estimated K factor and the $R_s C_s$ product, the overall maximum bandwidth BW_{Tmax} can be evaluated by Eqn (4.14) and it is found to be 4.2 GHz. This result is justified by a numerical calculation of the bandwidth versus normalised current curve as shown in Figure 4.11. It is clear that the modulation

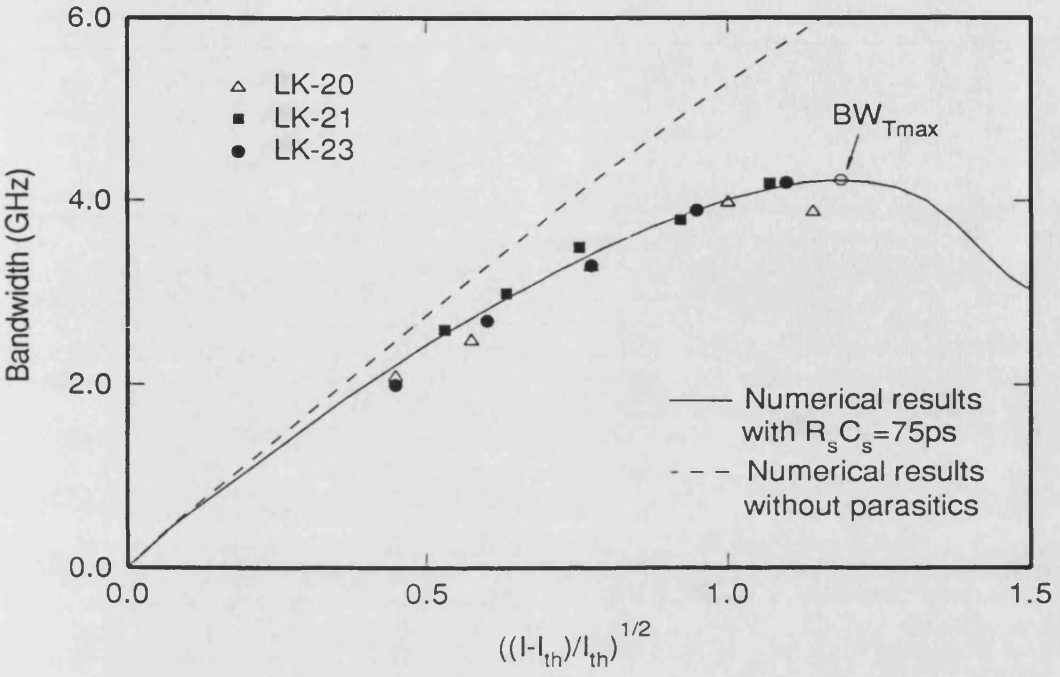

Figure 4.11: *Bandwidth versus square root normalised current. The numerical calculations and experimental results agreed well. Parameters used in the numerical calculation are* $g_o = 1.85 \times 10^{-6} cm^3 s^{-1}$, $\epsilon = 4 \times 10^{-17} cm^3$ *and* $R_s C_s = 75ps$.

bandwidth of the present ridge waveguide lasers are seriously hampered by the parasitic effects, since the intrinsic maximum bandwidth BW_{max}= 9.3 GHz are more than double of the overall (extrinsic) maximum bandwidth BW_{Tmax}= 4.2 GHz.

4.6 Conclusion

Chip parasitics are often the dominant parasitic effects inside a laser diode. The transfer function of the parasitics can be represented by a RC low pass filter which can cause limitation on the laser's overall modulation bandwidth. The intrinsic maximum bandwidth BW_{max} predicted by the K factor is therefore not applicable in this case. A modified relationship of the extrinsic maximum bandwidth BW_{Tmax} and the K factor has been derived.

An experiment based on a group of ridge waveguide laser diodes has been carried out. It has been shown that simply by measuring frequency response of the laser, one can estimate the parasitic R_sC_s product, the gain coefficient g_o, the extrinsic maximum achievable bandwidth BW_{Tmax} and also the gain suppression ϵ by assuming a typical value of photon lifetime τ_p.

In practice, by replacing parts of the laser diode structure with semi-insulated material [9], the chip parasitic effect can be reduced dramatically.

References

[1] R. S. Tucker, " High-frequency characteristics of directly modulated InGaAsP ridge waveguide and buried heterostructure lasers", *IEEE J. Lightwave Technol., vol. LT-2, pp. 385-393, 1984.*

[2] R. S. Tucker, "High-speed modulation of semiconductor lasers", *IEEE J. Lightwave Technol., vol. LT-3, pp. 1180-1192, 1985.*

[3] K. Y. Lau and A. Yariv, "Ultra-high speed semiconductor lasers", *IEEE J. Quantum Electron., vol. QE-21, pp. 121-138, 1985.*

[4] C.B. Su and V.A. Lanzisera, "Ultra-high-speed modulation of 1.3 *mu*m InGaAsP diode lasers", *IEEE J. Quantum Electron., vol. QE-22, pp. 1568-1578, 1986.*

[5] J.E. Bower, " High-speed semiconductor laser design and performance", *Solid State Electron., vol. 30, pp. 1-11. 1987.*

[6] N. K. Dutta, D. P. Wilt and R. J. Nelson, "Analysis of leakage currents in InGaAsP real index guide lasers", *IEEE J. Lightwave Technol., LT-2, pp.201-208, 1984.*

[7] R. Olshansky, P. Hill and W. Powazinik, "Frequency response of 1.3 μm InGaAsP high speed semiconductor lasers", *IEEE J. Quantum Electron., vol. QE-23, pp. 1410-1418, 1987.*

[8] R. Nagarajan, T. Fukushima, M. Ishikawa, J. E. Bowers, R. S. Geels and L. A. Coldren, "Transport limits in high-speed quantum well lasers : experiment and theory", *IEEE J. Photon. Technol. Lett., vol. 4, pp. 121-123, 1992.*

[9] K. Wakao, "InGaAsP/InP planar buried heterostructure lasers with semi-insulating InP current blocking layers grown by MOCVD", *IEEE J Quantum Electron., vol. QE-23, pp. 943-946, 1987.*

Chapter 5

Carrier Transport in QW Lasers

5.1 Introduction

The popularity of quantum well (QW) lasers has grown with the advancement in semiconductor crystal epitaxy technology in the past few years. The theoretical predictions [1] of the superior features of QW lasers over devices fabricated in more conventional bulk material, such as high differential gain, low threshold current, narrow linewidth and better temperature performance, are certainly the reasons for the wide-spread of QW lasers. Recently, considerable research interest in strained layer quantum well (SLQW) devices has also been driven by similar predictions that such material will further enhance the differential gain by the proper application of strain on the band structure of a semiconductor material [2, 3, 8].

Reduction in threshold current and spectral linewidth have been demonstrated experimentally in both QW [5, 6] and SLQW [4, 9, 11] lasers. However, the predicted enhancement in differential gain which should lead to a significant increase in the modulation bandwidth [14] has not yet been corroborated by

experimental work. The highest laser diode bandwidth reported so far is around 22-24 GHz which was in fact for a bulk material device [12, 13].

From a material viewpoint, part of the reason for such a contradiction between theoretical expectations and experimental realisations is the relatively higher non-linear gain effect (gain suppression) which occurs in QW/SLQW devices [15, 16, 17]. An increase in this gain suppression parameter will increase the damping mechanism inside the laser diode and therefore decrease the maximum achievable bandwidth as pointed out in Chapter 2. Nevertheless, the structural dependence of the differential gain in QW devices (refer to Table 2.2) suggests that material non-linear effects are not the only cause of the discrepancy. Recent reports [23, 25] show that the carrier capture into the quantum well and the carrier diffusion across the commonly used separated confinement heterostructure (SCH) seriously affect the modulation bandwidth of QW lasers.

In this chapter, a general picture of the carrier transport inside the QW laser is developed and then followed by the study of two different models :

(i) well barrier hole burning due to the quantum capture process suggested by W. Rideout [25]; and

(ii) carrier transport due to diffusion across the SCH layer and the thermionic emission from the quantum well [23].

By using small signal analysis, the detrimental effects of carrier transport on the modulation response of a QW laser will be demonstrated. A brief comparison between the two models will also be given. In fact, the inclusion of the carrier transport effects into the rate equations are shown to result in an intrinsic

third-order transfer function similar to that of the parasitics effects as given in Chapter 4. Hence, the modified K factor expression obtained previously can be used to estimate the intrinsic bandwidth providing other extrinsic effects, such as parasitics have been calibrated and eliminated from the analysis. Finally, considerations for quantum well structures which may be expected to minimise the carrier transport effects will be discussed.

5.2 The separated confinement heterostructure

Before going into any details of the modelling, it is helpful to have an understanding of the carrier transport processes involved inside a QW laser. The majority of QW laser diodes are made of separate confinement heterostructure (SCH) in order to improve carrier confinement into the active region. Figure 5.1 shows the layer structure of a QW laser which mainly consists of the SCH layers (which do not contribute gain) and the quantum wells (active region). The general picture of carrier injection mechanism inside the QW laser is as follows : the carriers are injected from the cladding layer and diffuse across the SCH/barrier layer and reach the edge of the quantum well where the carriers are still in their unbounded (unconfined) states. Not long after that, the carriers are then captured into bounded (confined) states of the QW by quantum capture process and ready for the lasing process. At the same time, there are carriers in the bound states which escape back to the unbounded states. As far as theory is concerned, the quantum capture process is via the absorption of an optical phonon [20, 21]; while the escape process can include thermionic emission [22]. It has been established by several research groups [23, 25, 26] that the carrier capture into the QW and carrier diffusion across SCH will cause additional limitation to the laser diode *intrinsic* bandwidth.

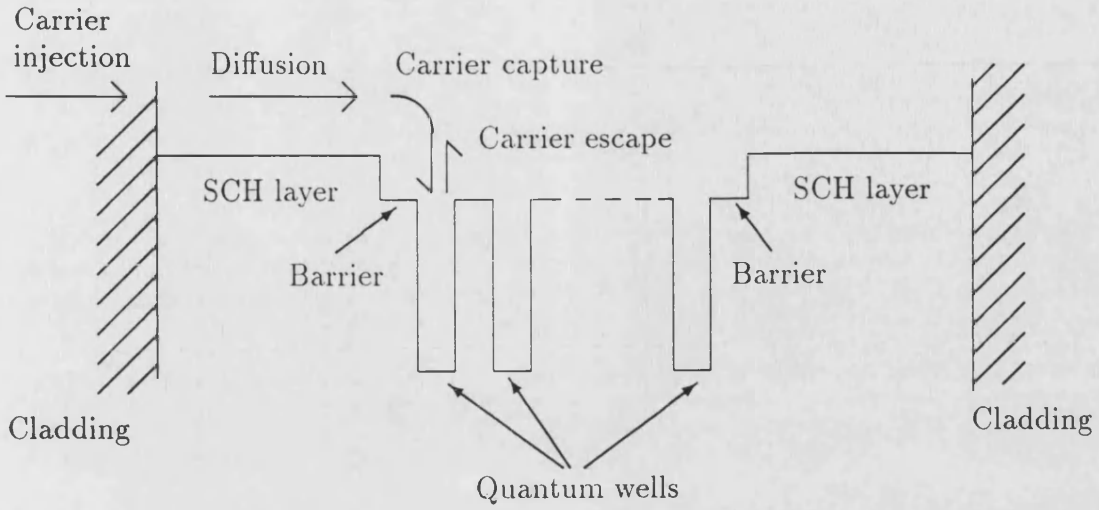

Figure 5.1: *Layer structure of a QW laser diode showing various carrier transport processes.*

5.3 The well-barrier hole burning

A research report by W. Rideout *et al* [25] first proposed that the photon density can cause changes in the distribution between the number of carriers in the well and those in the barriers/confinement region; and this results in a spatial variation of carrier distribution perpendicular to the active region. This *well-barrier hole burning* effect can cause additional damping to the modulation response of QW lasers and thus reduces the bandwidth.

In the present model, three coupled rate equations are used,

$$\frac{d\tilde{N}_b}{dt} = \frac{I}{qV_{qw}} - \frac{\tilde{N}_b}{\tau_e} - \frac{(\tilde{N}_b - \tilde{N}_w\eta_r)}{\tau_{cap}}$$

$$\frac{d\tilde{N}_w}{dt} = \frac{(\tilde{N}_b - \tilde{N}_w\eta_r)}{\tau_{cap}} - \frac{\tilde{N}_w}{\tau_e} - G(\tilde{N}_w)\tilde{P}$$

$$\frac{d\tilde{P}}{dt} = \Gamma G(\tilde{N}_w)\tilde{P} - \frac{\tilde{P}}{\tau_p} + R_{sp}(\tilde{N}_w)$$

$$G(\tilde{N}_w) = g_o(\tilde{N}_w - N_{tr})$$

$$\eta_r = \frac{\tau_{cap}}{\tau_{esc}} \tag{5.1}$$

It is pointed out that non-linear gain effects are not included. In the above $\tilde{N}_b$ and $\tilde{N}_w$ are the electron density in the barrier/confinement layers and quantum well respectively; τ_{cap} and τ_{esc} are the effective capture and escape time of carrier moving between the well and barrier/confinement layers; η_r is the ratio of N_b/N_w at equilibrium (or steady state) which can be given by carrier capture to the carrier escape time hence it can be regarded as the carrier escape/capture rate ratio; $\tau_e = 1/\gamma_e$ is the electron lifetime and is assumed to be a constant determined by the bimolecular recombination rate, hence differential recombination rate $d\gamma_e/dN = 0$; $G(N_w)$ is the optical gain for which the nonlinear gain coefficient ϵ is not explicitly included, instead the non-linearity will be derived by comparing the coefficients of the small signal transfer function of these equations to that obtained in Eqn (4.5) under certain conditions. $\tilde{P}$ and $\tilde{I}$ are the photon density and injected current; V_{qw}, g_o, Γ and τ_p are the volume of the quantum well active region, gain coefficient, confinement factor and the photon lifetime respectively.

From the above rate equations, it is obvious that this model is essentially describing the quantum capture process in the vicinity of the quantum well, ie. the transport of unbounded/bounded carriers at the well as depicted schematically in Figure 5.2. Therefore, the effects of carrier diffusion process across the SCH region is not explicitly included.

In the above laser threshold regime, d.c. solutions for the above rate equations show that N_w is essentially fixed at around threshold value similar to the results for the conventional pair of rate equations. However, the carrier density in the barrier/confinement region N_b increases with current even above threshold due to the finite carrier capture time τ_{cap}. As a result, the distribution of carrier densities

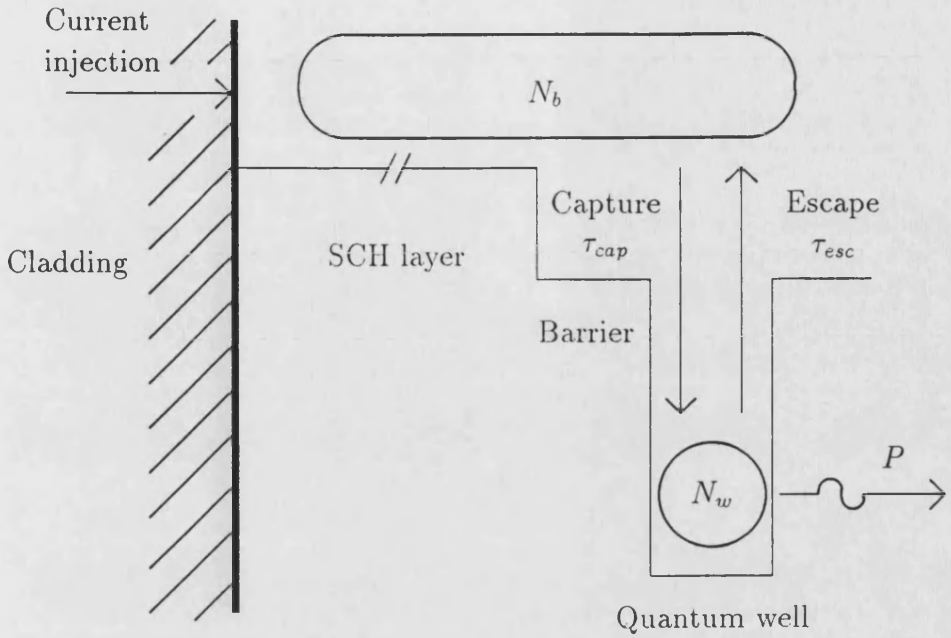

Figure 5.2: *Schematic diagram for the well-barrier hole burning model.*

perpendicular to the active region is uneven and a spatial *hole* is developed in the QW active region – well-barrier hole burning.

5.3.1 Intrinsic bandwidth

By applying small signal analysis to the above equations, the following third order transfer function can be obtained,

$$
\begin{aligned}
F_{whb}(\omega) &=: \frac{\frac{dG}{dN_w}P}{qV_{qw}} H_{whb}(\omega) \\
H_{whb}(\omega) &= \frac{1}{(jw)^3 + X(jw)^2 + Y(jw) + Z} \qquad (5.2) \\
X &= \left(\frac{dG}{dN_w}P + \frac{1}{\tau_e} + \frac{(1+\eta_r)}{\tau_{cap}}\right) \\
Y &= \Gamma G \frac{dG}{dN_w}P + \frac{1}{\tau_{cap}}\left(\frac{dG}{dN_w}P + \frac{1}{\tau_e}\right) \\
Z &= \frac{1}{\tau_{cap}}\Gamma G \frac{dG}{dN_w}P
\end{aligned}
$$

here P is the steady state photon density and the gain derivative $\frac{dG}{dN_w}$ is equivalent to the gain coefficient g_o.

This third order denominator can be approximately factorised to a form close to Eqn (4.5), which is the response function of the standard pair of rate equations Eqn (2.1) under the effect of parasitic RC roll off, that is,

$$\frac{1}{(1+j\omega RC_{eff})} \frac{1}{\left[\left(\frac{j\omega}{\omega_o}\right)^2 + 2\left(\frac{\alpha_r}{\omega_o}\right)\left(\frac{j\omega}{\omega_o}\right) + 1\right]}$$

where the undamped frequency ω_o and the damping rate α_r are given by Eqn (2.5) and (2.6) with $G = g_o(N - N_{tr})/(1 + \epsilon_{eff}P)$. By comparing coefficients, one can obtain the following expression for the effective RC constant RC_{eff} and gain suppression coefficient ϵ_{eff},

$$RC_{eff} \approx \frac{\tau_{cap}}{(1+\eta_r)} \tag{5.3}$$

$$\epsilon_{eff} \approx g_o\left(\tau_{cap}\left(\frac{\eta_r}{1+\eta_r}\right) - \eta_r\tau_p\right) \tag{5.4}$$

This suggests that the transport effects of the unbounded/bounded carriers at the quantum well, can be simplified to the case of an intrinsic laser diode (governed by the standard rate equations pair) under the influence of the parasitics effects as discussed in Chapter 4. In brief, a parasitic-like RC roll-off effect in the frequency response is produced by the extra pole, $(1 + j\omega RC_{eff})$ which limits the intrinsic bandwidth according to the magnitude of RC_{eff}. Moreover, further reduction in the intrinsic bandwidth via the damping effect is caused by the effective gain suppression term ϵ_{eff}. Figure 5.3 shows the numerically calculated intrinsic bandwidth of QW lasers whose dynamics are described by Eqn (5.1). It is clear that the intrinsic bandwidth BW is degraded as τ_{cap} increases. Note that the above analytic effective values are only valid when $\tau_{cap} \ll \omega_o$, while for $\tau_{cap} \approx \omega_o$, a numerical solution must be used.

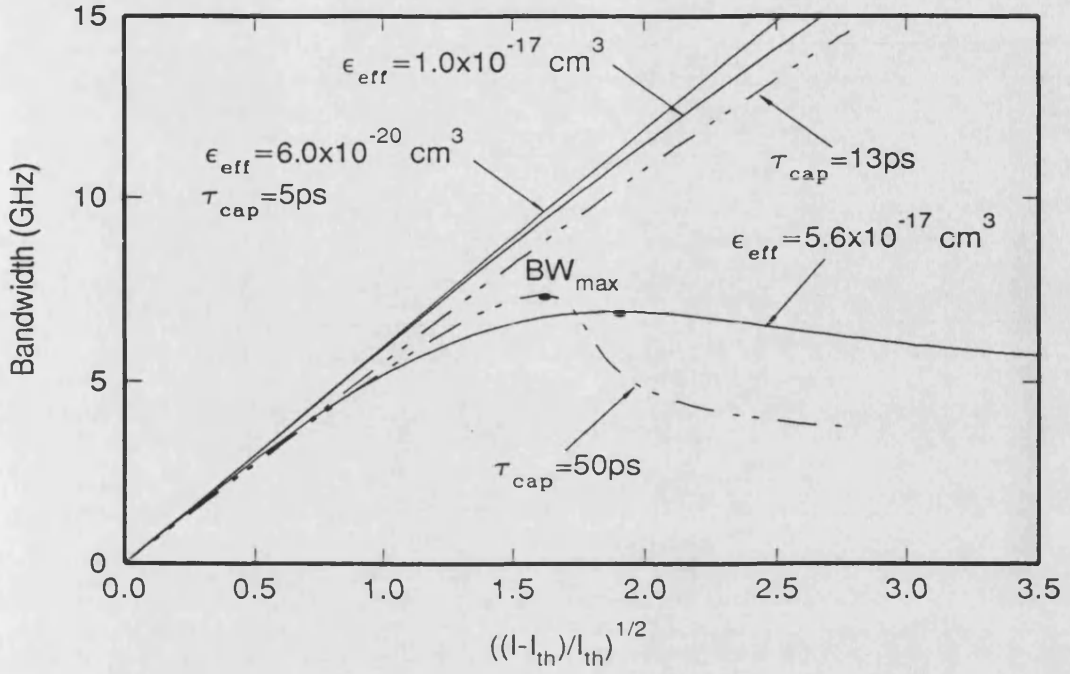

Figure 5.3: *The −3 dB bandwidth versus normalised bias current for different carrier capture time* τ_{cap}.

It is thus concluded that the well-barrier hole burning effect manifest itself as gain suppression through the quantum capture phenomenon and contributes:

(i) a damping effect; and

(ii) an equivalent parasitic-like RC roll-off effect;

which can cause reduction in the intrinsic bandwidth. These results also indicate the importance of carrier transport effect in modelling the dynamics of a QW laser diode.

Since the intrinsic bandwidth of a QW laser diode depends on the values of two parameters, τ_{cap} and η_r, typical or representative values for these parameters would be needed in order to validate these conclusions. It is found that the carrier

escape/capture rate ratio η_r is a structural dependent parameter [27] and hence the well barrier hole burning effect is bound to be structural dependent. Moreover, experimentally measured values of the absolute capture time τ_{cap} [18, 19, 20] lie between sub-picoseconds to a few picoseconds, which obviously indicates that the effective gain suppression is relatively small and causes virtually no effect on the intrinsic bandwidth. Therefore in order to explain the adverse effects of this model on the intrinsic bandwidth, an anomalously large τ_{cap} (a few tens picoseconds) has to be used [25] as illustrated in Figure 5.3. Such a large value of capture time τ_{cap} in fact suggests that the diffusion process across the SCH region should be included explicitly into the model as proposed Nagarajan *et al* [23].

5.4 The carrier diffusion across SCH layer

Not long after the proposal of well barrier hole burning model, Nagarajan *et al* [24] presented a better description of the carrier transport effect inside a QW laser using a set of four rate equations. This work predicted that carrier diffusion across the SCH region will cause a low frequency, parasitic-like roll-off which severely degrades the modulation bandwidth of a QW lasers and this theoretical prediction is also supplemented by an experiment with lasers of different sizes of SCH region. It is believed that the effect of the crucial carrier capture process, described in last section, has been excluded by this model [26, 27]. However, the following analysis will show that the effects of carrier capture, in fact, has been implicitly included through a carrier escape term in the model; and it is this carrier escape process which causes a significant damping effect and further limits the intrinsic bandwidth.

The set of rate equations used are very similar to the well barrier hole burning model, except that there are two rate equation for the SCH region – one for each side of the quantum well, that is :

$$\begin{aligned}
\frac{d\tilde{N}_{b1}}{dt} &= \frac{I}{qV_{sch}} - \frac{\tilde{N}_{b1}}{\tau_{tp}} - \frac{\tilde{N}_{b1}}{\tau_e} + \frac{\tilde{N}_w(V_{qw}/V_{sch})}{2\tau_{thm}} \\
\frac{d\tilde{N}_{b2}}{dt} &= -\frac{\tilde{N}_{b2}}{\tau_{tp}} - \frac{\tilde{N}_{b2}}{\tau_e} + \frac{\tilde{N}_w(V_{qw}/V_{sch})}{2\tau_{thm}} \\
\frac{d\tilde{N}_w}{dt} &= \frac{\tilde{N}_{b1}(V_{sch}/V_{qw})}{\tau_{tp}} + \frac{\tilde{N}_{b2}(V_{sch}/V_{qw})}{\tau_{tp}} - \frac{\tilde{N}_w}{\tau_e} - \frac{\tilde{N}_w}{\tau_{thm}} - G(\tilde{N}_w,\tilde{P})\tilde{P} \\
\frac{d\tilde{P}}{dt} &= \Gamma G(\tilde{N}_w,\tilde{P})\tilde{P} - \frac{\tilde{P}}{\tau_p} + R_{sp}(\tilde{N}_w) \\
G(\tilde{N}_w,\tilde{P}) &= \frac{g_o(\tilde{N}_w - N_{tr})}{1+\epsilon\tilde{P}}
\end{aligned} \tag{5.5}$$

where $\tilde{N}_{b1}$, $\tilde{N}_{b2}$ and $\tilde{N}_w$ are the carrier densities for the SCH layers and the quantum well respectively; τ_{tp} is the transport/dwell time of the carriers in the SCH which mainly due to carrier diffusion process; τ_{thm} is the thermionic emission time from the quantum well which is similar to the carrier escape time τ_{esc} in the well barrier hole burning model; V_{sch} is volume of one side of the SCH layer and V_{qw} is the volume of the quantum well. The other parameters are identical to those defined previously.

5.4.1 Intrinsic bandwidth

Applying small signal analysis to the above equations, the following transfer function, $F_{sch}(\omega)$ is obtained,

$$\begin{aligned}
F_{sch}(\omega) &= \frac{\frac{\partial G}{\partial N_w}P}{qV_{qw}\,\omega_o^2}\left(\frac{\tau_e}{\tau_e+\tau_{tp}}\right)H_{sch}(\omega) \\
H_{sch}(\omega) &= \frac{1}{(1+j\omega\tau_{tp})}\,\frac{1}{\left[\left(\frac{j\omega}{\omega_o}\right)^2 + 2\frac{\alpha_r}{\omega}\left(\frac{j\omega}{\omega_o}\right)+1\right]}
\end{aligned} \tag{5.6}$$

with

$$\omega_o^2 \approx \Gamma G \frac{\partial G}{\partial N_w} P \tag{5.7}$$

$$\alpha_r \approx \frac{1}{2}\left(\frac{\partial G}{\partial N_w} P - \Gamma \frac{\partial G}{\partial P} P + \frac{1}{\tau_e} + \frac{1}{\tau_{thm}}\right) \tag{5.8}$$

Under the influence of carrier diffusion across the SCH layer, an extra pole, $(1+j\omega\tau_{tp})$, is imposed on the transfer function, which thus causes a parasitic-like RC roll-off effect on the laser response. Furthermore, by comparing the expression for the damping rate α_r with that obtained from standard rate equations Eqn (2.6), it can be shown that there is an additional damping term caused by the thermionic emission, ie. $1/\tau_{thm}$. On the assumption that the thermionic emission is the major escape process from the quantum well, then one may write :

$$\frac{1}{\tau_{thm}} = \frac{\eta_r}{\tau_{cap}} \tag{5.9}$$

with the carrier escape ratio η_r range from 0.001 to 2.0 depending on the structural parameters [28]. The larger the η_r value the higher is the carrier escape rate. Hence, the extra damping effect is governed by the carrier capture/escape process into the quantum well which justifies the finding on what was found in the last section.

The diffusion time τ_{tp} across the SCH layer is calculated using

$$\tau_{tp} = \frac{L_{sch}^2}{2D} \tag{5.10}$$

where L_{sch} is the length of the SCH layer; D is the diffusion coefficient with typical values of 100 cm^2/s for electrons and 7 cm^2/s for holes. Therefore, for the slower carrier – the holes in the present case with a longer diffusion time, can result in a lower RC roll-off frequency. The intrinsic bandwidth of a QW laser calculated including the combined effects of the carrier diffusion (holes in this

case) across the SCH layer and the carrier capture/escape process is illustrated graphically in Figures 5.4 and 5.5.

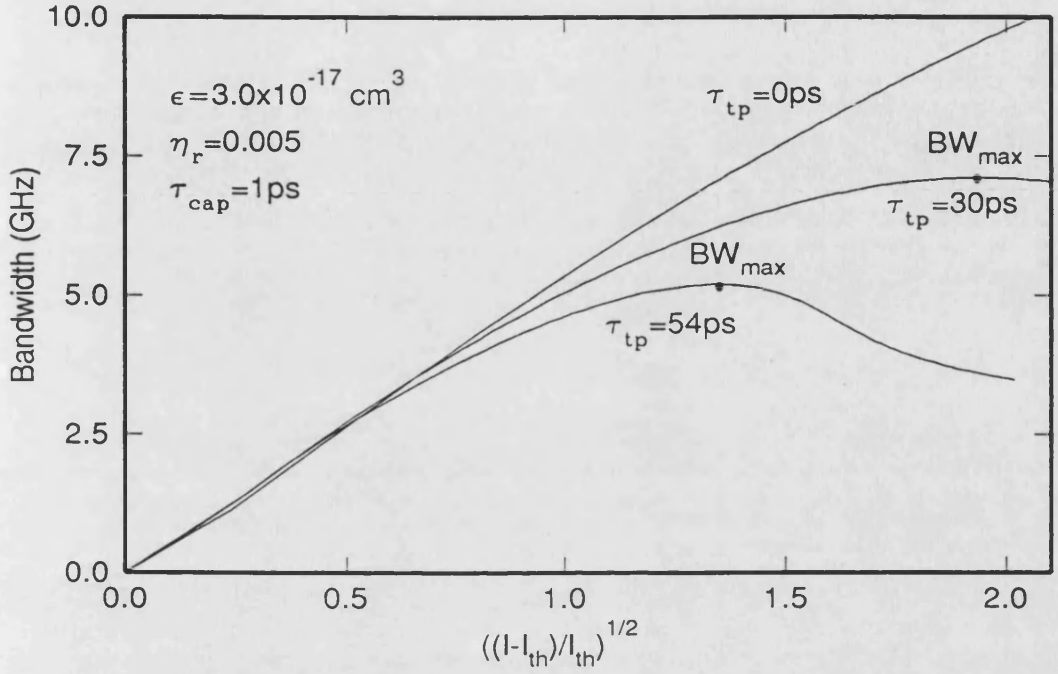

Figure 5.4: *The −3 dB bandwidth versus normalised bias current for different carrier diffusion time* τ_{tp}.

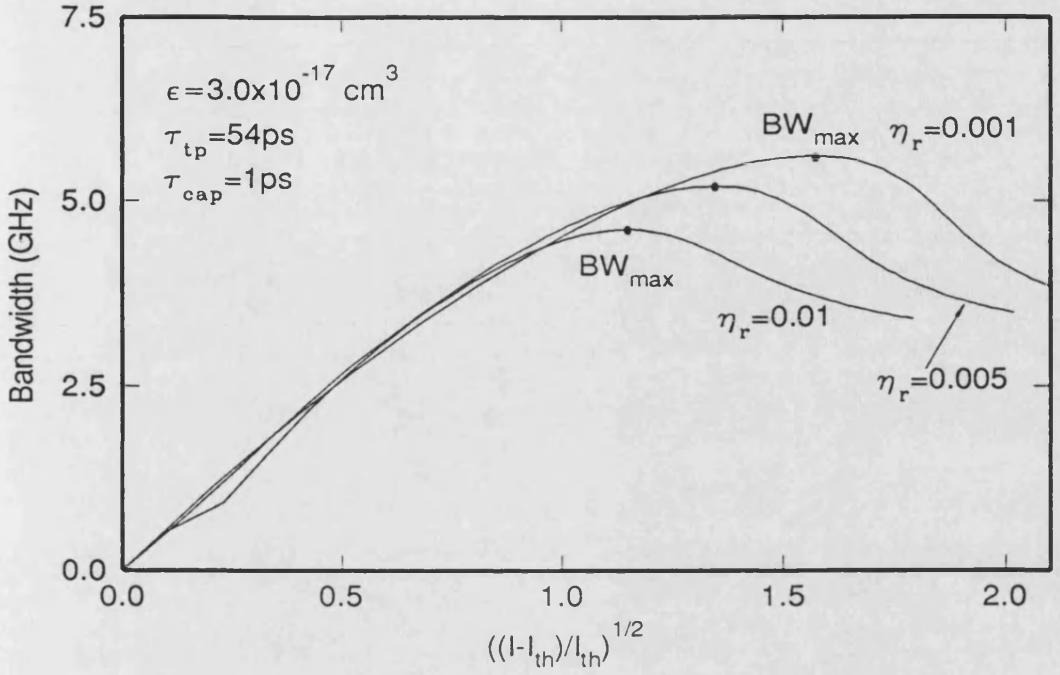

Figure 5.5: *The −3 dB bandwidth versus normalised bias current for different carrier escape/capture ratio* η_r.

Clearly, for large values of τ_{tp} and η_r, the intrinsic bandwidth is severely reduced. A larger τ_{tp} means the carriers need more time to complete the journey across the SCH region to reach the quantum well. This diffusion time is certainly a lot longer than the (sub-picoseconds/picoseconds) capture time, hence the SCH regions on both sides of the quantum well act like a carrier storage or reservoir which manifest itself as a capacitance effect. On the other hand, at the quantum well, a larger carrier escape/capture rate ratio η_r imposes a limit on the modulation response equivalent to a damping effect.

As a result, this comprehensive model predicts that

(i) the carrier diffusion across the SCH introduces a parasitics-like RC low frequency roll-off; and

(ii) the quantum capture/escape process contributes to the damping effect on

the intrinsic modulation response – which is not shown clearly in previous works [23, 24].

5.5 The modified K factor

As indicated in the past two sections, no matter which physical mechanisms assumed is used for specifying the carrier transport effects on the dynamic behaviour of a QW laser (well barrier hole burning or diffusion across SCH model), a third order transfer function with a first order pole causing significant low frequency roll-off is always obtained. This situation is equivalent to the parasitic effects on an intrinsic laser diode discussed previously in Chapter 4. The only conceptual difference is that the chip parasitics were considered as an extrinsic effect while the carrier transport process is viewed as an intrinsic property as illustrate in Figure 5.6.

Consequently, the results derived for obtaining the extrinsic maximum bandwidth affected by the parasitic effects, can also be used for analysing the intrinsic bandwidth of a QW laser BW_{QW} under the influence of carrier transport effects. This is given by

$$\begin{aligned} BW_{QWmax} &= \sqrt{\frac{-1+\sqrt{1+4(\tau_{eff})^2 BW_{max}^2}}{2(\tau_{eff})^2}} \\ &= \sqrt{\frac{-K+\sqrt{K^2+8(2\pi)^4(\tau_{eff})^2}}{2(\tau_{eff})^2 K}} \end{aligned} \tag{5.11}$$

where BW_{max} and K is the maximum bandwidth and the K factor obtained in the absence of carrier transport effects; τ_{eff} is an effective transport time which can be represented by RC_{eff} or τ_{tp} depending on which carrier transport model is being used.

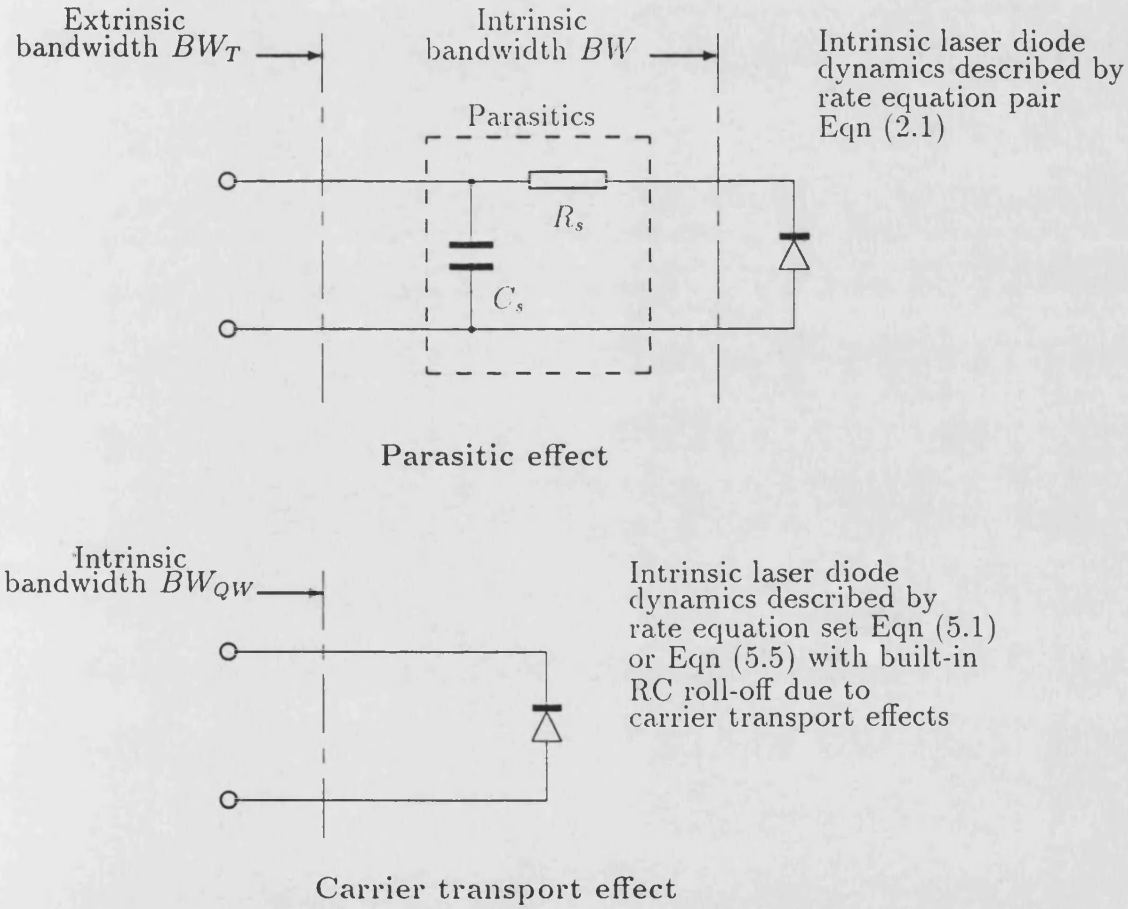

Figure 5.6: *The similarity between the parasitics and carrier transport effect.*

Providing that the chip parasitics are small, then by measuring the frequency response and matching it with the third order transfer function given by Eqn (5.2) or Eqn (5.6), the parameters α_r, ω_o and τ_{eff} can be measured. From the slope of the damping rate α_r versus the undamped frequency ω_o, the damping factor K and the maximum bandwidth BW_{max} without the influence of carrier transport are subsequently determined. The complete procedure is similar to that illustrated in Section 4.4. Substituting the values of τ_{eff} and BW_{max} or K into Eqn (5.11), the intrinsic maximum bandwidth BW_{QWmax} due to effect of carrier transport can be estimated.

It is noteworthy that another commonly used method for obtaining the K factor is to measure the relative intensity noise (RIN) spectrum instead of the frequency response of a QW laser. However, only the information of α_r and ω_o can be extracted by this method since the expression of the RIN spectrum is given by,

$$F_{RIN}(\omega) \approx F_{Lang}\frac{2\alpha_r + j\omega}{(j\omega)^2 + 2\alpha_r(j\omega) + \omega_o^2} \tag{5.12}$$

where F_{Lang} is the Langevin force of the field due to spontaneous emission which is assumed to be an uncorrelated white Gaussian noise. In deriving this equation pure optical modulating source, the Langevin sources, is used, hence the method is free from parasitic effects [30]. The only question remains is how to justify whether the α_r and ω_o obtained by this method are not influenced by the carrier transport effect.

In fact, it has been shown recently that the RIN method is free from carrier transport effects [29], that is, the equation will remain unchanged (does not contain the extra pole $1/(1+j\omega\tau_{eff})$) no matter whether there is carrier transport effect or not. Consequently, if one use the RIN method to determine the K factor and thereby to obtain the intrinsic maximum bandwidth via Eqn (2.23), an over-estimation of the intrinsic bandwidth is always obtained [29]. Since the

bandwidth value reflected by Eqn (2.23) is only BW_{max} and *not* BW_{QWmax}. However, by using the the new relationship provided in Eqn (5.11) together with an appropriate value of τ_{eff}, the intrinsic bandwidth may be accurately deduced.

5.6 Structural considerations

As indicated by the results obtained using the two different models, in order to reduce the carrier transport effects, both the diffusion time across the SCH τ_{tp} and the ratio of carrier escape/capture rate η_r have to be minimised.

In order to minimise τ_{tp}, a narrower SCH region width can be used at the expense of poor carrier confinement and greater internal losses which leads to reduction of differential gain A_o (or gain coefficient g_o). Consequently, for different structural parameters, there exists an optimal SCH width [23]. Similarly, the thickness of the barrier, sitting between wells in a multiple QW device, should also be minimised, but once again this will be offset by other effects such as tunnelling, optical confinement, etc. Doping the SCH region may help to reduce τ_{tp}, however, would also increase the internal losses slightly.

For reducing the carrier escape/capture rate ratio η_r, ie. the quantum escape effect, a graded index (GRIN) SCH could be of advantage, since its built-in electric field can speed up the capture process hence decrease the quantum escape rate. Nevertheless, the width of a GRIN SCH needed to achieve the optical confinement factor is twice that for SCH [23]. Hence the field enhancement of τ_{tp} must be larger by at least this factor to be significant. Moreover, a deeper and wider well can usually cause reduction in the η_r value, due to the effect of lowering the carrier Fermi level inside the well. Appropriate doping in the active

region can also be to lower the quasi-Fermi level of the carrier in the well. In addition, doping in the QW also induces a higher differential gain [31]. Two recent experiments based on carefully designed p-doped MQW lasers [32, 33], in fact, have successfully overcome the limits imposed by both the gain suppression and carrier transport effects and achieved a record high bandwidth.

In general, the structural design of quantum well laser requires careful considerations, and since most the parameters are structural dependent and interrelated, this make the whole process rather complicated. Undoubtly, the carrier transport effect is limiting the intrinsic bandwidth of a QW laser, however, a complete physical picture of the actual interaction is still in search and is currently open for debate.

5.7 Conclusion

Although the step like band structure of quantum well laser devices has been expected to achieve a higher bandwidth due to the enhanced differential gain, the carrier transport processes between the well and the adjacent SCH layers has producing serious detrimental effects on the modulation response. Two different models have been studied and it is found that the model proposed by R. Nagarajan *et al* is more comprehensive and complete. The carrier transport induced effects include :

(i) a low frequency parasitic-like RC roll off on the frequency response due to carrier diffusion across the SCH region; and

(ii) a damping effect on the frequency response caused by the quantum escape/capture processes at the quantum well.

This unveiled the importance of the escape/capture rate ratio which manifest itself as a damping effect and limits the intrinsic bandwidth.

Since the overall transfer function is described by a third-order system, the modified K factor/maximum bandwidth relationship derived in Chapter 4 can also be used to predict the intrinsic maximum bandwidth taking account of carrier transport effects. The RIN measurement method in determining the K factor and hence the intrinsic bandwidth of a QW laser used to give an over-estimating results, however, this over-estimation of the intrinsic bandwidth can be corrected by adopting the new relationship derived here.

Larger maximum bandwidth can be achieved by minimising the diffusion time across the SCH region and the quantum escape rate. Doping the SCH region and optimising its width with confinement factor can result in shorter diffusion time; while using GRIN SCH structure with a wider and deeper well can also reduce the quantum escape effects.

References

[1] Y. Arakawa and A. Yariv, "Quantum well lasers - gain, spectra, dynamics", *IEEE J. Quantum Electron., vol. QE-22, pp. 1887-1899, 1986.*

[2] A. Ghiti, E. P. O'Reily and A. R. Adams,"Improved dynamics and linewidth enhancement factor in strained layer lasers", *Electron. Lett., vol. 25, pp. 821-822, 1989.*

[3] T. Ohtoshi and N. Chinone,"Linewidth enhancement factor in strained quantum well lasers," *IEEE Photon. Technol. Lett., vol. 1, pp. 117-119, 1989.*

[4] J. S. Osinski, P. Grodsinski, Y. Zou and P. D. Dapkus, "Evidence of gain enhancement in long wavelength strained layer quantum well laser diodes", *Electron. Lett., vol. 27, pp. 469-470, 1991.*

[5] T. Tanase, Y. Kato, I. Mito, M. Yamaguchi, K. Nishi, K. Kobayashi, and R. Lang, "1.3 μm InGaAsP/InP multiquantum-well laser grown by vapour-phase epitaxy", *Electron. Lett. vol. 19, pp. 700-701, 1983.*

[6] N. K. Dutta, T. Wessel, N. A. Olsson, R. A. Logan, R. Yen and P. J. Anthony,"Fabrication and performance characteristics of InGaAsP ridge waveguide distributed-feedback multiquantum-well lasers," *Electron. Lett., vol. 21, pp. 571-573, 1985.*

[7] C. A. Zmudzinski, P. S. Zory, G. G. Lim, L. M. Miller, K. J. Beernink, T. L. Cockerill, J. J. Coleman, C. S. Hong and L. Figueroa,"Differential gain in Bulk and Quantum well diode lasers", *IEEE Photon. Technol. Lett., vol. 3, pp. 1057-1060, 1991.*

[8] I. Suemune, L. A. Coldren, M. Yamanishi and Y. Kan,"Extremely wide modulation bandwidth in a low threshold current strained quantum well laser," *Appl. Phys. Lett., vol. 53, pp. 1378-1380. 1988.*

[9] T. Chen, B. Zhao, Y. H. Zhuang, A. Yariv, J. E. Ungar and S. Oh, "Ultra low threshold strained layer multiquantum well InGaAs lasers", *Appl. Phys. Lett., vol. 60, pp. 1782-1784, 1992.*

[10] P. L. Derry, H. E. Hager, K. C. Chiu, D. J. Booher, E. C. Miao and C. S. Hong, "Low threshold current high-temperature operation of InGaAs/AlGaAs strained quantum well lasers", *IEEE Photon. Technol. Lett., vol. 4, pp. 1189-1191, 1992.*

[11] S. J. Wang, Y. Twu, T. Tanbun-ek, R. A. Logan, N. K. Dutta, A. B. Piccirilli, "Narrow linewidth strained layer 1.5μm multiquantum well distributed feedback lasers", *Electron. Lett., vol. 27, pp. 645-646, 1991.*

[12] E. Meland, R. Holmstrom, J. Schlafer, R. B. Lauer and W. Powazinik,"Extremely high frequency (24 GHz) InGaAsP diode lasers with

excellent modulation efficiency", *Electron. Lett., vol. 26, pp. 1827-1829, 1990.*

[13] R. T. Huang, D. Wolf, W. H. Cheng, C. L. Jiang, R. Aggrawal, D. Renner, A. Mar and J. E. Bower, "High speed, low threshold InGaAsP semi-insulating buried crescent lasers with 22 GHz bandwidth", *IEEE Photon. Technol. Lett., vol. 4, pp. 293-294, 1992.*

[14] K. Y. Lau, S. Xin, W. I. Wang, N. Bar-Chaim and M. Mittelstein,"Enhancement of modulation bandwidth in InGaAs strained-layer single quantum well lasers", *Appl. Phys. Lett., vol. 55, pp. 1173-1175, 1989.*

[15] Y. Arakawa and T. Takahashi, "Effect of nonlinear gain on modulation dynamics in quantum well lasers", *Electron. Lett., vol. 25, pp. 169-170, 1989.*

[16] Y. Arakawa and T. Takahashi, "Nonlinear gain effects in quantum well, quantum well wire and quantum well box lasers", *IEEE J. Quantum Electron., vol QE-27, pp. 1824-1829, 1991.*

[17] A. Ghiti and E. P. O'Reilly, "Non-linear gain effects in strained-layer lasers", *Electron. Lett., vol. 26, pp. 1978-1980, 1990.*

[18] H. Hirayama, J. Yoshida, Y. Miyake and M. Asada,"Estimation of carrier capture time of quantum-well lasers by spontaneous emission spectra", *Appl. Phys. Lett., vol. 61, pp. 2398-2400, 1992.*

[19] B. Deveaud, J. Shah, T. C. Damen and W. T. Tsang, " Capture of electrons and holes in quantum wells" *Appl. Phys. Lett., vol. 52, pp. 1886-1890, 1988.*

[20] S. Morin, B. Deveaud, F. Clerot, K. Fujiwara and K. Mitsunaga,"Capture of photonexcited carriers in a single quantum well with diffferent confinement structure ", *IEEE J. Quantum Electron., vol. 27, pp. 1669, 1991.*

[21] J. A. Brum, G. Bastard,"Resonant carrier capture by semiconductor quantum wells", *Phys. Rev., vol. B33, pp. 1420-1423, 1986.*

[22] H. Schneider and K. V. Klitzing,"Thermionic emission and Gaussian transport of holes in a $GaAs/Al_xGa_{1-x}As$ multiple-quantum-well structure",*Phys. Rev., vol. B38, pp. 6160-6165,1988.*

[23] R. Nagarajan, T. Fukushima, S. W. Corzine and J. E. Bowers,"Effects of carrier transport on high-speed quantum well lasers", *Appl. Phys. Lett., vol. 59, pp. 1835-1837, 1991.*

[24] R. Nagarajan, T. Fukushima, M. Ishikawa, J. E. Bowers, R. S. Geels and L. A. Coldren,"Transport limits in high-speed quantum-well lasers : experiment and theory", *IEEE Photon. Technol. Lett., vol 4, pp. 121-123, 1992.*

[25] W. Rideout, W. F. Sharfin, E. S. Koteles, M. O. Vassell and B. Elman,"Well-barrier burning in quantum well lasers", *IEEE Photon. Technol. Lett., vol. 3, pp. 784-786, 1991.*

[26] T. C. Wu, S. C. Kan, D Vassilovski, K. Y. Lau, C. E. Zah, B. Pathak and T. P. Lee,"Gain compression in tensile-strained 1.55 μm quantum well lasers operating at first and second quantised states", *Appl. Phys. Lett., vol. 60, pp. 1794-1796, 1992.*

[27] S. C. Kan, D. Vassilovski, T. C. Wu and K. Y. Lau,"On the effects of carrier diffusion and quantum capture in high speed modulation of quantum well lasers", *Appl. Phys. Lett., vol. 61, pp. 752-753, 1992.*

[28] S. C. Kan, D. Vassilovski, T. C. Wu and K. Y. Lau,"Quantum capture and escape in quantum-well lasers - implications on direct modulation bandwidth limitations",*IEEE Photon. Technol. Lett., vol. 4, pp. 428-431, 1992.*

[29] R. Nagarajan, M. Ishikawa and J. E. Bowers, "Effects of carrier transport on relative intensity noise and critique of K factor predictions of modulation response", *Electron. Lett., vol. 28, pp. 846, 1992.*

[30] K. Kikuchi and T. Okoshi,"Measurement of FM noise, AM noise, and field spectra of 1.3 μm InGaAsP lasers and determination of the linewidth enhancement factor", *IEEE J. Quantum Electron., vol. QE-21, pp. 1814-1818, 1985.*

[31] K. Uomi, "Modulation-doped multi-quantum well (MD-MQW) lasers. I. Theory", *Japanese J. Appl. Phys., vol. 29, pp. 81-87, 1990.*

[32] P.A. Morton, R.A. Logan, T. Tanbun-Ek, P.F.Sciortino Jr., A.M. Sergent, R.K. Montgomery and B.T. Lee, "25 GHz bandwidth 1.55 μm GaInAsP p-doped strained multiquantum-well lasers", *Electron Lett., vol. 28, pp. 2156-2157, 1992.*

[33] S. Weisser, J.D. Ralston, E.C. Larkins, I. Esquivias, P.J. Tasker, J. Fleissner and J. Rosenzweig, "Efficient high-speed direct modulation in p-doped $In_{0.35}Ga_{0.65}As/GaAs$ multiquantum well lasers", *Electron. Lett., vol. 28, pp. 2141-2143, 1992.*

Chapter 6

Non-linear distortions

6.1 Introduction

Frequency division multiplexing (FDM) is the multiplexing technique for most Subcarrier Multiplexed (SCM) lightwave communication systems, such as BSN (Broadband Service Network) [1] and CATV (Community Antenna Television) [2] systems, due to its flexibility and cost effectiveness. When a FDM multi-channel signal directly modulates a non-linear device such as a laser diode, the output optical signal contains not only the original frequency components but also the sums and differences between the original frequencies. This results in so called *non-linear distortions* which manifest themselves as noise and limit the performance of the lightwave system. The term non-linear distortions should be understood to include both harmonic distortion (HD) and intermodulation distortion (IMD).

The physical origins of these non-linear distortions can be classified into two categories depending upon their frequency of operation. At high frequencies ($f > f_o/2$), the distortions are mainly due to the resonant effect of the interaction

between photons and electrons – relaxation oscillation (RO) of the laser. For low frequency discussion ($f < f_o/2$), there has been suggestions that the spatial hole burning (SHB) in DFB lasers [3, 4, 5] and leakage current [6, 7] effects could be such mechanisms. In general, the non-linear distortions at high frequencies are usually much more serious when compared to the distortion level in the low frequency regime. Therefore, a SCM-BSN broadband distribution system operating up to microwave frequencies requires a careful consideration of the non-linear distortions due to the RO. However, a baseband AM-VSB CATV system at a frequency range of 50-500 MHz may suffer from the non-linear distortions due to SHB and current leakage.

In order to analyse the non-linear distortions generated by a laser diode, the pair of rate equations given by Eqn (2.1) can be used. Several methods are available for calculating the non-linear distortions, including :

(i) perturbation technique [8];

(ii) Volterra series [9]; and

(iii) Bessel function [10]

Qualitatively, with appropriate modification in method (iii), there is little difference between the results obtained by the above methods [11]. Both the perturbation and Volterra series approaches have been used in the present work to provide a double-checking facility in the numerical calculations. In fact, these two methods are quite similar, however, the Volterra series has the advantage of being capable of handling the calculations on a more general basis. Furthermore, it is particularly useful in dealing with cascaded non-linear systems which will be seen to be of use in in Chapter 7 in the analysis of the combined effect of SHB

and leakage current.

In this chapter, the basic terminologies and the fundamentals of frequency planning by counting the number of non-linear distortion terms will be given. This is followed by a brief description of the two different approaches – the perturbation method and Volterra series approach, used for calculating the intrinsic non-linear distortions for a laser diode. Finally, the discussions will concentrate on the RO induced non-linear distortions generated in the high frequency regime.

6.2 Basic terminologies and distortion terms counting

Considering the following set of equal-amplitude FDM multi-carrier (or multi-tone) signals as the input to a laser diode, that is,

$$\sum_{J=L}^{M} cos(J\ 2\pi f_c t)$$

where the carriers are separated by equal frequency increments of f_c beginning at Lf_c and ending at Mf_c with J and M as integers. Then in addition to the original carrier components, the output will consist of sum and difference frequencies of the original carrier components. The nth multiple of a particular carrier frequency is referred as nth order harmonic distortion (HDn); while the sums and differences between n carriers is the nth order intermodulation distortion (IMDn) as seen in Table 6.1 and 6.2. The complete set of second-order non-linear distortion, including both second harmonic (HD2) and second-order intermodulation products (IMD2), is sometimes referred as composite second-order (CSO) distortion. Similarly, the complete set of third-order non-linear distortion terms (HD3 and IMD3) is also called composite triple beat (CTB). In practice, the measurement

Frequency term	Distortion type	Number of terms
$2f_1$	Harmonic	1 if J/2 = integer
$f_1 + f_2$	Intermodulation	$Int(J+\frac{1}{2}) - L$ $(2L-1 \leq J \leq L+M)$
$f_1 - f_2$	Intermodulation	$M - L + 1$ $(0 < J < M - L + 1)$

Table 6.1: *Second order non-linear distortions (CSO) formed by a set of carrier with frequencies* $Lf_c, (L+1)f_c, \cdots, Mf_c$, *where L,J and M are integers.* f_1 *and* f_2 *are the arbitrary carriers fall within the carrier set.*

of all distortion products is always done with respect to the carrier components, hence the unit of 'dBc' (dB carrier) is often used.

The formulae in the last column of Tables 6.1 and 6.2 are for counting the number of distortion terms of particular frequency products [12]. These formulae have also been checked by a computer simulation program. The following interesting features concerning the distribution of the distortion terms can be observed from these formulae.

- if $L < M/2$, ie. carriers lie within one octave of the bandwidth, then no second-order distortion terms exists and leaves only the third-order terms;
- if $L < M/3$, ie. carriers lie within two octaves of the bandwidth, then no $f_1 + f_2 + f_3$ and $f_1 - f_2 - f_3$ type of distortion occurs;
- for channel number $J < 3L$, the $f_1 + f_2 + f_3$ and $2f_1 + f_2$ (two-tone third-

Frequency term	Distortion type	Number of terms
$3f_1$	Harmonic	1 if J/3 = integer
$2f_1 + f_2$	Intermodulation	$Int(\frac{J-L}{2}) - Int(\frac{J-1}{3}) - L + 1$ for $3L < J < 2L + 2M$
$2f_1 - f_2$	Intermodulation	$Int(\frac{M-J}{2}) + Int(\frac{J-L}{2})$ for $L \leq J \leq M$
$f_1 - 2f_2$	Intermodulation	$Int(\frac{M-J}{2}) - L + 1$ for $0 < J < M - 2L \text{and} M > 2L$
$f_1 + f_2 - f_3$	Intermodulation	$Int(\frac{J-L}{2}) \cdot Int(\frac{J-L-1}{2})$ $+(J - L) \cdot (M - J)$ $+Int(\frac{M-J}{2}) \cdot Int(\frac{M-J-1}{2})$ for $L \leq J \leq M$
$f_1 - f_2 - f_3$	Intermodulation	$Int(\frac{M-2L-J+1}{2}) \cdot IntM - 2L - J2$ for $0 < J < M - 2L - 1 \text{and} M \geq 2L + 1$
$f_1 + f_2 + f_3$	Intermodulation	$Int(\frac{3M-J+3}{6}) + Int(\frac{(3M-J-1)}{12})$ for $L + 2M - 1 \leq J \leq 3M - 3$

Table 6.2: *Third order non-linear distortions (CTB) form by a set of carrier with frequencies* $Lf_c, (L + 1)f_c, \cdots, Mf_c$, *where L,J and M are integers.* f_1, f_2 *and* f_3 *are the arbitrary carriers fall within the carrier set.*

order) terms will not occur;

- for channel number $J > M - 2L$, the $f_1 - f_2 - f_3$ and $f_1 - f_2$ terms are eliminated;

6.2.1 System examples

Consider the following two different types of SCM multi-channel systems :

(i) 60 FM video channels equally spaced over 2.4 to 4.8 GHz; and

(ii) 40 AM-VSB video channels equally spaced over 50 to 550 MHz similar to the operation of a CATV system.

Figure 6.1 shows the plots of the number of second-order and third order intermodulation distortions products, ie. IMD3, for the 60 FM channels SCM system operating in the 2.4-4.8 GHz band. The number of the dominant $f_1 + f_2 - f_3$ type IMD3 peaks at the band centre. Since the frequency band is occupied within one octave of bandwidth and thus no IMD2 terms exists.

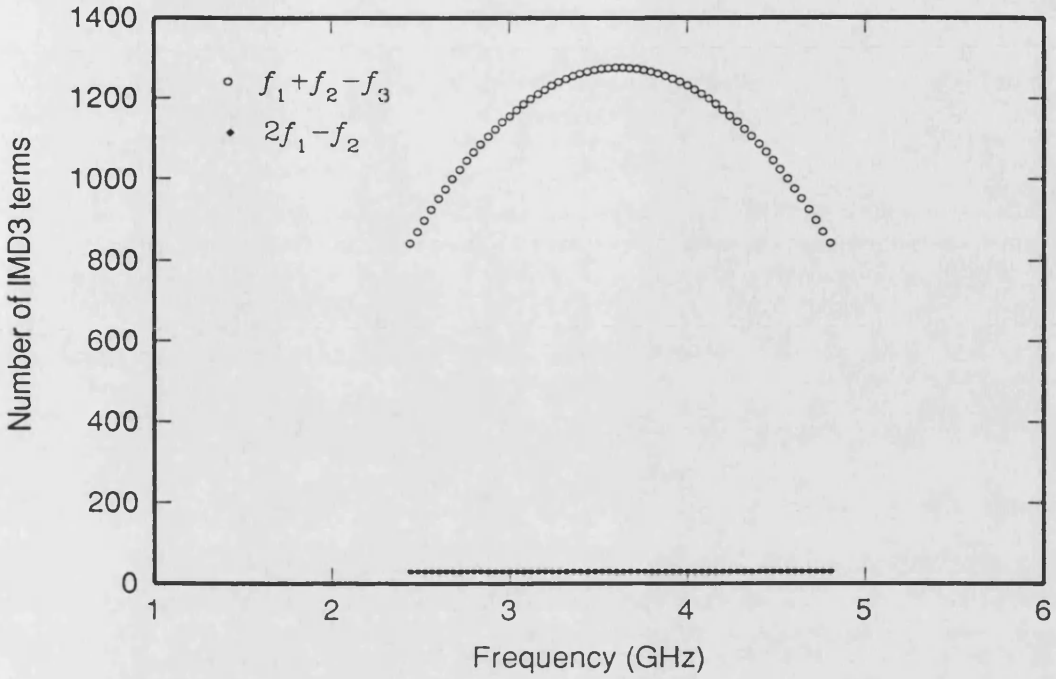

Figure 6.1: *The number of IMD3 terms is plotted against frequency for a 60 video channel FM SCM system.*

On the other hand, Figures 6.2 and 6.3 illustrate the number of IMD2 and IMD3 terms for the 40 AM-VSB channels SCM system equally spaced in the 50-550 MHz frequency range. A large number of IMD2 is present within the signal bandwidth and the maximum number of IMD2 appears at the band edges. The number of $f_1 + f_2 - f_3$ term is still dominant, though there exists a considerable number of other IMD3 terms, such as $f_1 - f_2 - f_3$ and $f_1 + f_2 + f_3$, which peak at the edges of the frequency span.

Therefore, the number of different distortion terms depends strongly on the frequency spectrum planning of a FDM system. This number will certainly affect the performance of a system, since the actual distortion level for a particular frequency term is given by :

$$10\ log_{10}(\text{no. of terms}) + \text{the amplitude of a particular distortion term}$$

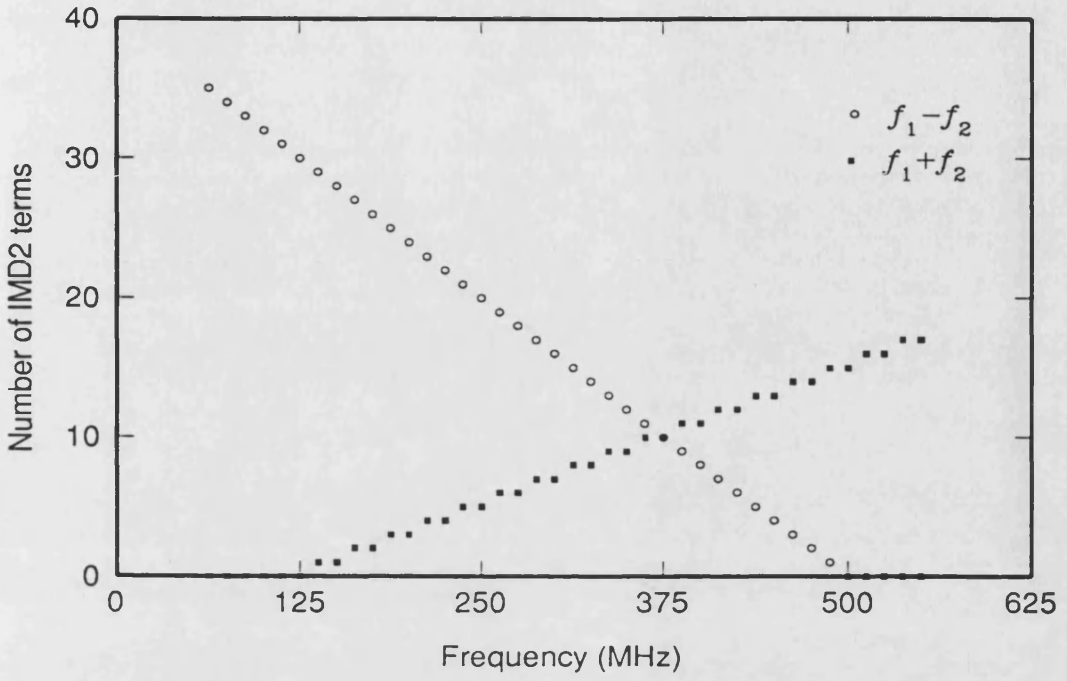

Figure 6.2: *The number of IMD2 terms is plotted against frequency for a 40 channel AM-VSB SCM system.*

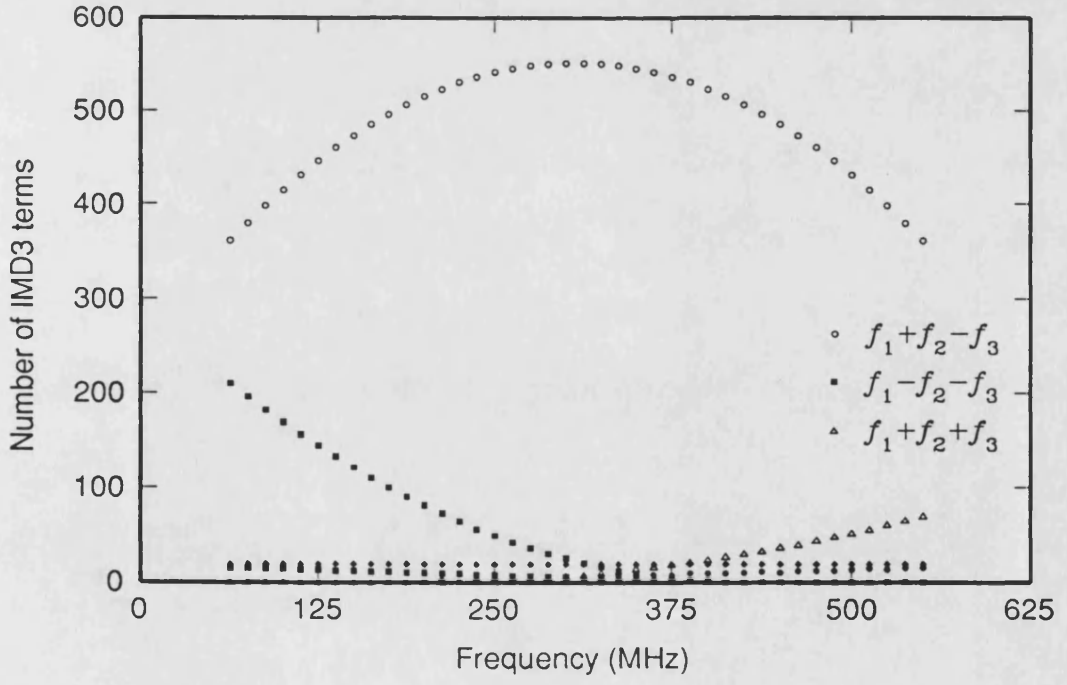

Figure 6.3: *The number of IMD3 terms is plotted against frequency for a 40 channel AM-VSB SCM system.*

For example, consider the previously mentioned 60 channel FM SCM system, the received FM signal usually requires at least a carrier-to-noise ratio (CNR) of 16-17 dB in order to give an acceptable signal-to-noise ratio (SNR) of 56 dB. The non-linear distortions are thus regarded as one kind of noise which degrades the system performance. Since no second-order non-linear distortions occur, this leaves only the dominant $f_1 + f_2 - f_3$ type of third-order distortions. The worst case of 1,276 $f_1 + f_2 - f_3$ distortion terms occurs at the mid-band channel of the upconverted frequency band and this corresponds to a rise of $10\log(1,276) = 31$ dB of the amplitude of a single $f_1 + f_2 - f_3$ distortion term. Assuming a margin of 10 dB for other noise sources, this restricts the amplitude of individual $f_1 + f_2 - f_3$ distortion to be no more than $-17 - 31 - 10 = -58$ dBc.

So far only the number of the distortion products has been considered, as illustrated above the magnitude of each individual distortion term should also be taken into account. The amplitude of the intrinsic distortion for a directly modulated laser diode can be calculated by using a rate equations analysis. This is treated in the next two sections.

6.3 Perturbation method

This method was first introduced into the analysis of laser diodes by K. Lau and A. Yariv [8]. By applying a small signal analysis technique to a pair of single mode rate equations Eqn (2.1) and expanding the parameters G, τ_e and R_{sp} in Taylor's series as shown in Appendix A, the following non-linear differential equations are obtained when terms higher than third-order are neglected :

$$\frac{d\delta n}{dt} = \frac{\delta i}{eV} + k_A \delta n + k_B \delta p + X_{NN}\delta n^2 + X_{PP}\delta p^2 + X_{NP}\delta n \delta p \qquad (6.1)$$

$$+X_{NNN}\delta n^3 + X_{PPP}\delta p^3 + X_{NNP}\delta n^2\delta p + X_{PPN}\delta p^2\delta n$$

$$\frac{d\delta p}{dt} = k_C\delta n + k_D\delta p + Y_{NN}\delta n^2 + Y_{PP}\delta p^2 + Y_{NP}\delta n\delta p \tag{6.2}$$

$$+Y_{NNN}\delta n^3 + Y_{PPP}\delta p^3 + Y_{NNP}\delta n^2\delta p + Y_{PPN}\delta p^2\delta n$$

The coefficients $k_A, k_B, k_C, k_D, X_{NN}, Y_{NN}, X_{NP}, Y_{NP}, \cdots$ are functions of the steady state photon density P and material parameters such as linear differential gain A_o, photon lifetime τ_p, gain suppression ϵ etc. Detailed expressions are given in Appendix A.

In order to obtain the magnitude of the frequency components for $f_1 \pm f_2 \pm f_3$ type IMD3, it is assumed that a small modulation current with three different carriers f_1, f_2 and f_3 (three tones), is applied to the laser. Hence,

$$\begin{aligned}\delta i &= Re\{\delta i^{\omega_1}e^{j\omega_1 t} + \delta i^{\omega_2}e^{j\omega_2 t} + \delta i^{\omega_3}e^{j\omega_3 t}\} \\ &= \frac{1}{2}[\delta i^{\omega_1}e^{j\omega_1 t} + (\delta i^{\omega_1})^* e^{-j\omega_1 t} + \delta i^{\omega_2}e^{j\omega_2 t} + (\delta i^{\omega_2})^* e^{-j\omega_2 t} \\ &\quad +\delta i^{\omega_3}e^{j\omega_3 t} + (\delta i^{\omega_3})^* e^{-j\omega_3 t}]\end{aligned}$$

where $\omega_n = 2\pi f_n$. Due to the non-linear nature of the rate equations, the perturbation quantities δn and δp will contain non-linear distortion terms and are given by :

$$\delta n^\omega = \frac{\mathcal{X}(\omega)(j\omega - k_D) + k_B\mathcal{Y}(\omega)}{\omega_o^2} H_{int}(\omega) \tag{6.3}$$

$$\delta p^\omega = \frac{\mathcal{Y}(\omega)(j\omega - k_A) + k_C\mathcal{X}(\omega)}{\omega_o^2} H_{int}(\omega) \tag{6.4}$$

where the driving terms $\mathcal{X}(\omega)$ and $\mathcal{Y}(\omega)$ for different distortion terms are given in Table 6.3.

ω	$\mathcal{X}(\omega)$
$\omega_1, \omega_2, \omega_3$	$\frac{\delta i^\omega}{eV}$
$2\omega_1, 2\omega_2, 2\omega_3$	$\frac{1}{2}\left[(\delta n^\omega)^2 X_{NN} + (\delta p^\omega)^2 X_{PP} + \delta n^\omega \delta p^\omega X_{NP}\right]$
$\omega_1 + \omega_2$	$\delta n^{\omega_1}\delta n^{\omega_2} X_{NN} + \delta p^{\omega_1}\delta p^{\omega_2} X_{PP} + \frac{1}{2} X_{NP}\left[\delta n^{\omega_1}\delta p^{\omega_2} + \delta p^{\omega_1}\delta n^{\omega_2}\right]$
$\omega_1 - \omega_2$	$\delta n^{\omega_1}(\delta n^{\omega_2})^* X_{NN} + \delta p^{\omega_1}(\delta p^{\omega_2})^* X_{PP}$ $+\frac{1}{2} X_{NP}\left[\delta n^{\omega_1}(\delta p^{\omega_2})^* + \delta p^{\omega_1}(\delta n^{\omega_2})^*\right]$
$3\omega_1, 3\omega_2, 3\omega_3$	$\delta n^\omega \delta n^{2\omega} X_{NN} + \delta p^\omega \delta p^{2\omega} X_{PP} + \frac{1}{2} X_{NP}\left[\delta n^{2\omega}\delta p^\omega + \delta p^{2\omega}\delta n^\omega\right]$ $+\frac{1}{4}\left[(\delta n^\omega)^3 X_{NNN} + (\delta p^\omega)^3 X_{PPP} + \delta n^\omega(\delta p^\omega)^2 X_{NPP} + \delta p^\omega(\delta n^\omega)^2 X_{NNP}\right]$
$2\omega_2 - \omega_1$	$\left[\delta n^{\omega_2-\omega_1}\delta n^{\omega_2} + \delta n^{2\omega_2}(\delta n^{\omega_1})^*\right] X_{NN}$ $+\left[\delta p^{\omega_2-\omega_1}\delta p^{\omega_2} + \delta p^{2\omega_2}(\delta p^{\omega_1})^*\right] X_{PP}$ $+\left[\delta n^{\omega_2-\omega_1}\delta p^{\omega_2} + \delta p^{\omega_2-\omega_1}\delta n^{\omega_2} + \delta n^{2\omega_2}(\delta p^{\omega_1})^* + \delta p^{2\omega_2}(\delta n^{\omega_1})^*\right] X_{NP}$ $+\frac{3}{4}\left[(\delta n^{\omega_2})^2(\delta n^{\omega_1})^* X_{NNN} + (\delta p^{\omega_2})^2(\delta p^{\omega_1})^* X_{PPP}\right]$ $+\frac{1}{4}\left[2\delta p^{\omega_2}\delta n^{\omega_2}(\delta p^{\omega_1})^* + (\delta p^{\omega_2})^2(\delta n^{\omega_1})^*\right] X_{PPN}$ $+\frac{1}{4}\left[2\delta n^{\omega_2}\delta p^{\omega_2}(\delta n^{\omega_1})^* + (\delta n^{\omega_2})^2(\delta p^{\omega_1})^*\right] X_{NNP}$
$\omega_1 + \omega_2 - \omega_3$	$\left[\delta n^{\omega_2-\omega_3}\delta n^{\omega_1} + \delta n^{\omega_1+\omega_2}(\delta n^{\omega_3})^* + \delta n^{\omega_1-\omega_3}\delta n^{\omega_2}\right] X_{NN}$ $+\left[\delta p^{\omega_2-\omega_3}\delta p^{\omega_1} + \delta p^{\omega_1+\omega_2}(\delta p^{\omega_3})^* + \delta p^{\omega_1-\omega_3}\delta p^{\omega_2}\right] X_{PP}$ $+\left[\delta p^{\omega_2-\omega_3}\delta n^{\omega_1} + \delta n^{\omega_1-\omega_3}\delta p^{\omega_2} + \delta n^{\omega_2-\omega_3}\delta p^{\omega_1}\right.$ $\left.+\delta p^{\omega_1-\omega_3}\delta n^{\omega_2} + \delta p^{\omega_1+\omega_2}(\delta n^{\omega_3})^* + \delta n^{\omega_1+\omega_2}(\delta p^{\omega_3})^*\right] X_{NP}$ $+\frac{3}{2}\left[\delta n^{\omega_1}\delta n^{\omega_2}(\delta n^{\omega_3})^* X_{NNN} + \delta p^{\omega_1}\delta p^{\omega_2}(\delta p^{\omega_3})^* X_{PPP}\right]$ $+\frac{1}{2}\left[2\delta p^{\omega_1}\delta n^{\omega_2}(\delta p^{\omega_3})^* + 2\delta p^{\omega_2}\delta n^{\omega_1}(\delta p^{\omega_3})^* + 2\delta p^{\omega_1}\delta p^{\omega_2}(\delta n^{\omega_3})^*\right] X_{PPN}$ $+\frac{1}{2}\left[2\delta n^{\omega_1}\delta p^{\omega_2}(\delta n^{\omega_3})^* + 2\delta n^{\omega_2}\delta p^{\omega_1}(\delta n^{\omega_3})^* + 2\delta n^{\omega_1}\delta n^{\omega_2}(\delta p^{\omega_3})^*\right] X_{NNP}$

Table 6.3: *Driving term $\mathcal{X}(\omega)$ for Eqn (6.3) and Eqn(6.4). $\mathcal{Y}(\omega)$ is obtained by replacing the corresponding coefficients, $X_{NN}, X_{NP}, X_{PP}, \cdots$ etc with $Y_{NN}, Y_{NP}, Y_{PP}, \cdots$.*

For non-linear distortions in the high frequency regime, ie. $\omega > \omega_o/2$, the following assumptions can be made:

- frequency spacing between ω_1, ω_2 and ω_3 is $\delta\omega \ll \omega_o$; hence $\omega_{av} \approx \omega_1, \omega_2, \omega_3$, where ω_{av} represents an average of the three carrier frequencies.
- the magnitude of the second-order terms is much bigger than the third order terms, for example, $X_{NP}\delta n^{\omega}\delta P^{\omega} \gg X_{NPP}\delta n^{\omega}\delta p^{\omega}\delta p^{\omega}$, therefore, third-order terms can be neglected.
- among the second-order terms, the terms with coefficient X_{NN} is comparatively smaller than the terms with X_{NP} and X_{PP}, and hence is neglected.
- terms with frequency $\delta\omega$ are small enough to neglect.

After some manipulations and simplifications of algebra, the following approximated expressions for the fundamental and distortion components are found to be:

$$\delta p^{\omega_{1,2,3}} \approx \Gamma\frac{\tau_p \delta i^{\omega_{1,2,3}}}{qV} H_{int}(\omega_{av}) \tag{6.5}$$

$$\delta p^{2\omega_{1,2,3}} \approx \frac{\Gamma^2\tau_p^2(j\omega_{av})^2(\frac{\delta i^{\omega_{1,2,3}}}{qV})^2}{\omega_o^2 P} H_{int}(\omega_{av})H_{int}(2\omega_{av}) \tag{6.6}$$

$$\delta p^{\omega_1+\omega_2} \approx \frac{2\Gamma^2\tau_p^2(j\omega_{av})^2(\frac{\delta i^{\omega_1}}{qV})(\frac{\delta i^{\omega_2}}{qV})}{\omega_o^2 P} H_{int}(\omega_{av})H_{int}(2\omega_{av}) \tag{6.7}$$

$$\delta p^{\delta\omega} \approx \frac{\Gamma^2\tau_p^2(j\delta\omega)(\frac{\delta i^{\omega_{av}}}{qV})^2}{\omega_o^2 P} \tag{6.8}$$

$$\delta p^{2\omega_1-\omega_2} \approx \frac{\Gamma^3\tau_p^3(j\omega_{av})^2(\frac{\delta i^{\omega_2}}{qV})^2(\frac{\delta i^{\omega_1}}{qV})^*}{4\omega_o^4P^2}(2\omega_{av}^2-\omega_o^2-j\omega_o^2\omega_{av}\frac{\epsilon}{g_o}) \cdot(H_{int}(\omega_{av}))^3H_{int}(2\omega_{av})(H_{int}(\omega_{av}))^* \quad (6.9)$$

$$\delta p^{\omega_1+\omega_2-\omega_3} \approx \frac{\Gamma^3\tau_p^3(j\omega_{av})^2(\frac{\delta i^{\omega_1}}{qV})(\frac{\delta i^{\omega_2}}{qV})(\frac{\delta i^{\omega_3}}{qV})^*}{2\omega_o^4P^2}(2\omega_{av}^2-\omega_o^2-j\omega_o^2\omega_{av}\frac{\epsilon}{g_o}) \cdot(H_{int}(\omega_{av}))^3H_{int}(2\omega_{av})(H_{int}(\omega_{av}))^* \quad (6.10)$$

$$\delta p^{3\omega_{1,2,3}} \approx \frac{3\Gamma^3\tau_p^3(j\omega_{av})^2(\frac{\delta i^{\omega_{av}}}{qV})^3}{4\omega_o^4P^2}(-2\omega_{av}^2-\omega_o^2-j\omega_o^2\omega_{av}\frac{\epsilon}{g_o}) \cdot(H_{int}(\omega_{av}))^3H_{int}(2\omega_{av})H_{int}(3\omega_{av}) \quad (6.11)$$

Defining the fundamental frequency components $\delta p^{\omega_{1,2,3}}$ as carrier $\mathrm{Cr}^{\omega 1,2,3}$, the optical modulation depth (OMD) can therefore be realised as :

$$\mathrm{OMD}_{1,2,3} = \frac{\mathrm{Cr}^{\omega 1,2,3}}{P} \quad (6.12)$$

Assuming all the three carriers are of the same amplitudes and hence the same modulation depth, the approximated expressions for the intrinsic non-linear distortions (with reference to the carrier Cr) for a laser diode are therefore given by,

$$\frac{\mathrm{HD2}}{\mathrm{Cr}} = \left|\frac{\delta p^{2\omega_{1,2,3}}}{\mathrm{Cr}}\right| = \mathrm{OMD}\frac{\omega_{av}^2}{\omega_o^2}\,|H_{int}(\omega_{av})| \quad (6.13)$$

$$\frac{\mathrm{IMD2}^{(f_1+f_2)}}{\mathrm{Cr}} = \left|\frac{\delta p^{2\omega_1+\omega_2}}{\mathrm{Cr}}\right| = 2\mathrm{OMD}\frac{\omega_{av}^2}{\omega_o^2}\,|H_{int}(\omega_{av})| \quad (6.14)$$

$$\frac{\text{IMD3}^{(f_1+f_2-f_3)}}{\text{Cr}} = \left|\frac{\delta p^{\omega_1+\omega_2-\omega_3}}{\text{Cr}}\right|$$

$$= \text{OMD}^2\left[\left(\frac{\omega_{av}^4}{\omega_o^4} - \frac{1}{2}\frac{\omega_{av}^2}{\omega_o^2}\right)^2 + \left(\frac{\epsilon}{g_o}\frac{\omega_{av}^2}{\omega_o^2}\omega_{av}\right)^2\right]^{1/2}$$

$$\cdot |H_{int}(1\omega_{av})H_{int}(2\omega_{av})| \tag{6.15}$$

$$\frac{\text{IMD3}^{(2f_1-f_2)}}{\text{Cr}} = \left|\frac{\delta p^{2\omega_1-\omega_2}}{\text{Cr}}\right|$$

$$= \frac{1}{2}\text{OMD}^2\left[\left(\frac{\omega_{av}^4}{\omega_o^4} - \frac{1}{2}\frac{\omega_{av}^2}{\omega_o^2}\right)^2 + \left(\frac{\epsilon}{g_o}\frac{\omega_{av}^2}{\omega_o^2}\omega_{av}\right)^2\right]^{1/2}$$

$$\cdot |H_{int}(1\omega_{av})H_{int}(2\omega_{av})| \tag{6.16}$$

$$\frac{\text{HD3}}{\text{Cr}} = \left|\frac{\delta p^{3\omega_{1,2,3}}}{\text{Cr}}\right|$$

$$= \frac{3}{2}\text{OMD}^2\left[\left(\frac{\omega_{av}^4}{\omega_o^4} + \frac{1}{2}\frac{\omega_{av}^2}{\omega_o^2}\right)^2 + \left(\frac{\epsilon}{g_o}\frac{\omega_{av}^2}{\omega_o^2}\omega_{av}\right)^2\right]^{1/2}$$

$$\cdot |H_{int}(2\omega_{av})H_{int}(3\omega_{av})| \tag{6.17}$$

It can be seen that in general the second-order non-linear distortion is proportional to the OMD; while third-order distortion is proportional to $(\text{OMD})^2$. Apparently, by increasing the OMD of a SCM lightwave system, a higher value of CNR can be achieved thus results in better SNR at the receiving end. However, as shown by the above equations, the non-linear distortion of the laser rises accordingly as OMD increases. In addition, a phenomenon called *clipping* [13], which occurs when the instantaneous amplitude of the modulating current falls below the threshold current of the laser diode and shutting the laser off, will also set a limit to the OMD. Practical OMD value for a multi-channel SCM system therefore lies around 2.5% to 6%/carrier [14] depending on the number of channels.

Figure 6.4 shows an example of the numerically calculated frequency dependence of different kinds of intrinsic nonlinear distortions of a laser diode subjected to a three-tone modulation signal with OMD = 2.5%/carrier; a comparison with the above approximated expressions is also shown and it is seen that among the different types of second-order non-linear distortions, the magnitudes of $f_1 - f_2$ (or $\delta\omega$) terms are very small and hence provided justification for the assumption made in deriving the approximated expressions. A 6 dB relationship is always maintained between the following distortion component pairs :

- IMD2 $(f_1 + f_2)$ = HD2 $(2f_{1,2})$ + 6 dB;
- IMD3 $(2f_1 + f_2)$ = HD3 $(3f_{1,2})$ + 6 dB; and
- IMD3 $(f_1 + f_2 - f_3)$ = IMD3 $(2f_1 - f_2)$ + 6 dB.

Further discussions of the functional behaviour of the non-linear distortions will be given in section 6.5. The following section will discuss the Volterra series method which provides a more general and systematic approach for evaluating the intrinsic distortions.

6.4 Volterra series approach

This approach is based on the functional expansion known as Volterra series which was first introduced into non-linear system analysis by Wiener *et al* [15]. Wiener perceived that the output $s(t)$ of a non-linear system can be related to the input $r(t)$ by the following series expansion,

$$s(t) = \sum_{n=1}^{\infty} \int_{-\infty}^{\infty} \cdots \int_{-\infty}^{\infty} H_n(\xi_1, \xi_2, \ldots, \xi_n) \prod_{i=1}^{n} R(\xi_i) e^{j\xi_i t} d\xi_i \qquad (6.18)$$

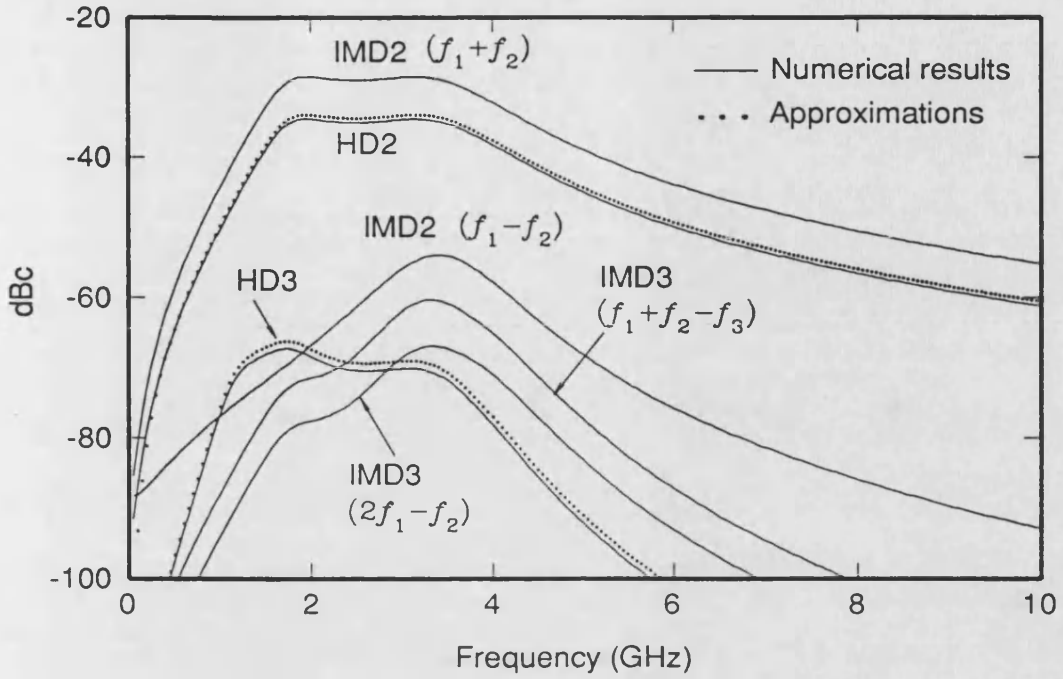

Figure 6.4: *The frequency dependence for various kind of non-linear distortions. OMD = 2.5%/carrier.*

in which $H_n(\xi_1, \xi_2, \ldots, \xi_n)$ are the nth order Volterra kernels (non-linear transfer functions); and $R(\xi)$ is the frequency spectrum (Fourier transform) of the input function in time $r(t)$. The first order Volterra kernel is the linear transfer function or the fundamental frequency response and higher order Volterra kernels are the non-linear transfer functions which generates various kind of non-linear distortion. When this expansion is applied to a small signal modulation regime, only the first few terms are required for an adequate approximation to $r(t)$. The model of a non-linear system for this approach is shown in Figure 6.5, which shows the output structured as the sum of parallelled low-order response.

The main objective is therefore to evaluate the Volterra kernels H_n which can be determined by using a so-called growing exponential approach [15] or probing method [16]. The approach is quite simple though the actual mathematical derivations is relatively complicated as summarised in Appendix B.

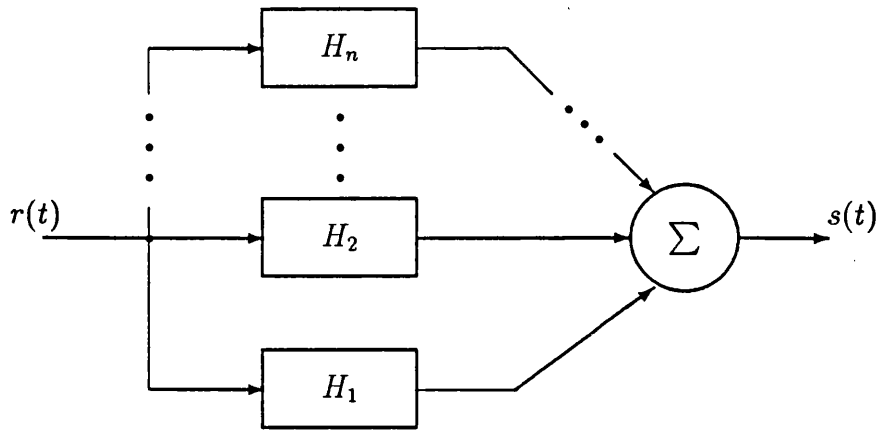

Figure 6.5: *Volterra/Wiener model of a non-linear system.*

In brief, to determine the nth order Volterra kernel, a linear combination of n growing exponentials is applied to the non-linear system,

$$\begin{aligned} r(t) &= \sum_{k=1}^{n} e^{j\omega_k t} \\ &= e^{j\omega_1 t} + e^{j\omega_2 t} + \cdots + e^{j\omega_n t} \end{aligned} \tag{6.19}$$

where $f_n = 2\pi\omega_n$. The corresponding output is the following Volterra series expansion,

$$\begin{aligned} s(t) &= H_1(\omega_1)e^{j\omega_1 t} + H_1(\omega_2)e^{j\omega_2 t} + H_1(\omega_2)e^{j\omega_2 t} \\ &\quad +2!H_2(\omega_1,\omega_2)e^{j(\omega_1+\omega_2)t} + 2!H_2(\omega_2,\omega_3)e^{j(\omega_2+\omega_3)t} \\ &\quad +2!H_2(\omega_1,\omega_3)e^{j(\omega_1+\omega_2)t} + 3!H_3(\omega_1,\omega_2,\omega_3)e^{j(\omega_1+\omega_2+\omega_3)t} \\ &\quad +\cdots \end{aligned} \tag{6.20}$$

Notice that only the essential non-linear transfer functions have been shown. Substituting Eqns (6.19) and (6.20) back into the system equations (rate equations in this case), the coefficient of $e^{(\omega_1+\omega_2+\cdots+\omega_n)t}$ will automatically be $n!H_n(\omega_1,\omega_2,\cdots,f_n)$. Thus all the required Volterra kernels can be found by

comparing the coefficient of $n!e^{j(\omega_1+\omega_2+\cdots\omega_n)t}$ on the both sides of the system equations.

However, if the input is a sum of n real sinusoidal modulating signals, then negative (decaying) exponentials are also involved, that is,

$$r(t) = \frac{1}{2}\sum_{k=1}^{n}(r_k e^{j\omega_k t} + r_k^* e^{-j\omega_k t})$$

with r_k is the magnitude of the modulating signals at frequency f_k where $\omega_k = 2\pi f_k$ and $(\cdot)^*$ denotes complex conjugate. In order to account for the permutation of different frequency terms, the Volterra kernels is then multiplied by a scaling factor for the actual amplitude of a particular type distortion term [16] as outlined in Appendix B.

6.4.1 Volterra kernels of the rate equations

To illustrate the Volterra series approach, the pair of laser diode rate equations Eqn (2.1) is rewritten into one single equation consisting only of the photon density P, (the electron density N is eliminated to avoid an additional Volterra series expansion for N) as given below,

$$\begin{aligned}\frac{I}{qV} &= \frac{d^2P}{dt^2}U(P) + \frac{dP}{dt}W(P) + \left(\frac{dP}{dt}\right)^2 X(P) \\ &\quad + \left(\frac{dP}{dt}\right)^3 Y(P) + Z(P) \qquad (6.21)\end{aligned}$$

where

$$\begin{aligned}U(P) &= \frac{1}{a(P)} \\ W(P) &= \frac{g(P) + A_{nr}}{a(P)} + \frac{b'(P)a(P) - a'(P)b(P) + 2B_r b(P)}{a^2(P)} + \frac{3Cb^2(P)}{a^3(P)} \\ X(P) &= \frac{B_r - a'(P)}{a^2(P)} + \frac{3C_{Auger}b(P)}{a^3(P)}\end{aligned}$$

$$
\begin{aligned}
Y(P) &= \frac{C_{Auger}}{a^3(P)} \\
Z(P) &= -g(P)N_{tr} + \frac{(g(P)+A_{nr})b(P)}{a(P)} + \frac{B_r b^2(P)}{a^2(P)} + \frac{C_{Auger}b^3(P)}{a^3(P)} \\
a(P) &= \Gamma g(P) + \Gamma\beta B_r N_{th} \\
b(P) &= \Gamma g(P)N_{tr} + \gamma_p P \\
g(P) &= \frac{g_o P}{1+\varepsilon P}
\end{aligned}
$$

and $'$ denotes $d(\cdot)/dP$.

A small signal analysis of Eqn (6.21), and then expanding U, W, X, Y and Z using Taylor series similar to that in Appendix A, one obtains in the following equation,

$$
\begin{aligned}
\frac{i}{qV} &= \left[Z'(P)p + W(P)\frac{dp}{dt} + U(P)\frac{d^2p}{dt^2}\right] \\
&\quad + \left[\frac{Z''(P)}{2}p^2 + X(P)\left(\frac{dp}{dt}\right)^2 + W'(P)p\frac{dp}{dt} + U'(P)p\frac{d^2p}{dt^2}\right] \\
&\quad + \left[\frac{Z'''(P)}{6}p^3 + Y(P)\left(\frac{dp}{dt}\right)^3 + X'(P)p\left(\frac{dp}{dt}\right)^2\right. \\
&\quad \left. + \frac{W''(P)}{2}p^2\frac{dp}{dt} + \frac{U''(P)}{2}p^2\frac{d^2p}{dt^2}\right] + \cdots\cdots
\end{aligned}
\tag{6.22}
$$

where small letters, i and p are small perturbations of the current injected input and the optical output respectively (analogy to the input and output time functions r and s mentioned previously). All other coefficients such as, $X(P), X'(P), Y(P), \cdots$ are therefore functions of the steady state photon density P. These coefficients are similar to the $k_A, k_B, \cdots, X_{NN}, Y_{NN} \cdots$ in Section 6.2, except that they are functions of steady state quantities both N and P.

For non-linear distortions up to third-order, the same order of Volterra kernel is needed. This implies a sum of three exponentials is adequate to act as the

probing input, that is,

$$i(t) = e^{j\omega_1 t} + e^{j\omega_2 t} + \cdots + e^{j\omega_n t} \tag{6.23}$$

Substituting the output series Eqn (6.20) and the probing input Eqn (6.23) into the system equation Eqn (6.22) and then equating the coefficients of $e^{j\omega t}$, $e^{j(\omega_1+\omega_2)t}$ and $e^{j(\omega_1+\omega_2+\omega_3)t}$ on the both sides, one can successively obtain the following Volterra kernels up to third-order,

$$H_1(\omega) = \frac{1}{Z'(P_o) + W(P_o)(j\omega) + U(P_o)(j\omega)^2} \tag{6.24}$$

$$H_2(\omega_1,\omega_2) = -\frac{1}{2}H_1(\omega_1)H_1(\omega_2)H_1(\omega_1+\omega_2)E(\omega_1,\omega_2) \tag{6.25}$$

$$\begin{aligned} E(\omega_1,\omega_2) = {} & Z''(P_o) + 2X(P_o)(j\omega_1)(j\omega_2) + W'(P_o)(j\omega_1 + j\omega_2) \\ & + U'(P_o)[(j\omega_1)^2 + (j\omega_2)^2] \end{aligned}$$

$$\begin{aligned} H_3(\omega_1,\omega_2,\omega_3) = {} & -\frac{1}{6}\left\{-4H_2(\omega_2,\omega_3)\frac{H_2(\omega_1,\omega_2+\omega_3)}{H_1(\omega_2+\omega_3)}\right. \\ & -4H_2(\omega_1,\omega_3)\frac{H_2(\omega_2,\omega_1+\omega_3)}{H_1(\omega_1+\omega_3)} \\ & -4H_2(\omega_1,\omega_2)\frac{H_2(\omega_3,\omega_1+\omega_2)}{H_1(\omega_1+\omega_2)} \\ & H_1(\omega_1)H_1(\omega_2)H_1(\omega_3)H_1(\omega_1+\omega_2+\omega_3) \\ & \left.\cdot F(\omega_1,\omega_2,\omega_3)\right\} \end{aligned} \tag{6.26}$$

$$\begin{aligned} F(\omega_1,\omega_2,\omega_3) = {} & Z'''(P_o) + 6(j\omega_1)(j\omega_2)(j\omega_3)Y(P_o) \\ & +2X'(P_o)\ [(j\omega_2)(j\omega_3) + (j\omega_1)(j\omega_3) + (j\omega_1)(j\omega_2)] \\ & +W''(P_o)(j\omega_1 + j\omega_2 + j\omega_3) \\ & +U''(P_o)\left[(j\omega_1)^2 + (j\omega_2)^2 + (j\omega_3)^2\right] \end{aligned}$$

order n	Frequency	Amplitude	Response type
1	f_1	$i_1 H_1(\omega_1)$	Cr
2	$2f_1$	$\frac{1}{2} i_1^2 H_2(\omega_1, \omega_1)$	HD2
2	$f_1 + f_2$	$i_1 i_2 H_2(\omega_1, \omega_2)$	IMD2
3	$2f_1 - f_2$	$\frac{3}{4} i_1^2 i_2^* H_3(\omega_1, \omega_1, -\omega_2)$	IMD3
3	$f_1 + f_2 - f_3$	$\frac{3}{2} i_1 i_2 i_3^* H_3(\omega_1, \omega_2, -\omega_3)$	IMD3
3	$3f_1$	$\frac{1}{4} i_1^3 H_3(\omega_1, \omega_1, \omega_1)$	HD3

Table 6.4: *Amplitudes of the non-linear distortion products.*

Consider an actual three-tone sinusoidal signal input,

$$\begin{aligned} i(t) &= \frac{1}{2}(i_1 e^{j\omega_1 t} + i_1^* e^{-j\omega_1 t} + i_2 e^{j\omega_2 t} + i_2^* e^{-j\omega_2 t} \\ &\quad + i_3 e^{j\omega_3 t} + i_3^* e^{-j\omega_3 t}) \end{aligned} \tag{6.27}$$

where i_1, i_2 and i_3 are the amplitudes of the modulating signal at frequency f_1, f_2 and f_3 respectively. By multiplying the above kernels with the corresponding scaling factor (see Appendix B), the complex amplitudes for different kinds of non-linear distortion are obtained as given in Table 6.4.

In Table 6.4, Cr denotes the carrier components centred at f_1, f_2 and f_3; HDn and IMDn refer to the nth order harmonic and intermodulation distortions respectively. Figure 6.6 depicts graphically the numerical results obtained using the Volterra series approach and by the perturbation method described earlier

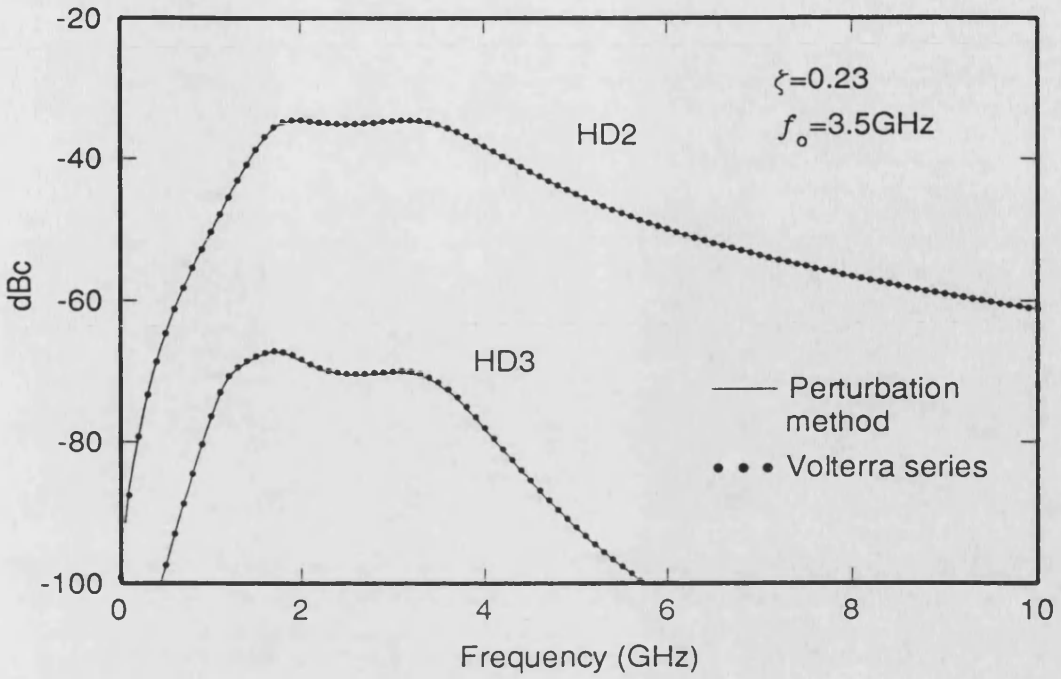

Figure 6.6: *The comparison between the results obtained by perturbation method and Volterra series approach. OMD = 2.5%/carrier*

on. It is clear that both methods agree very well. It is considered, however, that the application Volterra series approach is neater and more systematic than the perturbation method. To summarise, the perturbation method is a relatively quick method in studying system non-linearities while the Volterra series provides a general and systematic approach.

6.5 RO induced non-linear distortions

Regardless of which method is being used for evaluating the non-linear distortions, it is clear from Figures 6.4 and 6.6 that all distortion curves have maxima around the range $f_o/2$ to f_o where f_o is the undamped frequency, and they decrease rapidly with decreasing frequency below $f_o/2$. This confirms that resonance effect – relaxation oscillation (RO) due to the interaction between the electron and

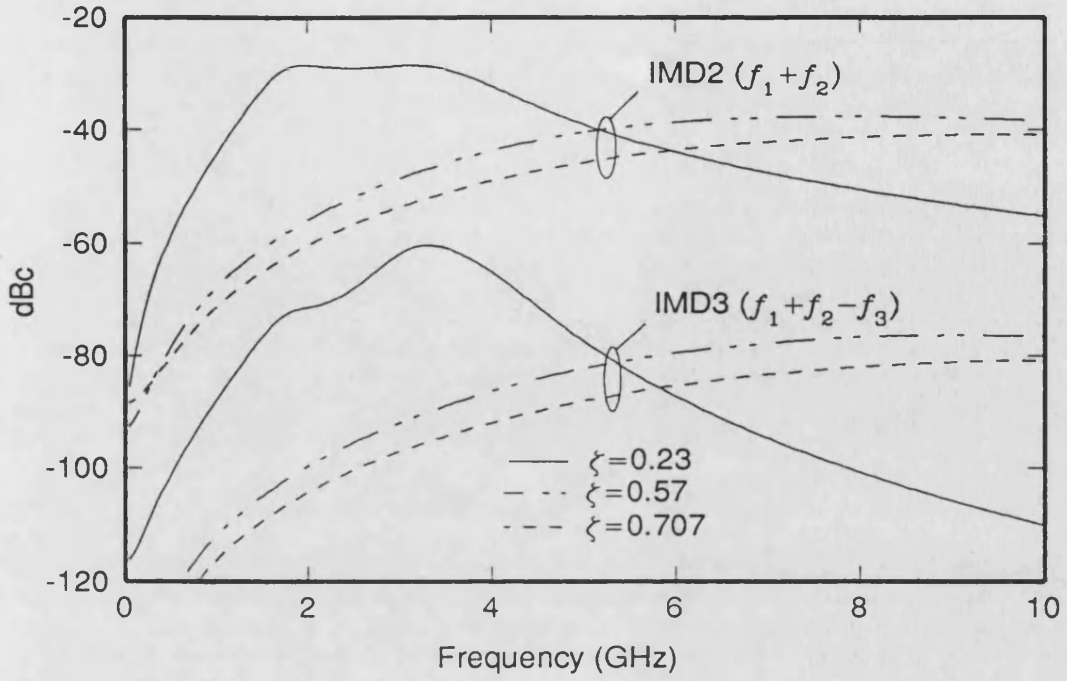

Figure 6.7: *The effect of damping factor ζ on the RO induced non-linear distortions. OMD = 2.5%/carrier.*

photon, is a dominant source of the non-linear distortions. However, as mentioned in Chapter 2, a stronger damping effect can result in suppression of the resonance peak and gives a more piece-wise response. This is also true in regard to the non-linear distortion level at high frequency regime ($f > f_o/2$) as illustrated in Figure 6.7 which shows the distortion level of a laser diode at different damping factor ζ due to increase in bias current. It can be seen that the distortion peaks due to the RO effect reduce as the damping factor ζ increases. Hence, a well-damped laser should exhibit less RO induced distortion.

Nevertheless, when the damping factor ζ goes beyond the optimal value of 0.707, the bandwidth of laser will reduce (see Chapter 2). In fact, when $\zeta > 0.707$, the reduction of the distortion is diminishing. Therefore, the optimal value of $\zeta = 0.707$ is also applicable to the case of minimising the RO induced non-linear distortion.

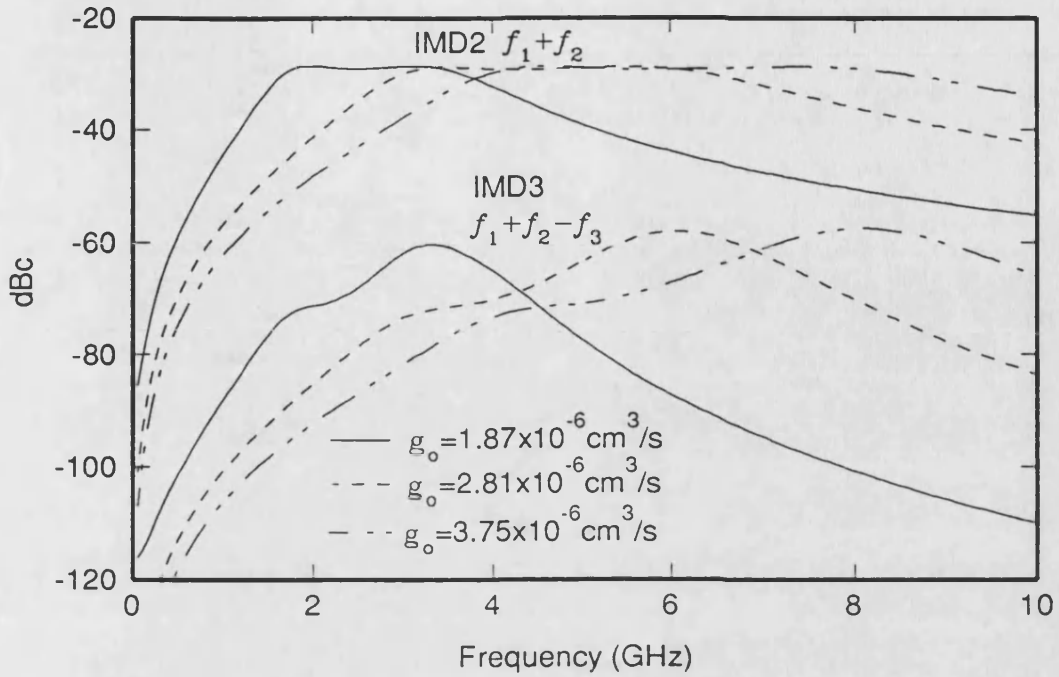

Figure 6.8: *The effect of different g_o on the RO induced non-linear distortions. OMD = 2.5%/carrier. In order to draw the comparison, the ζ value is maintained the same in all cases.*

For the same damping factor ζ, the effect of different gain coefficient g_o on the distortion spectrum is shown in Figure 6.8. As one may expect, the increase of g_o results in an increase of f_o as given by Eqn (2.7), hence, the non-linear distortion for a fixed frequency band decreases.

Modulation format	Required CNR (dB)
AM-VSB	50
FM	16.5-17 for SNR = 56 dB
FSK	15.5 for bit-error rate BER = 10^{-9}
PSK	12.5 for BER = 10^{-9}

Table 6.5: *CNR requirements for different modulation formats of a video signal.*

As may be seen in Figure 6.4 or 6.6, the magnitudes of the second-order non-linear distortions are typically much greater than the third-order counterparts. In a multichannel system, even though the number of second-order distortion terms is much smaller than the third-order ones, the resultant second-order non-linear distortion levels are usually much more serious than the third-order distortions. For instance, for 40 channels spanning across 50 Mz to 2 GHz, the dB difference in a worst case *terms count* between second-order (f_1+f_2)*and third-order distortion $(f_1+f_2-f_3)$ is $10\log(551)-10\log(39) = 12$ dB, while the *magnitude* difference for these two distortion terms is roughly 32 dB for a typical laser diode as depicted in Figure 6.4 (peak of IMD3 to peak of IMD2). Hence, the resultant second-order distortion level is still 20 dB above that of the third-order. Therefore, most SCM systems operating at high frequencies, always confine themselves to one octave of bandwidth, eg. 2.4-4.8 GHz, to eliminate the second-order distortion effects.

Although the distortion levels in the high frequency regime is relatively higher, one can still use this channel for transmitting signals by choosing a modulation format which is much more tolerant of non-linear distortions, for example, FM or even digital carrier modulation schemes FSK, PSK etc., at the expense of a larger bandwidth compared to an AM-VSB system. Table 6.5 shows the theoretical requirement of the CNR [18, 17] for different types of modulation format.

In terms of video signal transmission, the AM-VSB is the present standard for residential video and associated consumer electronics, hence it is attractive for a CATV system. Unlike AM-VSB, the FM format offers high-quality video system and is only currently used in point-to-point satellite and super-trunk links. Conversion from FM to AM-VSB format is required if it is used to reach the subscriber loop as mentioned in Chapter 1.

*$f_1 - f_2$ type has the highest number, however, its amplitude is extremely small and hence may be neglected.

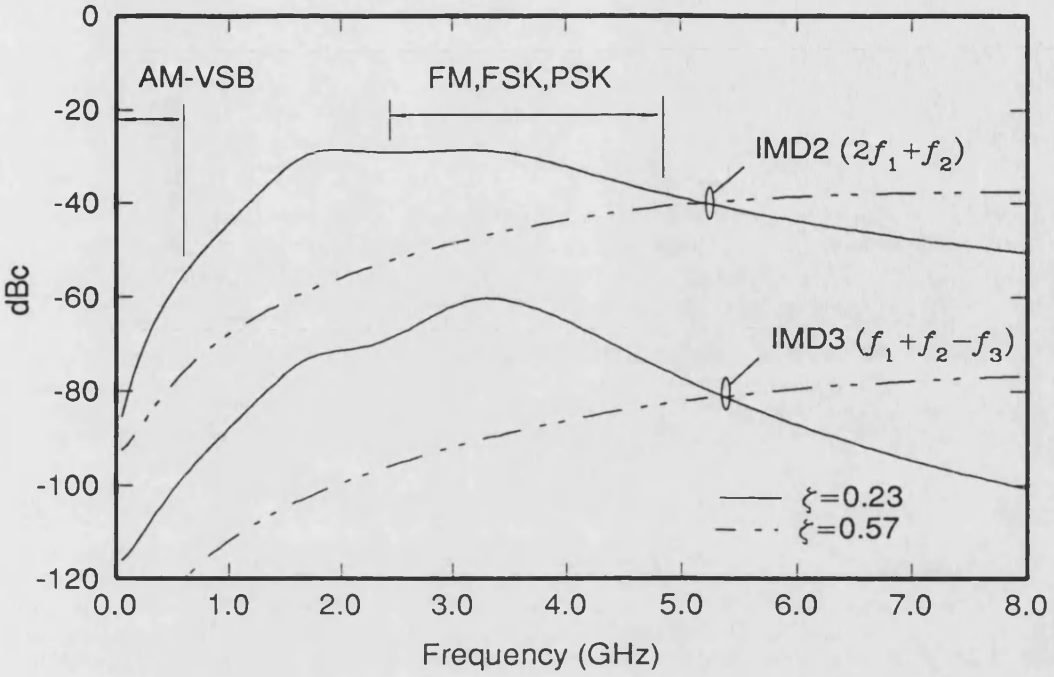

Figure 6.9: *The non-linear distortions of a typical laser diode with OMD = 2.5%/carrier. The possible operating frequency zones for different types of modulation formats are also shown.*

Due to high CNR required for the AM-VSB format, the linearity requirement is very stringent. For example, consider once again the previously mentioned video system with 60 FM channels SCM system, the required distortion level for the dominant $f_1 + f_2 - f_3$ term is -58 dBc. If the modulation format were changed to AM-VSB, then the required distortion level will be -91 dBc. It is almost certain that such a low third-order distortion level imposed by the AM-VSB format is not feasible for typical laser diode parameter values as shown in Figure 6.9. However, at the low end of the frequency spectrum, the linearity of the laser diode seems to improve greatly and can possibly meet this stringent linearity requirements. Therefore, a multi-channel FM SCM system can always utilise the high frequency region; while an AM-VSB multi-channel system is often restricted to the low frequency regime. Table 6.6 illustrates some examples of practical system requirements.

SCM system type	FM Video	AM-VSB CATV
no. of channels	60 × 30 MHz	42 × 6 MHz
Frequency range	2.4-4.8 GHz	50-500 MHz
Maximum terms count $f_1 \pm f_2$ $f_1 \pm f_2 \pm f_3$	 0 1276	 37 641
CNR required (dB)	16.5	50
Linearity requirement (dBc) $f_1 \pm f_2$ $f_1 \pm f_2 \pm f_3$	 – −58	 −74 −88

Table 6.6: *Typical linearity requirements for some practical system.*

Within the low frequency window, several additional non-linear effects must be considered, such as the spatial hole burning of DFB lasers and the leakage current, since these non-linearities may be dominant and can seriously hamper an AM-VSB system operates at that frequency range. These non-linear effects are studied in the next chapter.

6.6 Conclusion

The importance of frequency spectrum planning based on the distortion term count has been demonstrated. In terms of distortion components count, the second-order (f_1+f_2) and third-order $(f_1+f_2-f_3)$ intermodulation products are more numerous. Whilst the number of (f_1+f_2) peaks at high band edges of the FDM frequency band and the $(f_1+f_2-f_3)$ peaks at the middle of the frequency band. By keeping the bandwidth within one frequency octave, second-order non-linear distortion can be eliminated. This technique can be used in a broadband microwave SCM-BSN system.

The number of terms for a particular type of distortions, as well as, its amplitude, are the essential elements for determining the linearity requirements of a system. Two methods – the perturbation method and the Volterra series approach, for calculating the amplitude of different distortion terms have been studied. The Volterra series provides a more general and systematic approach.

The non-linear distortions are usually classified into two categories : high frequency $(f > f_o/2)$ and low frequency $(f < f_o/2)$ distortions. The distortions in the high frequency regime are mainly caused by the relaxation oscillation (RO) and can therefore be controlled by the damping factor ζ. The optimal value

of $\zeta = 0.707$ can be used to minimise the RO induced distortions (as well as providing maximum intrinsic bandwidth). Furthermore, a laser diode with a large differential gain such as QW devices which give a higher f_o are expected to experience a comparatively lower RO induced non-linear distortions.

At high frequencies, the relatively higher level of second-order non-linear distortions with smaller number of terms, is usually more serious than the large number of third-order distortions generated in a multichannel system. Hence, most high frequency SCM systems operate within one octave of bandwidth to eliminate these second-order products.

Because of the presence of RO induced non-linear distortions, the AM-VSB format with a stringent linearity requirement, is often restricted to operate in the low frequency window. On the other hand, SCM systems using other modulation formats, such as FM, PSK, FSK etc., which require relatively low CNR, can operate in the high frequency regime of the laser diode.

References

[1] R. Olshansky, V.A. Lanzisera, P.M. Hill,"Subcarrier multiplexed lightwave systems for broadband distribution", *IEEE Lightwave Technol., vol. 7, pp. 1329-1341, 1989.*

[2] T.E. Darcie, J. Lipson, C.B. Roxlo and C.J. McGrath, " Fiber Optic device for broadband analog video systems", *IEEE LCS Magazine, pp. 46-52, February 1990.*

[3] G. Morthier, F. Libbrecht, K. David, P. Vankwikelberge and G. Baets, "Theoretical investigation of the second-order harmonic distortion in the AM response of 1.55 μm F-P and DFB lasers", *IEEE J. Quantum Electron., vol. QE-27, pp. 1990-2002, 1991.*

[4] H. Kawamura, K. Kamite, H. Yonetani, S. Ogita, H. Soda and H. Ishikawa, "Effect of varying threshold gain on second-order intermodulation distortion in distributed feedback lasers", *Electron. Lett., vol. 26, pp.1720-1721, 1990.*

[5] A. Takemoto, H. Watanabe, Y. Nakajima, Y. Sakakibara, S. Kakimoto, J. Yamashita, T. Hatta and Y. Miyake, "Distributed feedback laser diode and module for CATV system", *IEEE J. Selected Areas in Comm., vol. 8, pp. 1359-1364, 1990.*

[6] S.Y. Huang, L.C. Upadhyayula, J. Lipson, E.L. Flynn and C.B. Roxlo, "Frequency-dependent distortions of composite triple beat in lightwave CATV transmission systems", *IEEE J. Selected Areas in Comm., vol. 8, pp. 1365-1367, 1990.*

[7] M.S. Lin, S.Y.J. Li and N.K. Dutta, "Measurements and modelling of the harmonic distortion in InGaAsP distributed feedback lasers", *IEEE J. Quantum Electron., vol. 26, pp. 998-1004, 1990.*

[8] K. Lau and A. Yariv, "Intermodulation distortion in a directly modulated semiconductor injection laser", *Appl. Phys. Lett., vol. 45, pp. 1034-1036, 1984.*

[9] T.E. Darcie and R.S. Tucker, "Intermodulation and harmonic distortion in InGaAsP lasers", *Electron. Lett., vol. 21, pp. 665-666, 1985.*

[10] M.T. Abuelma'Atti, "Carrier-to-intermodulation performance of multiple FM/FDM carriers through a GaAlAs heterojunction laser diode", *IEEE Trans. on Comm., vol. COM-33, pp. 246-248, 1985.*

[11] J.J. O'Reilly and H.M. Salgado, "Distortion analysis of semiconductor lasers : a caution", *Electron. Lett., vol. 27, pp. 946- 947, 1991.*

[12] J.C. Daly, "Fiber optic intermodulation distortion", *IEEE Trans. on Comm., vol. com-30, pp. 1954-1958, 1982.*

[13] A.A.M.Saleh, "Fundamental limit on the number of channels in subcarrier-multiplexed lightwave systems", *Electron. Lett., vol. 25, pp. 776-777, 1989.*

[14] M.R. Phillips and T.E. Darcie, "Numerical simulation of clipping-induced distortion in analog lightwave systems", *IEEE Photonics Technol. Lett., vol. 3, pp. 1153-1155, 1991.*

[15] W.J. Rugh, "Non-linear system theory : the Volterra/Wiener approach", *The Johns Hopkins University Press, 1981.*

[16] J.J. Bussgang, I. Ehrman and J.W. Graham, "Analysis of nonlinear systems with multiple inputs", *Proc. IEEE, vol. 62, pp. 1088-1119, 1974.*

[17] T.E. Darcie, "Subcarrier multiplexing for lightwave networks and video distribution systems", *IEEE J. Selected Areas in Comm., vol. 8, pp. 1240-1248, 1990.*

[18] W.I. Way, "Subcarrier multiplexed lightwave system design considerations for subscriber loop applications", *IEEE J. Lightwave Technol., vol. 7, pp. 1806-1818, 1989.*

Chapter 7

Low frequency non-linear distortions

7.1 Introduction

At relatively high modulation frequency ($f > f_o/2$), the standard rate-equation model, often predicts that the effect of the relaxation oscillation (RO) dominates the induced non-linear distortions and this agrees well with the experiments [1, 2]. However, at frequencies well below the relaxation frequency ($f < f_o/2$), the standard model often underestimates the non-linear distortions [3, 4]. This implies that other non-linear effects, such as, longitudinal spatial hole burning (SHB) and leakage current effects need to be taken into account.

Distributed feedback (DFB) laser diodes are a favourite candidate among all laser types in the application of optical analogue communications systems, for example, the broadband microwave frequencies (say 2.4-4.8 GHz) SCM and the mid-band (50-500 MHz) multichannel AM-VSB CATV systems. This is because the DFB lasers are capable of offering:

- stable single mode operation;
- less sensitivity to optical reflections in the system – hence exhibits a lower relative intensity noise (RIN) than Fabry-Perot lasers;
- a superior light-current (L-I) linearity than the Fabry Perot devices.

Despite all these merits, many DFB lasers suffer from a well-known detrimental effect called longitudinal spatial hole burning (SHB) which refers to the non-uniform carrier density distribution resulting from a non-uniform photon density along the lasing cavity.

It has been shown [6, 5] that the SHB effect causes a power-dependent loss (or threshold gain) and this represents an extra non-linearity in the device. In consequence the device suffers from additional non-linear distortions [7] which can severely limit the performance of an analogue system. The experimental results in [3] give further evidence that non-linear distortion depends strongly on the DFB κL product (where κ is the coupling coefficient and L is the length of laser diode). These results strongly suggest that SHB is the underlying mechanism for the distortions – varying the κL will directly alter the distribution of photon density along the lasing cavity and hence cause changes in the non-linear distortions.

It is noted that the SHB effect also exists, in principle, in FP (Fabry-Perot) lasers, however, due to the large facet reflectivities, the optical loss is virtually power independent. Thus FP laser diodes would not suffer much from SHB induced non-linear distortions. However, the disadvantage of multi-mode longitudinal mode operation, and high sensitivity to extrinsic optical reflection made the FP lasers less attractive compare to DFB devices for the applications in high quality analogue optical communication systems.

In order to obtain an accurate description of the processes occurring in the active region of the DFB laser, the present analysis includes the effect of a SHB induced power-dependent loss term into the rate-equations model is described in section 2. The consequences of that in terms of the non-linear distortions are given in section 3.

The confinement of current to the active region is also of significance in determining the non-linear properties of the laser. One typical class of index-guided structure is the buried heterostructure in which the active region is surrounded by higher index cladding and blocking layers. A substantial amount of leakage current may flow through these extra layers if the device's layer thickness, doping level or junction placement are not optimised. Such a leakage current may be responsible for increasing threshold current and non-linear distortions. It is possible to model this leakage current effect by using different combinations of active elements, eg. transistors and diodes, for different structures as given in [8].

The leakage current path and its electrical equivalent circuit is structure dependent. For the present purposes, the leakage path for the buried heterostructure and its variants is assumed to be represented by a simple p-n homo-junction diode formed by the p-blocking and n-buffering layers adjacent to the walls of the active region. Such an assumption is quite reasonable for most buried heterostructures as seen in [8]. A brief derivation based on the approach given by M.S. Lin *et al* [9] of the leakage current model is given in section 4.

By using the modified rate-equations model for the active region (section 3) and cascading that with the leakage diode model (section 4), a combined model for non-linearity can be obtained as is demonstrated in section 5. This combined model provides a theoretical predictions for the overall non-linear distortions of

a DFB laser.

7.2 Power-dependent loss due to SHB

DFB laser diodes predominantly oscillate in a single longitudinal mode because of a built-in index grating (corrugation) that provides dominant distributed feedback in the vicinity of Bragg wavelength determined by the grating period. But multi-longitudinal mode operation is sometimes observed due to the lack of control of the corrugation phase during the fabrication process. With the introduction of a quarter-wavelength shift at the centre of a conventional DFB laser, ie. $\lambda/4$ phase-shifted DFB, a more stable single longitudinal mode operation with lasing frequency at Bragg wavelength can be expected [12].

The theoretical threshold behaviour of both DFB and $\lambda/4$ phase-shifted DFB lasers is based on the coupled-wave theory by Kogelnik and Shank [11], which described the light intensity inside the cavity as two coupled travelling waves – forward and backward waves. The coupled-wave equations can be solved analytically to obtain an eigenvalue equation whose solution provides the required gain of the field for overcoming the grating loss – threshold gain, and the wavelength of the lasing mode. In addition, the resultant non-uniform intensity profile in the longitudinal direction is found to be dependent upon the coupling coefficient κ and also the facet power reflectivities r_0 and r_L (subscripts $_0$ and $_L$ stand for the facets at $z = 0$ and L respectively, whilst z is the propagation direction of the waves). This approach is justified since the photon density at threshold is very small, and the corresponding influence on the propagation constants of the travelling waves is negligible.

However, above threshold, such a variation in photon density distribution, often referred as spatial hole burning (SHB), causes a change in the carrier density distribution and thus results in spatial variation of optical gain and also the refractive index which are both functions of carrier density. In order to analysis a DFB laser diode with longitudinal variations of device parameters above threshold, a numerical approach is needed and is described in Appendix C.

In general, as the output optical power of a DFB laser increases, the shape of the intensity profile will change due to the SHB effect as shown in Figure 7.1. In the strong coupling case, ie. $\kappa L = 2.0$ the intensity profile is symmetrical in the longitudinal direction with light concentrated near the centre of the cavity and this leads to a highly non-uniform carrier density distribution.

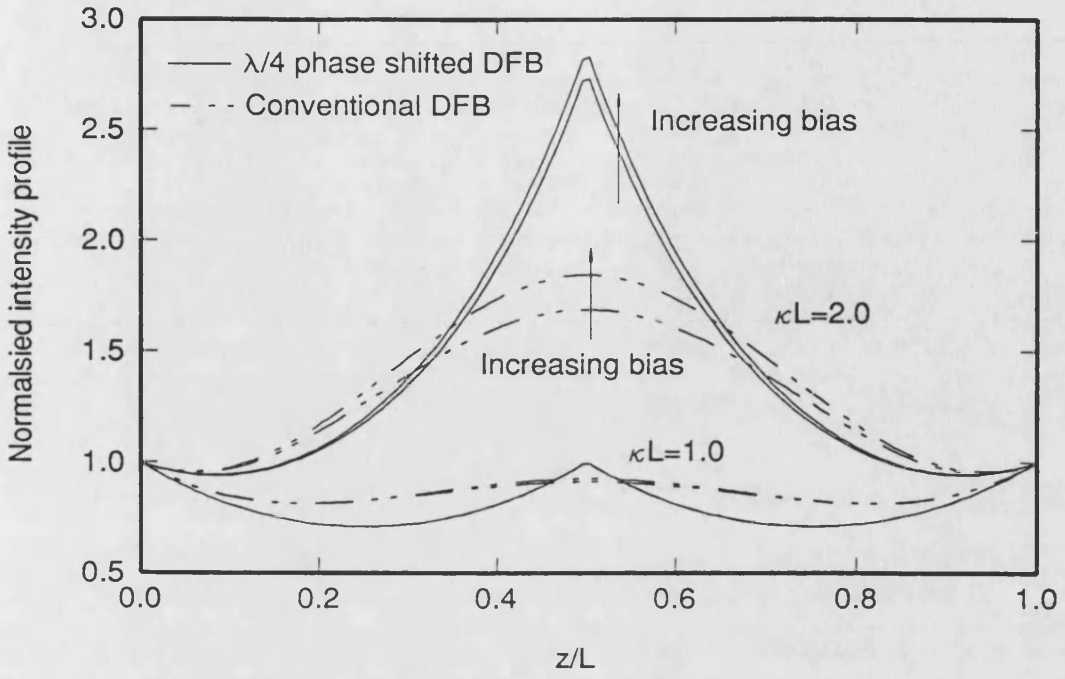

Figure 7.1: *The normalised intensity distributions of conventional DFBs $\lambda/4$ phase-shifted DFBs at different values of κL products. z is the longitudinal direction and L is the length of the device.*

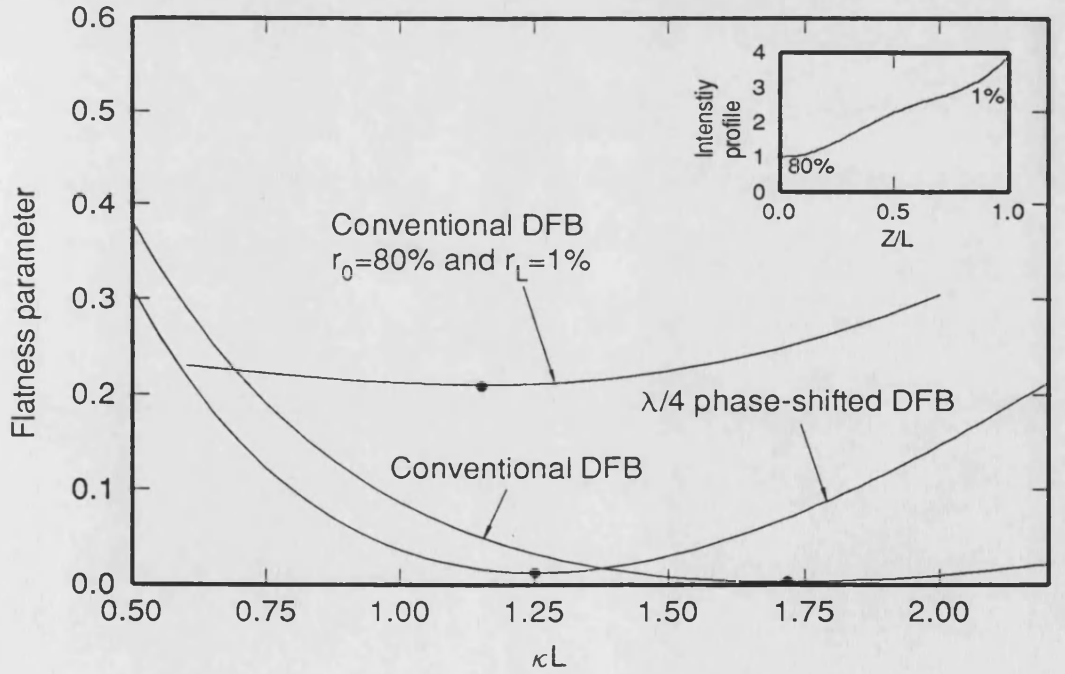

Figure 7.2: *The flatness parameter $\mathcal{F}$ against the κL product for a conventional DFB and $\lambda/4$ phase shifted DFB. Optimal values – values at which $\mathcal{F}$ are minimum, occurred at $\kappa L = 1.7$ and $\kappa L = 1.25$ respectively. Sub-plot shows the intensity profile of a conventional DFB of $\kappa L = 2.0$ with unequal facet reflectivities.*

It should be noted that a non-symmetrical intensity distribution is usually obtained when the end facet reflectivities are not equal (eg. $r_0 = 1\%$ and $r_L = 80\%$; $\kappa L = 1.0$) as depicted in sub-plot of Figure 7.2. However, in the following analysis equal facet reflectivities is often assumed unless otherwise specified.

A flatness parameter $\mathcal{F}$ for characterising the uniformity of the intensity profile is defined as [6]

$$\mathcal{F} \equiv \frac{1}{L}\int_0^L \left(\hat{RS}(z) - 1\right)^2 dz \tag{7.1}$$

where $\hat{RS}(z)$ is the photon distribution function normalised to the left end facet (refer to Appendix C). This flatness parameter $\mathcal{F}$ is normalised in such a way that a smaller value of $\mathcal{F}$ corresponds to a more uniform intensity distribution. Figure 7.2 displays the variation of $\mathcal{F}$ against the κL product for conventional and $\lambda/4$ phase shifted DFB laser diodes. In order to minimise the SHB effect, an optimal value of $\kappa L = 1.7$ is required for the conventional DFB while $\kappa L = 1.25$ is optimal for the $\lambda/4$ phase shifted DFB. However, if the facet reflectivities are not the same, the minimum point will shift accordingly as illustrated by the example with $r_0 = 1\%$ and $r_L = 80\%$, where the optimal $\kappa L \approx 1.1$.

In addition, the required gain for overcoming the distributed and facet loss, ie. the mode gain $\bar{\alpha}(P)$, is also power-dependent due to the effect of SHB. This results in a power-dependent optical loss $\gamma_p(P)$ [5, 6], since

$$\begin{aligned} \gamma_p(P) &= a_{th} v_g \\ &= (2\bar{\alpha}(P) + \alpha_{int}) v_g \end{aligned} \tag{7.2}$$

where α_{int} is the internal cavity loss including scattering, carrier absorption in the active region and cladding; a_{th} is the material threshold gain. Figure 7.3 illustrates the SHB induced power-dependent loss γ_p for several values of κL using the model in Appendix C with device parameters in Table 7.1. In all cases,

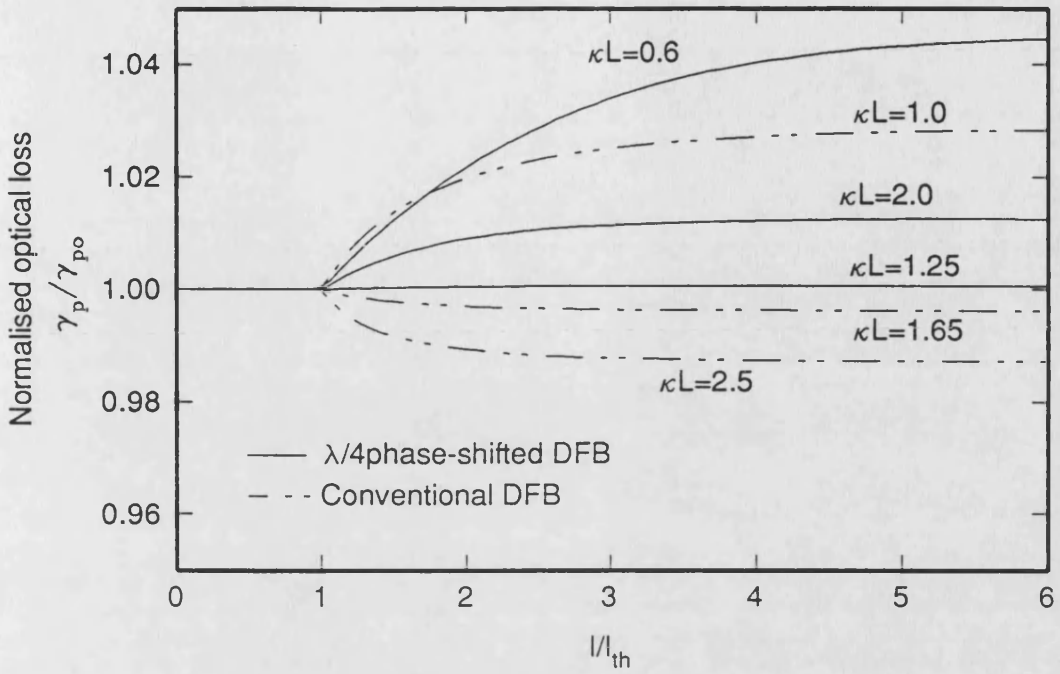

Figure 7.3: *The power-dependent optical loss (or threshold gain) versus the normalised bias current for several values of κL. At optimal κL, the variation of the optical loss is at minimum.*

the degree of variations, is mainly governed by the κL product. A saturation effect is always observed at high output power, this is due to the fact that the shape of the intensity profile does not change much when the optical output power is high. Although the magnitude of the variations in the optical loss is small, the effect of that in terms of non-linear distortion at low frequency can be tremendous [7].

7.3 SHB induced non-linear distortions

Since the power-dependence of the optical loss γ_p due to the SHB effect is highly non-linear, it is important to estimate its contribution to the intrinsic non-linear distortions of a DFB laser diode. The distortions in the low frequency regime, particularly between 50-500MHz, are of interest because a CATV AM-VSB multichannel system often works in this frequency range.

In order to analyse the non-linear effects due to power-dependent loss induced by SHB, the loss term $\gamma_p(P)$ included in the rate equations Eqn (2.1) is expressed as a polynomial of photon density with coefficients fitted to the results obtained in Figure 7.2, that is,

$$\gamma_p(P) = \gamma_{po}(1 + c_1 P + c_2 P^2 + c_3 P^3 + \cdots) \tag{7.3}$$

where γ_{po} is the grating loss at threshold (or threshold gain) and $c_1, c_2, \cdots$ are the curve fitting coefficients.

The non-linear distortions can then be calculated by using either the perturbation method or the Volterra series expansion approach. It is noted that modification of some terms are needed when using the perturbation method and is given in Appendix A. Figures 7.4 and 7.5 illustrate two examples for a $\lambda/4$ phase-shifted DFB of $\kappa L = 0.6$ and a conventional DFB with $\kappa L = 1.0$ respectively. The parameter values used for the numerical calculations are listed in Table 7.1.

In general, all the distortion curves show a strong frequency dependence and gradually rise with increasing frequency due to the RO resonance effect. On the other hand, the non-linear distortions also exhibit a bias dependence. The distortion levels in the vicinity of threshold are very high because of the strong

A_{nr}	$1 \times 10^{8} s^{-1}$	L	$250 \mu m$
B_r	$1 \times 10^{-10} cm^3 s^{-1}$	w	$1.8 \mu m$
C_{Auger}	$3 \times 10^{-29} cm^6 s^{-1}$	d	$0.12 \mu m$
Γ	0.3	β	1.7×10^{-4}
N_{tr}	$1 \times 10^{18} cm^{-3}$	A_o	$2.5 \times 10^{-16} cm^2$
n_o	3.5	α_{int}	$50 cm^{-1}$
Λ	$0.187 \mu m$	$\frac{dn}{dN}$	$-0.5 \times 10^{-20} cm^3$
v_g	$7.5 \times 10^{9} cm s^{-1}$	ϵ	$3 \times 10^{-17} cm^3$

Table 7.1: *Parameter values used for the couple-wave DFB laser diode model. L, w and d are the length, width and thickness of the active region where the active region volume $V = L \times w \times d$; n_o if the effective refractive index at threshold; Λ is the Bragg wavelength; $\frac{dn}{dN}$ denotes the variation in refractive index due to carrier density changes.*

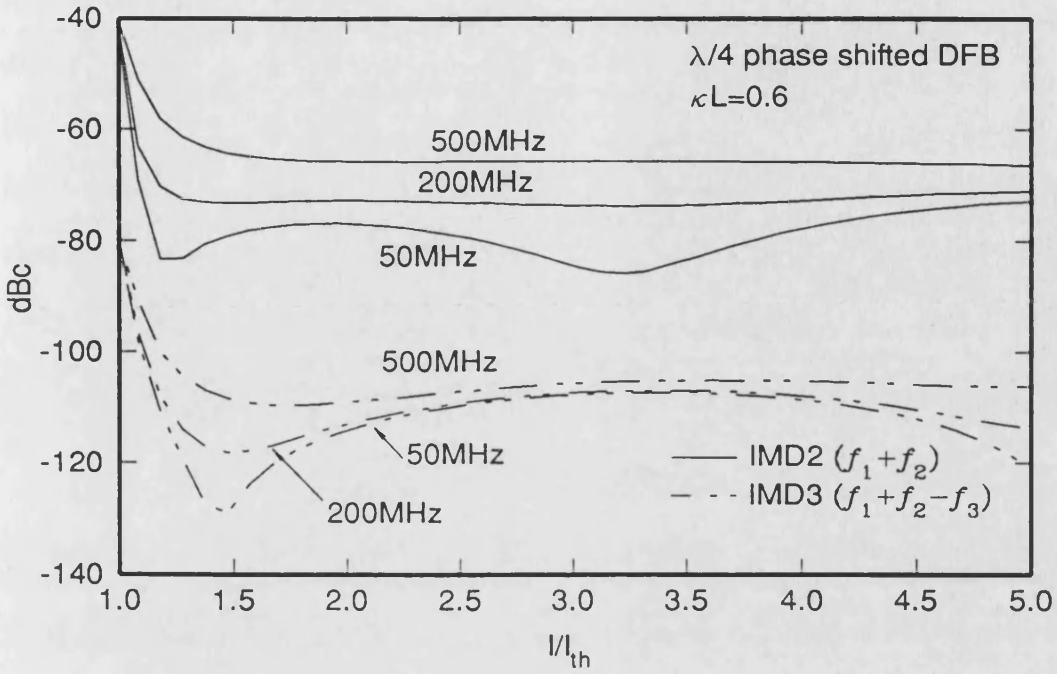

Figure 7.4: *The bias dependence of the non-linear distortions for a $\lambda/4$ phase shifted DFB with $\kappa L = 0.6$. The frequency labelled for each curve is f_2 where $f_1 = f_2 - 12.5MHz$ and $f_3 = f_2 + 12.5MHz$.*

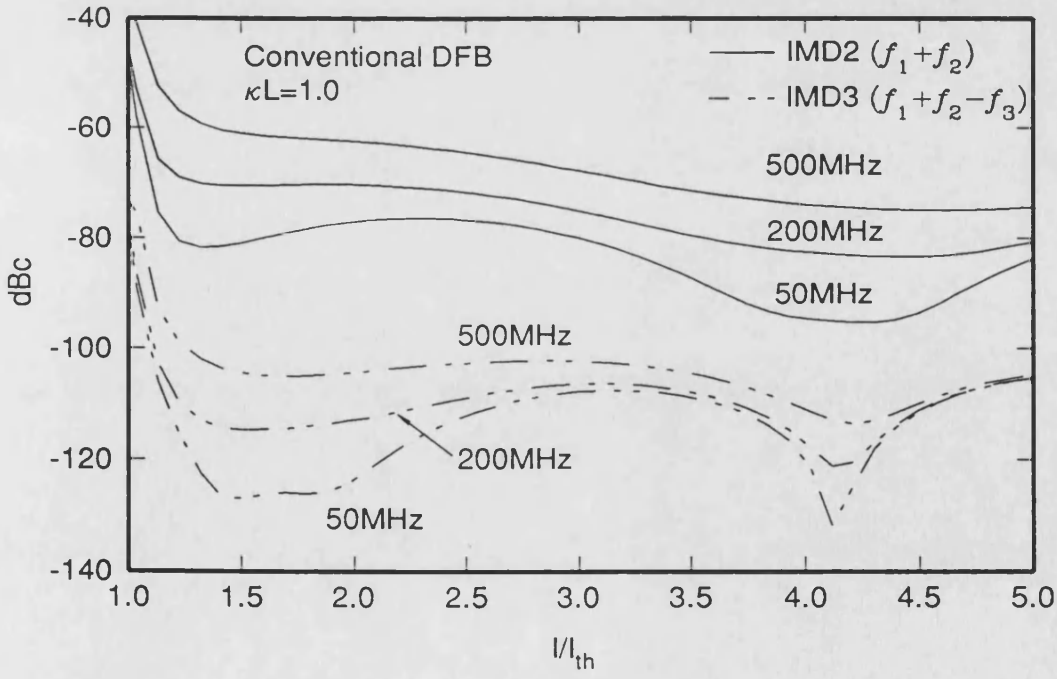

Figure 7.5: *The bias dependence of the non-linear distortions for a conventional DFB with $\kappa L = 2.0$. The frequency labelled for each curve is f_2 where $f_1 = f_2 - 12.5MHz$ and $f_3 = f_2 + 12.5MHz$.*

spontaneous emission around the turn-on point. In the above examples, the distortion levels decreases with increasing bias and then rise again at higher bias level. This is because the non-linear distortions at low bias are dominated by the SHB effect. As bias increases, the SHB induced power-dependent loss starts to saturate and thus the corresponding non-linear distortions is reduced. However, as the bias increases further, the gain non-linearity governed by the gain suppression coefficient ϵ becomes significant and non-linear distortions start to rise again.

In some cases, there may exist a dip in the bias dependence of the non-linear distortions at comparatively low frequency, say 50MHz. In fact, this dip is also found in some experimental results [7, 9]. The competition between the SHB and non-linear gain effect could be an explanation for this phenomenon. This can be justified, for instance, by manipulating the algebra of the IMD2 ($f_1 + f_2$) and obtain the following expression :

$$\frac{\text{IMD2}}{\text{C}_\text{r}} \propto |Re\{imd2(\omega)\} + j\omega Im\{imd2(\omega)\}| \tag{7.4}$$

$$\begin{aligned} Re\{imd2(\omega)\} &= P^2\left(\frac{\partial^2 G}{\partial N \partial P}\frac{d\gamma_p}{dP} - \frac{1}{2}\frac{\partial G}{\partial N}\frac{d^2\gamma_p}{dP^2}\right)\left(\frac{\partial G}{\partial N} + \frac{d\gamma_e \cdot N}{dN}\right) \\ &\quad + \Gamma\frac{\partial G}{\partial N}\left(2\frac{\partial G}{\partial N} + \frac{d\gamma_e \cdot N}{dN}\right)R_{sp} \\ &\quad + \left(\frac{\partial G}{\partial N} + \frac{\partial^2 G}{\partial N \partial P^2}P\right)\left(\frac{\partial G}{\partial N}\frac{d\gamma_p}{dP}P^2 - 2\omega^2\right) \\ Im\{imd2(\omega)\} &= \left(\frac{\partial G}{\partial N} + \frac{\partial^2 G}{\partial N \partial P}P\right)\left(2\frac{\partial G}{\partial N}P + \frac{\gamma_e \cdot N}{\partial N} + 2\Gamma\frac{R_{sp}}{P}\right) \\ &\quad + 2P^2\left(\frac{\partial^2 G}{\partial N \partial P}\frac{d\gamma_p}{dP} - \frac{1}{2}\frac{\partial G}{\partial N}\frac{\partial^2 \gamma_p}{\partial P^2}\right) \end{aligned}$$

At low frequencies, the magnitude of the real part $Re\{imd2(\omega)\}$ dominates the expression where the first term is the interference term between the SHB induced power-dependent loss γ_p and the gain non-linearity term $\frac{\partial G}{\partial P}$. At a particular bias

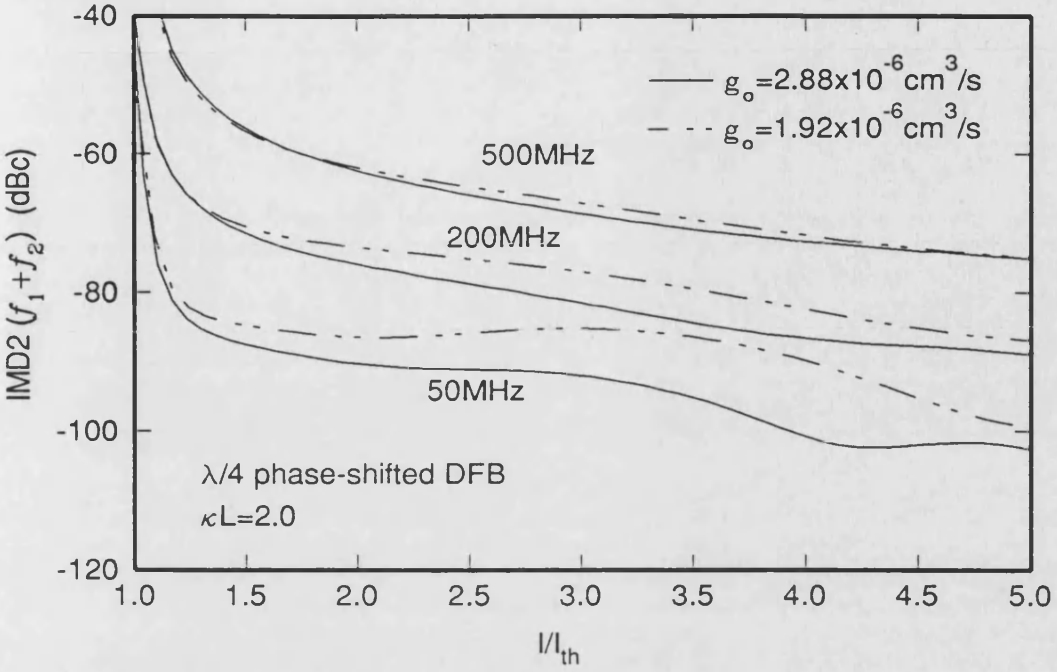

Figure 7.6: *The bias dependence of the non-linear distortions for a $\lambda/4$ phase shifted DFB with optimal $\kappa L = 1.25$ and different values of gain suppression ϵ. The SHB induced non-linear distortions are therefore at minimum.*

(output power), and depending on the sign of the derivatives of γ_p, the first term may vanish. This means that the two non-linearities may cancel each other out.

The example, shown in Figure 7.6, is a $\lambda/4$ phased-shifted DFB with $\kappa L = 1.25$ (ie. SHB is minimised). Here it is find that the non-linear distortions increases steadily with the bias, this is mainly contributed by the gain non-linearities, since gain suppression increase as the optical power increases.

For a given optical power, device with higher differential gain exhibit lower non-linear distortions as illustrated in Figure 7.7. Although high differential gain laser devices, such as, QW and SLQW, possess a relatively higher value of gain suppression than bulk devices and thus be liable to additional non-linear distortions. The increase of differential gain can in general compensate for the detrimental effects of the gain suppression.

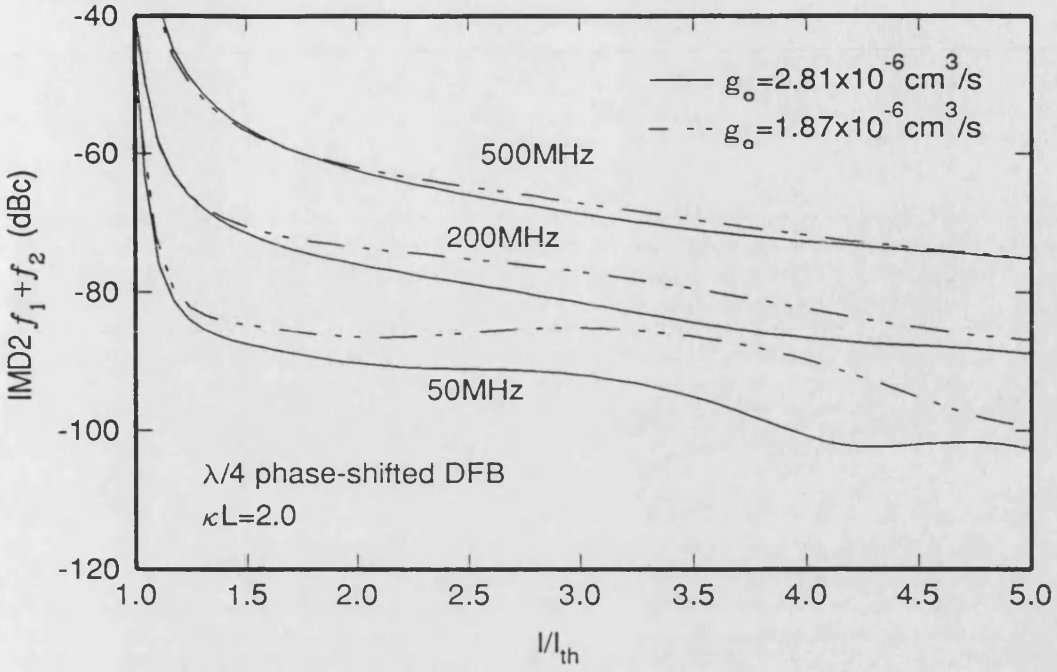

Figure 7.7: *The bias dependence of the non-linear distortions for a $\lambda/4$ phase shifted DFB with $\kappa L = 2.0$ and different values of gain coefficient g_o.*

The variation of the non-linear distortions are plotted against the coupling coefficient κL as given in Figures 7.8 and 7.9 for both conventional and $\lambda/4$ phase-shifted DFBs with $f_2 = 50$ MHz. The numerical results are calculated by examining a group of different κL lasers to the same output power; the error bars indicate the bias dependence of the non-linear distortions at different steps of constant output power values covering a bias range of $I/I_{th} = 1$ to 4. It is obvious that by designing a conventional DFB laser with an optimal value of $\kappa L = 1.7$ or a $\lambda/4$ phase-shifted DFB with $\kappa L = 1.25$, the low frequency non-linear distortions due to the SHB effect are minimised. For instance, an improvement of approximately 12 dB can be achieved by switching the κL product of a conventional DFB from $\kappa L = 2.0$ to $\kappa L = 1.7$. In general, it is not easy to control the value of κL, since the grating height which determines the κL, deforms easily during fabrication process.

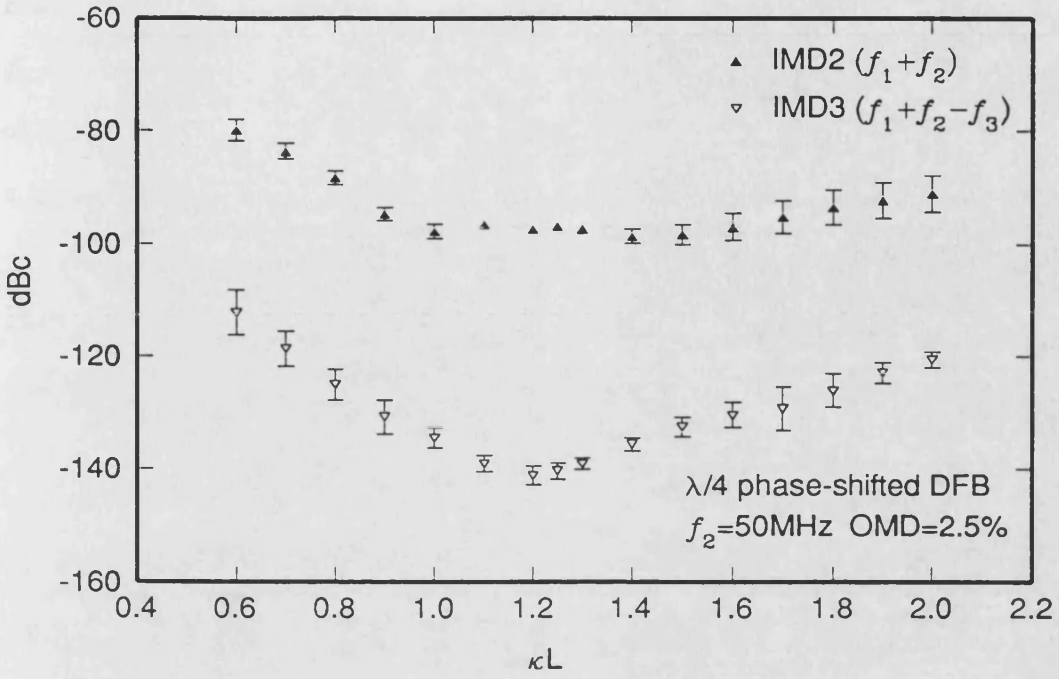

Figure 7.8: *Coupling coefficient dependence of the non-linear distortions for $\lambda/4$ phase shifted DFBs. Modulation frequency centered at 50 MHz with carrier separation of 12.5MHz.*

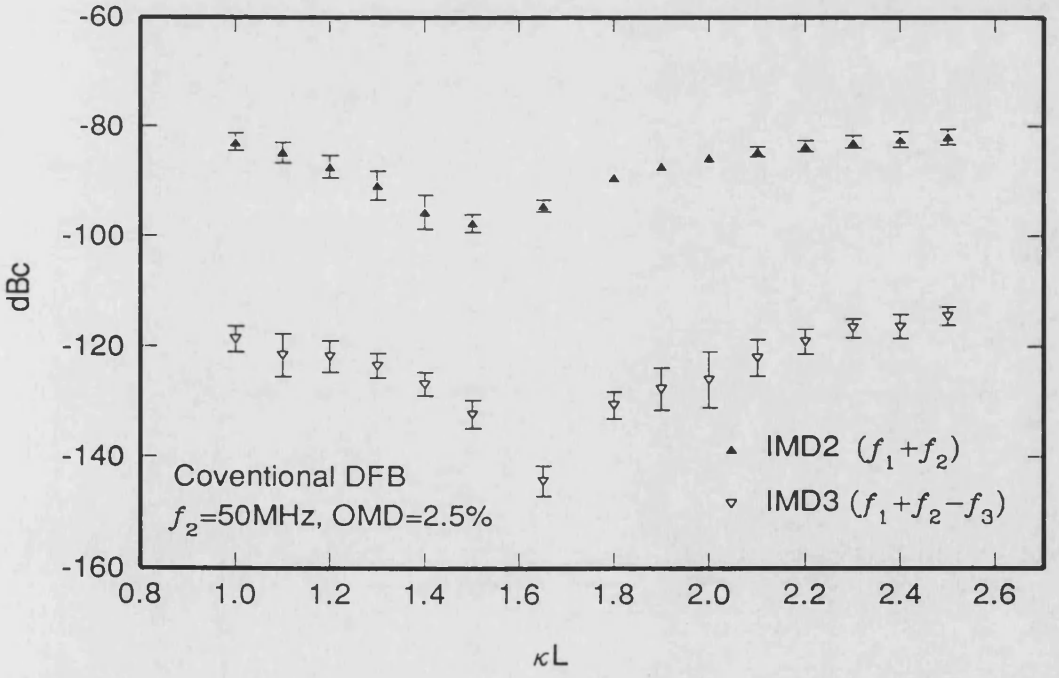

Figure 7.9: *Coupling coefficient dependence of the non-linear distortions for conventional DFBs. Modulation frequency centered at 50 MHz with carrier separation of 12.5 MHz.*

From the Figures 7.8 and 7.9, it is found that both IMD2 $f_1 + f_2$ and IMD3 $f_1 + f_2 - f_3$ at the modulation frequency of $f_2 = 50$ MHz are well within the limit of the linearity requirements (-74 dBc for IMD2 and -88 dBc for IMD3) set for a practical 42 channel CATV AM-VSB system listed in Table 6.6.

However, as the modulation frequency rises, say $f_2 = 500$ MHz, the non-linear distortions escalates due to the resonance effect of RO as given in Figures 7.10 - 7.13. In Figures 7.10 and 7.12, the IMD2 ($f_1 + f_2$) of some devices with unoptimised κL products, have already exceeded the limit of linearity requirement of -74 dBc; while there is still a large dB margin for the IMD3 ($f_1 + f_2 - f_3$) to reach the limit of -88 dBc as seen in Figure 7.11 and 7.13. Therefore, one can conclude that for typical CATV AM-VSB systems, the second-order distortions are more serious than their third-order relatives, even though the third-order may have a very large number of distortion terms.

It is worth pointing out that an optimal $\kappa L \approx 1$ for conventional DFBs is found experimentally by A. Takemoto *et al* [3] because the DFB lasers used are of unequal facet reflectivities, $r_0 = 1\%$ and $r_L = 80\%$. From Figure 7.2, the theoretical prediction of an optimal κL product for such kind of DFBs is around 1.1, and this agrees very well with the experimental results.

Nevertheless, when comparing with the experimental results [3], the theoretical predictions of the non-linear distortions due to the SHB effect still underestimate those measured. Therefore, it is necessary to account for the non-linear effect of another commonly occurring mechanism - the leakage current, which is highly structural dependent.

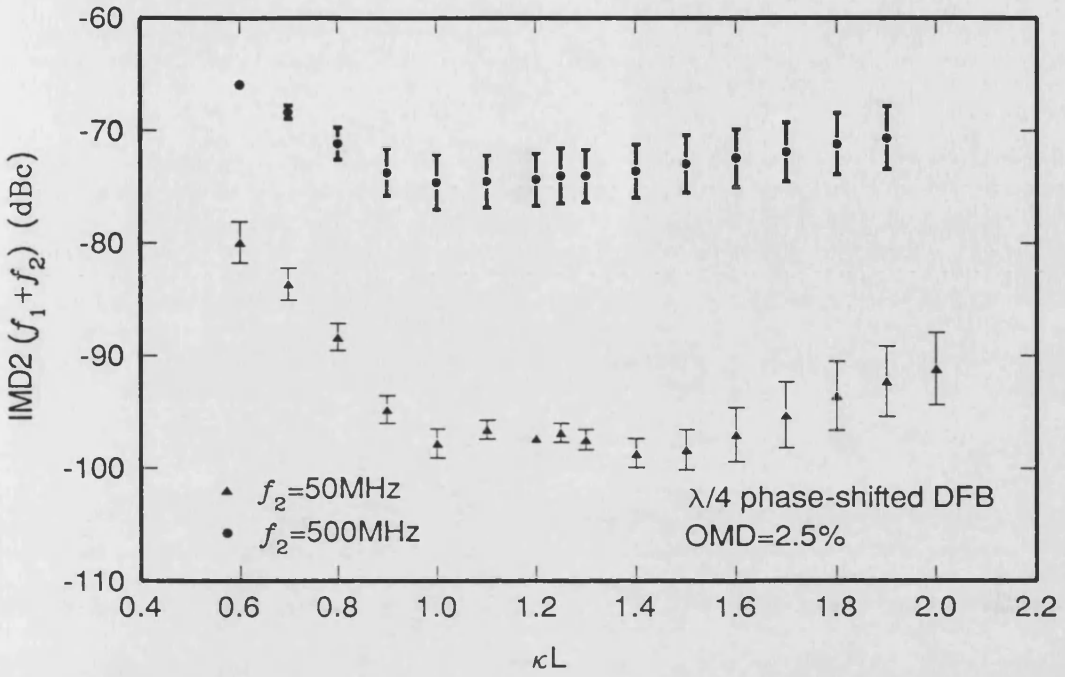

Figure 7.10: *Coupling coefficient dependence of the* $(f_1 + f_2)$ *type IMD2 for* $\lambda/4$ *phase shifted DFBs.* $f_2 = 500MHz$ *and carrier separation is 12.5MHz.*

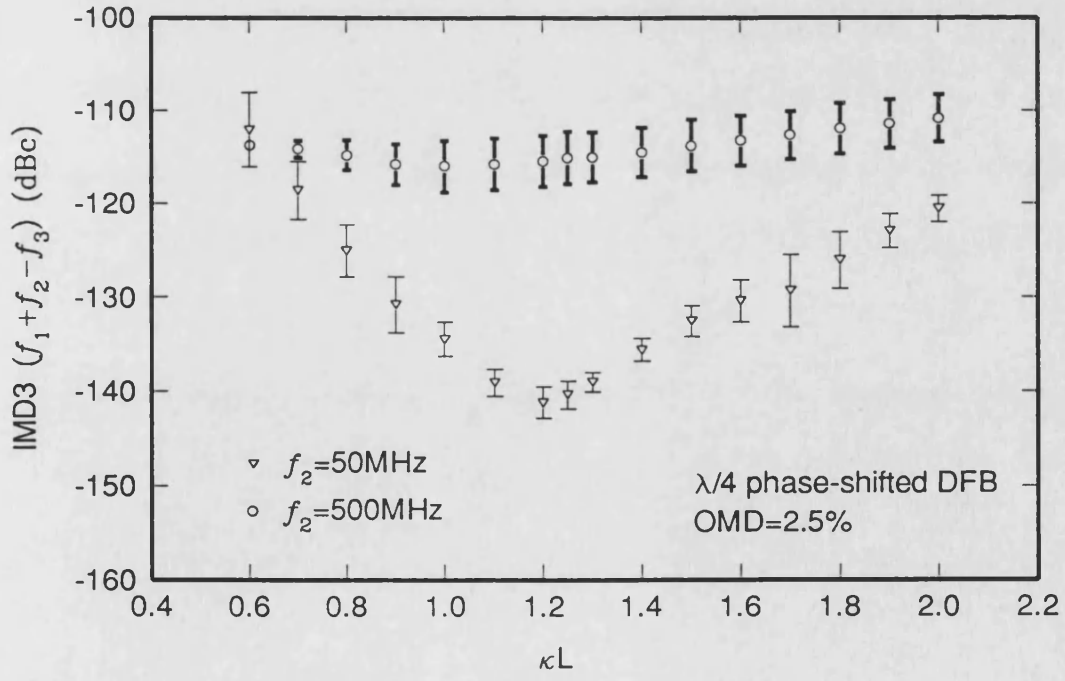

Figure 7.11: *Coupling coefficient dependence of the* $(f_1 + f_2 - f_3)$ *type IMD3 for* $\lambda/4$ *phase-shifted DFBs.* $f_2 = 500MHz$ *and carrier separation is 12.5 MHz.*

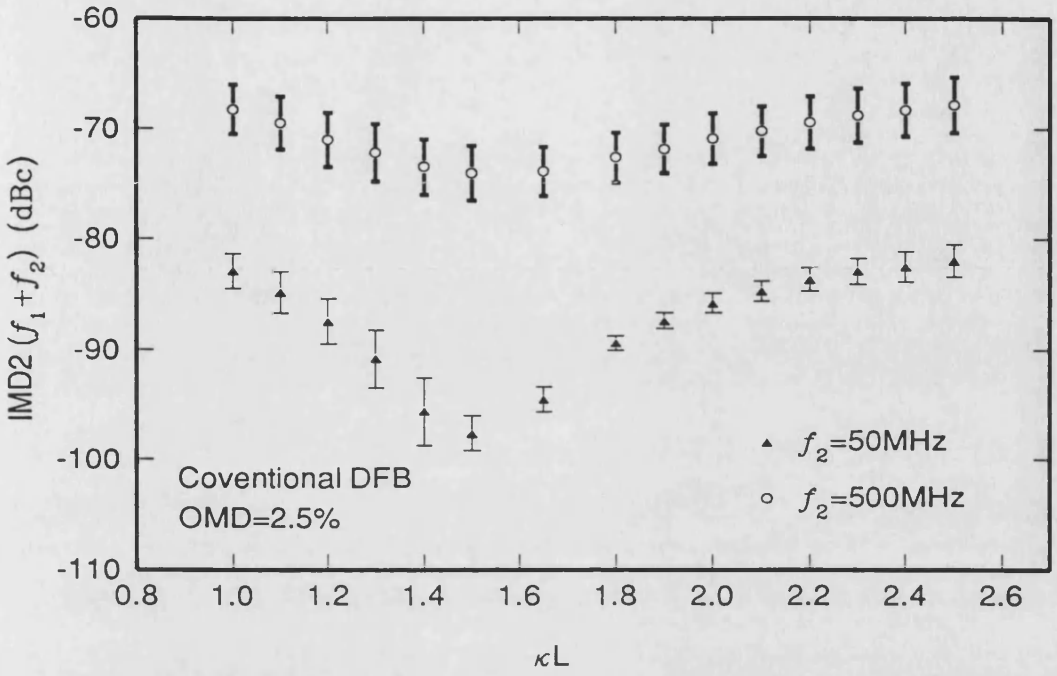

Figure 7.12: *Coupling coefficient dependence of the* $(f_1 + f_2)$ *type IMD2 for conventional DFBs.* $f_2 = 500MHz$ *and carrier separation is 12.5MHz.*

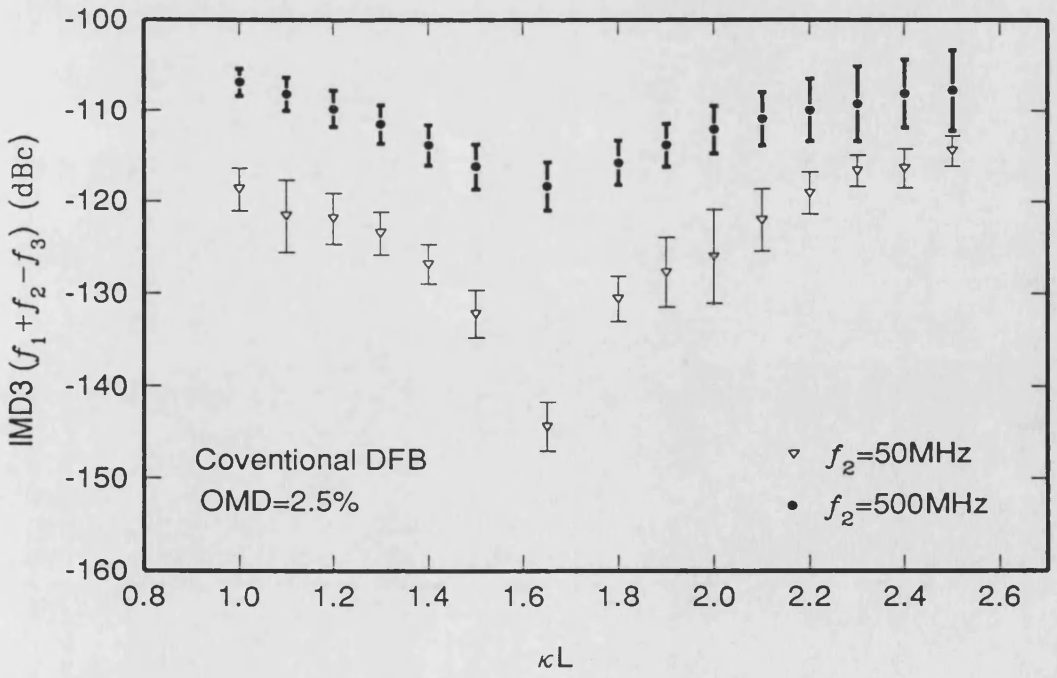

Figure 7.13: *Coupling coefficient dependence of the* $(f_1 + f_2 - f_3)$ *type IMD3 for conventional DFBs.* $f_2 = 500MHz$ *and carrier separation is 12.5 MHz.*

7.4 Leakage current non-linearities

So far, consideration has been devoted to the non-linearities arising in the active region of the laser, however, experiments show that the extrinsic non-linearities due to leakage current are also of importance. Current leakage may occur in most kinds of laser diodes, and its magnitude can usually be controlled by careful structural design. Here an example will be centre on the buried heterostructure and its variants of particular interest since they are commonly used in optical communication systems.

One of the major leakage paths of many laser diodes and particularly buried heterostructures, is due to the p-blocking layer and the n-buffering layer adjacent to the side walls of the active region [8]. It is this path which is considered here but it should be noted that in some types of buried heterostructure laser diode, this is not the only leakage path.

For most buried heterostructures, the above mentioned leakage path forms a p-n homo-junction which can be modelled by a leakage diode in parallel with the intrinsic laser diode (described by the rate-equation model) as shown in Figure 7.10 [9, 10]. In fact, by adjusting the parameters of the leakage diode, this model is adequate to describe the non-linear distortions induced by the leakage path of most laser structures.

In order to provide a straightforward analysis of the overall non-linear distortions generated by both the SHB effect and that of leakage current, the approach given by M. Lin *et al* [9] for the leakage current model is used but an extension of the analysis is made to include up to third order terms for the third-order non-linear distortions.

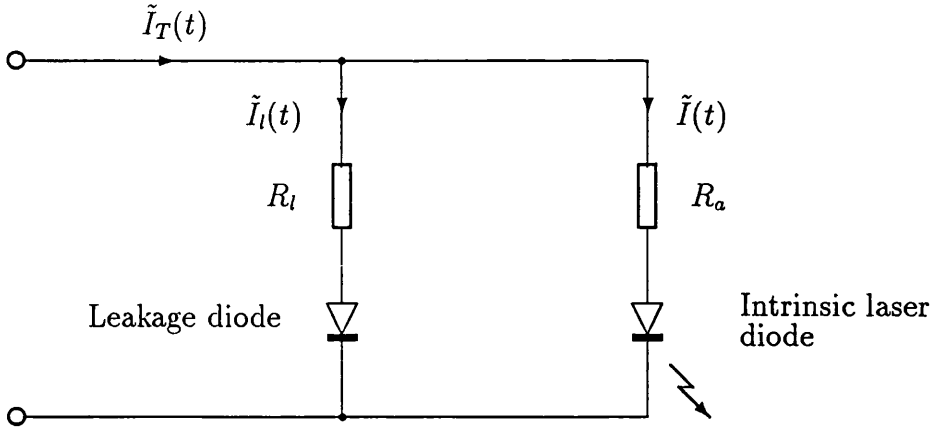

Figure 7.14: *Equivalent circuit model of a buried heterostructure laser diode with the leakage current modelled by a homo-junction diode and the active region (intrinsic laser diode) modelled by a pair rate equations with power-dependent loss.*

The injected current $\tilde{I}_T(t)$ can be represented by,

$$\tilde{I}_T(t) = \tilde{I}(t) + \tilde{I}_l(t) \tag{7.5}$$

where $\tilde{I}(t)$ is the instantaneous current through the intrinsic laser diode (active region); and $\tilde{I}_l(t)$ is the leakage current through the leakage diode. R_l and R_a are the resistances of the leakage diode and the active region respectively.

The relationship between the injected current $\tilde{I}_T(t)$ and the current through the active region $\tilde{I}(t)$ can be given by [9],

$$\tilde{I} = \tilde{I}_T - (\rho(\omega) + \sigma(\omega)\tilde{I}_T)(y(\tilde{I}_T) - 1) \tag{7.6}$$

with

$$\rho(\omega) = I_{so}\left[1 - (1 + j\omega\tau)^{1/2}\right]$$

$$\sigma(\omega) = \frac{I_{so}}{\tilde{I}_T}(1 + j\omega\tau)^{1/2}$$

$$y(\tilde{I}_T) = e^{\frac{qV_a}{\eta kT}}\, e^{\,a\tilde{I}_T \,-\, bI_{so}[\, y(\tilde{I}_T)-1\,]}$$

V_a	0.88-0.95 V	η	1-2
$\frac{kT}{q}$	0.0259	R_a	0.1-0.2 Ω [8, 9]
R_l	10-20 Ω [8, 9]	τ	0.2×10^{-9} sec [9]
I_{so}	1-3 $\times 10^{-11}$ A [8]	I_l @ I_{th}	0.3-1.0 $\times 10^{-3}$ A

Table 7.2: *Typical parameters values of the leakage diode model.*

here η is the leakage diode ideality factor; kT is the Boltzmann constant times the temperature; V_a is the voltage across the intrinsic laser diode; τ is the lifetime of the excess carriers in the p-blocking layer; I_{so} is the effective saturation current of the leakage diode. Typical values of all the relevant parameters are given in Table 7.2.

Performing a Taylor's series expansion of y and then applying the small signal analysis with $\tilde{I}_T(t) = I_T + i_T(t)$ and $\tilde{I}(t) = I + i(t)$, having I_T and I as the steady state values and i_T and i are the small perturbations, the following equations can be obtained,

$$\begin{aligned}\frac{i(t)}{qV} &= \frac{i_T(t)}{qV} - \frac{i_T(t)}{qV}\left[I_{so}y'(I_T) + \sigma(\omega)(y(I_T)-1)\right] \\ &\quad - qV\left(\frac{i_T(t)}{qV}\right)^2\left[\frac{1}{2!}I_{so}y''(I_T) + \sigma(\omega)y'(I_T)\right] \\ &\quad - (qV)^2\left(\frac{i_T(t)}{qV}\right)^3\left[\frac{1}{3!}I_{so}y'''(I_T) + \frac{1}{2!}\sigma(\omega)y''(I_T)\right] + \cdots\cdots \quad (7.7)\end{aligned}$$

where

$$y'(I_T) = \frac{D_o}{B_o}y(I_T)$$

$$
\begin{aligned}
y''(I_T) &= \frac{D_o}{B_o^3} y(I_T) \left[D_o - 2b\sigma(\omega) B_o y(I_T) \right] \\
y'''(I_T) &= \frac{D_o}{B_o^4} y(I_T) \left[D_o \{ D_o - 6b\sigma(\omega) B_o y(I_T) \} \right. \\
&\quad \left. + by(I_T) \{ I_{so} \frac{D_o}{B_o} + \sigma(\omega) \} \{ 6b\sigma(\omega) B_o y(I_T) - 3D_o \} \right] \\
a &= \frac{qR_a}{\eta kT} \\
b &= a + \frac{1}{2} \frac{qR_l}{\eta kT} \\
B_o &= a - b\sigma(\omega)[y(I_T) - 1] \\
D_o &= 1 + bI_{so} y(I_T)
\end{aligned}
$$

Following the *growing exponentials* approach described in Appendix B, the Volterra kernels for the leakage current effect can be obtained as given below,

$$G_1(\omega) = 1 - \left[I_{so} y'(I_T) + \sigma(\omega)(y(I_T) - 1) \right] \tag{7.8}$$

$$G_2(\omega_1, \omega_2) = -qV \left(\frac{i_T(t)}{qV} \right)^2 \left[\frac{1}{2!} I_{so} y''(I_T) + \sigma(\omega_1 + \omega_2) y'(I_T) \right] \tag{7.9}$$

$$
\begin{aligned}
G_3(\omega_1, \omega_2, \omega_3) &= -(qV)^2 \left(\frac{i_T(t)}{qV} \right)^3 \left[\frac{1}{3!} I_{so} y'''(I_T) \right. \\
&\quad \left. + \frac{1}{2!} \sigma(\omega_1 + \omega_2 + \omega_3) y''(I_T) \right]
\end{aligned} \tag{7.10}
$$

7.5 Combined non-linearities

In the previous two sections, the Volterra kernels H_1, H_2 and H_3 for the intrinsic laser diode including the effect of SHB and the kernels G_1, G_2 and G_3 for the leakage current represented by a homo-junction diode, have been found. These two non-linear systems can then be cascaded together to form a combined non-

linear system C as illustrated in Figure 7.11. By applying non-linear system

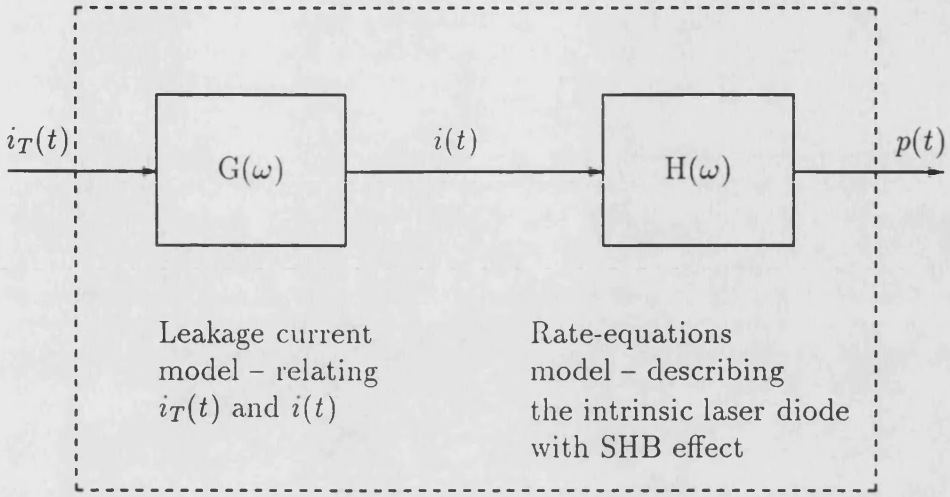

Figure 7.15: *The combined non-linear system C which consists of two cascaded stages – the leakage current stage and the rate-equations stage.*

theory, the combined Volterra kernels C_1, C_2 and C_3 are given by :

$$C_1(\omega) = G_1(\omega)H_1(\omega) \tag{7.11}$$

$$C_2(\omega_1,\omega_2) = G_1(\omega_1)G_1(\omega_2)H_2(\omega_1,\omega_2) + G_2(\omega_1,\omega_2)H_1(\omega_1+\omega_2) \tag{7.12}$$

$$\begin{aligned} C_3(\omega_1,\omega_2,\omega_3) &= G_1(\omega_1)G_1(\omega_2)G_1(\omega_3)H_3(\omega_1,\omega_2,\omega_3) \\ &+ \frac{2}{3}[\, G_1(\omega_1)G_2(\omega_2,\omega_3)H_2(\omega_1,\omega_2+\omega_3) \\ &+ G_1(\omega_2)G_2(\omega_1,\omega_3)H_2(\omega_2,\omega_1+\omega_3) \\ &+ G_1(\omega_3)G_2(\omega_2,\omega_3)H_2(\omega_3,\omega_1+\omega_2)\,] \\ &+ G_3(\omega_1,\omega_2,\omega_3)H_1(\omega_1+\omega_2+\omega_3) \end{aligned} \tag{7.13}$$

Eqn (7.11) represents the combined first order effect (transfer function) which can also be obtained by linear control theory. The combined second and third order effects are given by Eqns (7.12) and (7.13) respectively. The interpretation of Eqn (7.12) is that the component at $\omega_1+\omega_2$ in the output of C arises due to

the linear transmission through G and the second-order effects in H, or through the second-order effects in G but linear transmission through H. The terms in Eqn (7.13) may be similarly interpreted.

The combined non-linear effects are demonstrated using an example of a $\lambda/4$ phase-shifted DFB with $\kappa L = 2.0$ as given in Figure 7.16. Evidently, the incorporation of the leakage current effect causes an increase in the non-linear distortions in the low frequency regime. However, the sharp dip in the bias dependence, which appeared in the report by M. Lin *et al* [9], due to the leakage current effect is not seen. This is because in M. Lin *et at* report, a pure linear active region represented by the intrinsic diode is assumed and the leakage diode is therefore responsible for all the non-linear effects. The sharp dip is caused by the cancellations of some complex terms within the leakage diode model. However, when other non-linear effects, like SHB induced power-dependent loss and gain non-linearities are included as demonstrated here, the contribution of the leakage current non-linear effect on the bias dependence is reduced.

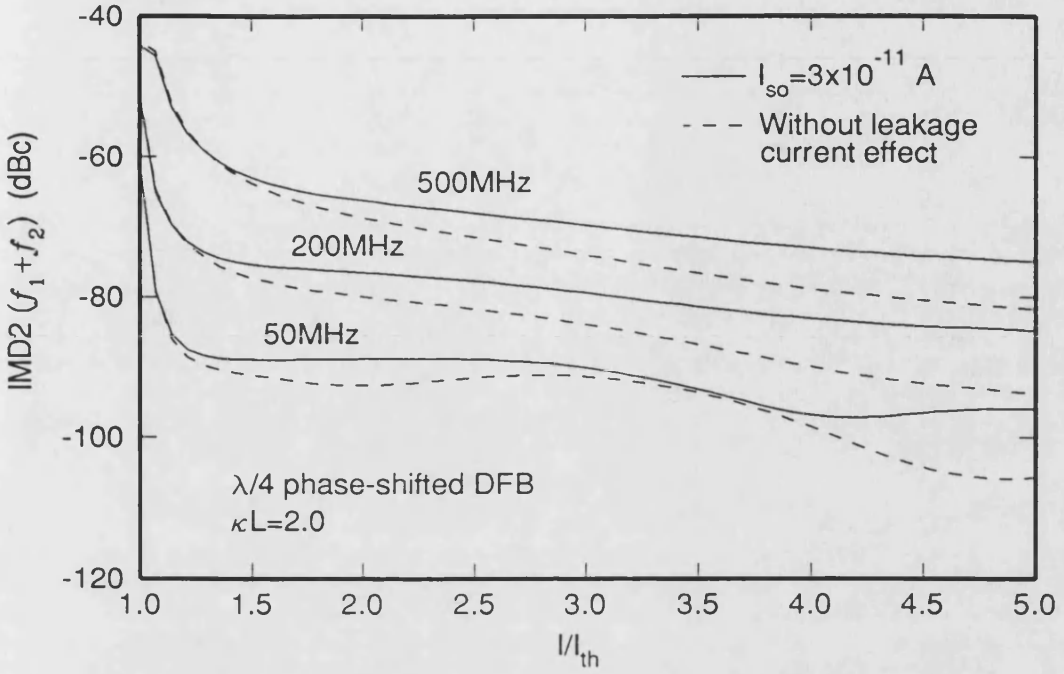

Figure 7.16: *Bias dependence of the second-order non-linear distortions for* $\lambda/4$ *phase-shifted DFBs with* $\kappa L = 2.0$.

Figures 7.17 and 7.18 show the variation of the non-linear distortions IMD2 and IMD3 at $f_2 = 50$ MHz for a $\lambda/4$ phased-shifted DFB are plotted against the κL respectively; similarly, Figures 7.19 and 7.20 show that of a conventional DFB. All laser diodes are driven with the same output power at various levels covering a bias range of $I/I_{th} \approx 1$ to 4 indicate by the error bars. In general, the leakage current effect has a stronger influence in the second-order non-linear distortions than on the third-order distortions.

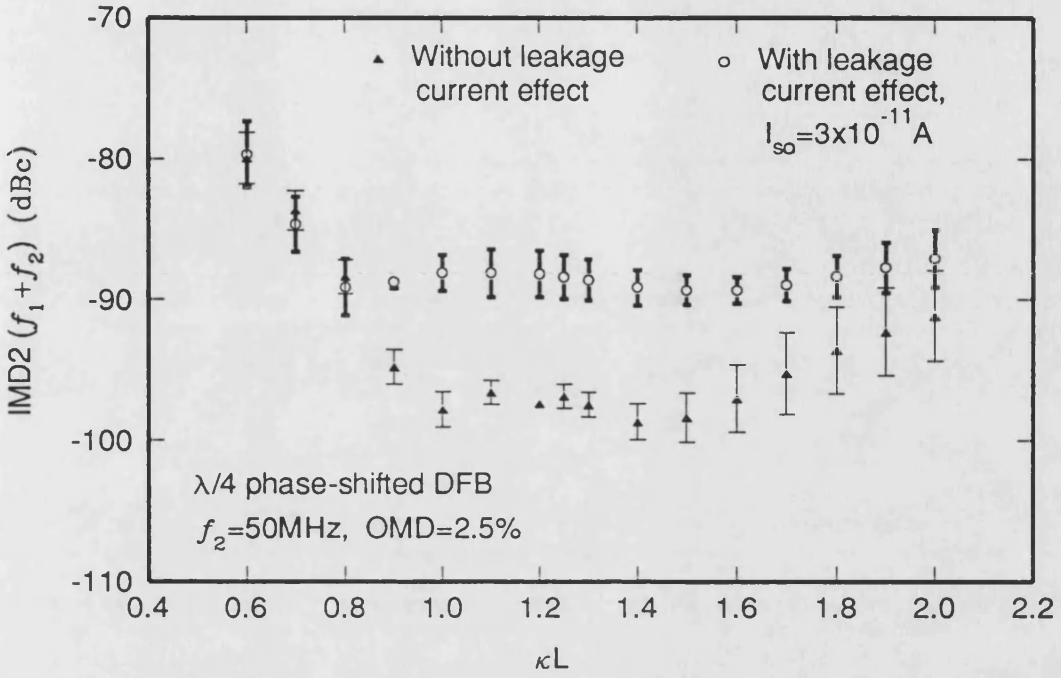

Figure 7.17: *Coupling coefficient dependence of the non-linear distortions for λ/4 phase-shifted DFBs.*

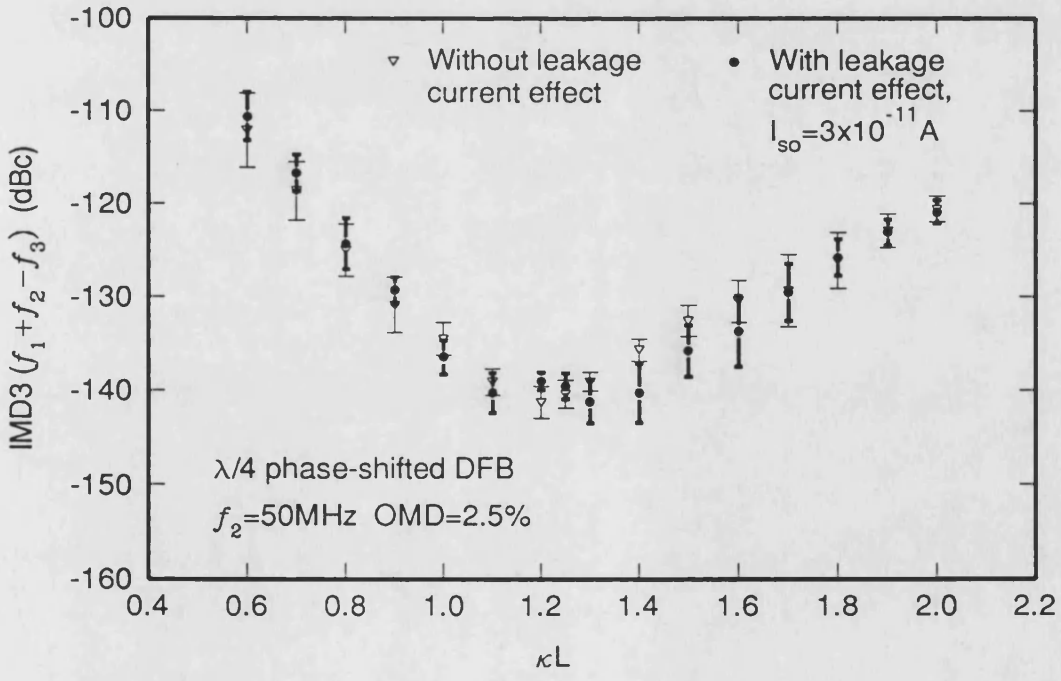

Figure 7.18: *Coupling coefficient dependence of the non-linear distortions for λ/4 phase-shifted DFBs.*

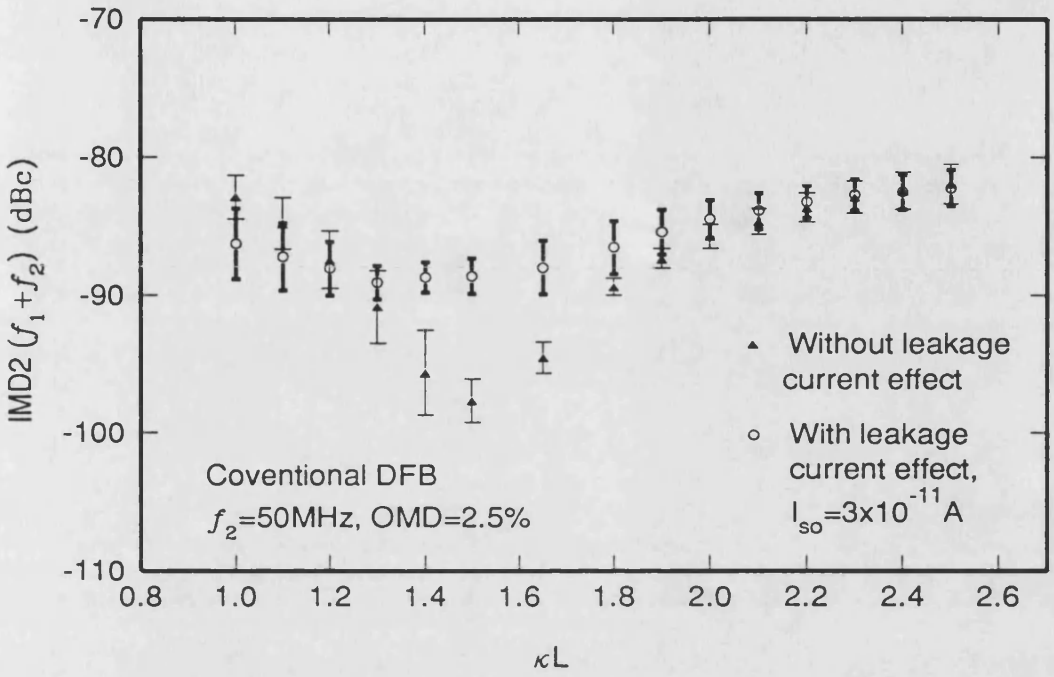

Figure 7.19: *Coupling coefficient dependence of the non-linear distortions for conventional DFBs.*

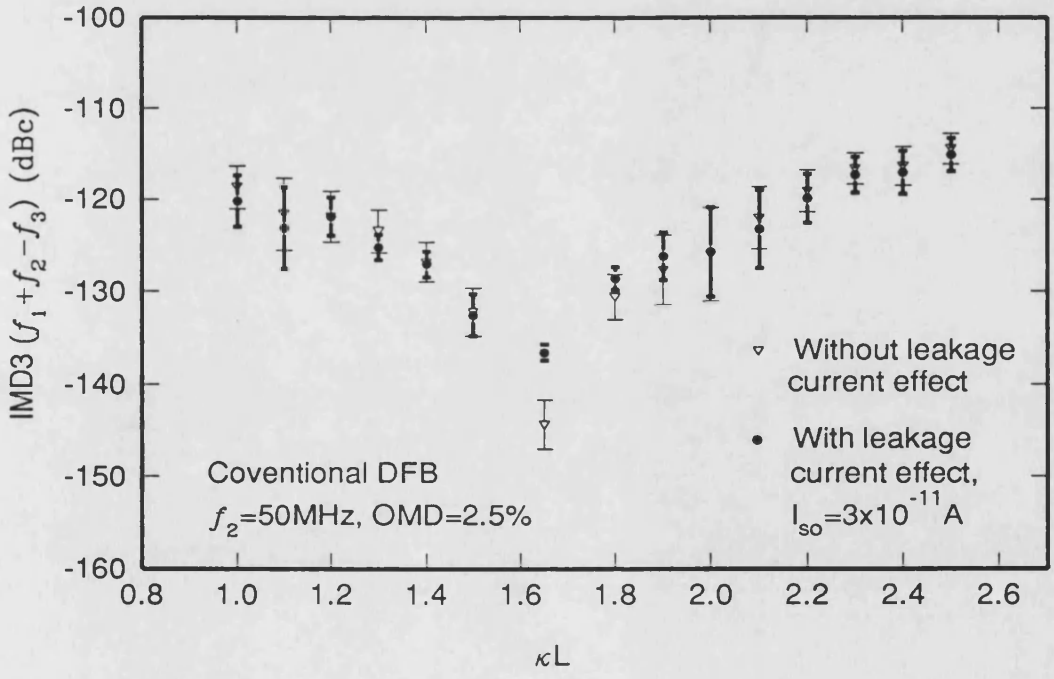

Figure 7.20: *Coupling coefficient dependence of the non-linear distortions for conventional DFBs.*

The benefit of selecting an optimal κL to minimise the non-linear distortion is less clear, because as the SHB effect is small at the optimal κL value, the leakage current becomes dominant as seen in Figures 7.17 and 7.19. Considering the same example of switching the κL product of a conventional DFB from $\kappa L = 2.0$ to $\kappa L = 1.7$, the improvement is now reduced to around 4.5 dB. In other words, the leakage current produces a non-linear distortion floor that degrades the performance of a laser diode.

The situation aggravates as modulation frequency reaches the high band edge, say 500 MHz. Figures 7.21-7.22 illustrate the second-order non-linear distortions at $f_2 = 500$ MHz for a conventional DFB with two different values of saturation current $I_{so} = 1 \times 10^{-11} A$ and $3 \times 10^{-11} A$, which corresponds to leakage current of $I_l = 0.3mA$ and $1.0mA$ respectively for the leakage diode. Comparing the two different cases at the optimal point, ie. $\kappa L = 1.7$, there is a rise of 2.5 dB and 6 dB for the $I_{so} = 1 \times 10^{-11} A$ and $3 \times 10^{-11} A$ respectively. Obviously, the inclusion of leakage current further degrades the linearity of the DFB laser, particularly, for the devices with optimal κL.

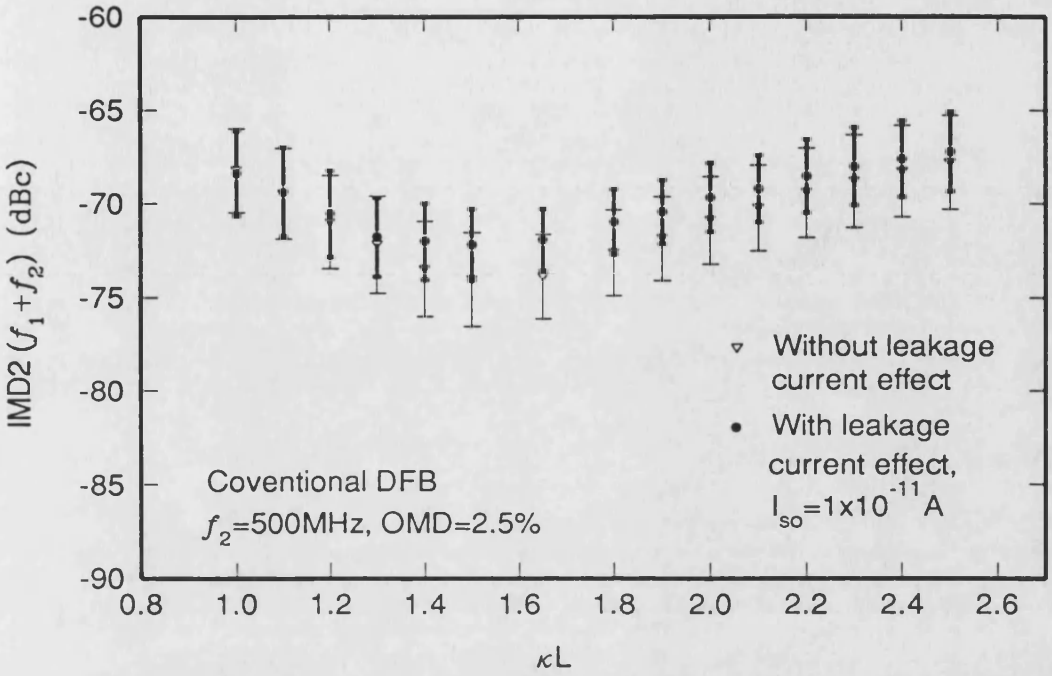

Figure 7.21: *Coupling coefficient dependence of the IMD2 for conventional DFBs at* $f_2 = 500MHz$.

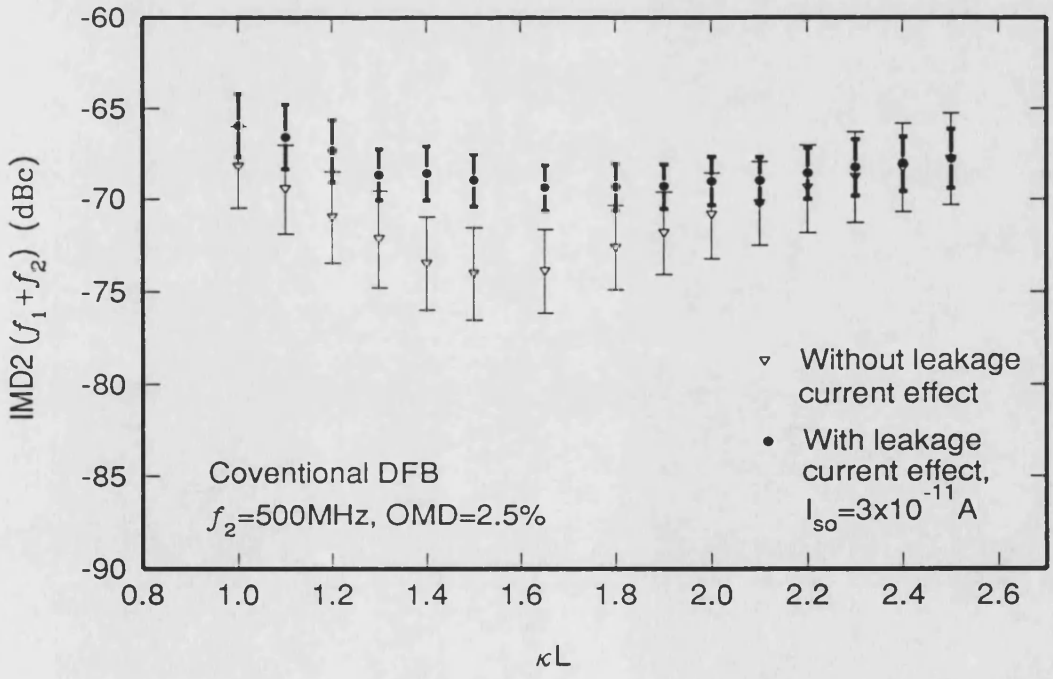

Figure 7.22: *Coupling coefficient dependence of the IMD2 for conventional DFBs at* $f_2 = 500MHz$.

7.6 Conclusion

The spatial hole burning (SHB) effect of widely used DFB lasers can cause a power-dependent optical loss $\gamma_p(P)$. The actual variation of $\gamma_p(P)$ against the optical output power is mainly governed by the shape of intensity profile and the facet reflectivities. As output optical power increases, the SHB induced power-dependence of the optical loss $\gamma_p(P)$ begins to saturate.

A flatness parameter $\mathcal{F}$ is defined to characterise the uniformity of the intensity profile inside the laser cavity. By utilising the flatness parameter $\mathcal{F}$, it is found that in order to minimise the non-linear distortions due to the SHB effect, optimal values of $\kappa L = 1.7$ and $\kappa L = 1.25$ are needed for the conventional DFB and $\lambda/4$ phase shifted DFB laser diodes respectively. For the case of unequal facet reflectivities, this optimal κL product may change.

Calculations performed here also show that although the SHB induced power-dependent variation in the optical loss term is small, it can cause an enormous non-linear distortion at low frequencies ($f < f_o/2$) which seriously impairs the performance of an analogue optical system, such as a multichannel CATV AM-VSB system operates within 50 to 500 MHz. In order to minimise this effect, the above mentioned optimal κL products should be used.

The bias dependence of the non-linear distortion at low modulation frequencies $f < f_o/2$, is mainly caused by the competition of SHB effect and the gain non-linearities. At low bias, the SHB induced power-dependent loss is the dominant non-linearity. However, as bias increases, the optical loss begins to saturate and the corresponding non-linear distortions reduced. On the other hand, the non-linear distortion due to the non-linear gain increases with increased bias. For a

DFB with unoptimised κL product, the non-linear distortions of the SHB effect is usually dominant over that of the gain non-linearities. In some cases, at given bias, the non-linear effects of SHB and that of the non-linear gain negate each other so that a dip appears in the non-linear distortion versus bias curves.

Similar to the high frequency distortion case, devices with high differential gain, for instance QW/SLQW lasers, exhibit a comparatively lower non-linear distortion level than bulk devices. Although these high gain device is expected to deliver a large gain suppression value liable to additional non-linear distortion, the increase in differential can in general compensate for this.

In regard to the linearity requirements of a CATV AM-VSB system, the second-order non-linear distortions have been shown to be more problematic than that of the third-order counterparts.

The leakage current which arises in the most laser diode devices, can also cause additional non-linear distortions in a laser diode. An example of the buried heterostructure type device has been given. By combining the leakage current model and the rate-equation model with a Volterra series approach, it is found that the SHB effect dominates the non-linear distortions in most circumstances, except for the case of an optimised κL DFB. The leakage current should be minimised in order to ensure that the benefits of choosing an optimal κL for reducing the non-linear distortions are preserved.

The combining process of the SHB and the leakage current effects via the use of Volterra can be generalised to include other types of laser diode structure provided an electrical equivalent circuit of the leakage path is obtained.

References

[1] T.E. Darcie and R.S. Tucker, "Intermodulation and harmonic distortion in InGaAsP lasers", *Electron. Lett., vol. 21, pp. 665-666, 1985.*

[2] W.I. Way, "Subcarrier multiplexed lightwave system design considerations for subscriber loop applications", *IEEE J. Lightwave Tech., vol. 7, pp.1806-1818, 1989.*

[3] A. Takemoto, H. Watanabe, Y. Nakajima, Y. Sakakibara, S. Kakimoto, J. Yamashita, T. Hatta and Y. Miyake, "Distributed feedback laser diode and module for CATV system", *IEEE J. Selected Areas in Comm., vol. 8, pp. 1359-1364, 1990.*

[4] P. Iannone and T.E. Darcie, "Mutichannel intermodulation distortion in high speed GaInAsP lasers", *Electron. Lett., vol. 23, pp. 1361-1362, 1987.*

[5] G. Morthier, F. Libbrecht, K. David, P. Vankwikelberge and G. Baets, "Theoretical investigation of the second-order harmonic distortion in the AM response of 1.55 μm F-P and DFB lasers", *IEEE J. Quantum Electron., vol. QE-27, pp. 1990-2002, 1991.*

[6] H. Soda, Y. Kotaki, H. Sudo, H. Ishikawa, S. Yamakoshi and H. Imai, "Stability in single longitudinal mode operation in GaInAsP/InP phase-adjusted DFB lasers", *IEEE J. Quantum Electron., vol. QE-23, pp. 804-814, 1987.*

[7] H. Kawamura, K. Kamite, H. Yonetani, S. Ogita, H. Soda and H. Ishikawa, "Effect of varying threshold gain on second order intermodulation distortion in distributed feedback lasers", *Electron. Lett., vol. 26, pp.1720-1721, 1990.*

[8] N.K. Dutta, D.P. Wilt and R.J. Nelson, "Analysis of leakage currents in 1.3μm InGaAsP real-index-guided lasers", *IEEE J. Lightwave Tech., vol. 2, pp. 201-208, 1984.*

[9] M.S. Lin, S.Y.J. Li and N.K. Dutta, "Measurements and modelling of the harmonic distortion in InGaAsP distributed feedback lasers", *IEEE J. Quantum Electron., vol. 26, pp. 998-1004, 1990.*

[10] S.Y. Huang, L.C. Upadhyayula, J. Lipson, E.L. Flynn and C.B. Roxlo, "Frequency-dependent distortions of composite triple beat in lightwave CATV transmission systems", *IEEE J. Selected Areas in Commun., vol. 8, pp. 1365-1367, 1990.*

[11] H. Kogelnik and C.V. Shank, "Couple-wave theory of distributed feedback lasers", *J. Appl. Phys., vol. 43, pp. 2327-2335, 1972.*

[12] H.A. Haus and C.V. Shank, "Antisymmetric taper of distributed feedback lasers", *IEEE J. Quantum Electron., vol. QE-12, pp. 532-539, 1976.*

[13] T.E. Darcie and G.E. Bodeep, "Lightwave multi-channel analog AM video distribution system", *ICC'89, pp. 32.4.1-32.4.4, 1989.*

[14] T.E. Darcie, J. Lipson, C.B. Roxlo and C. J. McGrath, " Fibre optic device technology for broadband analog video systems", *IEEE LCS Magazine, pp.46-52, February 1990.*

[15] K. Lau and A. Yariv, "Intermodulation distortion in a directly modulated semiconductor injection laser", *Appl. Phys. Lett., vol. 45, pp. 1034-1036, 1984.*

[16] H.M. Salgado and J.J. O'Reilly, "Volterra series analysis of distortion in semiconductor laser diode", *LEOS'91 San Jose, SDL10.2, pp. 53, 1991.*

Chapter 8

Conclusions

This thesis has been concerned with the investigation of the dynamical behaviour of laser diodes used in analogue lightwave systems, such as, subcarrier multiplexed – broadband service network (SCM-BSN) and cable television (CATV) systems. Particular emphasis has been given to study the bandwidth and non-linear distortion of these devices. The findings of these two areas are summarised in sections 1 and 2.

8.1 Bandwidth

Various aspects of the possible limitations on the bandwidth of laser diodes have been discussed. The following have been considered :

8.1.1 Damping effects

A damping factor ζ is defined for characterising the damping effect exhibits by a laser diode. From a small signal analysis of the single-mode rate equations, the

fundamental relationship between damping and intrinsic modulation bandwidth has been derived. The major contribution to the damping effect which has been considered is the material gain non-linearity (or gain suppression effect). Using the standard two-level non-linear gain model, bandwidth optimisation has been performed. It was found that by driving the laser diode to $\zeta = 0.707$, both maximum bandwidth and flat frequency response, which are the basic criteria for the laser diode deployed in an analogue lightwave system, can be achieved simultaneously.

8.1.2 Fundamental material effects

A simple linear equation relating the material properties, such as differential gain, gain suppression and photon lifetime to the intrinsic maximum bandwidth (or the Olshansky's K factor) was then obtained. This relationship shows that the advantage of using high differential materials for increasing the bandwidth is often offset by an enhanced gain suppression effect. For example, quantum well (QW) and strained-layer quantum well (SLQW) devices which have large differential gain are expected to produce a higher modulation bandwidth than bulk materials. However, due to their high gain suppression values, no real bandwidth enhancement over the bulk devices are observed for the QW/SLQW materials. Modulation p-doped multi-quantum well (MQW) devices, on the other hand, have recently been shown to break the bandwidth record of devices made from bulk materials. This is *partly* due to the enhancement in differential gain in these materials without causing any increase in their gain suppression values.

8.1.3 Non-linear gain effects

A study of two commonly used non-linear gain models : the so called *two level* and *non-perturbative* models, has been undertaken. The non-perturbative model does not predict, in contrast to the two-level model, any limits on the intrinsic bandwidth as optical output increases. This is certainly an advantage for high speed optical systems eg. subcarrier multiplexed - broadband service network (SCM-BSN), which seek to exploit the multi-GHz bandwidth of the laser diode. Nevertheless, to date, there has been little experimental work capable of distinguishing the two physical mechanisms, since very high power operation is required in order to test the predictions of the two models.

8.1.4 Parasitic effects

A modified K factor/maximum bandwidth relationship of a laser diode due to chip parasitics has been deduced. The frequency responses of several 1.3 μm ridge waveguide DFB lasers diodes provided by Northern Telecom, Paignton, UK, were measured. The differential gain and gain suppression coefficient of the devices were estimated by fitting the experimental results to the theory. The parasitics RC time constant was subsequently obtained. The results show that the present devices are seriously hampered by the parasitic effects.

8.1.5 Carrier transport effects in QW devices

Carrier transport processes (between the quantum well and the adjacent separated confinement heterostructure (SCH) layer) are another limiting factor on the

achievable bandwidth of QW laser devices. It has been found that the carrier transport model proposed by R. Nagarajan *et al* is capable of showing not just (i) a low frequency parasitic-like RC roll off on the frequency response due to carrier diffusion across the SCH region; but also (ii) a damping effect induced by the quantum capture/escape processes at the quantum well.

Therefore a larger maximum bandwidth is expected to be achieved by minimising the diffusion time across the SCH region and the quantum escape rate. Doping the SCH region and optimising its width with confinement factor can result in shorter diffusion time; while using GRIN SCH structure with a wider and deeper well can also reduce the quantum escape effects. This is another explanation for the high bandwidth obtained with modulation p-doped MQW lasers.

There exists a certain similarity between the parasitic and the carrier transport effects. The modified K factor/maximum bandwidth equation derived for the chip parasitics can therefore be used for the estimating the intrinsic bandwidth due to the carrier transport effects. It is suggested that the relative intensity method (RIN) measurement method can give an over-estimation of the maximum intrinsic bandwidth due to the neglect of carrier transport effect. However, the modified K factor/maximum bandwidth relationship can be used to correct the over-estimation.

8.2 Non-linear distortions

In a frequency division multiplexed (FDM) lightwave system such as SCM-BSN and cable television CATV system, the number of non-linear distortion components (distortion term count) and the magnitude of each individual distortion

component are of equal importance for estimating non-linear distortions. The principle of frequency spectrum planning based on the distortion term count has been introduced. In terms of number of terms, the second-order ($f_1 \pm f_2$) and third-order ($f_1 + f_2 - f_3$) intermodulation products have the highest number. Whilst the number of ($f_1 \pm f_2$) peaks at the band edges of the FDM frequency band and ($f_1 + f_2 - f_3$) peaks at the middle of the frequency band. Usually, the number second-order distortion terms is much less than that of its third-order counterpart. Furthermore, by keeping the bandwidth of the system within one frequency octave, the second-order non-linear distortions can be eliminated.

In analysing the amplitude of the distortion components generated in a laser diode, two methods – the perturbation method and the Volterra series approach have been used. The Volterra series provides a more general and systematic approach. The discussions of laser diode non-linear distortions have been categorised by the modulation frequency with reference to the half of the undamped frequency value $f_o/2$:

8.2.1 High frequency distortions ($f > f_o/2$)

The distortions in the high frequency regime are mainly caused by the relaxation oscillation (RO) effects and can therefore be controlled by the damping factor ζ. The optimal value of $\zeta = 0.707$ can be used to minimise the RO induced distortions (as well as providing maximum intrinsic bandwidth). Furthermore, a laser diode with a large differential gain such as QW/SLQW devices which give a higher f_o are expected to experience comparatively lower RO induced non-linear distortions.

At such a high frequency, the relatively higher level of second-order non-linear distortions with smaller number of terms, is usually more problematic than the large number of third-order distortions generated in a multichannel system. Hence, most high frequency SCM systems operate within one octave of bandwidth to eliminate these second-order products.

Because of the presence of RO induced non-linear distortions, the AM-VSB format with a stringent linearity requirement, is often restricted to operate in the low frequency window. On the other hand, SCM systems using other modulation formats, such as FM, PSK, FSK etc., which require relatively low CNR, can operate in the high frequency regime of the laser diode.

8.2.2 Low frequency distortions ($f < f_o/2$)

Two commonly occurring low frequency non-linear distortions, induced by spatial hole burning (SHB) and leakage current effects, have been discussed

The single-mode, low RIN and high linearity features have made distributed feedback (DFB) lasers superior to the Fabry-Perot (FP) device in analogue optical communication systems. However, the DFB lasers can suffer from the SHB effect, which can contribute an additional low frequency non-linear distortion. The mechanism which couples the standing wave SHB effect to generated non-linear distortion is the power-dependent optical loss.

By using a rate-equation model with power-dependent loss term, it was found that in order minimise such a SHB induced non-linear effects, the coupling coefficient and cavity length product, ie. κL has to be selected carefully. In general, a DFB

laser with anti-reflection (AR) coating on both sides, a $\kappa L = 1.7$ is needed for minimising such type of distortion. Similarly, an optimal value of $\kappa L = 1.25$ is required for a $\lambda/4$ phase-shifted DFB laser. For the case of unequal facet reflectivities, this optimal value of κL may change.

The model developed can also explain the bias dependence of the non-linear distortion. At low bias, the SHB induced non-linear distortion is dominant, however, as bias increases, this type of distortion begins to decrease due to saturation of the SHB effect. The non-linear distortions due to gain suppression will then follow when bias increases. In some case, at a given bias, the non-linear effects of the SHB and that of the gain non-linearity may negate each other so that a dip may appear in the non-linear distortion versus bias curve.

As in the high frequency distortion case, devices with high differential gain, for instance QW/SLQW lasers, exhibit a comparatively lower non-linear distortion level than bulk devices. Although these high gain devices are expected to deliver a large gain suppression value, which is liable to give an additional non-linear distortion, the increase in differential gain can in general compensate for this.

The leakage current which arises in most laser diode devices, can also cause additional non-linear distortions in a laser diode. An example of the buried heterostructure type device has been examined. By combining the leakage current model and the rate-equation model (including power dependent loss) with a Volterra series approach, it was found that the SHB effect dominates the non-linear distortions in most circumstances, except for the case of an optimised κL DFB. The leakage current should be minimised in order to ensure that the benefits of choosing an optimal κL for reducing the non-linear distortions are preserved.

8.3 Laser diode for SCM systems

In a subcarrier multiplexed (SCM) lightwave system such as SCM-BSN or SCM CATV system, the directly modulated laser diode is acting as the front end of the electrical-optical conversion process and therefore its dynamical behaviour can affect the system performance directly. DFB lasers are often used in SCM systems due to their capabilities of offering single mode operation with low RIN when compared to the FP devices. Summarising the above findings of this thesis, it is obvious that the QW/SLQW DFB lasers with optimal κL and minimised leakage should be an ideal candidate for a SCM system. If high bandwidth is of prior importance, then p-doped MQW DFB laser could be an option.

8.4 Suggestions for future work

Although, this thesis has provided some coverage related to the bandwidth and non-linear distortion of a laser diode, there is still quite a lot of research work to be done in those areas. The following is just to name a few of them.

As far as the material properties are concerned, the actual mechanism for the gain suppression is open for debate and a further insight on to this is necessary. The carrier transport phenomenon of the quantum well material, which is also one of the recent hot topic, should receive further investigation. Bandwidth improvement has been shown to be due to enhanced differential gain of p-doped quantum well devices, however, the effect of doping on the material non-linearity is still not quite clear and hence a thorough investigation seems worthwhile.

The intrinsic RIN of a laser diode is usually small, however, in the presence of external optical feedback, the overall RIN of a SCM system can be deteriorated. Hence, thorough examination of the interaction between the laser diode and the external optical feedback is necessary. The laser chirp, which can induced additional non-linear distortions due to its interaction with the fibre dispersion (particularly at 1.5 *mu*m wavelength), should also be scrutinised.

Appendix A

Small signal analysis

The small signal technique can be used for linearising a non-linear system to obtain the fundamental frequency response (linear transfer function). Providing the non-linearities of the system are not too strong, the technique is also applicable to the analysis of the higher order non-linear transfer functions which give rise to non-linear distortions.

A.1 Application to rate equations

Considering an injection current $\tilde{I}$ to a laser diode, comprising of steady state bias current I and small variation δi, the corresponding carrier $\tilde{N}$ and photon densities $\tilde{P}$ are assumed to be perturbed by a small amount δn and δp around their steady state values N and P, that is,

$$\tilde{I} = I + \delta i; \quad \tilde{N} = N + \delta n; \quad \tilde{P} = P + \delta p$$

where $I \gg \delta i, N \gg \delta n$ and $P \gg \delta p$. Then the terms G, τ_e and R_{sp} in the rate equation Eqn (2.1) can be expanded in a Taylor series in the small perturbation

in N and P, so that,

$$\begin{aligned}
G(\tilde{N},\tilde{P}) &= G(N,P) + \frac{\partial G}{\partial N}\delta n + \frac{\partial G}{\partial P}\delta p + \frac{1}{2}\frac{\partial^2 G}{\partial N^2}(\delta n)^2 + \frac{1}{2}\frac{\partial^2 G}{\partial P^2}(\delta p)^2 + \cdots \\
\gamma_e(\tilde{N}) &= \gamma_e(N) + \frac{\partial \gamma_e}{\partial N}\delta n + \frac{1}{2}\frac{\partial^2 \gamma_e}{\partial N^2}(\delta n)^2 + \cdots \\
R_{sp}(\tilde{N}) &= R_{sp}(N) + \frac{\partial R_{sp}}{\partial N}\delta n + \frac{1}{2}\frac{\partial^2 R_{sp}}{\partial N^2}(\delta n)^2 + \cdots
\end{aligned}$$

Substituting the above series expansions back into the rate equation Eqn (2.1), and rearranging terms, this leads to the following non-linear differential equations,

$$\begin{aligned}
\frac{d\delta n}{dt} &= \frac{\delta i}{eV} + k_A\delta n + k_B\delta p + X_{NN}\delta n^2 + X_{PP}\delta p^2 + X_{NP}\delta n\delta p \\
&\quad + X_{NNN}\delta n^3 + X_{PPP}\delta p^3 + X_{NNP}\delta n^2\delta p + X_{PPN}\delta p^2\delta n + \cdots \\
\frac{d\delta p}{dt} &= k_C\delta n + k_D\delta p + Y_{NN}\delta n^2 + Y_{PP}\delta p^2 + Y_{NP}\delta n\delta p \\
&\quad + Y_{NNN}\delta n^3 + Y_{PPP}\delta p^3 + Y_{NNP}\delta n^2\delta p + Y_{PPN}\delta p^2\delta n + \cdots \qquad \text{(A.1)}
\end{aligned}$$

where

$$\begin{aligned}
k_A &= -\left(\frac{\partial G}{\partial N}P + \frac{d\gamma_e \cdot N}{dN}\right) \\
k_B &= -\left(\frac{\partial G}{\partial P}P + G\right) \\
k_C &= \Gamma\left(\frac{\partial G}{\partial N}P + \frac{\partial R_{sp}}{\partial N}\right) \\
k_D &= \Gamma\left(\frac{\partial G}{\partial p}P + G\right) - \gamma \\
&= \Gamma\left(\frac{\partial G}{\partial P}P - \frac{R_{sp}}{P}\right) \\
X_{NN} &= -\left(\frac{1}{2}\frac{d^2\gamma_e}{dN^2}N + \frac{d\gamma_e}{dN}\right) \\
X_{PP} &= -\left(\frac{1}{2}\frac{\partial^2 G}{\partial P^2}P + \frac{\partial G}{\partial P}\right) \\
X_{NP} &= -\left(\frac{\partial^2 G}{\partial N\partial P}P + \frac{\partial G}{\partial N}\right)
\end{aligned}$$

$$
\begin{aligned}
X_{NNN} &= -\left(\frac{1}{2}\frac{d^2\gamma_e}{dN^2}+\frac{1}{6}\frac{d^3\gamma_e}{dN^3}N+\frac{\partial^3 G}{\partial N^3}\right)\\
X_{PPP} &= -\left(\frac{1}{6}\frac{\partial^3 G}{\partial P^3}P+\frac{1}{2}\frac{\partial^2 G}{\partial P^2}\right)\\
X_{NNP} &= -\left(\frac{1}{2}\frac{\partial^3 G}{\partial N^2\partial P}P+\frac{1}{2}\frac{\partial^2 G}{\partial N^2}\right)\\
X_{PPN} &= -\left(\frac{1}{2}\frac{\partial^3 G}{\partial P^2\partial N}P+\frac{\partial^2 G}{\partial N\partial P}\right)\\
Y_{NN} &= \Gamma\left(\frac{1}{2}\frac{\partial^2 G}{\partial N^2}P+\frac{d^2R_{sp}}{dN^2}\right)\\
Y_{PP} &= \Gamma\left(\frac{1}{2}\frac{\partial^2 G}{\partial P^2}P+\frac{\partial G}{\partial P}\right)\\
Y_{NP} &= \Gamma\left(\frac{\partial^2 G}{\partial N\partial P}P+\frac{\partial G}{\partial N}\right)\\
Y_{NNN} &= \Gamma\left(\frac{1}{6}\frac{\partial^3 G}{\partial N^3}P+\frac{1}{6}\frac{d^3R_{sp}}{dN^3}\right)\\
Y_{PPP} &= \Gamma\left(\frac{1}{6}\frac{\partial^3 G}{\partial P^3}P+\frac{1}{2}\frac{\partial^2 G}{\partial P^2}\right)\\
Y_{NNP} &= \Gamma\left(\frac{1}{2}\frac{\partial^3 G}{\partial N^2\partial P}P+\frac{1}{2}\frac{\partial^2 G}{\partial N^2}\right)\\
Y_{PPN} &= \Gamma\left(\frac{1}{2}\frac{\partial^3 G}{\partial P^2\partial N}P+\frac{\partial^2 G}{\partial N\partial P}\right)
\end{aligned}
$$

where all coefficients $k_A, k_B, k_C, k_D, X_{NN}, Y_{NN}, X_{NP}, \cdots$ are functions of the steady state quantities N and P. The coefficients k_A, k_B, k_C and k_D are related to the fundamental frequency response; while the terms with the coefficients $X_{NN}, Y_{NN}, X_{NP}, Y_{NP} \cdots$ contains quadratic and higher orders products of δn and δp are essential for calculating the small signal non-linear distortions as given in Chapter 6.

Eqns (A.1) are therefore linearised by neglecting all high powers terms of δn and δp, this results in the following coupled first order ordinary differential equations

(ODE),

$$\begin{aligned}\frac{d\delta n}{dt} &= \frac{\delta i}{eV} + k_A\delta n + k_B\delta p \\ \frac{d\delta p}{dt} &= k_C\delta n + k_D\delta p \end{aligned} \tag{A.2}$$

Differentiating Eqn (A.2) w.r.t. time again, the following second order ODE can be obtained,

$$\begin{aligned}\frac{d^2\delta n}{dt^2} - (k_A + k_D)\frac{d\delta n}{dt} + (k_Ak_D - k_Bk_C)\delta n &= \frac{1}{qV}\left(\frac{d\delta i}{dt} - k_D\delta i\right) \\ \frac{d^2\delta p}{dt^2} - (k_A + k_D)\frac{d\delta p}{dt} + (k_Ak_D - k_Bk_C)\delta p &= k_C\frac{\delta i}{qV} \end{aligned} \tag{A.3}$$

A.2 Step response

Assuming a step input current, hence setting $d\delta i/dt = 0$ and $\delta i = 0$, Eqn (A.3) becomes,

$$\frac{d\mathcal{Q}}{dt} - (k_A + k_D)\frac{d\mathcal{Q}}{dt} + (k_Ak_D - k_Bk_C)\mathcal{Q} = 0 \tag{A.4}$$

where $\mathcal{Q} = \delta n$ or δp. This second order ordinary differential equation can be solved by assuming the time dependence of $\mathcal{Q}$ as a damped sinusoidal, that is,

$$e^{-(\alpha_r \pm j\omega_r)t} \tag{A.5}$$

with

$$\alpha_r = -\frac{1}{2}(k_A + k_D) \tag{A.6}$$

$$\omega_r^2 = \omega_o^2 - \alpha_r^2 \tag{A.7}$$

$$\omega_o^2 = k_Ak_D - k_Bk_C \tag{A.8}$$

where $f_o = \omega_o/(2\pi)$ is the undamped frequency; $f_r = \omega_r/(2\pi)$ is the relaxation frequency; and α_r is the damping rate of the relaxation oscillation (RO). Notice

that only in the case that the damping rate $\alpha_r \ll \omega_o$, can the (angular) relaxation frequency ω_r be approximated by the (angular) undamped frequency ω_o; this is usually not the case for a laser diode.

A damping factor ζ for characterising the level damping in the system is defined as,

$$\zeta = \frac{\alpha_r}{\omega_o} \tag{A.9}$$

Figure A.1 shows the step response of a laser diode for different values of damping factor under various bias current. The frequency of the ringing is given by the relaxation frequency f_r. It is obvious the damping effect increases with the bias current and results in a reduced ringing effect. Furthermore, there exists a turn-on delay which is purely determined by the electron recombination processes inside the lasing cavity, hence it is a function of $\gamma_e(N)$.

A.3 Frequency response

The (fundamental) frequency response of the laser diode can be studied by either transforming Eqn (A.3) to the frequency domain using Fourier transform or using the following procedure. Representing $\delta i, \delta n$ and δp by a small sinusoidal modulation, therefore,

$$\begin{aligned} \delta i &= Re\{\delta i^{\omega} \exp^{j\omega t}\} \\ &= \frac{1}{2}[\delta i^{\omega} \exp^{j\omega t} + (\delta(i^{\omega})^{*} \exp^{-j\omega t}] \end{aligned}$$

similarly,

$$\delta n = \frac{1}{2}[\delta n^{\omega} \exp^{j\omega t} + (\delta n^{\omega})^{*} \exp^{-j\omega t}]$$

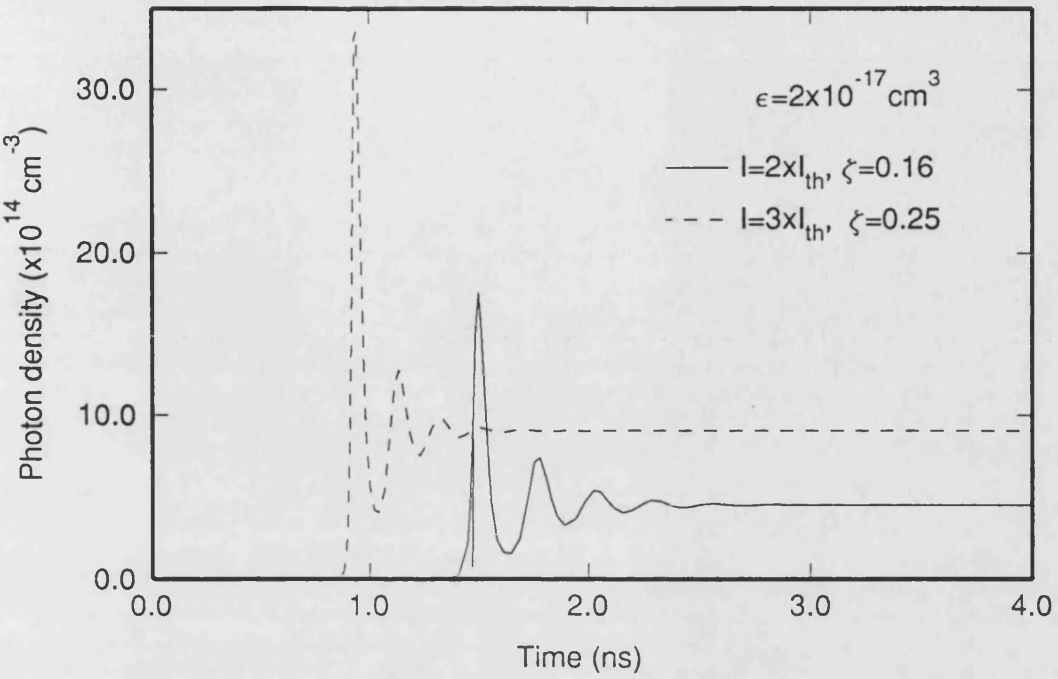

Figure A.1: *Time response for a step injection current at different amplitude leading to different values of damping factor* ζ

$$\delta p = \frac{1}{2}[\delta p^{\omega} \exp^{j\omega t} + (\delta p^{\omega})^{*} \exp^{-j\omega t}]$$

where $Re(\cdot)$ represents real part of the complex function and $(\cdot)^{*}$ denotes the complex conjugate. $\delta i^{\omega} = (\delta i^{\omega})^{*}, \delta n^{\omega} = (\delta n^{\omega})^{*}$ and $\delta p^{\omega} = (\delta p^{\omega})^{*}$ are the amplitude of the small signal quantities at a particular frequency ω. Collecting similar exponential terms, this gives,

$$\delta n^{\omega} = \frac{(\delta i^{\omega}/eV)(j\omega - k_D)}{\omega_o^2\left[\left(\frac{j\omega}{\omega_o}\right)^2 + 2\frac{\alpha_r}{\omega_o}\left(\frac{j\omega}{\omega_o}\right) + 1\right]} \tag{A.10}$$

$$\delta p^{\omega} = \frac{(\delta i^{\omega}/eV)k_C}{\omega_o^2\left[\left(\frac{j\omega}{\omega_o}\right)^2 + 2\frac{\alpha_r}{\omega_o}\left(\frac{j\omega}{\omega_o}\right) + 1\right]} \tag{A.11}$$

The intrinsic electro-optical frequency response $F_{int}(\omega) \equiv \delta p^{\omega}/\delta i^{\omega}$ is therefore given by,

$$F_{int}(\omega) = \frac{1}{qV}\frac{\Gamma\frac{\partial G}{\partial N}P}{\omega_o^2}H_{int}(\omega)$$

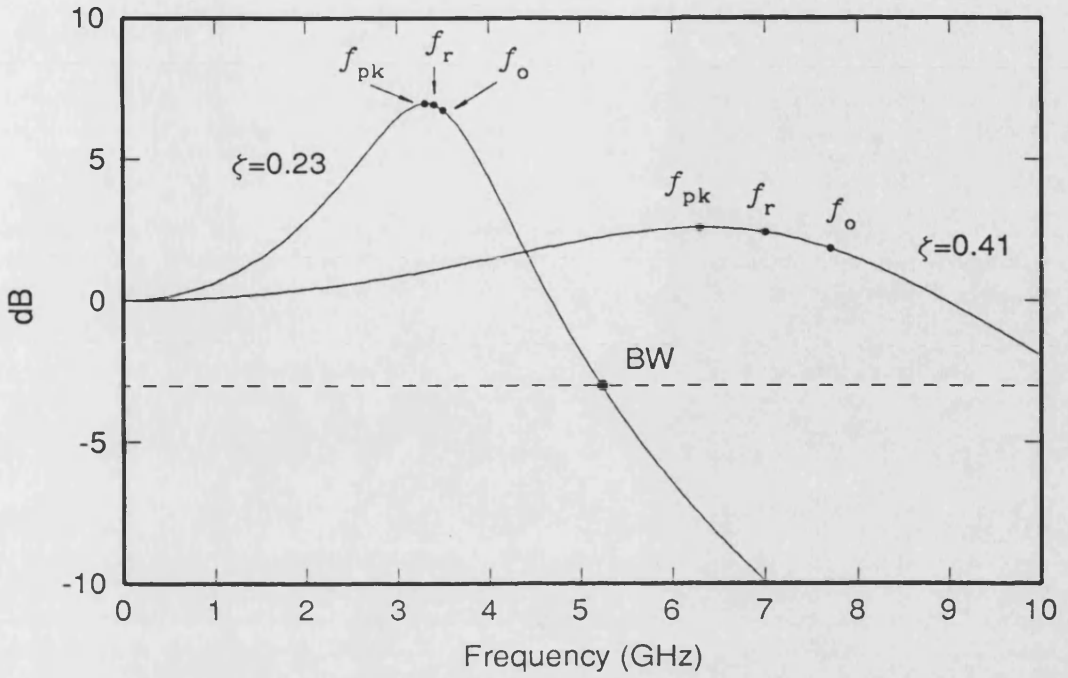

Figure A.2: *Frequency response for a laser diode at different of damping factor* ζ *due to increase in bias current.*

$$H_{int}(\omega) = \frac{1}{\left(\frac{j\omega}{\omega_o}\right)^2 + 2\frac{\alpha_r}{\omega_o}\left(\frac{j\omega}{\omega_o}\right) + 1} \tag{A.12}$$

where $H_{int}(\omega) = F_{int}(\omega)/F_{int}(0)$ is the normalised response function and is depicted in Figure A.2. Clearly, a stronger damping effect is obtained as bias current increases. The figure also illustrates the difference between the undamped frequency f_o, relaxation frequency f_r and peak response frequency f_{pk}. It is obvious that as damping factor ζ increases, the discrepancy between the three frequency terms grows and therefore they should not be assumed to be equal.

A.4 Power-dependent loss

Modification of the following terms are needed when the optical loss γ_p is expressed as a power-dependent function as in Chapter 7 :

$$\begin{aligned} k_D &= \Gamma\left(\frac{\partial G}{\partial P}P - \frac{R_{sp}}{P}\right) - \frac{d\gamma_p}{dP}P \\ Y_{PP} &= \Gamma\left(\frac{1}{2}\frac{\partial^2 G}{\partial P^2}P + \frac{\partial G}{\partial P}\right) - \left(\frac{d\gamma_p}{dP} + \frac{1}{2}\frac{d^2\gamma_p}{dP^2}P\right) \\ Y_{PPP} &= \Gamma\left(\frac{1}{6}\frac{\partial^3 G}{\partial P^3}P + \frac{1}{2}\frac{\partial^2 G}{\partial P^2}\right) - \left(\frac{1}{2}\frac{d\gamma_p}{dP} + \frac{1}{6}\frac{d^3\gamma_p}{dP^3}P\right) \end{aligned} \tag{A.13}$$

Appendix B

Volterra kernels and scaling factors

The Volterra series expansion, which relating the output $s(t)$ and the input $r(t)$ of a non-linear system, is given in Eqn (6.18) as,

$$s(t) = \sum_{n=1}^{\infty} \int_{-\infty}^{\infty} \cdots \int_{-\infty}^{\infty} H_n(\xi_1, \xi_2, \ldots, \xi_n) \prod_{i-1}^{n} R(\xi_i) e^{j\xi_i t} d\xi_i$$

in which $H_n(\xi_1, \xi_2, \ldots, \xi_n)$ are the nth order Volterra kernels (non-linear transfer functions); and $R(\xi)$ is the frequency spectrum (Fourier transform) of the input function in time $r(t)$. The kernels of this series expansion are usually obtained using the following *probing* method.

B.1 Probing method for evaluation of Volterra kernels

Assuming the input time function $r(t)$ is represented by a series of growing exponentials, that is,

$$r(t) = e^{j\omega_1 t} + e^{j\omega_2 t} + \cdots + e^{j\omega_n t}$$

and therefore its corresponding Fourier transform can be given by the following sum of delta function,

$$R(\xi) = \delta(\xi - \omega_1) + \delta(\xi - \omega_2) + \cdots + \delta(\xi - \omega_n) \tag{B.1}$$

Substituting Eqn (B.1) into the above Volterra series expansion, the following result can be obtained,

$$\begin{aligned} s(t) &= \sum_{n=1}^{\infty} \int_{-\infty}^{\infty} \cdots \int_{-\infty}^{\infty} H_n(\xi_1, \xi_2, \ldots, \xi_n) \prod_{i=1}^{n} \\ &\quad \cdot[\delta(\xi_i - \omega_1) + \delta(\xi_i - \omega_2) + \cdots + \delta(\xi_i - \omega_n)] e^{j\xi_i t} d\xi_i \end{aligned} \tag{B.2}$$

The product of the sum of delta functions generates a sum of all different terms of the form

$$\delta(\xi_i - \omega_{k_1})\delta(\xi_i - \omega_{k_2}) \cdots \delta(\xi_i - \omega_{k_n}) \tag{B.3}$$

where each index k_i is ranging from 1 to n. Then the number of permutations*(ie. where order of the terms is important) of the above term is given by,

$$\begin{aligned} &\frac{n!}{m_1! m_2! \cdots m_n!} \\ &m_1 + m_2 + \cdots + m_n = n \end{aligned} \tag{B.4}$$

where m_i the number of occurrence of f_{k_i} in the term given in Eqn (B.3). By carrying out Eqn (B.2) and accounting for the permutations of the terms, one results in,

$$s(t) = \sum_{n=1}^{\infty} \sum_{m} \frac{n!}{m_1! \cdots m_n!} H_n(\omega_{k_1}, \cdots, \omega_{k_n}) e^{j(\omega_{k_1} + \cdots + \omega_{k_n})t} \tag{B.5}$$

where m indicates that the sum includes *all* distinct set (or class) $\{m_1, m_2, \cdots m_n\}$, such that $m_i < m_{i+1}$ to guarantee no repetition of terms only differing by permutation.

*If given n things can be divided into c classes such that things belonging to the same class are alike while things belonging to different classes are different, then the number of permutations of these things taken all at a time is $\frac{n!}{m_1! m_2! \cdots m_n!}$ with $m_1 + m_2 + \cdots + m_n = n$ and m_i is the number of things in the ith class.

In Eqn (B.5), there exists a term of order n corresponding to $m_1 = m_2 = \cdots = m_n = 1$ given by,

$$n!H_n(\omega_1, \omega_2, \cdots, \omega_n)e^{j(\omega_1+\omega_2+\cdots+\omega_n)t}$$

and there are no other terms associated with $e^{j(\omega_1+\cdots+\omega_n)t}$ than this term since $\omega_1, \ldots, \omega_n$ are linearly independent. Therefore, the nth order kernel can be determined by the coefficient of $n!\ e^{j2\pi(\omega_1+\cdots+\omega_n)t}$ in the system output when the input is the sum of exponentials given in Eqn (B.1). A recursive process is required to determine all the kernels from the system equation which governs the system behaviour. The system equation is first excited by a single exponential the coefficient of which gives $H_1(\omega)$: then a sum of two exponentials is applied to yield $H_2(\omega_1, \omega_2)$ in term of $H_1(\omega)$, and so forth. This procedure continues to the required order of non-linearities with one extra exponential being added at each step.

B.2 Scaling factor

The scaling factor is in fact similar to the permutation factor shown in Eqn (B.4) and appeared in the expression Eqn (B.5). Due to the excitation of a sum of real sinusiodals signal instead of simple growing exponentials, this permutation factor needs some modifications. The modified permutation factor is here termed as *scaling factor.*

Consider the input as sum of L sinusoidal signals, that is,

$$\begin{aligned} r(t) &= \frac{1}{2}\sum_{k=1}^{L}(r_k e^{j\omega_k t} + r_k^* e^{-j\omega_k t}) \\ &= \sum_{k=1}^{L} Re\{r_k e^{j\omega_k t}\} \end{aligned} \tag{B.6}$$

with r_k is the magnitude of the modulating signals at frequency f_k where $\omega_k = 2\pi f_k$; $Re(\cdot)$ denotes real part of the function and $(\cdot)^*$ denotes complex conjugate. Therefore, the corresponding output amplitude expressed in Volterra series expansion will have a permutation factor of,

$$2\frac{n!r_1r_2\cdots r_n}{2^n m_{-L}\cdots m_L} \tag{B.7}$$

For the case of an input consisting of three sinusoidal carriers, ie. $L = 3$,

$$\begin{aligned} i(t) &= \frac{1}{2}(i_1e^{j\omega_1 t} + i_1^*e^{-j\omega_1 t} + i_2e^{j\omega_2 t} + i_2^*e^{-j\omega_2 t} \\ &\quad + i_3e^{j\omega_3 t} + i_3^*e^{-j\omega_3 t}) \end{aligned} \tag{B.8}$$

where i_1, i_2 and i_3 are the amplitudes of the modulating signal at frequency f_1, f_2 and f_3 respectively. The amplitudes of the second and third-order distortion terms are :

order	Combination						Response	Amplitude
n	m_{-3}	m_{-2}	m_{-1}	m_1	m_2	m_3	type	
1	0	0	0	1	0	0	C_r f_1	$i_1 H_1(\omega_1)$
2	0	0	0	2	0	0	HD2 $2f_1$	$\frac{1}{2} i_1^2 H_2(\omega_1, \omega_1)$
2	0	0	0	1	1	0	IMD2 $f_1 + f_2$	$i_1 i_2 H_2(\omega_1, \omega_2)$
3	0	1	0	2	0	0	IMD3 $2f_1 - f_2$	$\frac{3}{4} i_1^2 i_2^* H_3(\omega_1, \omega_1, -\omega_2)$
3	1	0	0	1	1	0	IMD3 $f_1 + f_2 - f_3$	$\frac{3}{2} i_1 i_2 i_3^* H_3(\omega_1, \omega_2, -\omega_3)$
3	0	0	0	3	0	0	HD3 $3f_1$	$\frac{1}{4} i_1^3 H_3(\omega_1, \omega_1, \omega_1)$

Table B.1: *Amplitudes of the non-linear distortion terms.*

Appendix C

Above-threshold DFB model

In order to obtain the power dependence of the optical loss induced by the spatial hole burning (SHB) effect, an above-threshold DFB model using a pair of coupled-wave equations and a carrier rate equation is built. The approach for solving the coupled-wave equations with longitudinal variation in the parameters due to the photon distribution, is based on the Transfer Matrix Method [2] – a method which is well established for microwave circuit analysis. The basic concept of this method is to describe the laser cavity by a finite number, say M, of two-port (2×2) matrices. The functional forms of the elements for each of these matrices is initially obtained by solving the coupled-wave equations at threshold. In this case, the propagation constant within each of these matrices has no longitudinal variation. In the above threshold case, calculation of the two-port matrix progressing along the longitudinal direction (z-direction) is done by consecutive pre-multiplication of the kth with the $(k+1)$th matrix. The propagation constant is changed using the carrier density equation calculated at each interface. In the present analysis, the non-linear effect of the gain suppression is coupled through the carrier equation.

C.1 Threshold analysis

The coupled-wave equations for the analysis of a DFB laser is thereby given below [1]:

$$\begin{aligned} -\frac{dR(z)}{dz} + (\alpha - j\sigma)R(z) &= j\kappa S(z) \\ \frac{dS(z)}{dz} + (\alpha - j\sigma)S(z) &= j\kappa R(z) \end{aligned} \tag{C.1}$$

with boundary conditions :

$$\begin{aligned} R(0) &= \sqrt{r_0}S(0) = \mathcal{R}_0 S(0) \\ S(L) &= \sqrt{r_L}R(L) = \mathcal{R}_L R(L) \end{aligned}$$

here R(z) and S(z) are the amplitude for forward and backward travelling waves; σ is the detuning from the Bragg frequency; α is the the mode gain which can be thought of as the required gain to overcome the distributed loss due to the presence of grating and any facet losses; κ is the coupling coefficient; r_0 and r_L are the facet (power) reflectivities; $\mathcal{R}_0$ and $\mathcal{R}_L$ are the amplitude reflectivities.

At threshold, where the photon density is extremely small, both σ and α are z independent and the above coupled-wave equations can be solved analytically to give the following general solution :

$$\begin{aligned} R(z) &= (cosh(\varphi z) + \frac{\alpha - j\sigma}{\varphi} sinh(\varphi z))R(0) - \frac{j\kappa}{\varphi} sinh(\varphi z)S(0) \\ S(z) &= \frac{j\kappa}{\varphi} sinh(\varphi z)R(0) + (cosh(\varphi z) - \frac{\alpha - j\sigma}{\varphi} sinh(\varphi z))R(0) \end{aligned} \tag{C.2}$$

with the dispersion relationship :

$$\varphi^2 = \kappa^2 + (\alpha - j\sigma)^2 \tag{C.3}$$

where φ is the propagation constant of the waves in the z direction.

The relationship between the travelling waves at both ends of the lasing cavity, ie. $z = 0$ and $z = L$, is thus given by :

$$\begin{bmatrix} R(L) \\ S(L) \end{bmatrix} = [T] \begin{bmatrix} R(0) \\ S(0) \end{bmatrix} \tag{C.4}$$

The transfer matrix T for such a periodic structure of length L can be written as [2, 3]:

$$[T] = \begin{bmatrix} cosh(\varphi z) + \frac{\alpha - j\sigma}{\varphi} sinh(\varphi z) & -\frac{j\kappa}{\varphi} sinh(\varphi z) \\ \frac{j\kappa}{\varphi} sinh(\varphi z) & cosh(\varphi z) - \frac{\alpha - j\sigma}{\varphi} sinh(\varphi z) \end{bmatrix} \tag{C.5}$$

The following eigenvalues equation has to be satisfied in order to guarantee lasing condition (obtained by substituting Eqn (C.2) into Eqn (C.1) and evaluating that at $z = -L/2$) :

$$\alpha - j\sigma = \varphi coth(\varphi L) \tag{C.6}$$

For a given value of κ, the complex transcendental equation Eqn (C.6) can be used to determine the possible values of the complex value $(\alpha - j\sigma)$. Each solution in fact corresponds to :

- a longitudinal mode with the mode gain α which contributes to the material threshold gain a_{th} that governs the lasing condition :

$$a_{th} = \frac{1}{\Gamma}(\alpha + \alpha_{int}) \tag{C.7}$$

- and a lasing wavelength λ, determined by the value of σ, given as :

$$\sigma = \frac{2\pi n}{\lambda} - \frac{\pi}{\Lambda} \tag{C.8}$$

where Λ is the Bragg wavelength; n is the refractive index.

Lasing will take place in the mode that has the lowest threshold gain, and provided the modal gain difference is sufficient large, a stable single longitudinal mode

operation can be obtained. In practice, the stability of the single mode operation may be offset by the SHB effect [4, 5]. In the following analysis, a stable single mode operation is often assumed.

It is note worthy that for a DFB laser with $\lambda/4$ phase-shifted at the centre, the value of σ will be zero, hence indicating the lasing wavelength is exactly at the Bragg frequency [6].

C.2 Above threshold analysis

As the bias current is increased above the threshold value, the photon density increases drastically and its non-uniform distribution along the z direction due to the distributed feedback grating can cause a significant spatial variation in both $\sigma(z)$ and $\alpha(z)$. This in consequence affects the local optical gain and refractive index. It was found that accurate results are obtained using an average mode gain $\bar{\alpha}(z)$. This also served to reduced computing time. A spatial variation of the gain should induce a slight smoothing of the photon density [8]. Therefore the coupled-wave equations and the related equations to account for the spatial variation of parameters is given below :

$$\begin{aligned} -\frac{dR(z)}{dz} &+ (\bar{\alpha} - j\sigma(z))R(z) = j\kappa S(z) \\ \frac{dS(z)}{dz} &+ (\bar{\alpha} - j\sigma(z))S(z) = j\kappa R(z) \end{aligned} \tag{C.9}$$

$$\sigma(z) = \frac{2\pi n(z)}{\lambda} - \frac{\pi}{\Lambda} \tag{C.10}$$

$$\begin{aligned} P(z) &= P_L \times \hat{RS}(z) \\ &= \frac{P_L}{|R(0)|^2 + |S(0)|^2}(|R(z)|^2 + |S(z)|^2) \end{aligned} \tag{C.11}$$

$$n(z) = n_o + \Gamma \frac{dn}{dN}(N(z) - N_{th}) \tag{C.12}$$

$$N(z) = N_{th} + \frac{N_{th}(I/Ith - 1) - \bar{\tau}_e v_g a_{th}\ P(z)/(1 + \epsilon P(z))}{1 + \bar{\tau}_e v_g A_o\ P(z)/(1 + \epsilon P(z))} \tag{C.13}$$

with

$$a_{th} = \frac{1}{\Gamma}(2\bar{\alpha} + \alpha_{int}) \tag{C.14}$$

$$\bar{\alpha} = \frac{1}{L}\int_0^L \alpha(z)dz \tag{C.15}$$

$$\bar{\tau}_e = \frac{1}{\gamma_e(\bar{N})} \tag{C.16}$$

here n is the refractive index with an effective index n_o at threshold; P is the photon density with P_L being the normalisation constant to be determined; $\hat{RS}(z)$ is the photon density distribution function normalised to that field intensity at $z = 0$, ie. $|R(0)|^2 + |S(0)|^2$; the threshold gain a_{th} is thereby expressed as the sum of the average mode gain $\bar{\alpha}$ and the internal cavity loss α_{int} by scattering, carrier absorption in the active region and cladding. An effective carrier lifetime $\bar{\tau}_e$ is defined as a function of the average electron density $\bar{N} = \frac{1}{L}\int_0^L N(z)dz$ instead of depending on the local variation $N(z)$.

The lasing condition is given by equating the gain and loss within the lasing cavity, that is,

$$\Gamma \int_0^L g(z)dz = (2\bar{\alpha} + \alpha_{int})L \tag{C.17}$$

where the spatial varying gain $g(z)$ is written as

$$g(z) = \frac{A_o(N(z) - N_{tr})}{(1 + \epsilon P(z))} \tag{C.18}$$

Finally, for the determination of P_L, the lasing condition Eqn (C.17) is used with Eqn (C.13), one can then obtain,

$$\int_0^L \frac{N_{th}(I/I_{th}-1)-\bar{\tau}_e v_g a_{th}\ P(z)/(1+\epsilon P(z))}{1+\bar{\tau}_e v_g A_o\ P(z)/(1+\epsilon P(z))}dz - \frac{2L(\bar{\alpha}-\alpha|_{I=I_{th}})}{\Gamma A_o} = 0 \qquad \text{(C.19)}$$

All the above equations are quite standard except Eqn (C.13), which can be obtained via manipulating the algebra of carrier rate equation of Eqn (2.1) with $dN/dt = 0$. Similarly, the lasing condition can also be visualised through the photon rate equation of Eqn (2.1).

In terms of transfer matrix representation, the DFB laser structure is therefore partitioned into M equal section with length h, with the kth section containing the transfer matrix T_k as illustrated in Figure C.1. For the kth section, the transfer matrix T_k is given by,

$$[T_k] = \begin{bmatrix} cosh(\varphi_k h)+\frac{\bar{\alpha_k}-j\sigma_k}{\varphi_k}sinh(\varphi_k h) & -\frac{j\kappa}{\varphi_k}sinh(\varphi_k h) \\ \frac{j\kappa}{\varphi_k}sinh(\varphi_k h) & cosh(\varphi_k h)-\frac{\bar{\alpha_k}-j\sigma_k}{\varphi_k}sinh(\varphi_k h) \end{bmatrix} \qquad \text{(C.20)}$$

The variation of the propagation parameter φ, which relies on α and σ, for each matrix is obtained via Eqns (C.10)-(C.13).

Therefore the matrix equation relating the wave amplitudes at both ends of the DFB laser with length L is given by :

$$\begin{bmatrix} R(L) \\ S(L) \end{bmatrix} = [T_M][T_{M-1}][T_{M-2}]\cdots[T_k]\cdots[T_2][T_1]\begin{bmatrix} R(0) \\ S(0) \end{bmatrix} \qquad \text{(C.21)}$$

For the case of $\lambda/4$ phase-shifted DFB laser, the intracavity field experiences a phase shift at the centre of the cavity length. The Transfer Matrix Method

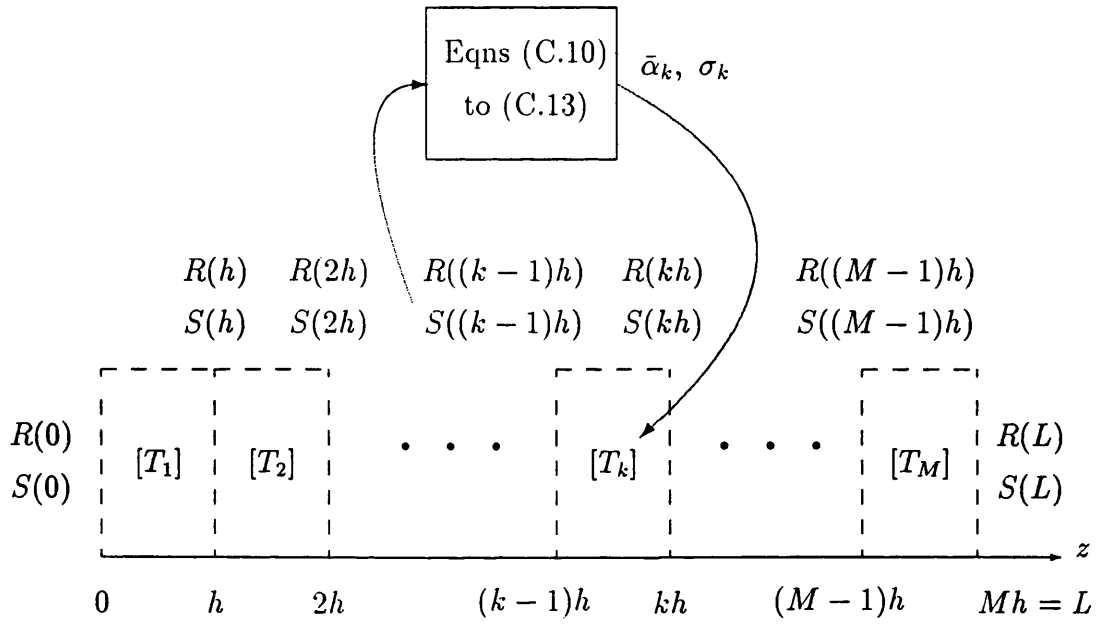

Figure C.1: *Analytical model for the Transfer Matrix Method (TMM). The DFB laser is divided into M transfer matrices $T_1, T_2, \cdots T_M$ and the propagation parameter for each matrix is obtained by applying Eqns (C.10) - (C.13) at each interface.*

(TMM) described above can easily be generalised to include the built-in phase shift by inserting the following phase shift matrix :

$$\begin{bmatrix} R(kh) \\ S(kh) \end{bmatrix} = \begin{bmatrix} e^{j\frac{\pi}{2}} & 0 \\ 0 & e^{j\frac{\pi}{2}} \end{bmatrix} \begin{bmatrix} R((k-1)h) \\ S((k-1)h) \end{bmatrix} \tag{C.22}$$

C.3 The numerical model

Figure C.2 shows the program flowchart of the DFB model, which includes the following basic steps of the numerical calculations :

(1) The threshold analysis is first performed using a Shooting method. Setting $P_L = 0$ and $I = I_{th}$, and then guess the value of α and σ at $z = 0$ boundary. Using this set of values, the wave $R(z)$ and $S(z)$ can then propagate through the DFB structure using TMM. Checking the boundary condition at $z = L$ (Eqn (C.13)) by assuming the error is,

$$\xi = S(L) - \mathcal{R}_L R(L)$$

If ξ is not within an expected error, by using two-dimensional Newton method, the adjustment to ξ is obtained by solving the following equation,

$$\frac{\partial \xi}{\partial \alpha}\delta\alpha + \frac{\partial \xi}{\partial \sigma}\delta\sigma = -\xi \tag{C.23}$$

Repeating the guess of the values of α and σ with the calculated adjustment until the required error at the boundary $z = L$ is reached.

(2) The corresponding results of the threshold – $\alpha, \sigma, R(z)$ and $S(z)$ are then used as an initial guesses for the above threshold analysis.

(3) Increment the bias current I above threshold.

(4) With the guesses, $R(z)$, $S(z)$ and $\bar{\alpha}$, Eqn (C.19) is solved using a fast root-finding method – Brent Method, to give an estimation of the normalised constant P_L.

(5) Save the value of $\bar{\alpha}$ to $\bar{\alpha}_{tmp}$ for later comparison.

(6) For the given P_L, applying the guesses $\bar{\alpha}$ and $\sigma(z = 0)$ to the boundary $z = 0$ and calculate the $R(z)$ and $S(z)$ with TMM. Using a similar shooting approach as that in step (1) to ensure the other boundary condition at $z = L$ is matched. The estimation of the adjustments is found by solving the following equation similar to Eqn (C.23):

$$\frac{\partial \xi}{\partial \bar{\alpha}} \delta\bar{\alpha} + \frac{\partial \xi}{\partial \sigma(0)} \delta\sigma(0) = -\xi \tag{C.24}$$

(7) Comparing the value of $\bar{\alpha}$ after the shooting method with $\bar{\alpha_{tmp}}$, if they do not fall within certain error, then go back to step (2) with the existing distributions $R(z)$ and $S(z)$. However, if the preset error is reached, this implies a self consistent solution between $\bar{\alpha}, \sigma(z), P_L, R(z)$ and $S(z)$ has achieved.

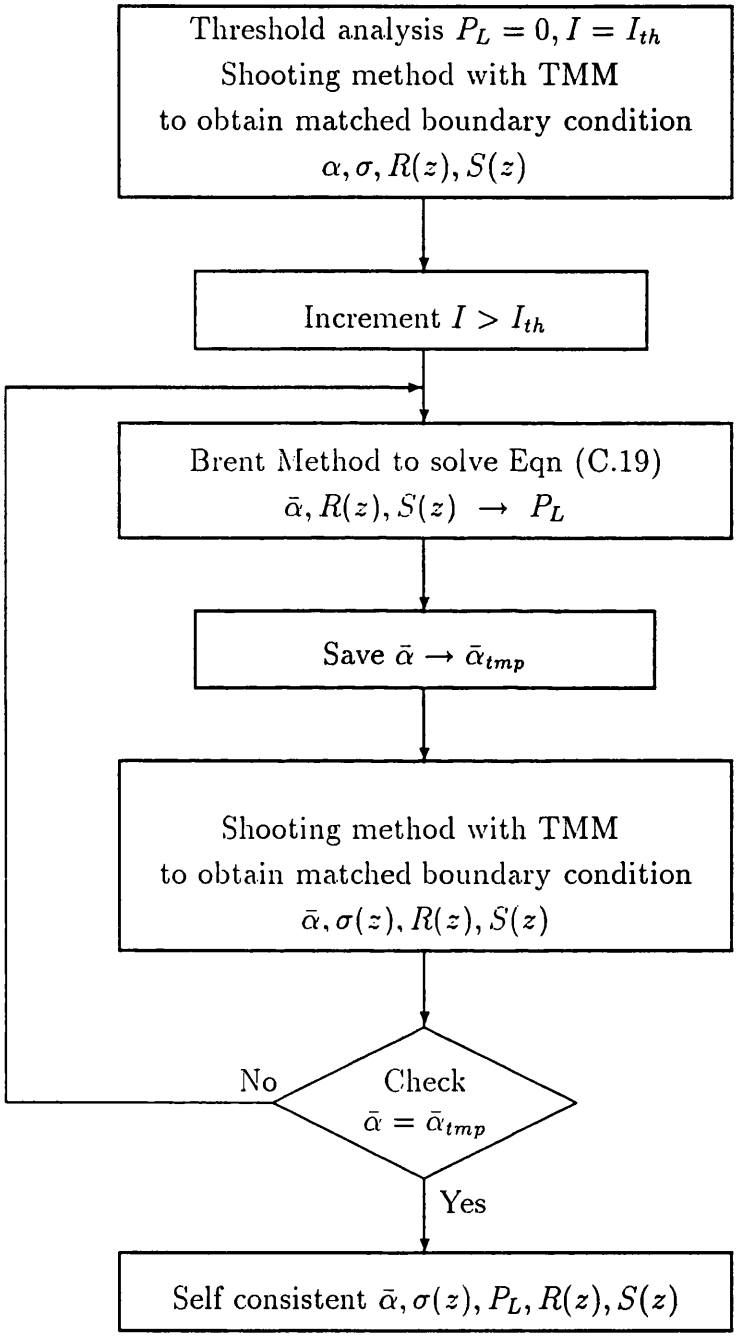

Figure C.2: *Program flowchart for the DFB model.*

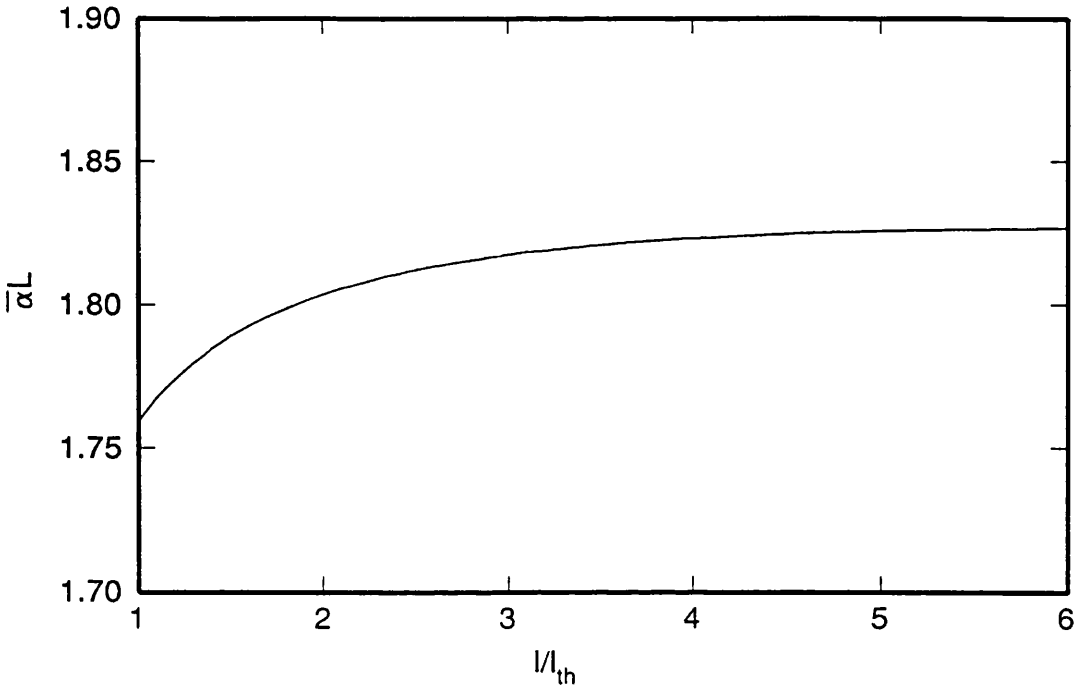

Figure C.3: *The power dependence of the mode gain $\bar{\alpha}$ for a DFB laser with $\kappa L = 1.0$.*

Figure C.3 shows the calculated power dependence of the mode gain $\bar{\alpha}$ for a DFB laser with $\kappa L = 2$. The main finding is that, the power dependence is strong at low bias and then starts to saturate as bias increases. This is mainly due to the increase of the denominator of Eqn (C.13) when bias increases. As a result, this implies that the SHB effect will decrease as bias increases.

References

[1] H. Kogelnik and C.V. Shank, "Couple-wave theory of distributed feedback lasers", *J. Appl. Phys., vol. 43, pp. 2327-2335, 1972.*

[2] G. Bjork, O. Nilsson, "A New exact and efficient numerical matrix theory of complicated laser structures : properties of asymmetric phase-shifted DFB lasers", *IEEE J. Lightwave Tech., vol. 5, pp. 140-146, 1987.*

[3] M. Yamada and K. Sakuda, "Analysis of almost-periodic distributed feedback slab waveguides via a fundamental matrix approach", *Applied Optics, vol. 26, pp. 3474-3478, 1987.*

[4] H. Soda, Y. Kotaki, H. Sudo, H. Ishikawa, S. Yamakoshi and H. Imai, "Stability in single longitudinal mode operation in GaInAsP/InP phase-adjusted DFB lasers", *IEEE J. Quantum Electron., vol. QE-23, pp. 804-814, 1987.*

[5] R. Schatz, "Longitudinal spatial instability in symmetric semiconductor lasers due to spatial hole burning", *IEEE J. Quantum Electron., vol. QE-28, pp. 1443-1449, 1992.*

[6] H.A. Haus and C.V. Shank, "Antisymmetric taper of distributed feedback lasers", *IEEE J. Quantum Electron., vol. QE-12, pp. 532-539, 1976.*

[7] G.P. Agrawal and A.H. Bobeck, "Modelling of distributed feedback semiconductor lasers with axially-varying parameters", *IEEE J. Quantum Electron., vol. QE-24, pp. 2407-2414, 1988.*

[8] I. Orfanos, T. Sphicopoulos, A. Tsigopoulos and C. Caroubalos, "A tractable above-threshold model for the design of DFB and phase-shifted DFB lasers", *IEEE J. Quantum Electron., vol. QE-27, pp. 946-956, 1991.*

List of Publications

(1) Y.C.A. Wong and K.A. Shore, " Diode laser bandwidth optimisation for analogue applications ", *Proc. IEE Colloquium on Microwave Optoelectronics, Digest No. 1990/139, pp. 1/1-1/3, 1990.*

(2) Y.C.A. Wong and K.A. Shore, " Influence of non-linear gain on bandwidth and damping factor of semiconductor lasers ", *Conference on Semiconductor and Integrated Optoelectronics (SIOE '91), UWCC, Cardiff, paper 27, 1991.*

(3) Y.C.A. Wong and K.A. Shore, " Influence of non-linear gain on the intrinsic bandwidth of quantum well and strained-layer semiconductor lasers ", *IEE Proc. Pt. J, vol. 138, pp. 413-419, 1991.*

(4) Y.C.A. Wong and K.A. Shore, " Non-linear gain effects in optimisation of semiconductor lasers for analogue applications ", *IEEE Lasers and Electro-Optics Annual Conference (LEOS '91), San Jose, California, USA, paper SDL 16.5, 1991.*

(5) Y.C.A. Wong and K.A. Shore, " Influence of photon lifetime variation on DFB laser dynamics", *Conference on Semiconductor and Integrated Optoelectronics (SIOE '92), UWCC, Cardiff, paper 29, 1992.*

(6) Y.C.A. Wong and K.A. Shore, " Analysis of two different forms of gain non-linearities on the dynamic response of a laser diode", *IEE Proc. Pt. J, vol. 139, 243-248, 1992.*

(7) Y.C.A. Wong and K.A. Shore, " Modification of laser diode bandwidth K factor due to parasitics including carrier transport in quantum well devices", *Optical Society of America Annual Meeting, Toronto, Canada, paper FB4, October 1993.*

(8) Y.C.A. Wong and K.A. Shore, " A modified K bandwidth factor relationship of semiconductor lasers due to parasitic effects", *Submitted to IEEE Photonics Technology Letter for publication.*

Influence of nonlinear gain on intrinsic bandwidth of quantum well and strained layer semiconductor lasers

Y.C.A. Wong
K.A. Shore

Indexing terms: Semiconductor lasers, Optical systems

Abstract: Optimisation of the bandwidth of semiconductor lasers subject to direct intensity modulation has been undertaken taking account of the effect of nonlinear gain suppression on the damping of relaxation oscillations. A novel relationship between the damping and the 3 dB intrinsic bandwidth of semiconductor lasers has been obtained and is used to examine the effect of the damping in limiting the intrinsic bandwidth of conventional and advanced (quantum well and strained layer) semiconductor lasers. It is shown that enhanced nonlinear gain in quantum well and strained layer lasers significantly limits bandwidth improvements anticipated for such advanced laser structures on the basis of their relatively high differential gain. The operating conditions appropriate to maximum intrinsic bandwidth have been identified in these cases.

1 Introduction

Semiconductor lasers are important light sources for broad-band optical communication systems using either analogue or digital direct modulation schemes for the transmission of e.g. video services together with voice and data. One such high performance optical system is the subcarrier multiplexed dystem (SCM) which, operating at microwave frequencies, seeks to exploit the multi-gigahertz bandwidth of laser diodes and optical fibres. In designing such a system, attention would need to be paid to the following two basic criteria. First of all, the intrinsic 3 dB bandwidth (BW) of the system should be as high as possible, in other words, the system should be capable of high speed operation. Secondly, a flat and smooth frequency response witihn the modulation frequency range should also be obtained to reduce the amount of harmonic and intermodulation distortions at high modulation frequencies.

It has been shown [1–4] that the intrinsic bandwith of the semiconductor laser is greatly influenced by the damping of relaxation oscillations (RO) arising due to nonlinear gain suppression. It is worth mentioning that although the exact origin of the gain suppression is still a matter of debate [5], spectral hole burning and carrier heating effects are widely believed to be primary sources [5–7]; although spatial carrier diffusion may be a secondary mechanism for gain suppression [8]. The main conclusions to be drawn in respect of the effect of relaxation oscillation damping are that if

(i) the damping is too small, a high resonance peak will appear in the frequency response — in contradiction with the second criterion given above

(ii) the damping is too large, a reduction in the intrinsic bandwidth occurs — violating the first criterion given above

It is clear therefore that optimisation of both the bandwidth and the damping are required to satisfy the design criteria.

The foregoing issues assume a particular importance when consideration is given to using advanced semiconductor laser structures incorporating quantum well (QW) and strained layer (SL) semiconductor material. In these cases it is expected that larger modulation bandwidths will be obtained owing to the larger differential gains which characterise these materials. However, it is found that the gain suppression is also enhanced by the quantum confinement of carriers [14] in such advanced laser structures and hence significantly reduces the effective intrinsic bandwidth. It will be argued here that because the gain suppression and the differential gain are of comparable importance in determining the bandwidth they must both be carefully considered in the use of advanced semiconductor lasers for high bandwidth applications. To date, however, rather less attention has been paid to the damping of the frequency response due to gain nonlinearities.

Some time ago, Olshansky implicitly performed a general bandwidth optimisation [1] by formulating a simple linear relationship between a damping parameter K and the maximum attainable intrinsic bandwidth. The K factor introduced by Olshansky (defined in Section 3.1 below) does not, however, indicate the role of damping in determining the response of the laser. The intention here is to introduce an alternative damping parameter which can be used to undertake a bandwidth optimisation taking damping effects into account and which also permits the evaluation of the operating conditions for the achievement of the identified maximum bandwidth. Within this formalism it is also possible to study the influence of differential gain and nonlinear gain suppression on the optimised bandwidth.

2 Basic terminologies and theory

In this work the laser diode modulation dynamics has been studied theoretically using a pair of single-mode

Paper 8446J (E3, E13), first received 27th March and in revised form 13th September 1991

The authors are with the University of Bath, School of Electronic and Electrical Engineering, Bath BA2 7AY, United Kingdom

te equations with nonlinear gain suppression taken to account thereby affecting the damping of the relaxation oscillation of the laser. All numerical calculations ere performed using the typical device and material arameters listed in Table 1.

able 1: Typical device parameters

$_{nr}$	$1 \times 10^{8}\ s^{-1}$
	$1 \times 10^{-10}\ cm^3\ s^{-1}$
	$1 \times 10^{-29}\ cm^6\ s^{-1}$
	1.7×10^{-4}
	$1 \times 10^{-10}\ cm^3$
$_{tr}$	$1 \times 10^{18}\ cm^{-3}$
	0.5
	1.5×10^{-12} s
	2.8×10^{-9} s
$_{th}$	$1.7 \times 10^{18}\ cm^3$
$_{th}$	9.77 mA
$_{g}$	$2.5 \times 10^{9}\ cm\ s^{-1}$

2.1 Rate equations with gain suppression

The pair of single-mode rate equations that we used are as follows:

$$\frac{dN}{dt} = \frac{I}{eV} - \gamma_e(N)N - G(N, P)P \tag{1}$$

$$\frac{dP}{dt} = \Gamma G(N, P)P - \gamma_p P + \Gamma R_{sp}(N) \tag{2}$$

with

$$\gamma_e(N) = \frac{1}{\tau} = A_{nr} + BN + CN^2$$

$$R_{sp}(N) = \beta\gamma_e(N)N$$

$$\gamma_p = \frac{1}{\tau_p}$$

where I, e and V are the injection current (A), electron charge (C) and volume of the active layer (cm^3); N and P are the carrier and photon densities (cm^{-3}); t, τ, τ_p are the time, carrier lifetime and photon lifetime (s); A_{nr}, B and C are the nonradiative (s^{-1}), radiative ($cm^3\ s^{-1}$) and Auger ($cm^6\ s^{-1}$) recombination rates; Γ and β are the optical confinement and the spontaneous emission factors; $G(N, P)$ is the optical gain which depends on both carrier and photon density. The functional form of this gain G is given by

$$G(N, P) = \frac{G_l}{(1 + \varepsilon P)} = \frac{g_0(N - N_{tr})}{(1 + \varepsilon P)} \tag{3}$$

where N_{tr} is the transparent carrier density (cm^{-3}); $G_l = G(N)$ which is the linear optical gain term; g_0 is the linear gain coefficient which is also termed as differential gain dG_l/dN($cm^3\ s^{-1}$); and finally, ε is the gain suppression or the nonlinear gain coefficient (cm^3). We point out that there exist alternative methods of expressing the nonlinear gain as shown, for example, in References 9 and 10. It is anticipated that such alternative expressions will result in quite different effects on the damping and bandwidth compared to those given here. These aspects will be explored in future work.

2.2 Damping rate, damping factor and bandwidth

2.2.1 Damping rate: The time response of the laser is obtained, in a conventional way, by considering the effect of a step current input using the above rate equations. In this way it is found that the carrier and photon densities have time dependences given by

$$\exp(-\alpha_r + j\Omega_r)t$$

which is in the form of a damped sinusoidal; where Ω_r is the angular relaxation frequency and α_r is the exponential decay rate or damping rate of the relaxation oscillation (RO). In addition, Ω_r is given by

$$\Omega_r = \sqrt{(\Omega_0^2 - \alpha_r^2)}$$

where Ω_0 is the angular undamped frequency. It can be seen therefore that Ω_0 will be approximately equal to Ω_r (as is often assumed), if and only if $\Omega_0 \gg \alpha_r$, i.e. when the damping is comparatively weak. That condition will not, in general, hold in the present work. It is obvious also that the higher the damping rate, the faster the relaxation oscillations die out.

Expressions for Ω_0 and α_r can be obtained if we consider the frequency response of the rate equations using the small signal analysis technique summarised in Appendix 8.1. In this way, it is found that the optical frequency response $Fr(\Omega)$ is given by

$$Fr(\Omega) = \left[\frac{j\Omega}{\Omega_0}\right]^2 + 2\frac{\alpha_r}{\Omega_0}\left[\frac{j\Omega}{\Omega_0}\right] + 1 \tag{4}$$

By keeping the dominant terms, both Ω_0 and α_r can be written as (Appendix 8.2)

$$\Omega_0 \approx \sqrt{\left[\frac{dG_l}{dN}\frac{P}{\tau_p}\frac{1}{(1 + \varepsilon P)}\right]} \tag{5}$$

$$\alpha_r \approx \frac{1}{2}\left(\varepsilon + \frac{dG_l}{dN}\tau_p\right)\frac{P}{\tau_p}\frac{1}{(1 + \varepsilon P)} \tag{6}$$

Eqns. 5 and 6 are very good approximations provided that α_r/Ω_0 is less than 1. The importance of this ratio will be emphasised in Section 3.2. Obviously, both Ω_0 and α_r are functions of the photon density P, which in turn is proportional to the injection (bias) current I. Also the optical output facet power P_{out} (intensity) can be obtained from the photon density P using the relationship

$$P_{out} = \tfrac{1}{2}\hbar\omega v_g \alpha_m \frac{PV}{\Gamma}$$

where $\cdot$ is the Planck constant, ω is the optical frequency, v_g is the group velocity ($cm\ s^{-1}$) and α_m is the mirror loss (cm^{-1}).

Hence, the damping rate will increase with the increase in optical output power. Nevertheless, the incremental change, i.e. the slope, is mainly controlled by the amount of gain suppression, ε.

2.2.2 Damping factor: In this work it is considered that insight into the laser dynamics is enhanced by the use of a damping factor ζ defined as

$$\zeta \equiv \frac{\alpha_r}{\Omega_0} \approx \frac{1}{2}\left(\varepsilon + \frac{dG_l}{dN}\tau_p\right)\Bigg/\sqrt{\left[\frac{P}{\frac{dG}{dN}\tau_p}\left(\frac{1}{1 + \varepsilon P}\right)\right]} \tag{7}$$

The damping factor ζ which will be used here is approximately proportional to the square root of the photon density P (or optical output power P_{out}) as seen in Fig. 1 which is obtained numerically. Thus the simplest way of changing this damping factor is via an alteration of the bias power or current. Clearly, one can also alter the slope of the curve by varying the differential gain dG_l/dN and photon lifetime τ_p

A typical range of ζ should be between 0 to 1, where $\zeta < 1$ is termed as underdamped, $\zeta > 1$ is called overdamped and $\zeta = 0.707$ will give a flat frequency response

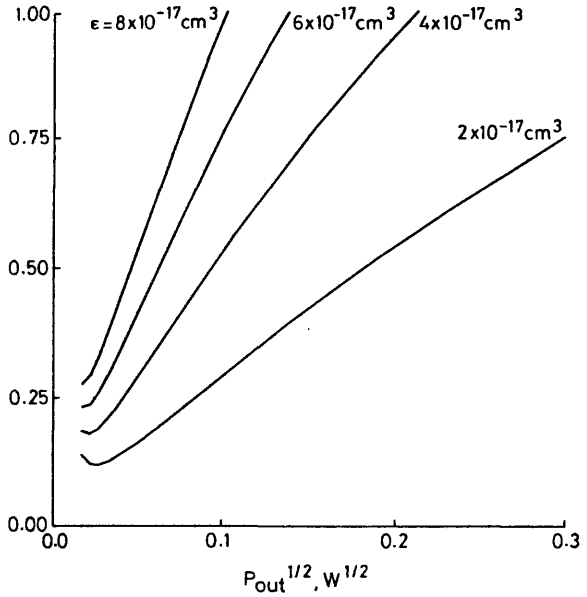

Fig. 1 *Variations of damping factor ζ with optical output power P_{out} at different values of gain suppression ε*

with no resonance peak. Therefore, ζ is not only a measure of the level of damping on the system, but it is also an indicator of the flatness of the frequency response.

Fig. 2 shows a graph of the frequency response at various levels of optical output power and which corresponds to a different level of damping factor ζ. As can be seen, the higher the ζ, the flatter the frequency response. In other words, the resonance peak shown in the frequency response is being suppressed as the damping factor ζ increases. Further usage of the damping factor ζ will be given in Section 3.

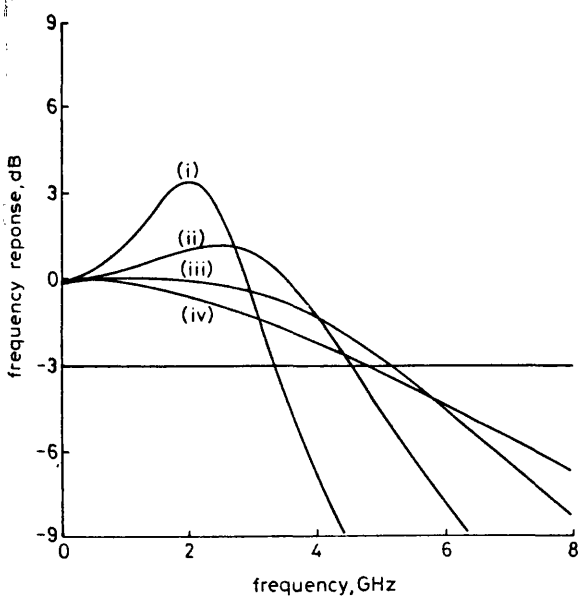

Fig. 2 *Frequency response of laser diode at different values of damping factor ζ due to various bias current I*

(i) $\zeta = 0.36$, $P_{out} = 6.2$ mW
(ii) $\zeta = 0.5$, $P_{out} = 9.5$ mW
(iii) $\zeta = 0.707$, $P_{out} = 16$ mW
(iv) $\zeta = 1.0$, $P_{out} = 32$ mW

2.2.3 Bandwidth: The -3 dB frequency in the frequency response diagram is used here to define the intrinsic bandwidth of the laser. As seen from Fig. 2 the bandwidth BW starts to increase as the damping factor ζ increases, but then at a certain value of ζ heavy damping begins to cause a reduction in the bandwidth. This effect may be understood by computing the bandwidth using the above definition, i.e. by setting $Fr(\Omega = -3\text{ dB}) = 1/\sqrt{(2)}$ from which we obtain

$$BW = Y(\zeta)\frac{\Omega_0}{2\pi} \tag{8}$$

where

$$Y(\zeta) = \sqrt{\{(1 - 2\zeta^2) + \sqrt{[(1 - 2\zeta^2)^2 + 1]}\}}$$

The square root term of eqn. 8, $Y(\zeta)$, is plotted against ζ in Fig. 3. As the damping factor ζ increases owing to an increase in bias current or power, $Y(\zeta)$ decreases. However, at the same time, the undamped frequency Ω_0 tends to increase with increasing bias current as given by eqn. 5. Therefore, a trade off exists between the square root term $Y(\zeta)$ and Ω_0, and this will result in bandwidth suppression or may even cause the bandwidth to undergo a maximum value as optical power increases. This point is discussed in detail in the following Section.

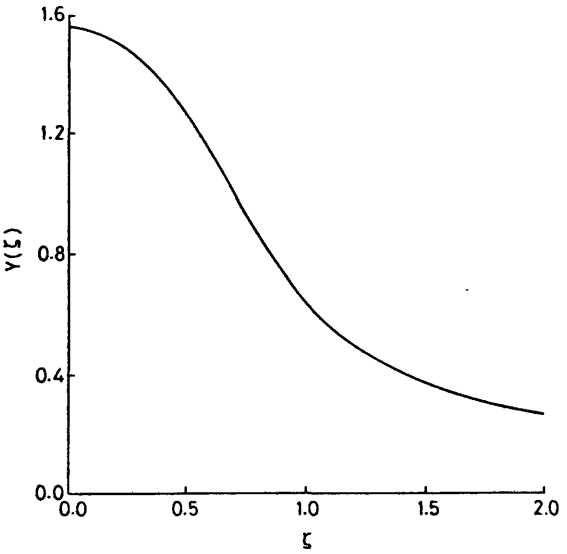

Fig. 3 *Plot of square root term $Y(\zeta)$ in eqn. 8 against damping factor ζ*

2.3 Bandwidth suppression and maximum achievable bandwidth

Bandwidth suppression: in our terminology, means that at a certain optical output power, a reduction occurs in the rate of increase of bandwidths with increasing optical power. This happens owing to the increase in damping effect which accompanies an increase of optical output power. If the damping is strong enough, the bandwidth against intensity may reach a maximum — the *maximum achievable bandwidth* BW_{max}.

Provided the laser diode can withstand high power, bandwidth suppression always exists and can easily be explained theoretically from eqn. 8 as given in the previous Section. However, the existence of the maximum achievable bandwidth solely depends on the actual functional form of both $Y(\zeta)$ (or ζ itself) and Ω_0 in terms of P.

The conditions for which the maximum bandwidth exists can be found by differentiating eqn. 8 with respect to ζ. This gives (Appendix 8.3)

$$\frac{dBW}{d\zeta} = BW\left(\frac{-2\zeta}{\sqrt{[(1 - 2\zeta^2)^2 + 1]}} + \frac{1}{\frac{d\zeta}{d\Omega_0}\Omega_0}\right) \tag{9}$$

Assuming

$$\frac{d\zeta}{d\Omega_0}\Omega_0 = \phi(P)\zeta$$

where $\phi(P)$ is either a function of P or a constant. If BW_{max} exists, then $dBW/d\zeta = 0$ at a certain value of P, which implies

$$2(\Phi(P)^2 - 1)\zeta^4 + 2\phi^2 - 1 = 0 \tag{10}$$

To retain real roots for eqn. 10, we require the discriminant to be greater than or equal to zero, that is,

$$2^2 - 4[2(\phi(P)^2 - 1)](-1) \geq 0 \Rightarrow \phi(P) \geq 0.707$$

In other words, if the bandwidth against intensity (or P) curve experiences a maximum point, i.e. maximum bandwidth BW_{max}, then the following criterion has to be fulfilled:

$$\frac{d\zeta}{d\Omega_0}\Omega_0 \geq 0.707\zeta \tag{11}$$

This criterion is very important in determining whether or not an intrinsic maximum bandwidth BW_{max} would actually occur in a laser diode. An important parameter which always affects both ζ and Ω_0 is the nonlinear gain G, where both ζ and Ω_0 are functions of P (if device parameters τ_p, dG_l/dN and ε are fixed).

3 Bandwidth optimisation

As seen in eqns. 5 and 7, for the nonlinear gain model used here, both ζ and Ω_0 are functions of

$$\sqrt{\left(\frac{P}{(1+\varepsilon P)}\right)}$$

It is easily seen that

$$\frac{d\zeta}{d\Omega_0}\Omega_0 = \frac{\zeta}{\Omega_0}\Omega_0 = \zeta > 0.707 \tag{12}$$

This proves that for our present rate equation model, with nonlinear gain as given in eqn. 3, the intrinsic bandwidth of the laser diode always experiences a maximum value, BW_{max}. The numerical results displayed in Fig. 4 (which shows the variation of the bandwidth BW with the optical output power at different values of gain suppression ε) also confirms this conclusion. With small gain suppression a higher BW_{max} can be obtained, albeit at a higher bias power than occurs for larger gain suppression.

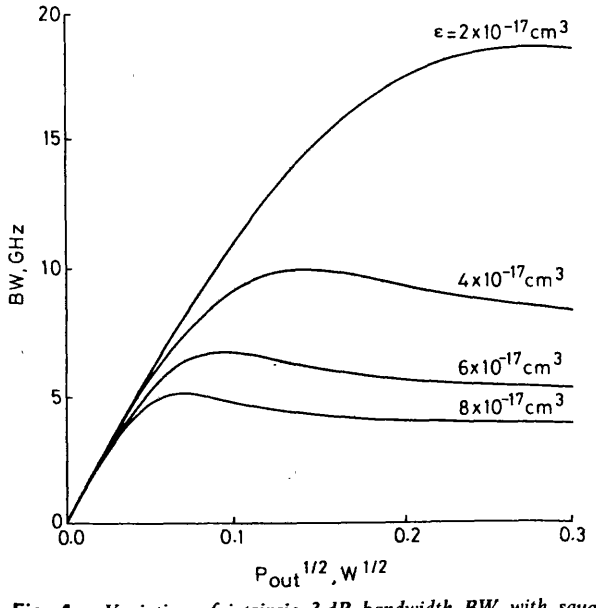

Fig. 4 *Variation of intrinsic 3 dB bandwidth BW with square root optical output power P_{out} at different damping factor ζ*

To obtain an optimal bandwidth from the laser, for a given gain suppression, it is obvious that the laser must be driven by a bias current corresponding to the relevant maximum point of the bandwidth against the square-root power curve given in Fig. 4. (i.e. BW_{max}). In addition, it is wished to characterise the flatness of the frequency response at this particular operating point.

This information can be easily extracted by substituting eqn. 12 back into eqn. 9. It is found that the damping factor ζ will always equal 0.707 whenever BW_{max} occurs. On the other hand, at this particular value of ζ ($\zeta = 0.707$), the frequency response is just flat and shows no resonance peak. This implies that the BW_{max} is actually our optimal bandwidth which satisfied the two basic criteria for a high performance system noted in the Section 1.

It is pointed out in Reference 12 that the optimal value of ζ for a high performance digital system is usually bigger than 1, i.e. corresponding to an overdamped system. The present result indicates a difference in optimisation criteria which would seem to be of particular importance for the design of high performance analogue systems.

The approximated bias current required to achieve this optimal bandwidth (BW_{max}) is then given by [11]

$$I_{BW_{max}} \approx \frac{2eV\dfrac{dG_l}{dN}}{\Gamma\left(\varepsilon + \dfrac{dG_l}{dN}\tau_p\right)^2} + I_{th} \tag{13}$$

where e is the electron charge and I_{th} is the threshold current. In general, it is desirable to have a moderate amount of gain suppression to reduce the required bias current to achieve $\zeta = 0.707$; however, with the gain suppression too high, the maximum achievable BW will be limited.

3.1 Damping parameter, K

In Reference 1, Olshansky has defined a 'damping' factor K as

$$K = \frac{2\alpha_r}{f_0^2} = 2(2\pi)^2\frac{\zeta}{\Omega_0} = (2\pi)^2\frac{\left(\varepsilon + \dfrac{dG_l}{dN}\tau_p\right)}{\dfrac{dG_l}{dN}} \tag{14}$$

which is independent of the photon density P. It is clear, therefore, that the K factor contains no information in relation to the effects of damping which have been shown above to be of considerable relevance. However, the utility of the K factor may be appreciated by noting that when the bandwidth reaches it maximum ($\zeta = 0.707$), it is found that

$$K = \frac{\sqrt{[2]}(2\pi)}{BW_{max}} \tag{15}$$

Thus, the 'damping' factor K is in fact a fast and powerful method of evaluating the maximum BW. In contrast, the strength of the damping experienced by the laser diode and the flatness of the frequency response are manifested by the damping factor ζ used in this work.

Furthermore, as mentioned in Section 2.1, there exists another functional form of nonlinear gain which gives no maximum bandwidth at all [9], in that case, the

damping' factor K loses its utility. Therefore, the K factor will only be a useful parameter if the functional form of the diode laser gain is as given by eqn. 3. On the other hand, the damping factor ζ always shows the level of damping no matter what functional form of nonlinear gain is used. In this way, the parameter ζ may always be used to identify the existence of the BW_{max} via the criterion given in eqn. 11 (as discussed in Section 2.3).

It is this general applicability of the parameter ζ which justifies its introduction as a measure of the dynamical behaviour of the laser diode.

Device material considerations

The calculations of the previous Sections emphasized the optical power or biase current dependence of the maximum bandwidth. In this Section, consideration is given to the dependence of the maximum BW on a number of device and material parameters. To high light the available options, an approximate form for the maximum bandwidth can be found by equalling eqns. 14 and 15. In this way the maximum BW can be expressed as

$$BW_{max} \approx \frac{1}{2\pi} \frac{\sqrt{(2)\dfrac{dG_l}{dN}}}{\left[\varepsilon + \dfrac{dG_l}{dN}\tau_p\right]} \qquad (16)$$

which shows that the maximum bandwidth is a function of the gain suppression ε; the photon lifetime, τ_p and the differential gain dG_l/dN.

The photon lifetime can be adjusted by varying the cavity length or else the facet reflectivities of the device. Variation of the differential gain can be achieved, for example, by changing the dopant concentrations in bulk semiconductor material or, more relevantly, by selecting a different device material. Of particular interest would be the use of advanced semiconductor materials such as quantum well or strained-layer materials for which higher differential gains than in bulk material are generally obtained [13, 14].

Work reported in Reference 15, for example, shows that QW devices also have a higher gain suppression ε than conventional bulk material whereas strained-layer devices exhibit an even higher gain suppression compared with unstrained QWs [16, 17, 18). The increases in gain suppression for such materials are, so far as we are aware, largely attributable to the quantum confinement of the carriers in these structures. Typical values of gain suppression for devices made in different semiconductor materials are given in Table 2. From currently available data it appears that strained layer devices should be anticipated to exhibit enhanced nonlinear gain suppression.

A plot of the maximum bandwidth BW_{max} with the differential gain at different gain suppression and photon lifetime is given in Fig. 5. The dotted curves corresponds to a photon lifetime of 3.7 ps and the solid curve is for a photon lifetime of 1.5 ps.

Table 2: Typical values of differential gain and gain suppression

g_0	Bulk	$1.5–2.0 \times 10^{-6}$ cm^3 s^{-1} 1.875×10^{-6} were assumed in calculations
	QW	2–3 × bulk [6, 21]
	Strained layer QW	4 × bulk [14, 22]
ε	Bulk	$1–3 \times 10^{-17}$ cm^3 [6, 19, 20]
	QW	1–2 × bulk [6, 21]
	Strained layer QW	3 × bulk [14, 22] $5.4–6.4 \times 10^{-17}$ cm^3* [16, 17, 18]

* ε value is obtained via RIN measurement

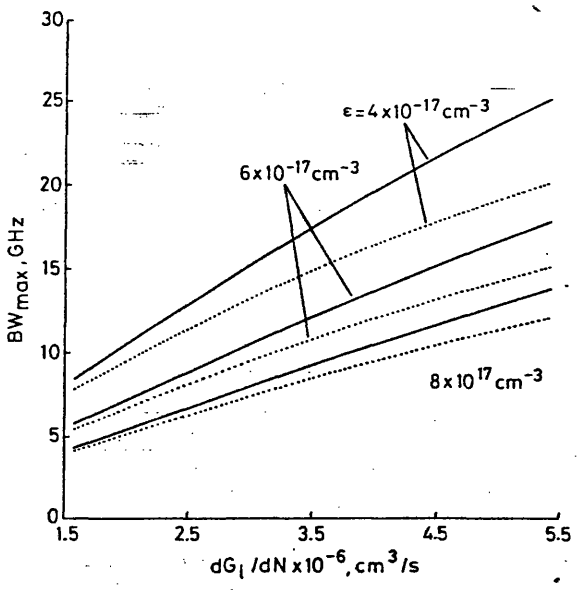

Fig. 5 *Variation of maximum achievable bandwidth BW_{max} against differential gain dG_l/dN at different values of gain suppression ε and photon lifetime τ_p*
——— $\tau_p = 1.5$ ps
- - - - $\tau_p = 3.7$ ps

It is obvious that an increase in differential gain can increase the maximum BW, however, the incremental change, i.e. the slope of curve, is mainly limited by gain suppression and photon lifetime. In other words, high differential gain devices do not always mean high BW, simply because they may have high gain suppression. One recent example is the strained-layer QW device [16, 17]. Consider for example, a strained-layer QW laser having an enhancement in the gain suppression of about three times that of a bulk laser as given in References and 16, 17 with equal photon lifetime; then owing to the linear relationship in eqn. 16, it sould be required that the strained-layer laser also has a differential gain of three times that of the bulk to maintain the same maximum achievable bandwidth. Real improvement in bandwidth can only be obtained if the differential gain of the strain-layer QW laser is actually more than three times that of the bulk. This implies that both the differential gain and the gain suppression are of equal importance to the bandwidth of a laser diode. It is clear, in particular that the effect of gain suppression on the bandwidth should not be overlooked.

5 Conclusions

A damping factor ζ has been defined to take into account the effects of relaxation oscillation damping on the frequency response. The relationship between damping factor ζ and bandwidth BW is also given (eqn. 3), which can be useful in analysing the effect of damping on the -3 dB bandwidth. Using a nonlinear gain in the form $g_0(N - N_{tr})/(1 + \varepsilon P)$, it has been shown that there exists a maximum achievable bandwidth due to the effect of damping. To obtain this maximum bandwidth with flat frequency response, ζ should be equal to 0.707; whereas for an optimal digital system ζ is usually greater than 1.

Approximate expressions for the maximum bandwidth and the corresponding bias current have been found. Both differential gain and gain suppression should be carefully considered to achieve high bandwidth. It has

been shown that high differential gain devices do not always imply large bandwidth due to the high gain suppression which may occur as, for example, in the strained-layer laser.

6 Acknowledgments

One of the authors (YCAW) wishes to acknowledge partial financial support from Northern Telecom/STC (Defence Systems), Paignton, Devon, UK. Both authors appreciate advice and discussions on this work from Dr. A. Janssen, Dr. B. Garrett and Dr. R. Gibb at Northern Telecom/STC.

7 References

1 OLSHANSKY, R., HILL, P., LANZISERA, V., and POWAZINIK, W.: 'Frequency response of 1.3 μm InGaAsP high speed semiconductor lasers', *IEEE J. Quantum Electron.*, 1987, QE-23, pp. 1410–1418
2 TRUCKER, R.S.: 'High speed modulation of semiconductor lasers', *J. Lightwave Technol.*, 1985, LT-3, pp. 1180–1192
3 BOWERS, J.E.: 'High speed semiconductor laser design and performance', *Solid-State Electron.*, 1987, 30, pp. 1–11
4 OLSHANSKY, R.: 'Effect of non-linear gain on the bandwidth of semiconductor lasers', *Electron. Lett.*, 1985, 21, pp. 721–722
5 AGRAWAL, G.P.: 'Gain non-linearities in semiconductor lasers: theory and application to DFB lasers', *IEEE J. Quantum Electron.*, 1987, QE-23, pp. 860–868
6 AGRAWAL, G.P.: 'Modulation bandwidth of high-power single-mode semiconductor lasers: effect of intraband gain saturation', *Appl. Phys. Lett.*, 1990, 57, pp. 1–3
7 AGRAWAL, G.P.: 'Spectral hole-burning and gain saturation in semiconductorlasers: strong-signal theory', *J. Appl. Phys.*, 1988, 63, pp. 1232–1235
8 TUCKER, R.S., and POPE, D.J.: 'Circuit modeling of effect of diffusion on damping in a narrow-stripe semiconductor laser', *IEEE J. Quantum Electron.*, 1983, QE-19, pp. 1179–1183
9 AGRAWAL, G.P.: 'Effect of gain non-linearities on the dynamic response of single-mode semiconductor lasers', *IEEE Photonics Technol. Lett.*, 1989, 1, pp. 419–421
10 SHORE, K.A., and WONG, A.Y.C.: 'Comparison of the effects between two different forms of non-linear gain models on the BW of a laser diode'. 1991, Internal report 4
11 SHORE, K.A., and WONG, A.Y.C.: 'Diode laser bandwidth optimisation for analogue application'. IEE Colloquium on microwave optoelectronics, Nov. 1990
12 AGRAWAL, G.P., and SHEN, T.M.: 'Importance of rapid damping of relaxation oscillations for high-performance optical communication systems', *Electron. Lett.*, 1990, 22, pp. 1087–1088
13 UOMI, K., and CHINONE, N.: 'Proposal on reducing the damping constant in semiconductor lasers by using quantum well structure', *Jap. J. Appl. Phys.*, 1989, 28, pp. L1424–1425
14 LAU, K.Y., XIN, S., WANG, W.I., BAR-CHAIM, N., and MITTELSTEIN, M.: 'Enhancement of modulation bandwidth in InGaAs strained-layer single quantum well lasers', *Appl. Phys. Lett.*, 1989, 55, pp. 1173–1175
15 ARAKAWA, Y., and TAKAHASHI, T.: 'Effect of nonlinear gain on modulation dynamics in quantum-well laser', *Electron. Lett.*, 1989, 25, pp. 169–170
16 SHARFIN, W.F., SCHLAFER, J., RIDEOUT, W., ELMAN, B., LAUER, R.B., LACOURSE, J., and CRAWFORD, F.D.: 'Anomalously high damping in strained InGaAs/GaAs single quantum well lasers'. IEEE Semiconductor Laser Conference, Sept. 1990, Davos, Switzerland, 1990
17 SHARFIN, W.F., SCHLAFER, J., RIDEOUT, W., ELMAN, B., LAUER, R.B., LACOURSE, J., and CRAWFORD, F.D.: 'Anomalously high damping in strained InGaAs/GaAs single quantum well lasers', *IEEE Photonics Technol. Lett.*, 1991, 3, pp. 193–195
18 GHITI, A., and O'REILLY, E.P.: 'Nonlinear gain effects in strained-layer lasers', *Electron. Lett.*, 1990, 26, pp. 1978–1980
19 LANG, R.J., MAYER, H.P., SCHWEIZER, H., MOZER, A.P., PANKNIN, P., and ELSASSER, W.: 'Measurement of relaxation resonance, damping, and nonlinear gain coefficient from the sidebands in the field spectrum of a 1.3 μm InGaAsP DFB laser', *Appl. Phys. Lett.*, 1989, 54, pp. 1845–1847
20 TSUJI, S., VODHANEL, R.S., and CHOY, M.M.: 'Measurement of nonlinear damping factor in 1.5 μm DFB lasers', *Appl. Phys. Lett.*, 1989, 54, pp. 90–92
21 SASAI, Y., OHYA, J., and OGURA, M.: 'Spectral linewidth and resonant frequency characteristics of InGaAsP/InP multiquantum well lasers', *IEEE J. Quantum Electron*, 1989, QE-25, pp. 662–667
22 RIDEOUT, W., YU, B., LACOURSE, J., YORK, P.K., BEERNINK, K.J., and COLEMAN, J.J.: 'Measurement of the carrier dependence of differential gain, refractive index, and linewidth enhancement factor in strained-layer quantum well lasers', *Appl. Phys. Lett.*, 1990, 56, pp. 706–708

8 Appendixes

8.1 Appendix A

For an injection current I, comprising the steady state bias current $\bar{I}$ and a small variation δI, N and P are assumed to be perturbed by a small amount δN and δP around their steady state values $\bar{N}$ and $\bar{P}$, that is

$$I = \bar{I} + \delta I;\ N = \bar{N} + \delta N \quad \text{and} \quad P = \bar{P} + \delta P$$

where

$$\bar{I} \gg \delta I;\ \bar{N} \gg \delta N \quad \text{and} \quad \bar{P} \gg \delta P$$

Then $G(N, P)$, $\tau_e(N)$ and $R_{sp}(N)$ of the rate eqns. 1 and 2 can be expanded in a truncated Taylor series up to the first order derivative due to the small perturbation in δN and δP, that is

$$G(N, P) = G(\bar{N}, \bar{P}) + G_N \delta N + G_P \delta P;$$

$$\gamma_e(N) = \gamma_e(\bar{N}) + \gamma_{eN} \delta N$$

$$R_{sp}(N) = R_{sp}(\bar{N}) + R_{spN} \delta N$$

where

$$G(\bar{N}, \bar{P}) = \frac{g_0(\bar{N} - N_{tr})}{(1 + \varepsilon \bar{P})}$$

$$G_N = \frac{\partial G(\bar{N}, \bar{P})}{\partial \bar{N}} = \frac{g_0}{(1 + \varepsilon \bar{P})}$$

$$G_p = \frac{\partial G(\bar{N}, \bar{P})}{\partial \bar{P}} = \frac{-g_0 \varepsilon (\bar{N} - N_{tr})}{(1 + \varepsilon \bar{P})^2}$$

$$\gamma_{eN} = \frac{\partial \gamma_e(\bar{N})}{\partial \bar{N}} = B + 2C\bar{N}$$

$$R_{spN} = \frac{\partial R_{sp}(\bar{N})}{\partial \bar{N}} = \beta(A + 2BN + 3C\bar{N}^2)$$

The above is substituted into the rate eqns. 1 and 2; which are then linearised to obtain

$$\frac{d\delta N}{dt} = \frac{\delta I}{eV} + k_A \delta N + k_B \delta P \tag{17}$$

$$\frac{d\delta P}{dt} = k_C \delta N + k_D \delta P \tag{18}$$

where

$$k_A = -[G_N \bar{P} + \gamma_{eN} \bar{N} + \gamma_e(\bar{N})]$$

$$= -\left(\frac{g_0 \bar{P}}{(1 + \varepsilon \bar{P})} + A + 2B\bar{N} + 3C\bar{N}^2\right)$$

$$k_B = -[G_P \bar{P} + G(\bar{N}, \bar{P})]$$

$$= \frac{-g_0(\bar{N} - N_{tr})}{(1 + \varepsilon \bar{P})^2}$$

$$k_C = \Gamma[G_N \bar{P} + R_{spN}]$$

$$= \Gamma\left[\frac{g_0 \bar{P}}{(1 + \varepsilon P)} + \beta(A + 2B\bar{N} + 3C\bar{N}^2)\right]$$

$$k_D = \Gamma G_p \bar{P} + \Gamma G - \gamma_p$$
$$= \Gamma\left[G_p \bar{P} - \frac{R_{sp}}{\bar{P}}\right]$$
$$= \Gamma\left[\frac{-\varepsilon \bar{P} g_0(\bar{N} - N_{tr})}{(1+\varepsilon\bar{P})^2} - \beta\frac{\gamma_e(\bar{N})\bar{N}}{\bar{P}}\right]$$
$$0 = \Gamma G\bar{P} - \gamma_p \bar{P} + \Gamma R_{sp}$$
$$\Rightarrow -\Gamma\frac{R_{sp}}{\bar{P}} = \Gamma G - \gamma_p$$

Differentiating both eqns. 17 and 18 with respect to time, we obtain two second order ODEs,

$$\frac{d^2\delta N}{dt^2} - (k_A + k_D)\frac{d\delta N}{dt} + (k_A k_D - k_B k_C)\,\delta N = \frac{1}{eV}\left[\frac{d\delta I}{dt} - k_D\,\delta I\right] \quad (19)$$

$$\frac{d^2\delta P}{dt^2} - (k_A + k_D)\frac{d\delta P}{dt} + (k_A k_D - k_B k_C)\delta P = k_C\frac{\delta I}{eV} \quad (20)$$

8.1.1 Step response: Assuming a step input current, $\delta I = 0$, the above two ODEs become

$$\frac{d^2X}{dt^2} - (k_A + k_D)\frac{dX}{dt} + (k_A k_D - k_B k_C)\delta X = 0 \quad (21)$$

where $X = \delta N$ or σP.

We can then solve this second order ODE by assuming the time dependence of δN and δP as a damped sinusoidal, that is,

$$\exp(-\alpha_r \pm j\Omega_r)t$$

where

$$\Omega_0^2 = k_A k_D - k_B k_C$$
$$\alpha_r = -\tfrac{1}{2}(k_A + k_D)$$
$$\Omega_r^2 = \Omega_0^2 - \alpha_r^2$$

and Ω_0 is the (angular) undamped frequency; Ω_r is the (angular) relaxation frequency; and α_r is the damping rate of the relaxation oscillation.

8.1.2 Frequency response: To study the frequency response, we can either transform eqn. 5 to the frequency domain by using the Fourier transform or we can assume δI, δN and δP represent small sinusoidal modulation, therefore,

$$\delta I = \delta I^{\Omega} e^{j\Omega t}; \quad \delta N = \delta N^{\Omega} e^{j\Omega t} \quad \text{and} \quad \delta P = \delta P^{\Omega} e^{j\Omega t}$$

where δI^{Ω}, δN^{Ω} and δP^{Ω} are the magnitude of the sinusoidal modulation at a particular frequency Ω. Notice that $\delta I \neq 0$, because δI is not the driving source for producing the corresponding small sinusoidal fluctuation in δN and δP which are given by

$$\delta N^{\Omega} = \frac{\frac{\delta I^{\Omega}}{eV}(j\Omega - k_D)}{\Omega_0^2 Fr(\Omega)} \quad (22)$$

$$\delta P^{\Omega} = \frac{k_C\frac{\delta I^{\Omega}}{eV}}{\Omega_0^2 Ft(\Omega)} \quad (23)$$

where

$$Fr(\Omega) = \left(\frac{j\Omega}{\Omega_0}\right)^2 + 2\frac{\alpha_r}{\Omega_0}\left(\frac{j\Omega}{\Omega_0}\right) + 1 \quad (24)$$

and the term α_r/Ω_0 is the way we defined our damping factor ζ. Furthermore, δI^{Ω}, δN^{Ω} and δP^{Ω} can also denote the Fourier transform or the corresponding time quantities.

8.2 Appendix B

From Appendix 8.1

$$\Omega_0^2 = k_A k_D - k_B k_C$$
$$= \left[G_p\left(R_{spN} - \Gamma\frac{d\gamma_e(\bar{N})\bar{N}}{d\bar{N}}\right) + \Gamma G(\bar{N}, \bar{P})G_N\right]\bar{P}$$
$$+ R_{sp}(\bar{N})\left(\frac{1}{\bar{P}}\frac{d\gamma_e(\bar{N})\bar{N}}{d\bar{N}} + G_N\right)$$
$$+ G(\bar{N}, \bar{P})R_{spN}$$
$$\alpha_r = \frac{1}{2}\left[G_N\bar{P} + \frac{d\gamma_e(\bar{N})\bar{N}}{d\bar{N}} - \Gamma G_P\bar{P} + \frac{R_{sp}}{\bar{P}}\right]$$

Retaining the dominant terms, we have

$$\Omega_0^2 \approx \Gamma G(\bar{N}, \bar{P})G_N\bar{P}$$
$$\approx \frac{dG_l}{dN}\frac{\bar{P}}{\tau_p}\left(\frac{1}{1+\varepsilon\bar{P}}\right) \quad (25)$$
$$\alpha_r \approx \tfrac{1}{2}(G_N - \Gamma G_P)\bar{P}$$
$$\approx \frac{1}{2}\left[\varepsilon + \frac{dG_l}{d\bar{N}}\tau_p\right]\frac{\bar{P}}{\tau_p}\left(\frac{1}{1+\varepsilon\bar{P}}\right) \quad (26)$$
$$\zeta = \frac{\alpha_r}{\Omega_0}$$
$$\approx \frac{1}{2}\left(\varepsilon + \frac{dG_l}{dN}\tau_p\right)\sqrt{\left[\frac{P}{\frac{dG_l}{dN}\tau_p}\left(\frac{1}{1+\varepsilon\bar{P}}\right)\right]} \quad (27)$$

8.3 Appendix C

$$BW^2 = \frac{Y(\zeta)^2\Omega_0^2}{2\pi^2}$$
$$\frac{dBW}{d\zeta} = \frac{1}{2BW}\frac{dBW^2}{d\zeta}$$
$$= \frac{1}{2BW}\frac{Y(\zeta)^2}{(2\pi)^2}\left(\frac{-4\zeta\Omega_0^2}{\sqrt{[(1-2\zeta^2)^2 +)]}} + \frac{d\Omega_0^2}{d\zeta}\right)$$
$$= BW\left(\frac{-2\zeta}{\sqrt{[(1-2\zeta^2)^2 + 1]}} + \frac{1}{\frac{d\zeta}{s\Omega_0}\Omega_0}\right)$$

because

$$\zeta = \frac{\alpha_r}{\Omega_0}$$
$$\frac{s\zeta}{d\Omega_0^2} = \frac{1}{2\Omega_0}\frac{d\zeta}{d\Omega_0}$$
$$\frac{d\Omega_0^2}{d\zeta} = \frac{2\Omega_0}{\frac{d\zeta}{d\Omega_0}} = \frac{2\Omega_0^2}{\frac{d\zeta}{d\Omega_0}\Omega_0}$$

Analysis of two forms of gain nonlinearities on the dynamic response of a laser diode for high frequency applications

C.A. Wong
A. Shore

Indexing term: Laser diodes

Abstract: The implications on the dynamic response of a laser diode for two nonlinear gain models are studied theoretically. The nonperturbative model, recently introduced by Agrawal, leads to a quantitative difference with the previous commonly used two-level model in terms of both the intrinsic bandwidth and damping. The present work is compared with predictions made by Agrawal for the nonperturbative model.

Introduction

Broadband high performance optical communication systems, e.g. subcarrier multiplexed system, which can accommodate both digital and analogue signals and operate at microwave frequencies, seek to exploit the multigigahertz bandwidth of the laser diodes and optical fibres. In designing a laser diode to be used in such a system attention needs to be paid to two basic criteria. First, the intrinsic 3 dB bandwidth of the laser diode needs to be as high as possible which enables the system to operate at high speed. Secondly, a flat and smooth frequency response is also needed to minimise the amount of nonlinear distortions at high frequency; this can be done by imposing damping on the frequency response of the laser diode.

By using small signal analysis of the pair of rate equations shown in Section 2, we formulate the relationship between the damping and the intrinsic 3 dB bandwidth BW [1],

$$BW = Y(\zeta)\Omega_o \tag{1}$$

where

$$Y(\zeta) = \sqrt{\{(1 - 2(\zeta^2) + \sqrt{[(1 - 2\zeta^2)^2 + 1]}\}}$$

$$\zeta \equiv \frac{\alpha_r}{\Omega_o}$$

Here, ζ is defined as a damping factor which directly reflects the level of damping experienced by the laser diode; α_r is the damping rate (s^{-1}) and Ω_o is the angular undamped frequency (Hz). The function $Y(\zeta)$ is shown in Fig. 1 from which it is seen that as ζ increases, the whole function $Y(\zeta)$ decreases. Typical range for damping factor is $0 < \zeta < 1$.

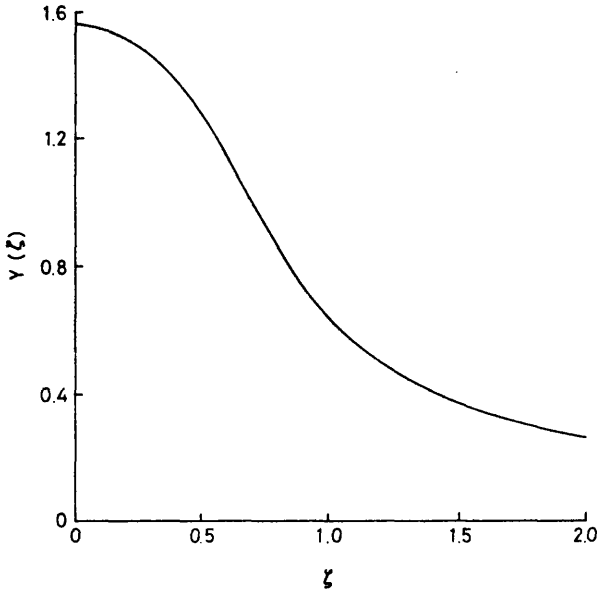

Fig. 1 *Plot of square-root term $Y(\zeta)$ in eqn. 1 against damping factor ζ*

Obviously, eqn. 1 shows that the damping and bandwidth are closely related. As the damping factor increases due to increase in optical output power, $Y(\zeta)$ begins to decrease while Ω_o increases. Hence, a tradeoff between $Y(\zeta)$ and Ω_o exists. Depending on the rate of changing of these two terms with the increase in optical output power, the bandwidth will inevitably experience suppression or even undergo a maximum point BW_{max} as the optical intensity increases.

An important parameter which can affect the damping rate α_r and indirectly controls the changing rate of $Y(\zeta)$ and Ω_o as intensity increase, is the optical gain G. Several forms of functional dependence of G on the photon density P and the carrier density N have been proposed in the literature in recent years. Two common functional

Paper 8888J (E13), first received 25th October 1991 and in revised form 30th March 1992

The authors are with the University of Bath, School of Electronic and Electrical Engineering, Claverton Down, Bath BA2 7AY, United Kingdom

This work has been partially supported by Northern Telecom, Paignton, Devon, UK

forms for G which have been used are

$$G(N, P) = G_l(1 - \varepsilon P) = g_o(N - N_{tr})(1 - \varepsilon P) \quad (2)$$

$$GG(N, P) = \frac{G_l}{1 + \varepsilon P} = \frac{g_o(N - N_{tr})}{1 + \varepsilon P} \quad (3)$$

where $G_l = G(N)$ is the linear optical gain; g_o is the gain coefficient or the linear differential gain; N_{tr} is the transparency carrier density; and ε is the gain suppression coefficient. Eqn. 2 is always used as a simple model related to small optical power, i.e. $\varepsilon P \ll 1$, since the model actually breaks down when $\varepsilon P \geqslant 1$. In dealing with the high-power regime of semiconductor laser, the relationship in eqn. 3, which is in direct analogy to a homogeneously broadened two-level system [2], can be used (in fact, eqn. 2 is an approximation of eqn. 3 when εP is small). For convenience we refer to this form of nonlinear gain in eqn. 3 as the two-level model.

More recently, Agrawal has derived another form of nonlinear gain model [3–5],

$$G(N, P) = \frac{G_l}{\sqrt{(1 + \varepsilon P)}} = \frac{g_o(N - N_{tr})}{\sqrt{(1 + \varepsilon P)}} \quad (4)$$

This nonperturbative nonlinear gain model is obtained by considering the intraband relaxation effect in high power lasers which has been neglected in the two-level model. Both nonlinear gain models (eqns. 3 and 4), can be expected to have different effects on the damping rate and undamped frequency of a laser diode and hence on the damping factor and bandwidth.

In this paper, we use both functional forms of nonlinear gain models (eqns. 3 and 4) in the rate equations and study their effects on the bandwidth and damping of semiconductor lasers. Based on small-signal analysis on the single-mode rate equations model, we obtain both the numerical and analytical results for the α_r, Ω_o and ζ of the two nonlinear gain models. Both the bandwidth and criterion for the maximum bandwidth are found by using eqn. 1. In addition, a comparison between our results and those obtained by Agrawal for the nonperturbative nonlinear gain model is given. Consideration is also given to experimental means for distinguishing between the two nonlinear gain models.

2 Damping parameters

The pair of single-mode rate equations for the carrier density N and photon density P used throughout this paper is

$$\frac{dN}{dt} = \frac{I}{eV} - \gamma_e(N)N - G(N, P)P$$
$$\frac{dP}{dt} = \Gamma G(N, P)P - \gamma_p P + R_{sp}(N) \quad (5)$$

with

$$\gamma_e(N) = \frac{1}{\tau} = A_{nr} + BN + CN^2$$

$$\gamma_p = \frac{1}{\tau_p}$$

$$R_{sp} = \beta(BN)N$$

where I, e and V are the injection current (A), electron charge (col) and active layer volume (cm^3); τ, τ_p are the carrier lifetime and the photon lifetime (s); A_{nr}, B and C are the nonradiative (s^{-1}), radiative (cm^3 s^{-1}) and Auger (cm^6 s^{-1}) recombination rates respectively; Γ and β are the optical confinement and the spontaneous emission factors.

From a standard small-signal analysis of this pair of equations, it is found that [1],

$$\alpha_r \approx \frac{1}{2}\left(\frac{dG}{dN} - \Gamma\frac{dG}{dP}\right)P \quad (6)$$

$$\Omega_o^2 \approx \Gamma G \frac{dG}{dN} P \quad (7)$$

$$\zeta = \frac{1}{2}\sqrt{\left(\frac{dG/dN}{\Gamma G}\right)\left(1 - \Gamma\frac{dG/dP}{dG/dN}\right)}\sqrt{P} \quad (8)$$

A laser diode with high nonlinear gain suppression coefficient ε and low differential gain g_o will exhibit a high damping effect as indicated by the significant term $(dG/dP)(dG/dN)$ in eqn. 8.

Substituting the two different nonlinear gain models into the above equations, we obtained the following sets of results:

(i) for the two-level model:

$$\alpha_r \approx \frac{1}{2}\left(1 + \frac{\varepsilon}{g_o\tau_p}\right)\frac{g_o}{\varepsilon}\frac{x}{(1 + x)} \quad (9)$$

$$\Omega_o^2 \approx \frac{g_o}{\tau_p\varepsilon}\frac{x}{(1 + x)} \quad (10)$$

$$\zeta \approx \frac{1}{2}\frac{1}{\sqrt{(\varepsilon/g_o\tau_p)}}\left(1 + \frac{\varepsilon}{g_o\tau_p}\right)\sqrt{\left(\frac{x}{(1 + x)}\right)} \quad (11)$$

where $x = \varepsilon P$ is introduced as a form of normalisation.

(ii) for the nonperturbative model:

$$\alpha_r \approx \frac{1}{4}\left(2 + \frac{\varepsilon}{g_o\tau_p}\right)\frac{g_o}{\varepsilon}\frac{x}{(1 + x)} \quad (12)$$

$$\Omega_o^2 \approx \frac{g_0}{\tau_p\varepsilon}\frac{x}{\sqrt{(1 + x)}} \quad (13)$$

$$\zeta \approx \frac{1}{4}\frac{1}{\sqrt{(\varepsilon/g_o\tau_p)}}\left(2 + \frac{\varepsilon}{g_o\tau_p}\right)\sqrt{\left(\frac{x}{(1 + x)^{3/2}}\right)} \quad (14)$$

Comparing eqns. 9 and 12, the growth rate of α_r against x (or intensity) produced by the two-level nonlinear model

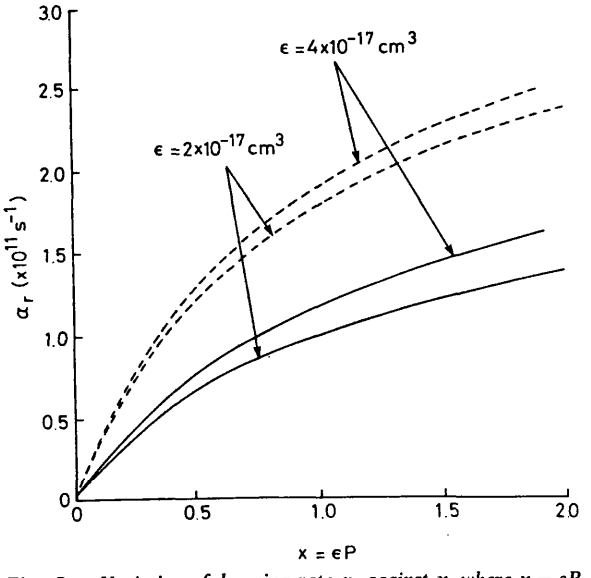

Fig. 2 *Variation of damping rate α_r against x, where $x = \varepsilon P$, for two different forms of nonlinear gain models*

——— nonperturbative model
- - - - two-level model

is twice that obtained by the nonperturbative model as evident by numerical results shown in Fig. 2. This shows that the two-level model implies a comparatively higher damping than that of the nonperturbative model.

In Fig. 3, numerical results also show that the two-level model is subject to a higher suppression in Ω_o than

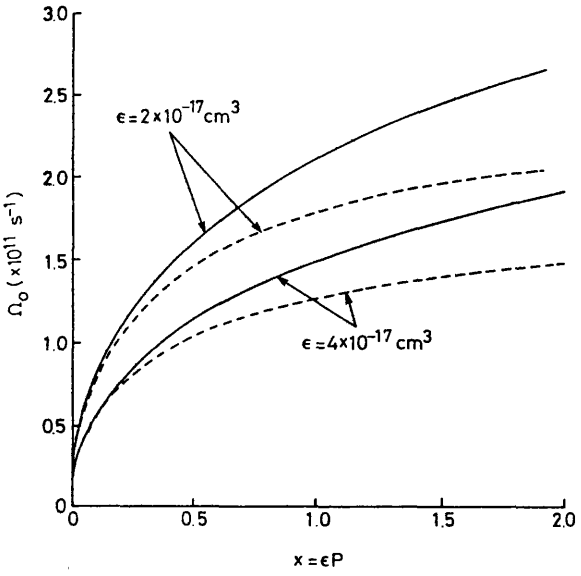

Fig. 3 *Variation of undamped frequency Ω_o against x, where $x = \varepsilon P$, for two different forms of nonlinear gain models*

——— nonperturbative model
- - - - two-level model

of the nonperturbative model as x (or intensity) increases which is obvious when viewing the denominators of the approximated expression in eqns. 10 and 13. All the parameter values used in the numerical calculations are listed in Table 1.

Table 1: Typical device parameters

A_{nr}	$1 \times 10^{8}\ s^{-1}$
B	$1 \times 10^{-10}\ cm^3\ s^{-1}$
C	$1 \times 10^{-29}\ cm^6\ s^{-1}$
β	1.7×10^{-4}
V	$1 \times 10^{-10}\ cm^3$
N_{tr}	$1 \times 10^{18}\ cm^{-3}$
Γ	0.5
τ_p	$1.5 \times 10^{-12}\ s$
τ	$2.8 \times 10^{-9}\ s$
N_{th}	$1.7 \times 10^{18}\ cm^{-3}$
I_{th}	9.77 mA
g_o	$1.8 \times 10^{-6}\ cm^{-3}\ s^{-1}$

Fig. 4 displays the numerical calculations of the damping factor ζ against x for the two different nonlinear gain models. Within the practical regime of ζ (i.e. $0 \leqslant \zeta \leqslant 1$), it is clear that the ζ of the nonperturbative model has a relatively smaller growth rate (approximately half that of the two-level model) and tends to saturate at a certain optical output power.

By differentiating eqn. 14 with respect to x, it is found that the ζ of the nonperturbative model always saturates at $x \simeq 2$ regon with a value of

$$\zeta_{sat} = 0.155 \frac{[2 + (\varepsilon/g_o \tau_p)]}{\sqrt{(\varepsilon/g_o \tau_p)}} \tag{15}$$

It is this saturation effect and the reduced growth rate of ζ of the nonperturbative model which causes a dramatic

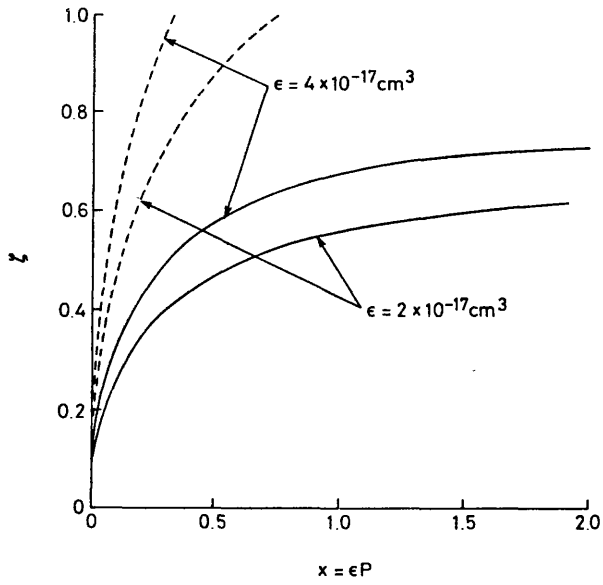

Fig. 4 *Variation of damping factor $\zeta \equiv \alpha_r/\Omega_o$ against x, where $x = \varepsilon P$, for two different forms of nonlinear gain models*

——— nonperturbative model
- - - - two-level model

change in the intrinsic bandwidth when compared with that of the two-level model.

3 Bandwidth suppression and maximum bandwidth

In this work we take bandwidth suppression to mean that a certain optical output power, a reduction occurs in the rate of increase of bandwidth with increasing optical power. This happens due to the increase in damping effect which accompanies an increase of optical output power as explained in Section 1. If the damping effect in the system is strong enough, then bandwidth against intensity may reach a maximum — the maximum achievable bandwidth BW_{max}.

It has already been shown [1] that the criterion for the maximum bandwidth BW_{max} to occur is

$$\frac{d\zeta}{d\Omega_o} \Omega_o \geqslant 0.707\zeta \tag{16}$$

Checking this criterion for the two different nonlinear gain models, it is found that

(*i*) *for the two-level model:*

$$\frac{d\zeta}{d\Omega_o} \Omega_o = \zeta \geqslant 0.707\zeta \tag{17}$$

which indicates that a maximum bandwidth always exists for this functional form of gain nonlinearity. Further calculation shows that $\zeta = 0.707$ whenever the BW_{max} occurs

while

$$BW_{max} \approx \frac{\sqrt{2}}{2\pi} \frac{\Gamma G}{[1 - \Gamma(dG/dP)/(dG/dN)]}$$

$$= \sqrt{(2)}(2\pi) \frac{1}{2\alpha_r/f_o^2}$$

$$= \frac{\sqrt{(2)}g_o}{2\pi(\varepsilon + g_o\tau_p)} \quad (18)$$

where $f_o = \omega_o/2\pi$. This equation points out that the maximum bandwidth is power independent and depends mainly on device parameters. For example, an increase in the differential gain g_o, say by using quantum well material, will usually achieve a higher maximum bandwidth provided the gain suppression coefficient remains unchanged or small [1]. The term $2\alpha_r/f_o^2$ is the Olshansky's K factor, a powerful tool for evaluating BW_{max}.

Substituting $\zeta = 0.707$ in eqn. 11, we find that at $BW = BW_{max}$

$$x = \frac{2(\varepsilon/g_o\tau_p)}{1 + (\varepsilon/g_o\tau_p)^2} \quad (19)$$

which indicates that x has a maximum value of unity at $\varepsilon/g_o\tau_o = 1$. Therefore the maximum bandwidth will always occur at $0 < \varepsilon P < 1$ and depends purely on the value of $\varepsilon/g_o\tau_p$. Typical values lie between 0.5 to 15 for bulk and quantum well materials.

(ii) for the nonperturbative model:

$$\frac{d\zeta}{d\Omega_o}\Omega_o = \frac{2 - x}{2 + x}\zeta \quad (20)$$

which suggests that BW_{max} may or may not exist, since $\zeta(2 - x)/(2 + x)$ can be bigger or smaller than 0.707ζ.

However, it is certain that if there exists a local maximum or turning point in bandwidth against optical intensity then (to meet the criterion in eqn. 16) $x = \varepsilon P$ must fulfil the condition

$$\frac{2 - x}{2 + x}\zeta \geqslant 0.707\zeta$$

$$\text{i.e. } 0 < \varepsilon P \leqslant 0.34 \quad (21)$$

In fact, the existence of the local maximum for this nonperturbative nonlinear gain model also depends on the parameter $\varepsilon/g_o\tau_p$. This can be visualised by manipulating eqn. 14 and expressing x as a cubic in $\varepsilon/g_o\tau_p$. For typical parameter values such a local maximum point hardly exists. Consequently, the K factor will lose its utility as a measurement of maximum bandwidth and becomes a power-dependent parameter.

Fig. 5 shows numerically calculated bandwidth against x using the two nonlinear gain models. For the two-level model, the bandwidth always experiences a maximum bandwidth at $\zeta = 0.707$, which confirms the finding. In brief, when the intensity increases, Ω_o begins to rise linearly while $Y(\zeta)$ decreases. As intensity increase further, the nonlinear gain term $1 + x$ in the denominator of eqn. 10 starts to cause Ω_o to increase sublinearly; and at the same time $Y(\zeta)$ decreases continuously. Hence a tradeoff between terms exists, and its effect is so strong that it actually causes a maximum point in the bandwidth against intensity. In this nonlinear model, it is noteworthy that if the laser diode is being driven to operate at $\zeta = 0.707$ where $BW = BW_{max}$, then both basic criteria mentioned in Section 1 will be fulfilled automatically and the laser diode is actually working at its optimal point.

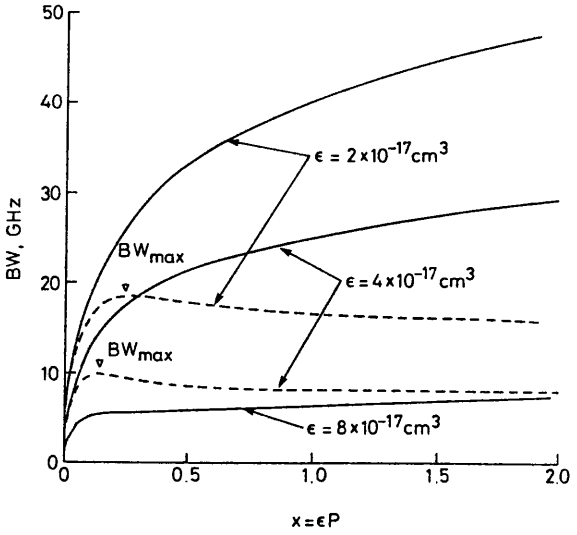

Fig. 5 *Variation of 3 dB intrinsic bandwidth BW against x, where $x = \varepsilon P$, for two different nonlinear gain models*

——— nonperturbative model
- - - - two-level model

On the other hand, for the nonperturbative model, bandwidth suppression exists which causes the bandwidth to increase sublinearly at high intensity but no maximum point is observed. This is due to the fact that the growth rate of ζ is reduced when compared to the two-level model. Hence $Y(\zeta)$ decreases relatively slower and may even become constant as ζ saturates at high value of x (i.e. $\varepsilon P \simeq 2$). Furthermore, the sublinear increase effect in Ω_o is also comparatively weak (since the denominator is $\sqrt{(1 + x)}$ rather than $1 + x$ in the previous case, refer to eqns. 10 and 13 respectively). Consequently, the total bandwidth suppression effect is far less than that obtained from the two-level nonlinear gain model and therefore a maximum point in bandwidth against x is rarely seen for typical parameter values. The

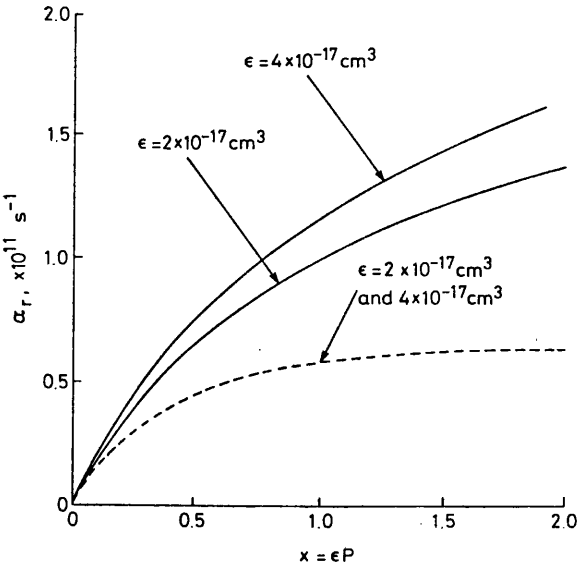

Fig. 6 *Comparison of results obtained by two different approaches on damping rate α_r for nonperturbative nonlinear gain model*

——— this approach
- - - - Agrawal's approach

bottom curve in Fig. 5 illustrates that a local maximum point may arise at a value of x which corresponds to the range in eqn. 20 due to strong damping effect caused by high value of ε and low differential gain g_o, e.g. $\varepsilon = 8 \times 10^{-17}\,\text{cm}^3$ and $g_o = 0.9 \times 10^{-6}\,\text{cm}^3\,\text{s}^{-1}$ (i.e. $\varepsilon/g_o\tau_p \simeq 60$); however, this is a very unusual case.

It is constructive to compare our results to those obtained by Agrawal for the nonperturbative nonlinear gain model. From References 4, 5, the analytical results obtained by Agrawal are (in our notation):

$$\alpha_r = \frac{1}{4}\frac{1}{\tau_p}\frac{x}{(1+x)^{3/2}} \tag{22}$$

$$\Omega_o^2 = \frac{g_o}{\tau_p \varepsilon}\left(1 + \frac{x}{2}\right)\frac{x}{(1+x)^2} \tag{23}$$

The results obtained by Agrawal and ourselves are shown graphically in Figs. 6, 7 and 8 for α_r, Ω_o and BW,

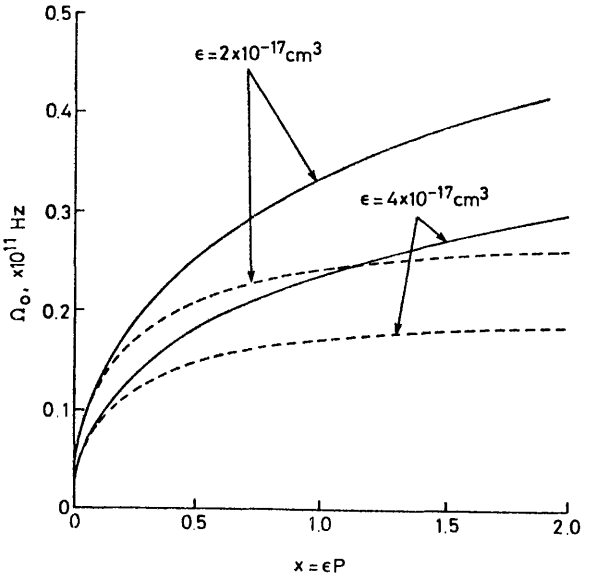

Fig. 7 *Comparison of results obtained by two different approaches on undamped frequency Ω_o for nonperturbative nonlinear gain model*

——— this approach
- - - - Agrawal's approach

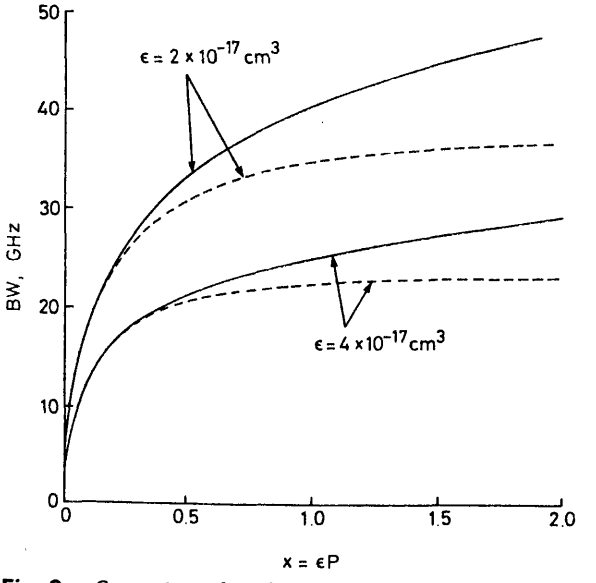

Fig. 8 *Comparison of results obtained by two different approaches on 3 dB intrinsic bandwidth BW for nonperturbative nonlinear gain model*

——— this approach
- - - - Agrawal's approach

respectively. The reasons for the big discrepancy in the two sets of results are explained as follows:

- In References 4 and 5, Agrawal has implicitly assumed $\Omega_o \approx \Omega_r$, where Ω_r is the relaxation frequency which should be approached by $\Omega_r = \sqrt{(\Omega_o^2 - \alpha_r^2)}$.
- A significant term, $g_o x/2\varepsilon\sqrt{(1+x)}$ in eqn. 21, has been omitted by Agrawal during the approximation procedure.
- An assumption that $\tau_p = 1/\Gamma G_l = 1/\Gamma g_o(N - N_{tr})$ has been made by Agrawal, whereas $\tau_p = 1/\Gamma G = \sqrt{(1 + \varepsilon P)}/\Gamma g_o(N - N_{tr})$ should be used.

4 Practical considerations

A large intrinsic bandwidth is normally required for the laser diode deployed in a high performance optical system. It has been shown that no matter which form of nonlinear gain model is being used, bandwidth suppression always occurs. The most striking feature of the nonperturbative model is that there is virtually no limitation imposed on the intrinsic bandwidth as optical power increase; on the contrary, the bandwidth produced by the two-level model always experiences a maximum point within $0 < \varepsilon P < 1$.

Based on this difference in behaviour, one can apparently determine which nonlinear gain model best describes a particular laser diode by driving it up to $\varepsilon P \simeq 1$ to obtain a trace of BW against $\sqrt{(\varepsilon P)}$. If a maximum point exists then the two-level model is appropriate to the laser diode under the test; otherwise, if a reasonably linear relationship persists between BW and $\sqrt{(\varepsilon P)}$, then the nonperturbative model could be a good alternative. This is demonstrated by the simulated results shown in Fig. 9.

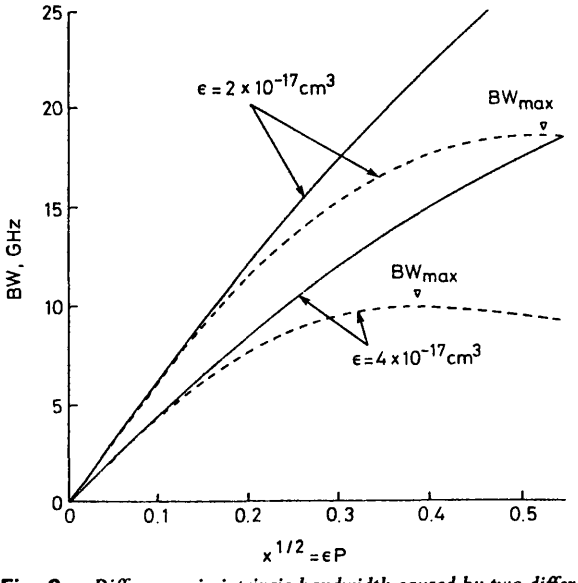

Fig. 9 *Differences in intrinsic bandwidth caused by two different forms of nonlinear gain models at practical range of intensity [$\sqrt{(\varepsilon P)}$ is used by analogy with $\sqrt{(output\ power)}$]*

——— nonperturbative model
- - - - two-level model

The K factor can be another parameter to observe, to check whether the nonperturbative model should be used in place of the two-level model for an experiment. If the measured K factor shows a moderate amount or even strong power dependence, this suggests that one should

switch from the two-level model to the nonperturbative model.

There is at present very little experimental work available which permits a test of the model. Thermal effects restrict the nominal output power of a typical laser diode to $0 < \varepsilon P < 0.3$, thus a specially designed high power laser diode would be required for the experimental observation. However, Agrawal [5] has suggested that the data obtained in an experiment described in Reference 6 for high power DFB lasers supports the use of the nonperturbative nonlinear gain model.

5 Conclusion

We have compared the effect of two nonlinear models on both the damping and bandwidth. The nonperturbative model does not cause any maximum bandwidth in bandwidth against intensity, in contrast the two-level model always induces a BW_{max} within $0 < \varepsilon P < 1$. Such an unlimited growth of bandwidth in the nonperturbative model is due to the saturation effect of the damping factor in this model.

6 References

1 WONG, Y.C.A., and SHORE, K.A.: 'Influence of nonlinear gain on the intrinsic bandwidth of quantum well and strained layer semiconductor lasers', *IEE Proc. J.*, 1991, **138**, pp. 413–419

2 BOWERS, J.E., HEMENWAY, B.R., GNAUCK, A.H., and WILT, D.P.: 'High-speed constricted-mesa lasers', *IEEE J. Quantum Electron.*, 1986, **QE-22**, pp. 833–844

3 AGRAWAL, G.P.: 'Effect of gain nonlinearities on the dynamic response of single-mode semiconductor laser', *IEEE Photonics Technol. Lett.*, 1989, **1**, pp. 419–421

4 AGRAWAL, G.P.: 'Modulation bandwidth of high power single-mode semiconductor lasers: Effect of intraband gain saturation', *Appl. Phys. Lett.*, 1990, **57**, pp. 1–3

5 AGRAWAL, G.P.: 'Effect of gain and index nonlinearities on single-mode dynamics in semiconductor lasers', *IEEE J. Quantum Electron.*, 1990, **QE-26**, 1901–1909

6 KAMITE, K., SUDO, H., YANO, M., ISHIKAWA, H., and IMAI, H.: 'Ultra-high-speed InGaAsP/InP DFB lasers emitting at 1.3 μm wavelength', *IEEE J. Quantum Electron.*, 1987, **QE-23**, pp. 1054–1058